The Synthesis and Self-Assembly of MPC Block Copolymers

COWIE, LAUREN

The Synthesis and Self-Assembly of MPC Block Copolymers

Lauren Cowie

A Thesis Presented for the Degree of Doctor of Philosophy

Department of Chemistry
University of Durham
2012

Abstract

Biocompatible and biodegradable poly(lactide)-2-methacryloyloxyethyl phosphorylcholine (PLA-PMPC) amphiphilic block copolymers were synthesized by a combination of Ring Opening Polymerization (ROP) and Reversible Addition-Fragmentation Chain Transfer (RAFT) polymerization techniques. The PLA-macroRAFT agent was synthesized by the derivatization of PLA-OH with RAFT agent 4-cyano-4-(phenylcarbonothioylthio)pentanoic acid (CPADB) achieving high levels of functionalization and narrow weight distributions (PDI range of 1.02-1.17). PLA-PMPC with varied MPC block lengths were synthesized yielding polymers with a narrow polydispersity PDI = 1.16-1.21. Triblock copolymers PMPC-PLA-PMPC with varying hydrophilic weight ratios were synthesized following an analogous method, the polymerizations were shown to be controlled with PDI's of 1.24 and 1.36.

PLA-PMPC block copolymers with varied compositions were self-assembled using several techniques to target different morphologies. Nanostructures were characterised by DLS and TEM. Block copolymers with a larger PLA block length were shown to generate smaller aggregates i.e. micelles. The morphologies observed for the various block copolymers were consistent amongst different preparative techniques. Vesicle structures were reproducible by the self-assembly of $PMPC_{50}$-PLA_{51}-$PMPC_{50}$, however, by preparing nanoparticles by direct dissolution micelles formed. The block copolymers were shown to encapsulate a hydrophobic dye in aqueous media thereby demonstrating its potential drug delivery applications.

Declaration

The work reported in this thesis is based on research carried out in the Department of Chemistry, University of Durham, England between November 2008 and March 2012. No part of this thesis has been submitted elsewhere for any other degree or qualification and it is all my own work unless referenced to the contrary in the text.

Statement of Copyright

Acknowledgements

I would firstly like to take this opportunity to thank Prof. Neil Cameron for giving me the opportunity to undertake the project, as well as for his ideas, time and continuous guidance and support throughout my PhD it was much appreciated. To Dr Ezat Khosravi, Dr Mike Driver and Brian Tarbit I would like to thank them for their additional supervision and input.

To all those in the NRC group and in office 235, past and present, it has been a pleasure working alongside each and every one of you, certainly my time at Durham would not have been as enjoyable without you all. Special mentions go to Greg and Ali for all their knowledge and training. To Sarah for her encouragement and company which kept me going and I will forever be grateful of her help in providing me with a place to rest my head! David thanks go to him for all his advice and support especially during the last stretch, you kept me sane! Finally to Scott, thank you for your support and uplifting presence providing me with plenty of laughs when I needed them, the past 4 years would not have been the same without you.

Special thanks also to Dr Alan Kenwright for all his help and to Christine Richardson thanks for all your assistance with TEM. I'm also extremely grateful to Nick Warren who readily ran and analyzed the data for several polymers samples obtained on the mixed solvent GPC. Thanks go to, Doug, Jeff, Tony and Phil for providing me with all my labware needs and their company.

Finally I'd like to thank my family especially my parents for their continuous support and advice. Their presence has been much appreciated during my PhD and without them I don't think I would have got this far.

Abbreviations

ACVA	4, 4’-azobis(4-cyano-pentanoic acid)
AIBN	2, 2’-azobis(2-methylpropionitrile)
APC	2-(acryloyloxy)ethyl phosphorylcholine
APCN	Amphiphilic Cone Network
ATRP	Atom Transfer Radical Polymerization
BMA	*n*-Butyl methacrylate
BSTSE	2-(benzylsulfanylthiocarbonylsulfanyl)ethanol
CMC	Critical Micelle Concentration
CPAD	4-cyano-4-[(dodecylsulfanylthiocarbonyl)sulfanyl]pentanoic acid
CPADB	4-cyano-4-(phenylcarbonothioylthio)pentanoic acid
DBU	1, 8-diazabicyclo[5.4.0]undec-7-ene
DCC	N,N-dicyclohexylcarbodiimide
DCM	Dichloromethane
DEA	2-(diethylamino)ethyl methacrylate
DLS	Dynamic Light Scattering
DMA	2-(dimethylamino)ethyl methacrylate
DMAP	4-dimethylaminopyridine
DMF	Dimethylformamide
DDMAT	S-1-dodecyl-S-(α,α’-dimethyl-α’’-acetic acid) trithiocarbonate
DMSO	Dimethylsulfoxide
DOX	Doxorubicin
DP	Degree of Polymerization
DPA	2-(diisopropylamino)ethyl methacrylate
ECM	Cells and Extracellular Matrix
GPC	Gel Permeation Chromatography
HEA	2-hydroxyethyl acrylate
HECPD	2-[N-(2-hydroxyethyl)-carbamoyl]prop-2-yl dithiobenzoate
HEMA	2-hydroxyethyl methacrylate
HPMA	2-hydroxypropyl methacrylate
IPA	Isopropanol
LCST	Lower Critical Solution Temperature
MPC	2-methacryloyloxyethyl phosphorylcholine
MPS	Mononuclear Phagocyte System

MRA	MacroRAFT agent
MTT	(3-(4, 5-Dimethylthiazol-2-yl)-2, 5-diphenyltetrazolium) bromide
NMP	Nitroxide Mediated Polymerization
NMR	Nuclear Magnetic Resonance
PA	Poly(anhydride)
PC	Phosphorylcholine
PCl	Poly(caprolactone)
PDMAEMA	Poly(dimethylaminoethyl methacrylate)
PDI	Polydispersity Index
PDMS	Poly(dimethylsilane)
PEG/PEO	Poly(ethylene glycol)/Poly(ethylene oxide)
PGA	Poly(glycolide)
PHEMA	Poly(2-hydroxyethyl methacrylate)
PLA	Poly(lactide)
PMPC	Poly(2-methacryloyloxyethyl phosphorylcholine)
PMPS	Poly(methylphenylsilane)
PNIPAM	Poly(N-isopropylacrylamide)
POEGMA	Poly(oligoethylene glycol methacrylate)
PS	Polystyrene
RAFT	Reversible Addition-Fragmentation Chain Transfer
RI	Refractive Index
ROP	Ring Opening Polymerization
TE	Tissue Engineering
TEM	Transmission Electron Spectroscopy
THF	Tetrahydrofuran

Contents

List of Figures

List of Tables

Aims

The aim of the work is to prepare amphiphilic 2-methacryloyloxyethyl phosphorylcholine (MPC) containing block copolymers with a biodegradable hydrophobic block using reversible addition-fragmentation chain transfer (RAFT) polymerization and self-assemble these amphiphilic block copolymers into nanostructures with potential biomedical applications e.g. drug delivery. MPC provides excellent blood compatibility and is therefore ideal for the development of drug carriers. The outer shell of the nanoparticle composed of PMPC would increase the efficiency of the drug carrier by preventing reticuloendothelial system (RES) recognition resulting in premature removal from the bloodstream. PMPC combined with a biodegradable segment allows for the release of the drug under biological conditions.

1. Introduction

1.1 2-Methacryloyloxyethyl phosphorylcholine (MPC)

Biomimicry is the discipline of designing materials by mimicking biology and nature. It was born through the discovery by Zwaal *et al*.[1] that "phospholipids composing the inner membrane of cells were thrombogenic i.e. resulted in blood clots, while lipids composing the outer membrane were non-thrombogenic".[1, 2] Biomimicry aims to reproduce the properties of the outer surface of cell membranes by incorporating cell membrane constituents onto polymers e.g. synthetic phospholipids (a naturally occurring molecule containing a phosphate group) analogues or phosphorylcholine (PC) moieties.[3, 4] PC is used as the polar head group for major lipid components e.g. phosphatidylcholine and sphinogomyelin, that compose the outer membrane of intact blood cells.[2] Therefore surfaces functionalised with PC groups would be rendered non-thrombogenic. Chapman was the first to synthesize a PC containing polymer via the polymerisation of diacetylenic phosphatidylcholine monomer, which demonstrated enhanced haemocompatibility.[5] Following this development Nakabayashi[6] *et al*. synthesized another PC containing monomer; 2-methacryloyloxyethyl phosphorylcholine (MPC), a methacrylate derivative with a zwitterionic PC moiety shown in **Figure 1.1**.[6]

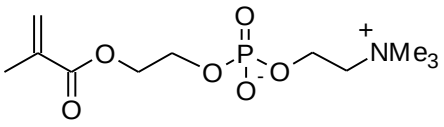

Figure 1-1. Structure of MPC.

1.1.1 Controlled Polymerization of MPC

Atom Transfer Radical Polymerization (ATRP) is the method most often used to control the polymerization of MPC. ATRP is effective for the polymerization of hydrophilic monomers in aqueous media under mild conditions and therefore would be ideal for MPC due to its insolubility in many organic solvents. Armes *et al*. reported the first controlled polymerization of MPC in water at 20 ^{o}C achieving 90 % conversion within 5 minutes generating polymers with a narrow PDI range of 1.12-1.28.[7] However, less control was experienced when the MPC wt% was increased from 17 to 40 (PDI=1.23-1.45).[7] Additionally MPC was polymerized in methanol to avoid the occurrence of autopolymerization of MPC which occurs in aqueous media at room temperature.[7, 8] The

polymerization was shown to be highly controlled (PDI=1.12) with 70 % conversion reached in 4 h.[7]

ATRP is inadequate for the synthesis of polymers intended for biomedical use due to the presence of metal catalyst residues which can range from 10-880 ppm depending on the purification procedure used and thus RAFT polymerization presents an attractive alternative.[9, 10] The RAFT polymerization of MPC procedure has been development from its first reported use; the initial method for RAFT polymerization used 4-cyano-4-(phenylcarbonothioylthio)pentanoic acid (CPADB) as the RAFT agent and initiator 4,4'-azobis(4-cyanopentanoic acid) (ACVA) which was rapid reaching greater than 90 % conversion within 1 h.[11] The polymerization was not as controlled as that achieved by ATRP which was attributed to the incomplete dissolution of RAFT agent and initiator.[11] The method was further altered by the addition of 5 wt% sodium hydrogen carbonate to the polymerization mixture which was then stirred for 4 h in an ice bath prior to the polymerization to give a narrow dispersed homopolymer (PDI = 1.12).[12] Bhuchar *et al*. reported the RAFT polymerization of MPC in methanol with CPADB and CTAm, which avoids dissolution problems and possible hydrolysis of the RAFT agent leading to a lack of control over the polymerization.[13] The polymerization of MPC was slower reaching 80% conversion in 10 h, however, polymerization was controlled. Studies showed that CPADB demonstrated greater control over the polymerization of MPC than the trithiocarbonate RAFT agent with a PDI of 1.08.[13] The copolymerization of MPC with 2-aminoethyl methacrylamide hydrochloride under the conditions analogous to the homopolymerization was shown to be controlled with a PDI of 1.2 which is significantly less if carried out in aqueous media.[13]

1.1.2 Blood Compatibility

It is well-known that when biomedical materials come into contact with bodily fluids such as blood and plasma protein adsorption occurs which can elicit unfavourable biological responses e.g. formation of a blood clot, thus biocompatibility in particular blood compatibility is vital for biomedical devices. Plasma proteins adsorbed on to the artificial surface are believed to mediate cell adhesion. The protein undergoes conformational changes on the surface exposing domains which can bind to the cell surface which can lead to thrombus formation. It is well-documented that PC moieties reduce protein adsorption and cell adhesion (**Figure 1-2**), the mechanism by which PC interact with proteins has not been elucidated, however, there have been several explanations.[2, 14]

The first mechanism was by competitive adsorption in which plasma lipids were adsorbed preferentially at the surface forming a self-assembled bilayer suppressing the adsorption of proteins attributed to the easier diffusion.[15, 16] However, in the *in vitro* protein assays in the absence of lipids PC surface still demonstrates anti-biofouling properties thus showing that several mechanisms are active in resisting protein adsorption.[17] The state of water molecules surrounding the protein and at the polymeric surfaces is also known to influence protein adsorption. It was that reported that MPC polymers possess a large free water fraction surround the PC moieties forming a hydration layer which allows for the reversible adsorption of proteins prohibiting the binding and conformational change of proteins which leads to irreversible adsorption and subsequent denaturation on the surface.[18] At a surface the binding of proteins is driven by the hydrophobic effect, the releasing of water surrounding the protein and at the solid interface results in a decrease in entropy as water becomes less ordered in the bulk. A positive enthalpic contribution to the free energy of adsorption comes from the intermolecular forces acting between the protein and the surface. Irreversible binding and denaturation of the protein occurs more extensively at hydrophobic surfaces. There is a greater degree of unfolding of the protein at a hydrophobic surface which results in stronger interfacial interactions as non polar groups which are hidden within the protein structure can become exposed to the surface by conformational changes.[19] Proteins deposited on the surface provides cells a way of binding to the surface via receptors.[20] .Another factor which influences protein adsorption is the flexibility and mobility of the PC moiety, it has been reported that longer PEO block lengths increase flexibility and effectively reduce protein adsorption.[21]

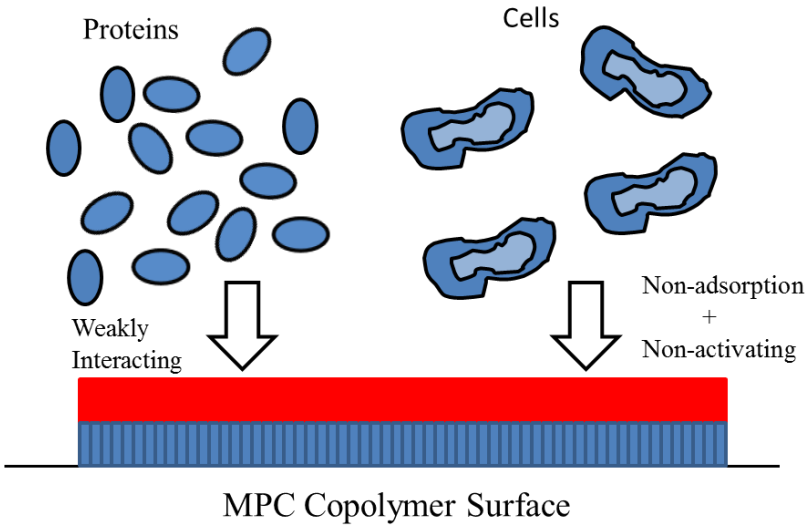

Figure 1-2. Blood compatibility of MPC copolymer surface.

1.1.3 MPC Diblock Copolymer Colloids

Nanostructures e.g. micelles, vesicles have found widespread applications in coatings and in nanomedicine. The properties of PMPC makes it ideal for biomedical applications; the biomimcry of the phosphorylcholine moiety inhibits both protein adsorption and platelet adhesion increasing the stealthiness of the material. A range of amphiphilic PMPC block copolymers have been synthesized and their self-assembly studied.

PMPC amphiphilic block copolymers have been studied as potential drug carriers, the loading and drug release kinetics of the cancer drug Pacitaxel by PMPC-poly(butyl methacrylate (PBMA) prepared by RAFT polymerization has been investigated.[22] The block copolymers self-assembled encapsulated the drug to form micelles with an average diameter of 18 nm.[22] These nanoparticles were shown to demonstrate high loading content (the weight ratio of the drug encapsulated to the weight of the polymeric micelles was >13 %) and a slow sustainable release of the drug which was influenced by the PMPC block length.[22] MPC has also been copolymerised with 2-(diisopropylamino)ethyl methacrylate (DPA) and 2-(diethylamino)ethyl methacrylate (DEA) by ATRP to form biocompatible pH responsive nanoparticles for drug delivery (**Figure 1-3**).[23, 24] Block copolymers of various compositions were shown to form micelles with micellation occurring at pH≥8 for PMPC-PDEA and at pH ≥7.4 for PMPC-PDPA.[23] Above these pH values the tertiary amine becomes deprotonated creating a hydrophobic block which induces self-assembly. The ability of PMPC-PDPA block copolymers to further entrap hydrophobic dyes at physiological pH demonstrates its potential as a drug carrier. PMPC-PDPA nanoparticles were shown to be less cytotoxic than PMPC-PDEA.[23] PMPC-PDPA has therefore been the focus of much research in drug delivery determining drug loadings and release kinetics.[25] Furthermore PMPC-PDPA vesicles have been shown to be a potential vehicle for DNA encapsulation and intracellular delivery which can be utilised to treat diseases by altering gene expression within specific cells.[26, 27]

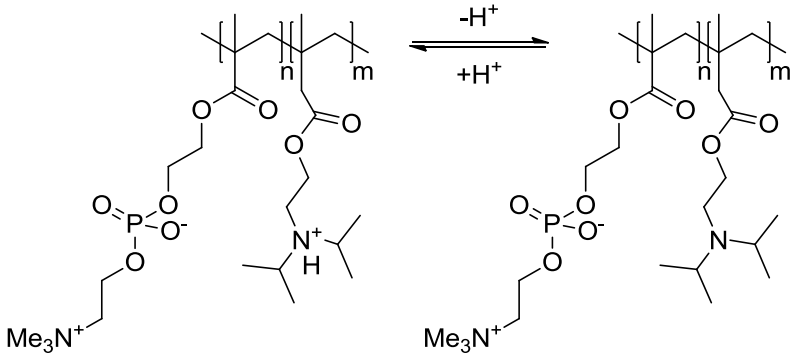

Figure 1-3. pH induced self-assembly of PMPC-PDPA block copolymer.

Armes *et al.* reported a novel polymerization system which drives *in-situ* self assembly.[28] The target block copolymer is PMPC-P(2-hydroxypropyl methacrylate) (HPMA) (**Figure 1-4**) synthesized using a PMPC macroRAFT agent to mediate the RAFT polymerization in aqueous solution.[28] The increase in the HPMA block length drives the self-assembly due to the insolubility of the resulting polymer.[28] A range of $PMPC_{25}$-$PHPMA_X$ (x = 100-400) block copolymers were used to elucidate a morphological transition diagram investigating the effects of two parameters; the hydrophobic block length and the total solid concentration.[28]

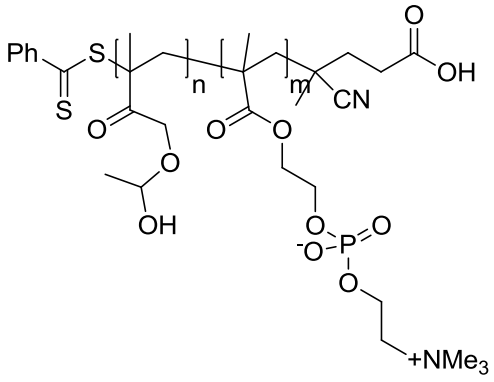

Figure 1-4. Structure of PMPC-PHPMA.

The range of polymers and conditions produced pure morphological phases allowing for the reproducible preparation of specific morphologies i.e. sphere, worm or vesicle.[28] The polydispersity of these polymers were shown to broaden upon increasing the hydrophobic block length ranging from 1.22 to 1.73 due to the presence of a high molecular weight shoulder attributed to branching of the dimethacrylate impurity.[28] Branched polymers are composed of a main chain with one or more substituents i.e. side chains or branches, branching can result in the broadening the PDI because the branched chains contribute more to the M_w than M_n therefore as polymers rapidly build up molecular weight the molecular weight distribution increases.

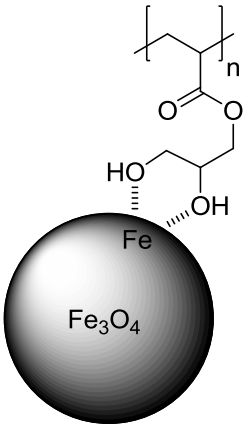

Figure 1-5. Coordination of PMPC- Poly(glycerol monomethacrylate) to iron atoms.

Double hydrophilic block copolymers composed of MPC and poly(glycerol monomethacrylate) have been used to stabilise a dispersion of magnetite nanoparticles.[29] The diol moiety of glycerol monomethacrylate can form a five membered chelate with iron atoms as shown in **Figure 1-5** and PMPC imparts steric stabilization and as a surface coating increases the biocompatibility of the nanoparticle .[29] These sols can be utilised as contrast agents for magnetic resonance imaging.[29] PMPC-PDMA block copolymers have been utilised as a surface coating for gold nanoparticles as DMA acts as a reducing agent for $HAuCl_4^-$.[30] The resulting tertiary amine subsequently binds to the surface of the gold nanoparticle, these biocompatible block copolymer stabilised gold sols have applications in biomedicine e.g. cell imaging.[30]

Synthesis of PCl_{60}-$PMPC_{37}$ diblock copolymers was reported by combining ROP and ATRP.[31] Chain extension of the PCl-Br macroinitiator generated a diblock copolymer with a narrow polydispersity of 1.29.[31] The block copolymer was shown to form vesicles upon self-assembly via direct dissolution at 70 ^oC with a diameter range 40-500 nm for the same vesicles.[31] These nanoparticles were subsequently stabilised by aqueous sol-gel chemistry; solubilising tetramethyl orthosilicate in the hydrophobic membrane before silification to generate water soluble polymer/silica hybrid vesicles.[31]

1.1.4 PMPC Triblock Copolymers

Several MPC based triblock copolymers have been evaluated for biomedical applications researching thermoresponsive and pH amphiphilic triblock copolymers. pH responsive PDPA-PMPC and PDEA-PMPC triblock copolymers were prepared by ATRP using the bifunctional initiator, diethyl-meso-2,5-dibromoadipate.[32] Under basic conditions the

amine residues become deprotonated and therefore hydrophobic which induces self-assembly.[32] High concentrations of the copolymer result in the formation of micellar gel networks where longer PMPC block lengths bridge adjacent micelles whereas at low concentrations flower micelles are observed.[32] These systems were evaluated for the drug release of the cardiovascular drug dipyridamole, at pH 7.4 a slow sustained release was observed but under acidic conditions release was rapid and thus demonstrates potential for biomedical applications.[32]

Armes reported a range of thermo-responsive gelators based on PMPC ABA and ABC type triblock copolymers via ATRP.[33-35] PNIPAM-PMPC triblock gelators formed at 37 ^{o}C at high concentrations of the block copolymer.[33] The cell viability experiments proved gels could act as a cell medium and for 5-10 % gels cells were cultured on tissue culture plastic. [33] However, cells were not viable when cultured in 20 % gel attributed to the higher viscosity of the gel resulting in poor diffusion of nutrients and waste from the cells.[33] Theses gelators show potential for drug delivery as well as for tissue engineering. PPO-PMPC-PNIPAM doubly thermoresponsive triblock copolymers were synthesized and self-assembled targeting different morphologies based on the different LCSTs leading to micellization or gelation.[34] These gelators were less effective than ABA types forming free standing at only 20 % concentration or by increasing the temperature above 40 ^{o}C.[34] A new class of biochemically degradable thermo-responsive gelators was reported; $PNIPAM_x$–$PMPC_y$-S-S-$PMPC_y$–$PNIPAM_x$.[36] The triblock copolymer was synthesized using the ATRP bifunctionalized initiator (bis[2-(2-bromoisobutyryloxy)ethyl] disulfide previously reported by Tsarevsky and Matyjaszewski (**Figure 1-6**).[37] The triblock copolymer was shown to form a free standing gel at 10 % w/v at 37 ^{o}C.[36] Glutathione was utilised to cleave the disulfide bonds forming amphiphilic block copolymers as evidenced by the GPC results and with the formation of a free flowing liquid.[36] These triblock copolymers have been shown to degrade under physiological conditions using naturally occurring glutathione.[36]

$PHPMA_x$–$PMPC_y$-S-S-$PMPC_y$–$PHPMA_x$ was synthesized using a similar methodology to form biochemically degradable thermoresponsive gelators for biomedical applications.[38] NIPAM is unfortunately not suitable for use in the biomedical field as it is relatively expensive and a potent neurotoxin thus HMPA was explored as an alternative. The HMPA based triblock copolymers has been shown to be biodegradable with the intermicellar bridges cleaved at the disulfide bond under mild conditions.[38] The biocompatibility of these gels were investigated for wound dressing applications. Cell viability tests showed

that the gels displayed no adverse effects when in contact with tissue engineered skin thus providing further scope for these materials as wound dressings.[38]

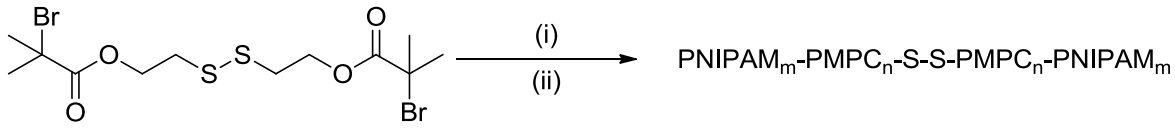

Figure 1-6. Synthesis of MPC triblock copolymer; (i)MPC, CuBr/bipyridine, methanol, 20^{o}C (ii).NIPAM, CuBr/Me$_4$Cyclam methanol, 0 ^{o}C.

PDMS–PMPC triblock copolymers were used to impart biocompatibility to a PDMS surface reducing bio-fouling and as a result improve the performance of biomedical devices. PEGylation is often employed for this purpose but has demonstrated cell adhesion following long term exposure as a result of the hydrolytic degradation of the poly(oligo(ethylene glycol) methylether methacrylate) (POEGMEMA) backbone coating, thus an alternative anti-biofouling surface was investigated.[39, 40] The triblock copolymers were synthesized by RAFT polymerization of MPC using RAFT functionalised poly(vinyl methyl siloxane-*co*-dimethylsilane) producing polymers with a PDI range of 1.27-1.63.[40] The triblock copolymer was covalently bound to the surface by hydrosilation, the surface was shown to reduce platelet adhesion and protein adsorption and the results were influenced by the molecular weight and MPC density of the block copolymer.[40] The biological responses on a phase separated PDMS-PMPC triblock surface was also tested finding protein adsorption on the hydrophobic domains and minimal cell adhesion for high PMPC compositions.[41] At 45 % PMPC composition considerable cell adhesion occurred although the surface is regarded as a hydrophilic surface the hydrophobic domains determined the biological response.[41]

1.1.5 Synthesis and Self Assembly of PLA-PMPC Block Copolymers

PLA-PMPC diblock copolymers have been synthesized and their self-assembly studied due to their potential in drug delivery. The combination of biocompatibility and biodegradability makes these amphiphilic block copolymers ideal for biomedical applications. The block copolymer is prepared by a combination of ROP and ATRP; where the ROP of lactide is terminated by 2-bromo-2-methylpropionyl bromide forming the macroinitiator used for ATRP of MPC (**Figure 1-7**).[42-44] The self-assembly of these

polymers have been studied examining various hydrophilic weight fractions (f_{MPC}) using various preparation techniques. Ji *et al*. reported the formation of large compounds micelles with an average diameter of $1.1x10^3$ nm for low molecular weight block copolymer PLA_{37}-$PMPC_3$ with f_{MPC} of 0.23.[43] Aggregates were prepared via an injection method.[43] Giant vesicles were similarly prepared from block copolymers with f_{MPC} of 0.48 and 0.53 with diameters of 3.5 ± 1.6 µm and 11.0± 3.9 µm, respectively, and are of great interest as a cell model.[44] PLA_{126}-$PMPC_{36}$ with f_{MPC} of 0.54 self-assembled via dialysis to form vesicle morphologies.[44] Vesicles with a diameter range of 118-156 nm were shown to form from the self-assembly of block copolymers composed of a significantly larger PMPC block length.[42] The aggregates formed by the self-assembly of PLA-PMPC diblock copolymers were shown to encapsulate fluorescent dyes thus providing scope for drug delivery

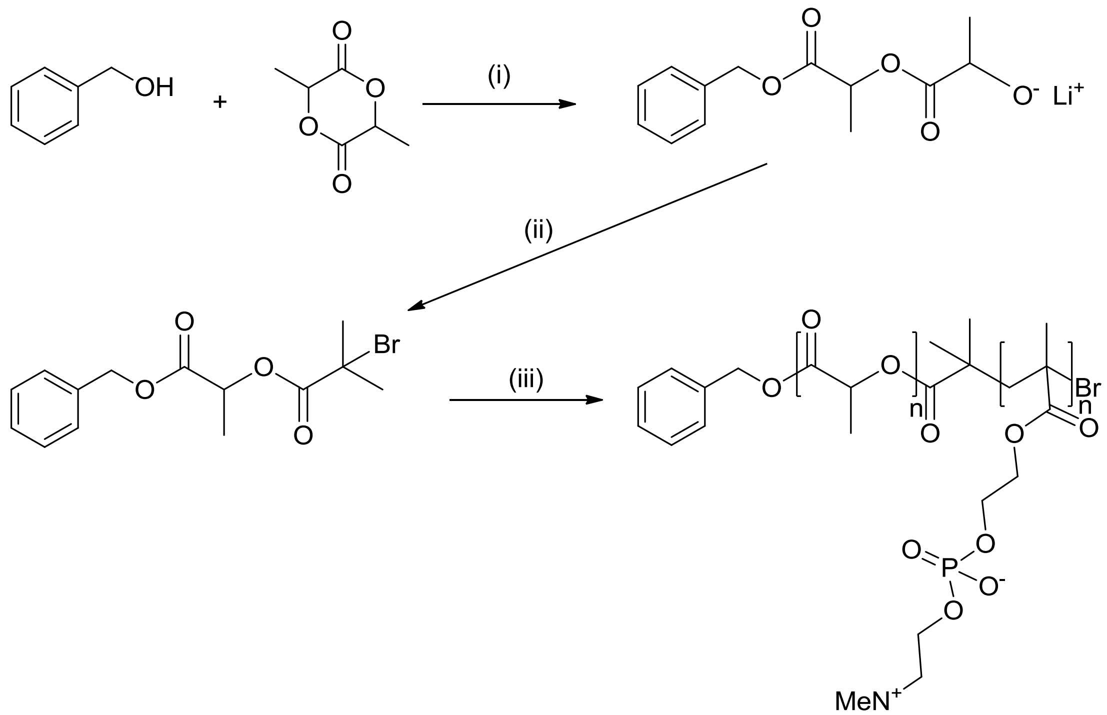

Figure 1-7. Synthesis of PLA-PMPC block copolymer; (i) *n*-butyl lithium, lactide, toluene, 70 °C (ii) 2-bromo-2-methylpropionyl bromide,(iii). MPC, CuBr/bipyridine, DMSO/methanol.

PLA-PMPC micelles and polymersomes have been applied for the delivery of the potent anti-cancer doxorubicin (DOX) evaluating its efficacy and cytotoxicity.[45] The micelles formed were less than 50 nm which is advantageous for drug delivery as small nanoparticles (10-100 nm) e.g. micelles, can evade uptake by the mononuclear phagocyte system (MPS) due prolonging circulatory time in the blood stream and suppresses unfavourable immuno-response.[45] Polymeric micelles of 20-100 nm have are been shown

to preferentially accumulate in tumour tissue due to the enhanced permeability and retention effect; the increased porosity of the vascular surrounding the tumour and poor lymphatic drainage system.[46] Slow drug release from the DOX loaded micelles was observed for lower drug loading content which is required to maintain therapeutic effect.[45] The cytotoxicity of LO2 cells after incubation for 24 h with PLA-PMPC nanoparticles was determined using MTT method showing low cytotoxicity to cells with approximately 100 % cell viability observed over 0.05-0.5 mg/ml micelle concentration.[45] The cytotoxic effects on HepG2 cells (liver carcinoma cell line) by DOX loaded micelles after 48 h was similar to that of the free drug with 80 % cell death observed, thus the nanoparticle had been successfully internalised and the drug released in to the carcinoma cells.[45]

PLA-PMPC based polymersomes loaded with the hydrophobic drug DOX in the PLA membrane and the hydrophilic drug DOX.HCl in the aqueous interior showed great potential in pharmaceutical applications.[47] At pH 5 the degradation of PLA chains drives the morphological transition of polymersomes to micelles within 90 h; pH dependent morphological transition is a highly desirable property of nanoparticle drug carriers eliciting the release of the drug at the target site.[47] The drug loading efficiency was reported to be higher in the membrane (34 %) than the polymersome interior (13 %).[47] At pH 5, 98 % of the DOX.HCl was released in comparison to 52 % of the hydrophobic drug.[41] The difference in release kinetics was attributed to the morphological transition under acidic conditions to form micelles.[47] The cytotoxic effect of PLA-PMPC nanoparticles was determined using LO2 (normal cells) and HepG2 cells by the MTT method was minimal with approximately over 90 % cells viability observed for 0.05-0.5 mg/ml micelle concentration.[47] The MTT assay tests for the reduction of the MTT dye by mitochondrial succinate dehydrogenase, the reduction process can only occur in metabolic active cells thus indicating the viability of the cells. The cytotoxicity of the drug loaded nanoparticles was studied on tumour cells using the MTT method which reported similar results to the free DOX.HCl with 20 % cell viability.[47] The acid endocytic compartments of tumour cells can therefore elicit the degradation of these nanoparticles releasing the hydrophilic drug effectively with the same potency as the free drug. PLA-PMPC nanoparticles show great potential in the delivery of cancer drugs.[47]

1.2 Biodegradable Synthetic Polymers

Synthetic biodegradable polymers are extremely versatile as their properties can be tailored to meet the requirements for specific applications through copolymerization and blending .[48] Synthetic biodegradable polymer have been utilised in the biomedical field since the 1960's, but only over the last twenty years has there been a real interest in developing a new range of these polymers.[49, 50] During this period new biodegradable polymers have emerged; poly(carbonates), poly(caprolactone) (PCL), poly(anhydrides) (PA).[49, 51, 52] The drive for progress coincided with the advances in biomedical technologies such as tissue engineering, gene therapy and controlled drug delivery.[49]At that time the properties of the current synthetic biodegradable polymers i.e. PLA and poly(glycolide) PGA, would not have met the requirements of the increasing number of applications.[51]

1.2.1 Ring Opening Polymerization

Aliphatic polyesters are synthesized via two routes; ROP and polycondensation. There are several drawbacks associated with the latter route, firstly the reaction is limited by equilibrium and is hence carried out under extreme conditions to remove the water from the system.[53] High temperatures will drive the reaction forward to achieve high conversion and high molecular weight polymers. The monomer units are, however, thermally unstable and thus high temperatures will favour side reactions such as dehydration and decarboxylation.[53] Other disadvantage of this method include the inability to prepare high molecular weight polymers as well as the inability to control the polymer molecular weight which results in a broader polydispersity index (PDI) limited by Carothers equation.[53]

The ROP method first demonstrated by Carothers in 1932 is a more favoured route for the preparation of polyesters.[54] There are several mechanisms for ROP; anionic, cationic, coordinative, radical and enzymatic. ROP is a form of chain growth polymerization generates high molecular weight polymers under mild conditions in contrast to polycondensation (step growth polymerization). The molecular weight for chain growth polymerization increases rapidly at the initial stages of polymerization and remains the same throughout the polymerization whereas during stepwise polymerization molecular weight increases slowly and to obtain high molecular weight polymers high conversions must be reached. Furthermore, a greater control over the degree of polymerization (DP) is obtained by chemical ROP by using a specific monomer to initiator molar ratio which leads to a narrow PDI.[55, 56]

1.2.1.1 Thermodynamics

Since the 1930's many cyclic monomers have been successfully polymerised via the ROP method. ROP of cyclic monomers is driven by the relief of ring strain, this favourable enthalpic contribution will overcome the unfavourable entropic contribution observed for all polymerizations.[53] Generally the ring strain associated with three and four membered cyclic esters is greater than that for five and seven membered rings and hence there is a greater driving force for their ring opening.[53] The ring strain associated with 3 and 4 membered rings is due to bond angle distortion which is greater than both the conformational strain in a 5-membered ring and the transannular strain in a 7-membered rings.[57] **Table 1-1**[58] provides the enthalpic and entropic contributions for ROP of 4-7 membered lactones and lactide. The enthalpy for the ROP of γ-butyrolactone is positive, the monomer will therefore not undergo polymerisation unlike the 6 membered lactone δ-valerolactone despite both having a ring strain energy of approximately 33 $kJmol^{-1}$.[59] Houk *et al.*[59] explained the difference in reactivity was attributed to the low ring strain associated with the five membered lactone which demonstrated little distortion around the ester functionality in comparison to valerolactone.[59, 60]

Table 1-1. Enthalpy and entropy of the ROP of cyclic esters at 298 K.

Cyclic Ester	**Propiolactone**	**Butyrolactone**	**Valerolactone**	**Lactide**	**Caprolactone**
ΔH_p **/kJ mol^{-1}**	-82.3	5.1	-27.4	-22.9	-28.8
ΔS_p **/J mol^{-1} K^{-1}**	-74.0	-29.9	-65.0	-25.0	-53.9

1.2.1.2 Transfer Processes

There are two predominant side reactions which occur during propagation of polyester chains; intramolecular and intermolecular transesterification. These transfer reactions lead to the broadening of the PDI.[48]

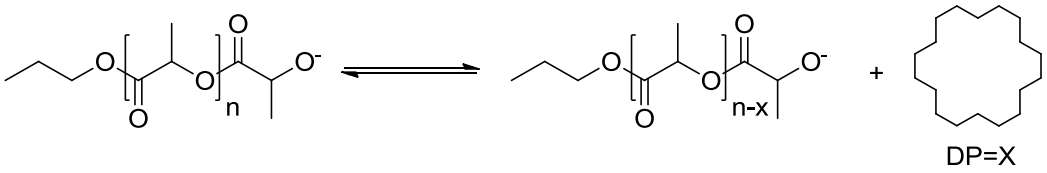

Figure 1-8. Intramolecular tranesterification or back-biting of a propagating polymer chain.

Intramolecular transesterification or back-biting shown in **Figure 1-8**[48] occurs through the nucleophilic attack of the reactive chain end upon labile ester linkages resulting in the formation of cyclic oligomers which lowers the molecular weight of the polymer.[48] The cyclic oligomer can react further with propagating polyester chains to generate polymers of various chain lengths.[48] Intermolecular transesterification (**Figure 1-9**[48]) involves the reaction of two propagating chains without losing the reactive chain ends giving rise to variation of the polymer sequence.[48] The occurrence of these reactions are influenced by the choice and concentration of polymerization catalyst or initiator, temperature, reaction time and nature of monomer.[61, 62]

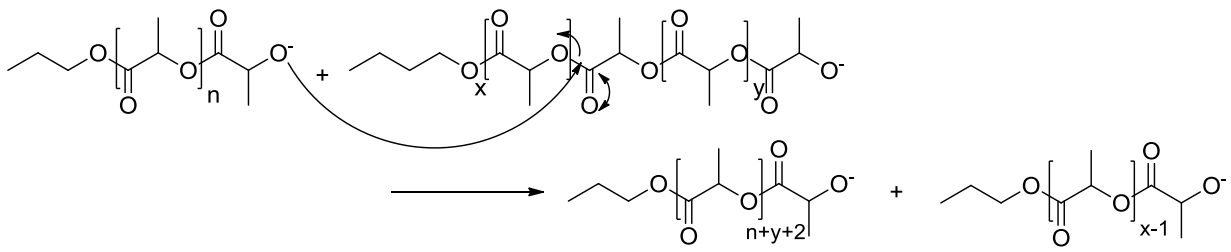

Figure 1-9. Intermolecular transesterification of growing PLA chains.

1.2.1.3 Coordination Ring Opening Polymerization

Coordination polymerization has been used extensively for the synthesis of polyesters, using a wide variety of catalysts. Many organometallic species have been reported for use in coordination insertion ROP such as various lanthanide complexes and non-toxic metal salts e.g. Zn.[55, 63-65] The most common catalysts used are aluminium and tin alkoxides or carboxylates.[54]

Coordinative insertion ROP is more favourable than ionic ROP due to the nature of the growing chain. The propagating species is covalent in character and is therefore less reactive thus reducing the number of side reactions.[66] For coordinative ROP there are two main reaction pathways with the organometallic reagent determining the route which is followed. The organometallic reagent will act as either a catalyst or an initiator which gives rise to these two mechanisms.[55, 66] The first is shown in **Figure 1-10**[55] where the organometallic catalyst activates the monomer by complexation with the carbonyl moiety, enhancing the electrophilicity and thus increasing susceptibility towards nucleophilic attack.[55] Nucleophiles added to the mixture e.g. alcohols, will subsequently attack the cyclic ester which initiates ROP.[55] The second is a coordinative insertion mechanism illustrated in **Figure 1-11**[55], in which the organometallic initiator coordinates to the

carbonyl group.[55] The coordination increases the nucleophilicity of the ligand and the electrophilicity of the carbonyl moiety which leads to the *O*-acyl bond scission and simultaneous insertion of the monomer.[55] Metal alkoxides will act as initiators whereas metal carboxylates take on a catalytic role as they are less nucleophilic.[66] Both methods use a predetermined amount of initiator is used to control molecular weight and each have demonstrated controlled polymerisations with low PDIs. The advantage of using the organometallic reagent as a catalyst is that these reagents are often toxic and in this method are utilised at lower concentrations.

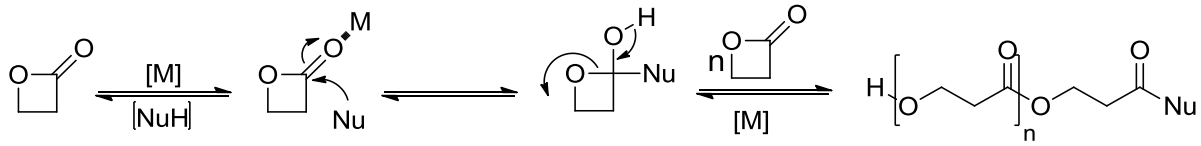

Figure 1-10. Coordinative ROP in which the organometallic reagent (M) acts as a catalyst.

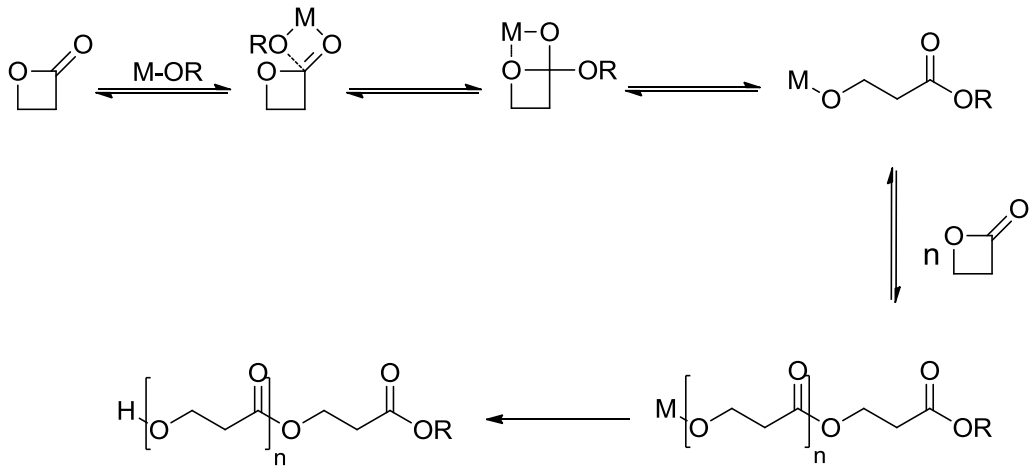

Figure 1-11. Coordinative ROP in which the organometallic reagent (M-OR) acts as an initiator.

1.2.2 Aliphatic Esters

1.2.2.1 Poly(lactide)

Poly(lactide) (PLA) is prepared by the polymerisation of the lactide monomer. The cyclic diester possesses two chiral centres giving to rise to three possible stereoisomers; LL, DD and LD isomers. The polymers derived from *LL* and *meso* lactide will therefore be stereochemically different and thus will exhibit properties distinct from each other.

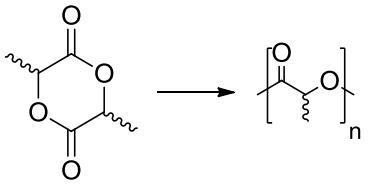

Figure 1-12. Polymerization of Lactide to PLA.

PLLA is a semicrystalline polymer (37% crystalline) with a T_m range 170-183 ^oC and a T_g of 55-65 ^oC whilst PDLLA is completely amorphous with a T_g of 59 ^oC.[67] The morphological and thermal property differences are attributed to the stereochemical outcome; stereoregularity results in the formation of the crystalline domain and will also raise the T_g. It is also due to the crystallinity of PLLA that this polymer exhibits high mechanical strength with demonstrated tensile strength of 59 MPa.[67] For PDLLA the random distribution of chiral configurations along the backbone impedes the ability of chains to form crystalline structures thus lowering the tensile strength of the polymer.[68]

The morphology of the two stereoisomers also affects the rate of degradation since the crystalline domain is more resistant to hydrolysis than the amorphous domain.[67] Generally PLLA is a slow degrading polymer due to its lipophilicity which will impact water uptake furthermore the degradation of PLLA is significantly slower than that of PDLLA.[49] PDLLA when hydrolysed loses its strength within 1-2 months whereas in comparison PLLA loses its strength after six months due to the resistance of crystalline regions to degrade .[49, 69]

The stereoisomers are appreciably different in chemical, physical and mechanical properties and are thus utilised in different applications. Due to the low strength mechanical properties and faster rate of degradation PDLLA for has been developed as a drug delivery device and as a low strength scaffold for tissue engineering.[67] PLLA is predominantly used for load bearing applications such as orthopaedic fixation devices e.g. Phantom Suture Anchor®, but has also been investigated for use as scaffolds for ligament replacement.[49, 70, 71] PLA has gained widespread use in the biomedical field due to the range of chemical, physical and mechanical properties demonstrated as well as the fact that PLA degrades to form non toxic by-product lactic acid which is a normal human metabolic by-product which is further broken down to carbon dioxide and water.[49]

1.2.2.2 Poly(glycolide)

Poly(glycolide) (PGA) was one of the first synthetic biodegradable polymers to be used for biomedical applications. In the 1960's Davis and Greck developed PGA as a resorbable suture marketed as Dexon®, because of its excellent fibre forming ability.[49, 68] PGA is a semi-crystalline (45-55 % crystallinity) polymer, the close packing of the ester groups contributes to a high T_m(224-230 ^oC) and T_g of the polymer ranges from 35-40 ^oC.[50] This polymer demonstrates excellent mechanical strength, which is due to its high crystallinity.[49] PGA exhibits a high tensile strength and a tensile modulus of 12.5 GPa.[49, 69] PGA degrades to form glycine which is non-toxic and biocompatible which is metabolised in the citric acid cycle to water and carbon dioxide.[49]

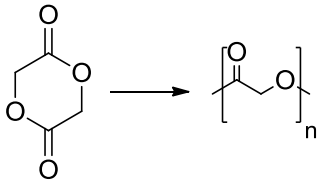

Figure 1-13. Polymerization of glycolide to PGA.

PGA has also been developed as bone internal fixation devices (Biofix®) due to its mechanical properties which are ideal for load bearing applications.[49] Glycolide is often copolymerised with monomers to improve the mechanical properties of homopolymers e.g. poly(trimethylene carbonate) and broaden the scope of these polymers.[49] The most researched glycolide copolymer is Poly(LA-*co*-GA) i.e. P(LGA), using both the *L*, *L* and *meso*-isomer. A wide variety of compositions have been developed for a wide array of biomedical applications.[49] PLGA are predominantly used to form sutures which vary in their rate of degradation depending on the LA:GA ratio.[49, 72] PLGA has also been used to develop tissue engineering applications as it demonstrates good cell adhesion and proliferation.[49] Another application of PGLA is drug delivery; Lupron Depot® composed of PLGA releases gonodotropin for prostrate cancer.[49]

1.2.2.3 Poly(caprolactone)

Poly(caprolactone) (PCL) is formed by the ROP of the seven membered lactone ε-caprolactone.[49] This polymer demonstrates extremely useful properties and has therefore been extensively studied for potential applications in the biomedical field. PCL is a semicrystalline (50 % crystalline) polymer with a T_m range of 59-64 ^oC and a low T_g of approximately -60 ^oC, therefore will exist in a rubbery state and demonstrates low tensile

strength (23 MPa).[48, 49] In addition this polymer is hydrolytically labile degrading over a period of 2-3 years which is slower than that of PLA, chain scission of PLA is 2.8 times faster than PCL.[49, 73] PCL degrades chemically and enzymatically yielding non-toxic and biocompatible 6-hydroxycaproic acid which is completely metabolized in the citric acid cycle.[65, 74]

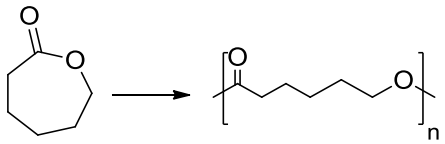

Figure 1-14. Polymerization of ε-caprolactone to PCL.

The slow degradation rate coupled with its permeability to small molecules makes PCL ideal for sustained drug delivery.[65] Capronor® is a one year contraceptive delivery device composed of PCL which releases the drug levonorgestrel.[75] Copolymerisation has been significant to the versatility of PCL in drug delivery, orthopaedics and tissue engineering, having been used to manipulate the degradation rates and improve mechanical properties. PCL demonstrates low mechanical strength and stiffness (0.4 GPa), copolymerisation with glycolide improves mechanical properties - poly(CL-*co*-GA) is used as a monofilament suture which is commercially known as Monocryl®.[68] Caprolactone has also been copolymerized with D,L-lactide to accelerate the rate of degradation by disrupting structural regularity.[68] It is important in tissue engineering for degradation rates of polymers to be adjusted to meet the new tissue formation rate e.g. bladder, liver and skin.

1.2.3 Degradation via Hydrolytic Chain Scission

1.2.3.1 Mechanism

The mechanism and kinetics of the degradation of polyesters has been extensively investigated.[76-78] The hydrolytic degradation of aliphatic polyesters and their copolymers are similar.[73, 79] Initially water penetrates the amorphous domain and will cleave ester linkages since the crystalline domain is more resistant to hydrolysis. The crystalline regions will begin to degrade when most or all of the amorphous regions have degraded. Chain scission is random generating shorter polymer chains with hydroxyl and carboxylic acid end groups. The degradation of polyesters is an autocatalytic process therefore the increase of carboxylic end groups of the degradative products accelerates chain scission which ultimately increases the rate of degradation.[78] The polymer degrades generating

lower molecular weight chains and water soluble monomers and oligomers which leads to a loss of polymeric material.[78]

1.2.3.2 Factors Affecting Degradation

1.2.3.2.1 Chemical Bonding

The rate of degradation is determined primarily by the type of functionality present in the backbone.[80] Generally PAs and poly(ortho ester)s are more reactive towards hydrolysis with half lives of 0.1 h and 4 h, respectively, poly(ester)s degrade more slowly with a half life of 3.3 yr.[81, 82] These figures are variable with the chemical environment surrounding labile bonds for example the degradation of PLA is relatively slow due to sterics as the methyl group impedes hydrolysis.[51]

1.2.3.2.2 Water Uptake

Hydrophilic polymers are able to adsorb large quantities of water, thereby increasing water concentration and in turn the degradation rate. In comparison, hydrophobic polymers for which water uptake is minimal, display degradation rates which are much slower.[83, 84]

1.2.3.2.3 The Effect of Copolymer Composition

Copolymerization affects the rate of degradation in two ways; the first is that copolymerization influences polymer morphology. A homopolymer or a polymer composed mainly of one type of monomer is likely to be semicrystalline and it is well established that the rate of degradation of semi-crystalline polymers is slower than that of completely amorphous polymers.[78] The other way is that the rate of hydrolysis for ester linkages are not the same; hydrolytic studies of PLGA of various compositions showed that by increasing the PGA content the rate of hydrolysis also increased.[85] There are several explanations for the faster hydrolysis rate; glycolide repeating units are more hydrophilic than lactide units thus increases water uptake, and encourages dissolution of higher molecular weight glycolide oligomers.[85]

1.2.3.2.4 The Effect of pH

The hydrolysis of ester linkages can either be acid or base catalysed. The degradation of PLA and PLGA sutures were reported in terms of retained tensile strength it was found that the degradation of PLGA sutures was greatest at both pH 5 and 10 whilst for PLA degradation was higher in an alkaline environment.[86] Degradation rates were high at low

pH due to autocatalysis; the acidic carboxylic acid end groups generated accelerate hydrolysis by lowering pH.[87] Hydrolysis of PAs is also catalysed by acid or base but increases with an increase in pH, the rate of degradation of poly(bis-(*p*-carboxyphenoxy)propane anhydride), for example, increases 10 fold by increasing the pH from 7.4 to 10.[83]

1.2.4 Biomedical Applications

1.2.4.1 Tissue Engineering

Tissue engineering (TE) is a relatively new interdisciplinary field bringing together cell biology, materials science, reactor engineering and clinical research to construct new tissues and organs.[88] The creation of this field was prompted by the donor shortage situation in the United States where only a tenth of patients waiting on a liver transplant proceed to surgery.[89] The scope of TE is vast; the ability to restore and improve tissue function has huge therapeutic potential in diseases synonymous with aging and lifestyle such as diabetes, heart disease and osteoarthritis.[90]

The concept of TE is based on the ability of cells to form tissues and, if cultured in three dimensions, ultimately organs.[88, 91] Tissue regenerated from patient cells has the advantage that it is free of immune rejection and unfavourable immune response.[92] Most tissues are composed of cells and extracellular matrix (ECM), hence any tissue lost through damage or disease will result in the loss of the ECM.[92] TE involves the incorporation of cells into a three dimensional framework i.e. a scaffold. These scaffolds provide a substrate for cells to attach, proliferate, differentiate and subsequently form the ECM.[65, 92] The physical and chemical properties of the scaffold help create a favourable environment for tissue formation.[88] A wide range of materials have been investigated for use as a scaffold e.g. ceramics and metals, but it is the chemical and mechanical properties of polymeric material which have been shown to closely resemble that of most biological tissues.[88, 93]

Synthetic polymers have been investigated as possible scaffolds as their properties can be tailored to match that of the biological tissue in terms.[88, 94] It is essential that scaffolds be biodegradable to avoid disrupting tissue regeneration or provoking a foreign body reaction.[92] The rate of tissue regeneration should correspond to the rate at which the scaffold degrades.[92] It is essential that a polymeric scaffold be permeable, cell adhesive and porous with pore sizes that match the candidate cells for the scaffold to be effective.[65] Polyesters; PLA, PGA and PCL and copolymers, are widely used in tissue engineering,

however, their shortcoming is the hydrophobicity of the polymer backbone which can lead to a lack of cellular attachment and interaction.[88, 95-97] Other biodegradable polymers which have been investigated for use in TE include poly(carbonate)s, poly(orthoester)s and poly(phosphagene).[98] Stevens and Howdle have both made significant contributions to the area, creating scaffolds composed of polymeric and inorganic material and composites of both.[99-101] Howdle *et al*. has published a lot of work on the use of supercritical carbon dioxide to create porous polymeric scaffolds these foams have been studied for gene therapy and the regeneration of cartilage tissue.[99, 102] Stevens *et al*. reported the use of hydrogel scaffolds that incorporates growth factors for cartilage TE and developed functionalised poly(glutamic acid) fibrous scaffolds with potential TE applications.[103, 104]

1.2.4.2 Controlled Drug Delivery

Drugs have been traditionally and more commonly been administered orally or intravenously as a single dose. The disadvantages of this are that the drug is administered at a close to toxic concentration causing side effects, poor absorption, repetitive administration and the potential for overdose. The therapeutic effect of drugs is only achieved by administered and maintaining a long term drug concentration.[105] Controlled drug delivery devices were developed to change the release of the drug in the body in order to eliminate possible under- and over-dosing, reduce dosages, provide site specific delivery and reduce drug side effects. The challenges faced by these systems is finding a suitable delivery system which is biocompatible, generates non-toxic metabolites, mechanically strong, capable of loading high amounts of drugs and provide site specific delivery.[106] Drug delivery devices based on polymeric material meet the majority of these requirements.[106]

The strategy is for the drug to be released by the pH triggered hydrolysis of nanoparticles or a degradable polymer matrix as material is lost by erosion, or by dissolution or diffusion of the drug.[105] Biodegradable polymers are preferred because these polymers and their metabolites are biocompatible and bioresorbable and there is no need for a second surgery.[105] The rate of degradation and type of erosion of these devices is important because it ultimately controls the rate of drug delivery and is a factor considered for the type of therapy and duration of release.[105, 107] Polyesters, poly(ortho-ester)s and PAs have all been studied as a potential drug delivery matrix.[49, 105]

1.2.4.3 Orthopaedic Applications

In the field of orthopaedics, biodegradable polymers have been utilised to construct fracture fixation devices; screws, pins, staples, clips and suture anchors.[108] It is believed that biodegradable polymers will eventually replace the use of metallic implant.[65] In 2011 Johnson & Johnson recalled the DePuy ASR hip implant after patients reported adverse effects arising from metal poisoning which required medical attention and in some cases corrective surgery.[109] The benefits of this are that a second surgery to remove the implant which poses a degree of risk to the patient is no longer required and it avoids corrosion.[65] The main problem with using metallic fixation devices is that the fractured bone has a greater tendency to re-fracture upon removal of the implant as the load is predominantly carried by the implant rather than the bone during the healing process.[68] This will, according to Wolff's law, result in a stress shielding effect which increases the potential for re-fracture.[108] The shielding stress effect does not occur with the use of biodegradable polymeric fixtures as the mechanical properties deteriorate during polymer degradation.[65, 108] The device can, therefore, only support a decreasing amount of stress thus allowing for the gradual transfer of load from the implant to the healing bone. Although advantageous these materials can induce an inflammatory response at the location of the implant through acidosis caused by polymeric degradation.[110, 111]

1.2.4.4 Other Biomedical uses

Biodegradable polymers have long been used as resorbable sutures, this was in fact one of the first applications of aliphatic polyesters for biomedical use. The success of these polymers as sutures was due to their rapid degradation and ability to be produced as strong filaments. The most widely resorbable sutures are all based on PGA and PLA copolymers. In addition specialty packaging composed of polymeric material has been utilised for the packaging of drugs and wound dressing as it acts as barrier against gas and liquid.

1.3 Reversible Addition-Fragmentation Chain Transfer (RAFT) Polymerization

1.3.1 History

Radical addition fragmentation has been used in organic chemistry since the early 1970's such as the Barton-McCombie deoxygenation process with xanthates.[112] This chemistry

was exploited in the late 1980's as a means of controlling polymerization reactions using addition fragmentation chain transfer agents including allyl sulphides,[113] allyl bromides,[114] vinyl ethers[113] and thioesters.[115] Polymerizations exhibiting living characteristics with the reversible addition fragmentation transfer were reported in 1995.[116, 117] Reversible addition-fragmentation chain transfer (RAFT) polymerization was first devised in 1998; reporting the first use of thiocarbonylthio RAFT agents mediated polymerization.[118] RAFT polymerization has become one of the most widely used polymerization techniques alongside nitroxide mediated polymerization (NMP) and atom transfer radical polymerization (ATRP).

The advantages of RAFT polymerization over other controlled radical polymerization techniques i.e. NMP and ATRP, is that it demonstrates compatibility with a wide range of polymers and reaction conditions as well as a high tolerance to functional monomers. RAFT polymerisation has been employed to access block copolymers, stars and other complex architecture. However there are several shortcomings; a particular RAFT agent is only suitable for a limited selection of monomers. The synthesis of RAFT agents is usually a multistep procedure with further purification steps which often leads to low product yields. Furthermore the C-S bond of the thiocarbony thio moiety is particularly labile and can therefore undergo several side reactions e.g. hydrolysis.

1.3.2 Mechanism

RAFT polymerization demonstrates living characteristics controlling the molecular weight and architecture through the suppression of termination processes by the reversible trapping of a propagating radical as a dormant species using a RAFT agent.[119] The general structure for a RAFT agent is given in **Figure 1-15**.

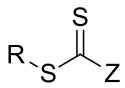

Figure 1-15. General structure of RAFT agent.

The mechanism of RAFT polymerization is given in **Figure 1-16**. The mechanism is similar to the conventional radical polymerization, however, the key feature of RAFT polymerization is the sequence of addition–fragmentation equilibria. During the reversible chain transfer step the addition of the propagating radical to the thiocarbonyl moiety of the

RAFT agent occurs to form an intermediate carbon centered radical.[120] The radical intermediate subsequently undergoes β-scission to either form the leaving group radical (R) or re-form the propagating radical.[120] The chain equilibrium step involves the reaction of propagating radical with the macroRAFT agent.[120] Rapid equilibrium between the propagating radicals (P_n and P_m) and the dormant macroRAFT agents allows for an equal probability for all chains to grow at equal rates thus leading to a controlled polymerization generating polymers with narrow polydispersities.[120] The rapid interchange in the addition-fragmentation steps (reversible chain transfer and chain equilibrium) maintains a low concentration of propagating radicals thus limiting termination reactions via combination and disproportionation.

Initiation

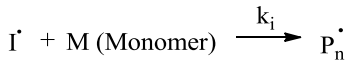

Reversible Chain Transfer

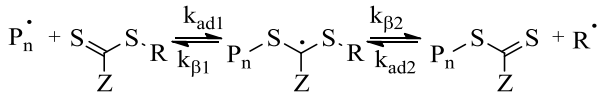

1 2 3

Reinitiation

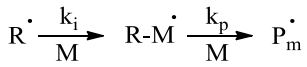

Chain equilibrium

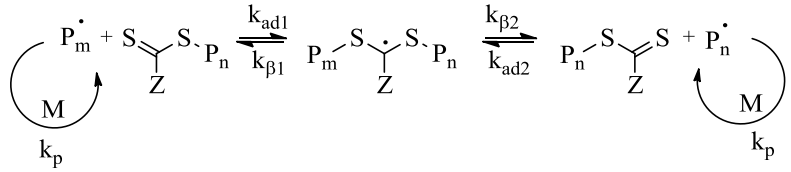

Termination via combination and disproportionation

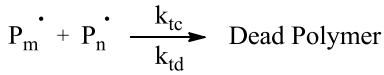

Figure 1-16. RAFT polymerization mechanism.[119]

1.3.2.1 Rate Transfer Constants

The efficacy of the RAFT polymerization is evaluated by the consumption of the RAFT agent and monomer which depends on two transfer coefficients, $C_{tr}=k_{tr}/k_p$ and $C_{-tr}=k_{tr}/k_i$ which describes the reactivity of both the propagating and expelled radical.[120, 121] The rate coefficient k_{tr} of a RAFT agent is given in **equation 1**, it is influenced by the rate of addition of the propagating radical (P_n) to the RAFT agent and a partition coefficient which gives the partitioning of the radical intermediate between the starting material i.e. the release of the propagating radical and products i.e. release of R radical leaving group.[121]

$$k_{tr} = k_{ad1}\frac{k_{\beta 1}}{k_{ad2} + k_{\beta 1}} \qquad (\mathbf{1})$$

The rate coefficient associated with the formation of the macroRAFT (**Figure 1-16**, **3**) agent is given by equation 2 where the leaving group radical is partitioned between reinitiating polymerization and addition to the macroRAFT agent.[121] Knowledge of these rate coefficients provides an understanding of the RAFT agent activity.

$$k_{-tr} = k_{\beta 2}\frac{k_{ad2}}{k_{ad2} + k_{\beta 1}} \qquad (\mathbf{2})$$

1.3.3 RAFT Agent

The choice of RAFT agent is significant to the success of the polymerization, a range of common RAFT agents are shown in **Figure 1-17**. For a successful polymerization there are several requirements of the RAFT agent; the thiocarbonyl moiety must be reactive enabling high rates of addition during the reversible chain transfer step (pre-equilibrium), the fragmentation of the radical intermediate should occur rapidly avoiding side reactions and should fragment in favour of product macroRAFT agent to expel the R radical which should subsequently reinitiate polymerization.[119] The efficacy of the RAFT agent depends on the properties of the R and Z groups which will influence the rate of addition, fragmentation and reinitiation.

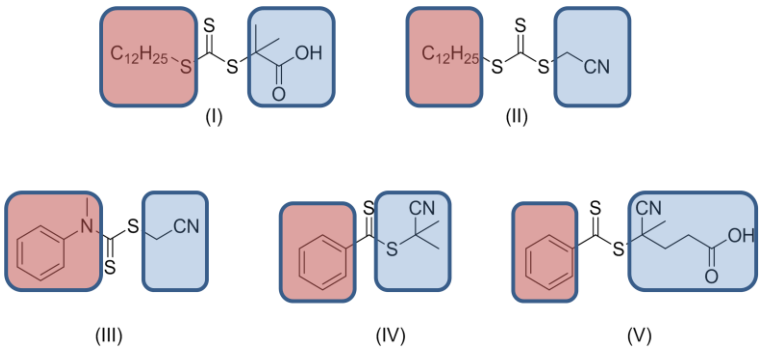

Figure 1-17. Selection of RAFT agents (I) 2-(dodecylthiocarbonothiolthio)-2-methylpropionic acid (DDMAT), (II) cyanomethyl dodecyl trithiocarbonate, (III) cyanomethyl methyl(phenyl)carbamodithioate, (IV) 2-cyanopropan-2-yl benzodithioate, (V) CPADB. Z groups (pink) and R groups (blue) are indicated.

The role of the R group is such that a balance is required between the leaving and reinitiating abilities. The triphenylmethyl radical for example is a good leaving group however is inadequate for reinitiating polymerization and would result in retardation of polymerization.[120] Factors which influence the efficiency of the R group include sterics, radical stability (conjugated systems) and polar effects.[119] Increased radical stability and steric bulk improves the leaving group capabilities favouring the fragmentation of R relative to the propagating species (P_n), however, this can impede the reinitiation of polymerization if R is too stable.[122] Electron withdrawing groups improves the fragmentation of R by increasing the electrophilicity of the resultant radical and also increases the rate of reinitiation due to its greater affinity for the electron rich vinyl moieties of the monomer.[122] It is suggested that R should be structurally similar to the monomer of the propagating radical, however, this is incorrect as the strain relieved on rehybridization of the active centre increases in the order tertiary > secondary > primary therefore the polymeric radicals are better leaving groups than monomeric radicals.[120] This was evidenced by the polymerization of methyl methacrylate with a RAFT agent (**Figure 1-18**) where R is 2-ethoxycarbonylpropyl which was shown to be a poor leaving group w.r.t to the methyl methacrylate propagating radical.[123]

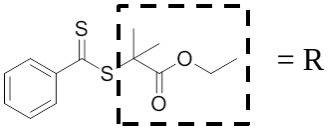

Figure 1-18. Structure of RAFT agent 2-(ethoxycarbonyl)prop-2-yl dithiobenzoate.

The Z group influences the reactivity of the thiocarbonyl bond towards radical addition by the propagating species and stability of the radical intermediate.[119] The Z group should impart minimal stability to the radical intermediate, enhanced stability can lead to side reactions can lead to polymerization retardation and inhibition.[122] The rate of addition is higher when Z=aryl, alkyl dithioesters and lower when z = O-alkyl xanthates.[120] The chain transfer coefficient generally follows the trend dithioesters>trithiocarbonates>dithiocarbonates (xanthates)>dithiocarbamates.[120] The low activity of *O*-alkyl xanthates and *N'N*-dialkyldithiocarbamates towards addition is explained w.r.t the zwitterionic canonical forms (**Figure 1-19**) as a result of the interaction between the lone pair on the O or N and the thiocarbonyl bond.[119] An electron withdrawing group on the Z group can enhance the activity of the xanthates/dithiocarbamates by making the lone pair on the O and N less available for delocalization.[120] The low activity of these RAFT agents makes them ideal for the polymerization of VAc and NVP where the propagating radical is a poor homolytic leaving group.[119] Electron withdrawing groups generally enhance the activity of the RAFT agent by increasing the electrophilicity of the thiocarbonyl bond and in turn the rate of addition e.g. ring substituted cyanisopropyldithiobenzoate.[120, 124]

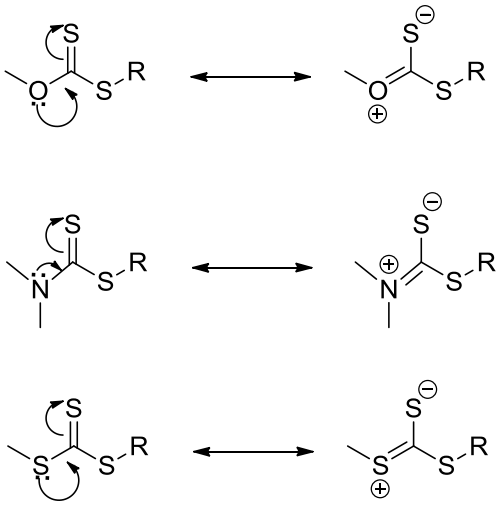

Figure 1-19. Canonical structures of xanthates, dithiocarbonates and trithiocarbonates.[119]

1.3.3.1 Cytotoxicity of RAFT Agents

The cytotoxicity of a selection of RAFT agents was evaluated due to the increasing utilization of RAFT polymerization for the generation of polymers for biomedical applications and availability of RAFT agents. Biocompatible polymers; P(OEG-A), P(OEG-MA) and P(HPMA) bearing either a trithiocarbonate or a dithiobenzoate RAFT

end group were studied on different cell lines.[125] The cells incubated with POEG based polymers after 24 h shows high cell viability of 99 % thus no cytotoxic effect was observed for CHO-K1 (hamster ovary) and NIH3T3(mouse embryonic fibroblast), however with respect to the murine macrophage cell line the cell viability was significantly lower for dithiobenzoate end-capped P(OEG-MA) and P(OEG-A) cell viability 73 % and 85 % respectively.[125] The trithiocarbonate showed little toxic effects with approximately 100 % cell viability observed. Long term incubation i.e. 3 days, was assessed for trithiocarbonate and dithiobenzoate end capped P(OEG-A), for each cell line cell viability either slightly decreased or remained the same as that observed after 24 h incubation.[125] The cytotoxicity studies of RAFT functionalized P(HPMA) showed dithiobenzoate endcapped P(HPMA) were highly toxic to all cell lines - it was suggested that the hydroxylpropylmethacrylamide side groups interact with the dithiobenzoate RAFT group or residual impurities in the RAFT agent leading to this toxic effect.[125] Upon removal of the RAFT end group the cell viability was reported to be 100 %, in addition all cell lines were viable upon reducing the concentration of dithiobenzoate end capped PHPMA.[125] The cytotoxicity study showed that the toxicity is influenced by both the chosen RAFT agent and the class of polymer. Cytotoxicity of RAFT also varies amongst different cell types therefore each potential polymer for biomedical applications should be assessed and trends cannot be derived between the polymer and toxicity.

1.3.4 Synthesis of Diblock Copolymers by RAFT Polymerization and other Polymerization Techniques

The combination of RAFT polymerization with other polymerization techniques e.g. ROP and ATRP, has enabled the synthesis of a range of block copolymers with advantageous properties. There are several reported strategies for the synthesis of block copolymers composed of RAFT and non-RAFT polymers (**Figure 1-20**). Non RAFT polymers are generally polyesters, PDMS and PEO. The most widely used approach is to covalently attach a RAFT agent to a pre-formed functionalised polymer via either the R or the Z group and using the resultant polymer as a macroRAFT agent (**Figure 1-20 strategy 1**). RAFT agents or RAFT formed polymers may possess the functionality to initiate other polymerization techniques such as ROP generating the macroRAFT agent (**Figure 1-20 – strategy 4**) and block copolymer (**Figure 1-20**, **strategy 3**). The least common pathways involve the conjunction of two preformed polymers with functionalities complementary to

each other (**Figure 1-20**, **strategy 2**) and a one pot synthesis for the block copolymer where RAFT and non-RAFT polymerization occur concurrently (**Figure 1-20**, **strategy 5**).

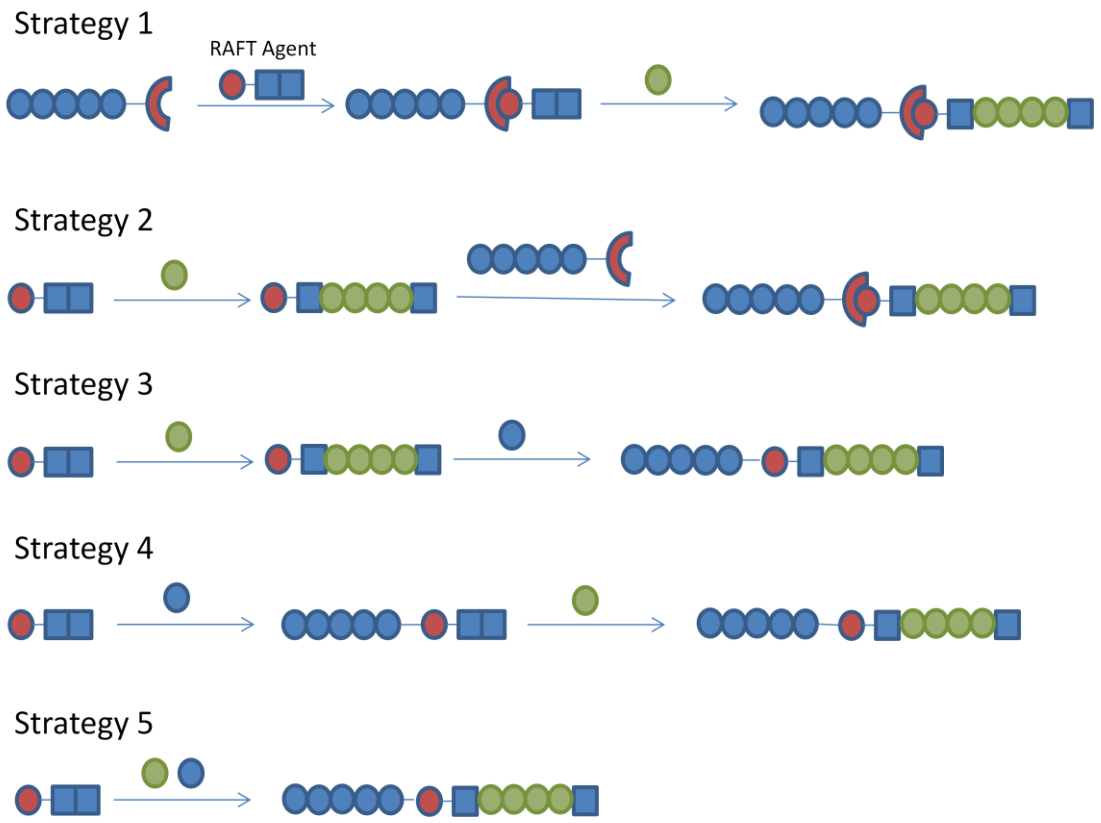

Figure 1-20. Range of strategies employed for block copolymer synthesis combining a RAFT polymer (green sphere) with a non-RAFT polymer (blue spheres).[126]

1.3.4.1 RAFT Functionalization of Non-RAFT Polymer followed by RAFT Polymerization

Strategy 1 (**Figure 1-20**) is the most frequently used route for combining RAFT and non-RAFT polymers together. The RAFT agent can be covalently attached to the preformed polymer via the R group or the Z group. Generally this involves the derivatization of functional end groups of the preformed polymer by esterification, amination or nucleophilic substitution. The hydroxyl end groups of PLA and PCl are often coupled to RAFT agents with carboxyl moieties e.g. CPADB and DDMAT, via dicyclohexylcarbodiimide (DCC) mediated esterification to generate the macroRAFT agent which is subsequently chain extended.[127-129] Barz *et al*. reported the synthesis of PLA-poly(pentafluorophenyl methacrylate) (PFMA), the PFMA acted as an activated ester precursor which was reacted with 2-hydroxypropylamine to form PLA-PHMPA, the cellular uptake of the amphiphilic block copolymer was studied.[127] The macroRAFT agent was formed by esterification of the terminal hydroxyl with CPADB (**Figure 1-21**), ^{1}H NMR spectroscopic analysis showed 69% functionalization of PLA was achieved.[127] PCl-

macroRAFT agent was prepared following an analogous methodology gaining near 100% functionalization, the polymer was subsequently chain extended by DEA giving a PDI range of 1.20-1.43.[129] PEO based macroRAFT agents have also been synthesized by esterification with a RAFT agent.[130-132] Ester bonds are, however, more susceptible to nucleophilic attack and thus in cases stable amide linkages are preferred. The amination of amino terminated PEO with the carboxyl moiety of 4-cyano-4-(ethylsulfanylthiocarbonyl)sulfanylpentanoic acid provided a PEO-macroRAFT agent demonstrating 94 % efficient end capping by ^{1}H NMR spectroscopy.[133] The macroRAFT agent was utilised to synthesize the triblock copolymer PEO-PAPMA-PNIPAM a potential drug carrier with a PDI of 1.21. [133]

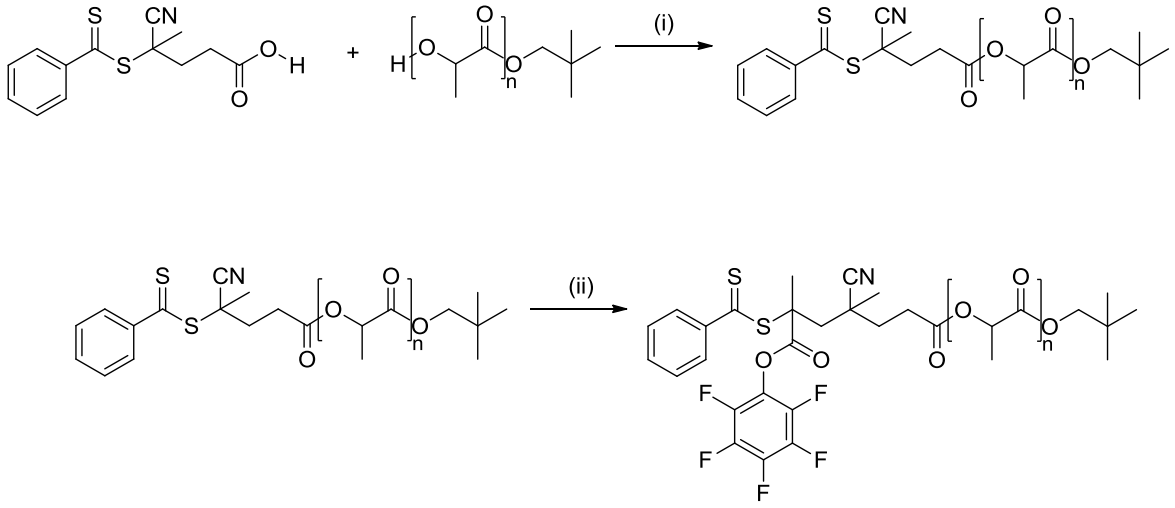

Figure 1-21. Synthesis of PLA-PFMA; (i) dicyclohexylcarbodiimide (DCC)/4-(dimethylamino)-pyridine (DMAP), DCM, (ii) 4,4′-Azobis(4-cyanovaleric acid (ACVA), PFMA, dioxane, 80 ^{o}C.

Synthesis of xanthate based macroRAFT agents involves a halogen substitution. PCl macroRAFT agent was synthesized by transforming the hydroxyl terminated PCl into 2-bromopropionyl end capped PCl via a nucleophilic substitution which was further reacted with potassium *O*-ethyl dithiocarbonate.[134] The PCl-macroRAFT agent was shown to effectively control the polymerization of *N*-vinylpyrrolidone.[134] PDMS and PEG xanthate macroRAFT agents have been reported following an analogous procedure.[135, 136] ATRP polymers and RAFT copolymers can be combined using this strategy. The synthesis of p(*t*-butyl acrylate)-p(vinyl acetate) was reported converting the terminal bromine of the *t*-butyl acrylate macroinitiator into a xanthate based macroRAFT agent which was subsequently chain extended.[137] This approach was required as the chosen RAFT agent does not exert the same control over the polymerization of both monomers.[137]

1.3.4.2 RAFT agent utilised as an Initiator for non RAFT polymerization followed by RAFT polymerization

Strategy two (**Figure 1-22**) produces block copolymers by using the RAFT agent to initiate the non-RAFT polymerization to form the macroRAFT agent. This pathway focuses on the dual initiator (2-benzylsulfanylthiocarbonylsulfanyl)ethanol (BSTSE) as the RAFT agent Z group possesses a hydroxyl functionality. Hale *et al*. reported a two step synthesis in which BSTSE initiates the ROP of lactide the resulting macroRAFT agent was subsequently chain extended by NIPAM. The initiator demonstrated little control over the polymerization with a broad PDI=2-2.2, these polymerizations have since been repeated reporting narrower PDIs.[138] Poly(lactic acid-co-glycolic acid)-co-poly(ethyleneglycolmethacrylate) was synthesized as shown by in **Figure 1-22** as a potential drug carrier using BSTSE, similar results were reported presenting mono-modal curves however broad polydispersities were observed with a PDI range of 1.4-1.8.[139] Ting *et al*. reported the synthesis of poly(lactide)-block-poly(6-*O*-acryloyl-*R*-d-galactopyranose) following an analogous procedure with low polydispersities.[140] These polymers were cross-linked followed by the removal of the core by degradation of PLA using hexylamine resulting in the formation of hollow nanocages.[140]

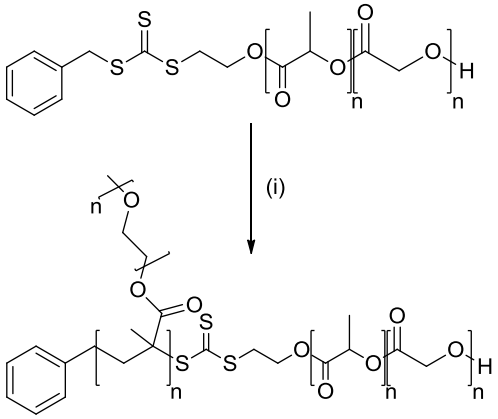

Figure 1-22. Synthesis of PLGA–PEGMA block copolymer; (i)EGMA, AIBN, THF, 80^{o}c.

1.3.4.3 Polymer prepared by RAFT Polymerization initiates Non –RAFT Polymerization

Strategy three (**Figure 1-20**) involves the initiation of a non RAFT polymerization using a functionalised polymer prepared by RAFT polymerization; this technique is rarely used for block copolymer synthesis but for more complex architectures. Barner-Kowollik reported the RAFT polymerization of styrene using RAFT agent dibenzyltrithiocarbonate and the subsequent conversion of the trithiocarbonate moiety within the polymer chain into terminal hydroxyl end groups thus effectively halving the M_n of the polymer (**Figure 1-23**).[141] The resultant hydroxyl terminated polystyrene (PS) initiates ROP of caprolactone.

The polydispersity of sulphur free polymers generated via this method were shown to be well-defined with PDI range of 1.1-1.3.[141] Similarly PS and polyethylene derived from dibenzyltrithiocarbonate mediated RAFT polymerization can be converted into thiol functionalised polymers via the reduction of the central trithiocarbonate moiety by aminolysis.[142] The styrylmercaptan initiated ROP of lactide produces broad polydisperse polymers (PDI=1.38-1.6).[142] Polymers prepared by dithioester mediated RAFT polymerization have the potential to initiate non-RAFT polymerization following several end group transformations. Dithioester moieties have been shown to be converted into hydroxyl groups via a hydroperoxide polymer which can be employed as an initiator for ROP.[143] RAFT agents have been synthesized in which the R group possesses a hydroxyl moiety; 2-[*N*-(2-hydroxyethyl)-carbamoyl]prop-2-yl dithiobenzoate (HECPD), however, this RAFT agent is not often used due to the low yields in which it is obtained. Akimoto *et al*. utilised HECPD to polymerize lactide subsequent to the RAFT polymerization of NIPAM and DMAAm.[144] The dithiobenzoate end group was reduced to form a thiol which reacted with maleimide - the resulting polymers were shown to self-assemble to form micelles and their degradation and drug encapsulation studied.[144]

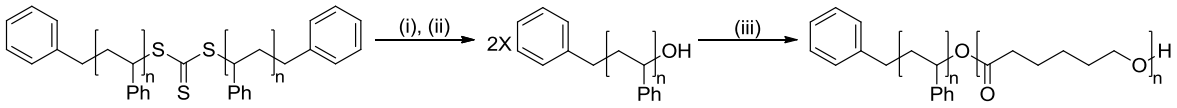

Figure 1-23. Synthesis of PS-PCl; (i)AIBN, triphenylphosphine, THF, 60 ^{o}C, (ii)caprolactone, 1, 5, 7 triazabicyclo[4, 4, 0]dec-5-ene, toluene.

1.3.4.4 Reaction between Complimentary Moieties on a RAFT and Non-RAFT polymer

RAFT and non-RAFT polymers have been combined by a hetero Diels-Alder. Barner-Kowollik *et al*. reported a [4+2] cycloaddition of a diene terminated PCL with the Z group of a dithioester terminated PS (**Figure 1-24**).[145] Electron deficient Z groups of the RAFT agent were phosphoryl and pyridyl moieties which are known to make excellent heterodienophiles. The [4+2] cycloaddition reactions were successful showing complete conversion.[145]

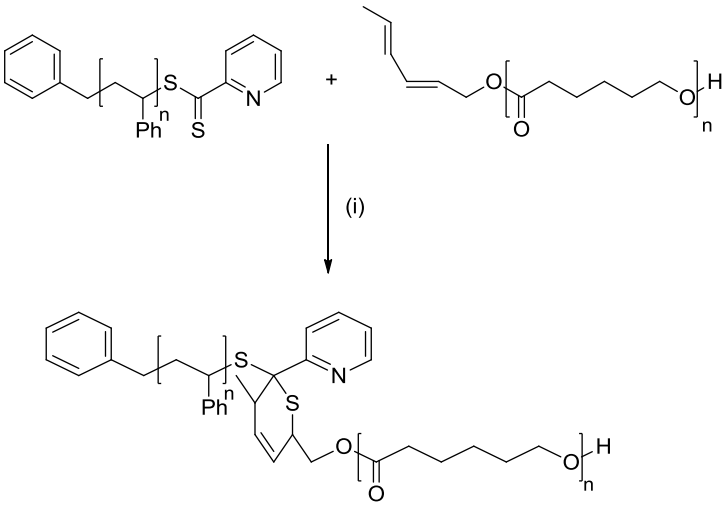

Figure 1-24. Hetero Diels-Alder cycloaddition of PS with PCl; (i) TFA, 50 ^{o}C.

1.3.4.5 Simultaneous Polymerization

A one pot synthesis of PS-PCl was reported in supercritical CO_2 using the dual headed initiator BSTSE which simultaneously initiates the ROP of caprolactone and RAFT polymerization of PS (**Figure 1-25**).[146] The PDI of the polymers generated were relatively high ranging from 1.5-2.1 which was attributed to the uncontrolled enzymatic catalysed polymerization of caprolactone.[146]

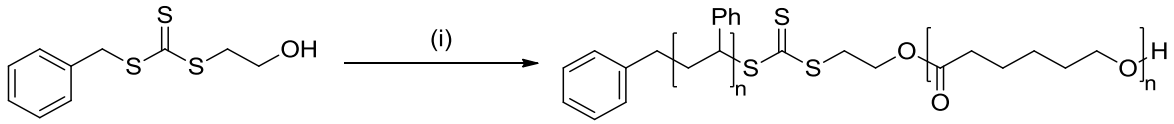

Figure 1-25. Synthesis of PS-PCl. (i) Novozym-435, caprolactone, AIBN, styrene, supercritical CO_2.

1.3.5 Triblock Copolymers

ABA and BAB type triblock copolymers based on poly(dimethylsiloxane) (PDMS), poly(ethylene glycol) (PEG), poly(ethylene oxide) (PEO) and PCl generating both ABA and BAB type triblock copolymers have been prepared and evaluated for biomedical applications e.g. drug delivery. The synthesis of the macroRAFT agents generally involves the esterification of the preformed polymer with the carboxyl moiety of a RAFT agent.

Zhu *et al*. reported the synthesis of PCl-poly(dimethylaminoethyl methacrylate)$_2$(PDMAEMA) and application for the co-delivery of siRNA and Paclitaxel

drug.[147] PCl is often utilised as the hydrophobic component of amphiphilic block copolymers due its biodegradability and biocompatibility. Di-hydroxypolycaprolactone was synthesized via the ROP utilising ethylene glycol and subsequently coupled to a 4-cyanopentanoicacid dithionaphthalenoate.[147] These nanoparticles have been shown to effectively bind with siRNA and deliver the drug into cancer cells with increased cellular uptake with low cytotoxicity.[147]

Amphiphilic triblock copolymers have often been used to form amphiphilic conetworks (APCN). APCN's are novel materials where hydrophobic and hydrophilic regions are interconnected in a 3D structure which can be applied to drug delivery and tissue engineering. Achilleos *et al*. synthesized a range of well defined BAB block copolymers (PDI = 1.15-1.16) by the chain extension of PEG terminated by two 4-cyanopentanoicacid dithiobenzoate RAFT agents with styrene, methyl methacrylate and butyl acrylate with the inclusion of a cross-linker.[148] An APCN was synthesized using PDMS end capped by DDMAT chain extended by *N*,*N*-dimethyl acrylamide and allyl methacrylate which was cross-linked by hydrosilation.[149] Hydrogels based on PEO-P(NIPAM)$_2$were reported using xanthate mediated RAFT polymerization, the macroRAFT agent was prepared by esterification and an atom transfer radical reaction giving 31 % yield.[150] P(NIPAM) hydrogels can exhibit volume phase transitions in response to temperature alterations due to its LCST in water (32 ^{o}C).[150] Amphiphilic triblock copolymer with the PEG segment was to increase the diffusion of water and investigate the reswelling and deswelling of the hydrogel.[150]

Triblock copolymers have also been synthesized using xanthate end capped PEO macroRAFT agents. The functionalization of the PEO is a five step synthesis via series of end group derivatisations forming a dialdehyde intermediate affording a 50 % yield of the macroRAFT agent.[151] The macroRAFT agent was shown to effectively mediate the RAFT polymerization of poly(vinyl acetate) giving a PDI range of 1.21-1.23.[151] Alternatively PEO-macroRAFT agent has been synthesized via a two step reaction involving a halogen intermediate with higher product yields reported (>70 %).[135]

Another synthetic methodology for triblock copolymers is the use of a RAFT agent which can initiate polymerization from both the Z and R group. ROP of caprolactone was initiated using the two carboxyl moieties of the RAFT agent 2-(2-arboxyethylsulfanylthiocarbonylsulfanyl)propionic acid using an aluminium catalyst to generate well defined polymers (**Figure 1-26**).[152] The RAFT polymerization of NIPAM using the PCL macroRAFT agent gave polymers with broad PDI's of 1.38-1.71.[152] The

polymers formed micelle structure with diameters of 100 nm and have demonstrated thermosensitive drug release behaviour.[152]

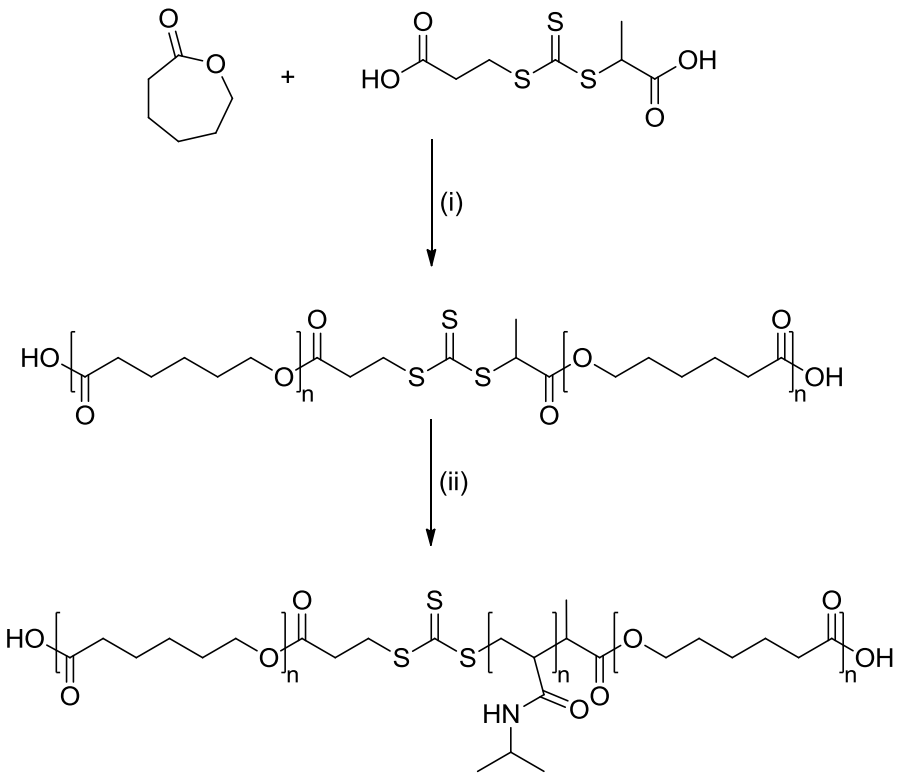

Figure 1-26. Synthesis of triblock copolymer PCL(PNIPAM)$_2$; (i) Al ($OCH(CH_3)_2)_3$, 120 ^oC, (ii) AIBN, NIPAM, THF, 70 ^oC.

1.4 Self-Assembly of Amphiphilic Block Copolymers

The development of controlled polymerization techniques has led to the synthesis of a range of polymer architectures e.g. linear amphiphilic block copolymers, graft copolymers and star-like polymers. Of these it is the self-assembly of linear block copolymers that is the most researched due to the wide range of potential applications. The self-assembly of block copolymers in solution has generated various morphologies; micelles, cylindrical micelles, lamellae and vesicles. The self-assembly of systems such as PS-PAA and PS-PEO have been extensively studied.[153-156]

1.4.1 Aggregate Preparation Techniques.

It is well know that micellization occurs in dilute solution at a concentration above the critical aggregate concentration.[157] The two main techniques used for the self-assembly of block copolymers are by the solvent switch method and direct dissolution.[157] The solvent

switch method involves the initial dissolution of the polymer in a common solvent, self-assembly is induced by varying conditions such as temperature or solvent composition.[157] The latter is more commonly referred to as the solvent switch method in which a precipitant is added for one of the blocks. The common solvent is subsequently removed by evaporation or dialysis.[157] Dialysis is often employed due to its compatibility with a wider range of water miscible solvents. The method of preparation has been shown to have a morphogenic effect on the self-assembled structures.[153, 158]

Other methods include film rehydration which is employed to target vesicle formation.[159] The block copolymer is dissolved in a common solvent, the solvent is allowed to evaporate to form a film.[160] The polymeric film is rehydrated in aqueous media aided by heat or sonification.[160] Electroformation invented by Angelova and Dimitrov, involves the formation of a polymeric film on the surface of an electrode e.g. platinum wire or indium tin oxide, the polymeric film is rehydrated in the presence of an electric field to induce self-assembly.[158, 159, 161, 162] Giant vesicles (2 to 10 μm) have been generated using both procedures.[158, 163] Microfluidics is also used to produce vesicles by preparing double emulsions in a glass microcapillary device; this method gives great control over the size of vesicles formed unlike the methods described above.[164]

1.4.2 Self-Assembled Structures

1.4.2.1 Micelles

Micelles are typically sized between 10-100nm and classified as either being regular or reverse.[155, 165] Block copolymers self assembled in aqueous medium form regular micelles which possess a hydrophobic core and hydrophilic corona.[155] In organic solvents reverse micelles are formed; as the solvent is now selective for the hydrophobic segment the blocks reverse i.e. the hydrophilic block forms the core.[155]

Regular and reverse micelles can be further divided into two types depending on the hydrophilic:hydrophobic composition of the block copolymer; star and crew-cut micelles.[155] Star micelles form by the association of block copolymers composed of a larger hydrophilic segment whereas micelles which possess a significantly larger hydrophobic block exist as crew-cut micelles.[155] Crew cut micelles have been prepared from the highly asymmetric PS_{500}-poly(acrylic acid)$_{58}$.[155]

Preparative techniques differ for the preparation of these two type of micelles. Star micelles are formed by direct dissolution of the block copolymer in a solvent selective for

the larger hydrophilic block.[155] Direct dissolution is not suitable for the formation of crew cut micelles due to the presence of the larger hydrophobic block which would result precipitate as opposed to aggregation.[155] Crew cut micelles are prepared by adding a precipitant for the larger block to a solution of the polymer dissolved in a common solvent to induce self-assembly.[155]

1.4.2.2 Rods/Worm-like Micelles

Rods/worm-like micelles possess a cylindrical core surrounded by the corona, the diameter of these structures are similar to that of micelles (*ca.* 30nm) however the length of these aggregates can vary significantly.[159] It is the flexibility of these aggregates which differentiates stiff rods from worm-like micelles.[166] Rods/worm-like micelles form by the growth of micelles along an axis, at either end of the cylindrical structure a hemispherical cap is present reducing unfavourable interactions between the core and solvent.[166] Cylindrical micelles of dodecylpyridinium bromide have been shown to solubilise hydrophobic dyes and more effectively than spherical micelles of dodecylpyridinium bromide.[167]

1.4.2.3 Polymersomes

Polymersomes are a class of vesicles formed by the self-assembly of amphiphilic block copolymers. Vesicles are hollow spheres composed of a hydrophobic wall with an internal external hydrophilic corona and contain a pool of the dispersing medium in their interior. Polymersomes have received a lot of attention due to their potential for biomedical applications, the aqueous core allows for the encapsulation and delivery of hydrophilic drugs and DNA whilst the membrane can be loaded with hydrophobic drugs. The aggregates form via a two step process; first a bilayer is formed followed by its closure.[168] Vesicles are formed preferentially due to their higher thermodynamic stability.[159] The two techniques typically used to target vesicle morphology are the solvent switching and polymer rehydration.[169] Vesicle formation is also influenced by polymer concentration and choice of common solvent.[153, 159] The size and membrane thickness have been shown to be dependent on method of preparation and molecular weight of the polymer.[156, 170]

1.5 Summary

Progress in controlled polymerization techniques has allowed for the preparation of an array of amphiphilic block copolymers. The strategies discussed in section **1.3.4**, have enabled us to develop methods to synthesize PLA-PMPC block copolymers which are of biomedical interest by a combination of ROP and RAFT techniques. These block copolymers have been previously synthesized by a combination of ROP and ATRP however the use of a copper catalyst would lead to metallic contamination.

Many triblock copolymers based on PDMS, PCl and PEO have been prepared and evaluated for biomedical application. ABA triblocks where B=PLA has not to our knowledge been reported therefore PMPC triblock copolymers will be synthesized and their self-assembly studied in addition to the diblock copolymers which has yet to be reported.

2. Synthesis of Poly(lactide) MacroRAFT Agents For the Synthesis of PLA-PMPC Block Copolymers

2.1 Introduction

To synthesize PLA-*b*-PMPC block copolymers two polymerization techniques are combined; ROP and controlled radical polymerization. The solubility of PMPC is limited to alcohols and aqueous solutions which are incompatible with ROP therefore, the ROP of lactide must precede the polymerization of MPC. PLA-*b*-PMPC has been previously synthesized by combining ROP and ATRP but the combination of ROP and RAFT has not, to the best of our knowledge, been reported.[42] There are two strategies for preparing a PLA-macroRAFT; utilization of a dual headed initiator and post polymerization modification (**Figure 2-1**).[42, 127, 171]

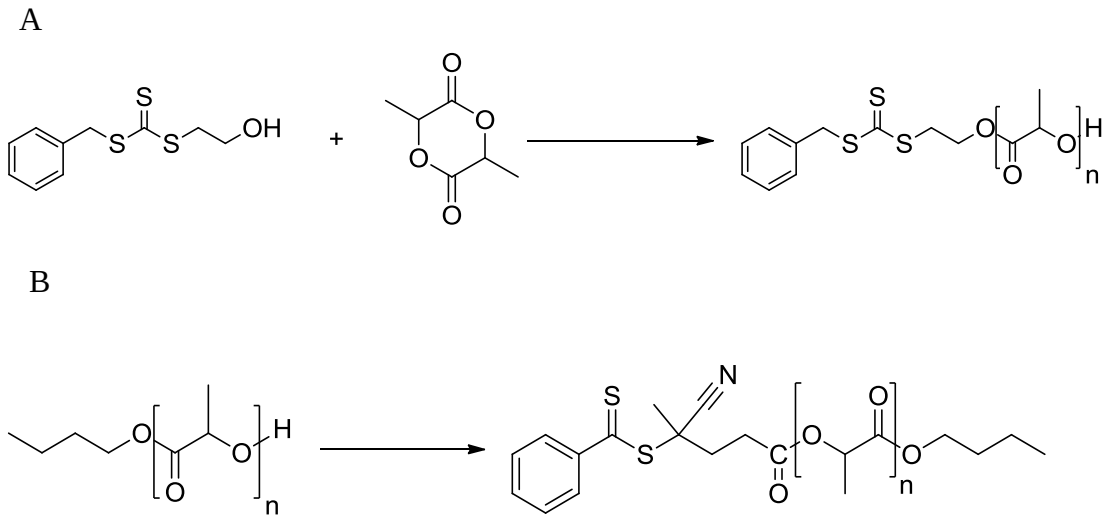

Figure 2-1. Proposed synthesis of PLA-macroRAFT agents via A) a dual headed initiator method and B) post polymerization modification.

2.2 Synthesis of MacroRAFT agent via a Dual Headed Initiator

2.2.1 Synthesis of 2-(Benzylsulfanylthiocarbonylsulfanyl)ethanol (BSTSE)

Dual headed initiators have been utilised for the synthesis of PLA based block copolymers, 2-(Benzylsulfanylthiocarbonylsulfanyl)ethanol (BSTSE) has been to shown to ROP lactide effectively and the resulting macroRAFT agent utilised for the RAFT polymerization of methacrylates. BSTSE-PLA could, therefore, be used to polymerize MPC generating the target block copolymer. BSTSE was first reported by Hale *et al*. who applied it to the synthesis of PLA-*b*-PNIPAM.[138] The trithiocarbonate dual headed initiator BSTSE was prepared using a literature procedure reported by O'Reilly *et al*..[172] This methodology was preferred as this RAFT agent was generated in high yields (>99%) under mild reaction conditions with a less extensive purification procedure (**Figure 2-2**). BSTSE was synthesized by reacting the thiolate formed upon selective deprotonation of the thiol, with carbon disulphide (**Figure 2-2**). The resulting anion reacted via nucleophilic substitution with benzyl bromide to generate the trithiocarbonate RAFT agent (**Figure 2-2**). The reaction was monitored using thin layer chromatography and the RAFT agent was obtained at 90% yield.

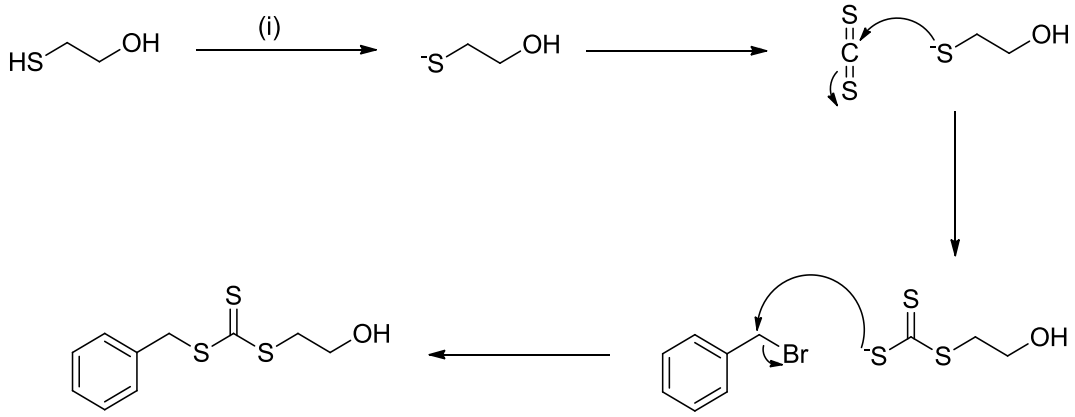

Figure 2-2. Synthesis of BSTSE RAFT agent; (i) potassium phosphate tribasic (1.0 eq.), acetone, RT, 35 min.

2.3 Synthesis of PLA-macroRAFT Agent

2.3.1 Tin Octanoate Catalyzed ROP of Lactide

Tin (II) octanoate was chosen to catalyze the ROP of lactide. It is reported to be a highly effective catalyst which generates high molecular weight polymers and demonstrates a

high catalytic activity.[173] The polymerization of lactide proceeds via coordination-insertion which is shown in **Figure 2-3**. The polymerization is initiated by a metal alkoxide formed upon reacting the catalyst with an alcohol.

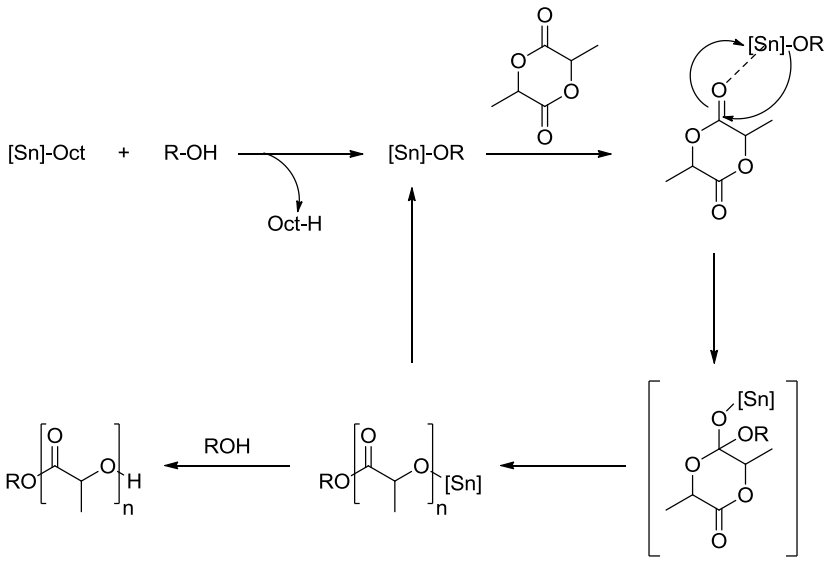

Figure 2-3. Mechanism for tin octanoate catalyzed polymerization of lactide.[174]

The PLA-macroRAFT agent lactide with a target of DP 50 was synthesized by ROP of which was catalysed by tin octanoate and initiated by BSTSE (**Figure 2-4**). The polymerization reached 90 % conversion after 12 h. The DP of the crude polymer was 67±10% determined by the ^{1}H NMR spectrum and the end group ratio 2:3:2 was observed which was in keeping with that expected. Errors associated with determining the DP of the polymer arise from processing the ^{1}H spectrum such as phasing, setting integral limits and using a baseline correction. The theoretical ratio of integrals for end group signals $i_A/i_{B+C}/i_D$ should be 2:3:2 which corresponds to the ratio of the benzyl methylene signal (A):RAFT end group methylene signal (B) and PLA methylene signal (C): RAFT end group methylene signal (D) (**Figure 2-4, 2-5**). The DP of the polymer purified by precipitating into methanol increased to 75 and the end group ratio deviated from the target as shown in **Figure 2-5**. GPC analysis gave M_n=5,900 gmol^{-1} (theoretical M_n=5600 gmol^{-1}) and the PDI=1.35. The changes observed in the ^{1}H NMR spectrum post precipitation suggest that the RAFT end group may have cleaved either pre- or post purification. Based on these results alternative catalysts for the ROP of lactide were investigated. Furthermore the concentration of tin present post purification (1000-2000 ppm) would exceed the concentration of tin in commercially used medical polymers (20-50 ppm) and therefore the polymer could not be used for biomedical applications.[175]

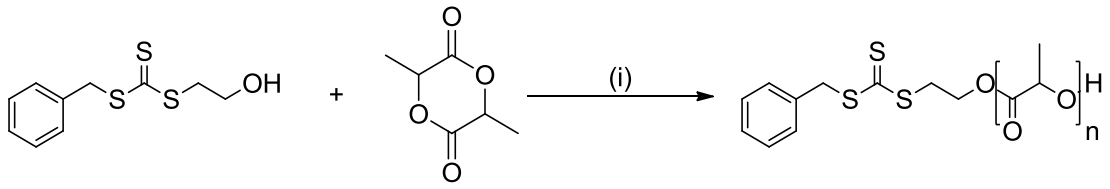

Figure 2-4. Tin octanoate catalyzed ROP of lactide. (i) tin octanoate (0.025 eq.), toluene, 110 ^{o}C, 24 h.

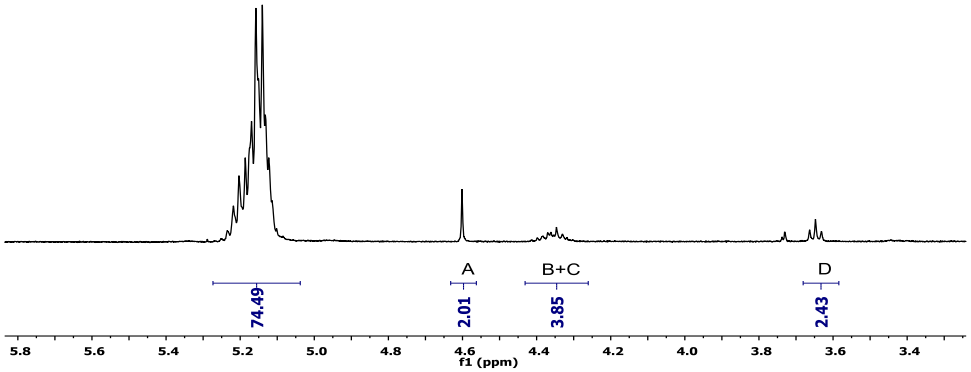

Figure 2-5. ^{1}H NMR spectrum (400 MHz, $CDCl_3$) of R-PLA_{50}-OH prepared by tin octanoate catalysed ROP.

2.3.2 Organocatalysts

Organocatalysts have been widely used for the preparation of polyesters.[176] The tertiary amine 1, 8-diazabicyclo[5.4.0]undec-7-ene (DBU) was chosen as an alternative to tin octanoate as it is highly active towards the ROP of lactide, generates well-controlled polymers (PDI<1.1) at a faster rate, under mild conditions and without metallic contamination.[177] DBU is a weak base with a pKa_H of ~12 so will not full deprotonate the alcohol(pKa ~15). The mechanism by which the base catalyses the polymerization is depicted in **Figure 2-6** - the base activates both the alcohol initiator and the chain end via hydrogen bonding.[174] Hydrogen bonding enhances the nucleophilicity of the alcohol by attracting the proton via the nitrogen lone pair which results in an increase in the partial positive charge on the proton and the negative charge on oxygen. The enhanced nucleophilicity of the initiating and propagating hydroxyl moieties facilitating the nucleophilic attack on the monomer.[174] DBU has previously been reported to catalyze the ROP of lactide with BSTSE as an initiator in DCM at room temperature to generate well-defined polymers (PDI 1.15).[177]

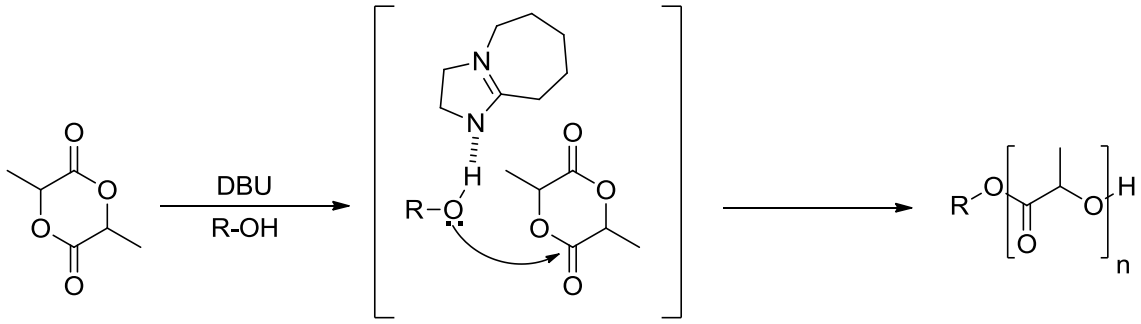

Figure 2-6. Mechanism for DBU catalyzed ROP of lactide[178]

2.3.2.1 DBU Catalyzed ROP of Lactide

The ROP of lactide was catalyzed by DBU, aiming for a target DP of 50 following the conditions described in **Figure 2-7**.[176] The polymerization reached 98 % conversion after 35 min and was subsequently quenched by the addition of benzoic acid. Post purification R-PLA-OH was obtained in high yields (72-97 %) with a PDI less than 1.1 (**Table 2-1**). These results were comparable with those obtained by Hedrick for 4-pyrenebutanol initiated ROP of lactide which reached high conversions of ≥99 % and generated polymers with narrow polydispersity of 1.05 and 1.08 and when BSTSE was used as an initiator the PDI was given as 1.15.[176]

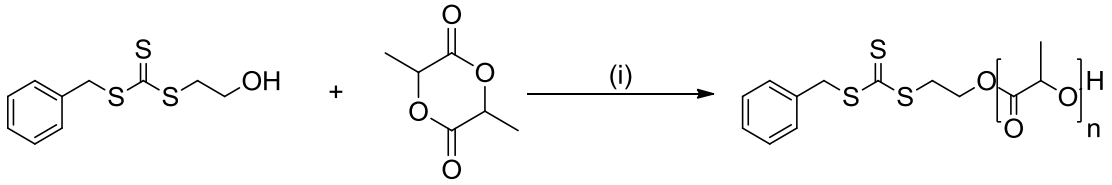

Figure 2-7. DBU catalyzed ROP of lactide. (i) DBU (0.8 eq.), chloroform, RT, 35mins.

The DP of the polymer was determined by the integral ratio of the benzyl methylene signal at 4.62 ppm (peak 3, **Figure 2-8**) with respect to the PLA methine signal at 5.17 ppm (peak 2, **Figure 2-8**) and was found to be DP 50. BSTSE was shown to have successfully initiated and controlled the polymerization of lactide; the ratio of RAFT end group signals to the PLA end group is 1:1 as evidenced by the ^{1}H NMR spectrum shown in **Figure 2-8** where the ratio of end group signals i_3:$i_{2',+4}$:i_5 is shown to be 2:3:2.

The BSTSE initiated polymerization of lactide is an effective way of generating RAFT agent end capped PLA chains. The DBU catalyzed ROP was controlled and generated narrow polydisperse PLA (PDI = 1.03). The M_n determined by ^{1}H NMR spectroscopy was in agreement with the theoretical M_n and that determined by GPC with THF (**Table 2-1**). The method utilised is limited to RAFT agents that possess a hydroxyl group but the RAFT

agent most used for methacrylate polymerization possesses a carboxyl moiety which cannot initiate ROP. Instead the RAFT agent with a carboxyl functionality must be coupled to the hydroxyl end group of PLA to generate the macroRAFT agent.

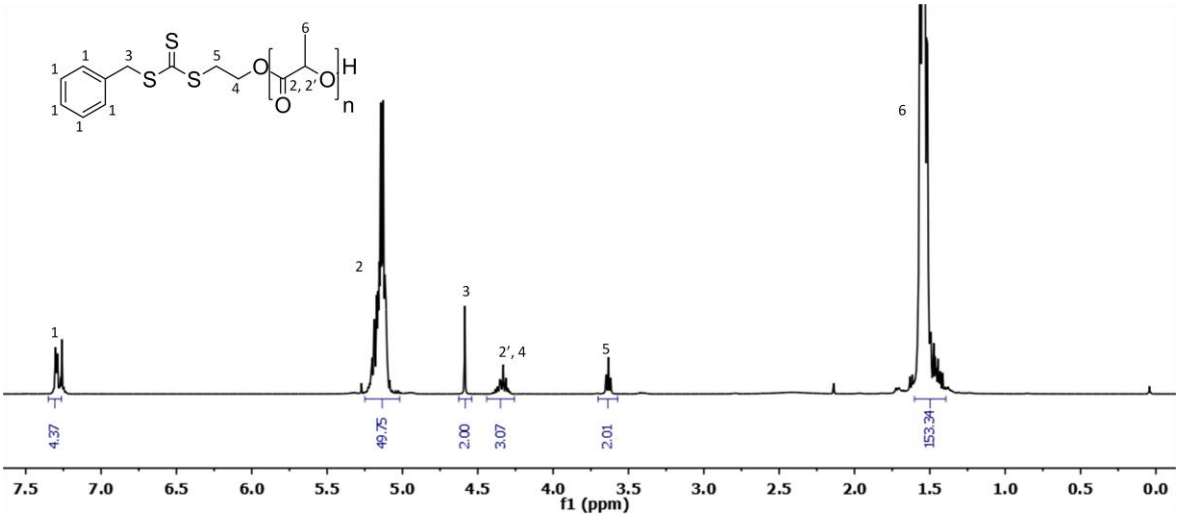

Figure 2-8. ^{1}H NMR spectrum (400 MHz, $CDCl_3$) of R-PLA_{50}-OH

Table 2-1. Molecular Weight Data for PLA and PLA-macroRAFT agents

PLA Polymer[a]	Conv. (%)	M_n (Theory 100% Conv.)	M_n (^{1}H NMR)	M_n[b] (GPC)	M_w[b] (GPC)	PDI[b]	Yield (%)
PLA_{50}-OH [c]	98	3700	3500	3600	4100	1.14	80
PLA_{200}-OH [c]	99	14500	16200	12300	12600	1.02	97
HO-PLA_{50}-OH [d]	97	3700	3800	4400	4700	1.07	72
HO-PLA_{200}-OH[d]	98	14500	12800	11100	12000	1.09	74
HO-PLA_{400}-OH[d]	95	28900	29000	17600	20500	1.16	83
PLA_{50}-R [e]	100	3900	3700	3700	3800	1.02	72
PLA_{200}-R[e]	99	14700	16200	13600	14100	1.03	92
R-PLA_{50}-R[f]	99	4200	4300	4400	4500	1.02	91
R-PLA_{200}-R[f]	99	15100	12100	12400	13100	1.06	92
R-PLA_{400}-R[f]	100	29400	28700	18500	21600	1.17	91
R-PLA_{50}-OH[g]	99	3800	3900	3900	4100	1.03	96

[a] Sample codes: general formula PLA_x-Y and Y-PLA_x-Y, where x represents the target DP of PLA and Y indicates the end group present where Y is either a hydroxyl group (OH) or a RAFT agent moiety (R)

[b] data obtained by THF GPC using triple detection. Calibrated with a single narrow molecular weight distribution PS standard. Sample concentration used was ~1mg/ml except for PLA with a DP of 50 for which 5mg/ml was used.

[c]Synthesized by the ROP of lactide initiated by butanol

[d] Synthesized by the ROP of lactide initiated by butanediol

[e] Synthesized by the esterification of a mono-hydroxyl endcapped PLA with CPADB

[f] Synthesized by the esterification of a di-hydroxyl endcapped PLA with CPADB

[g] Synthesized by the ROP of lactide initiated by BSTSE

2.4 Post Polymerization Modification

2.4.1 Synthesis of Mono-functionalized MacroRAFT agent

2.4.1.1 Synthesis of PLA Initiated by Butanol

PLA with a target DP of 50 was synthesized following the conditions described in **Figure 2-9** utilising butanol as the initiator. The DP of the polymer was determined by the integral ratio of the methylene end group signal (**Figure 2-10**, peak 2) to the PLA methine signal (**Figure 2-10**, peak 1) from the ^{1}H NMR spectrum shown in **Figure 2-10** as DP 48. The intensity of the methylene end group signal (**Figure 2-10**, peak 2) is greater and was therefore was used instead of the PLA methine end group signal (**Figure 2-10**, peak 1') to calculate DP. PLA with a higher molecular weight (DP 200) was also synthesized by altering the monomer:initiator ratio. Both polymerizations reached conversions above 98 % within 35 min and generated polymers in high yields (80-97%) with narrow molecular weight distributions (**Table 2-1**).

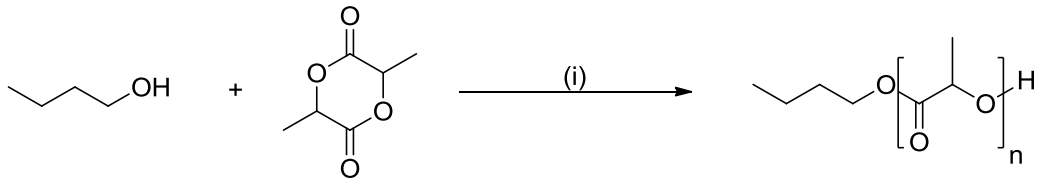

Figure 2-9. DBU catalyzed ROP of lactide; (i) DBU (1.0 eq.), chloroform, RT, 55 min.

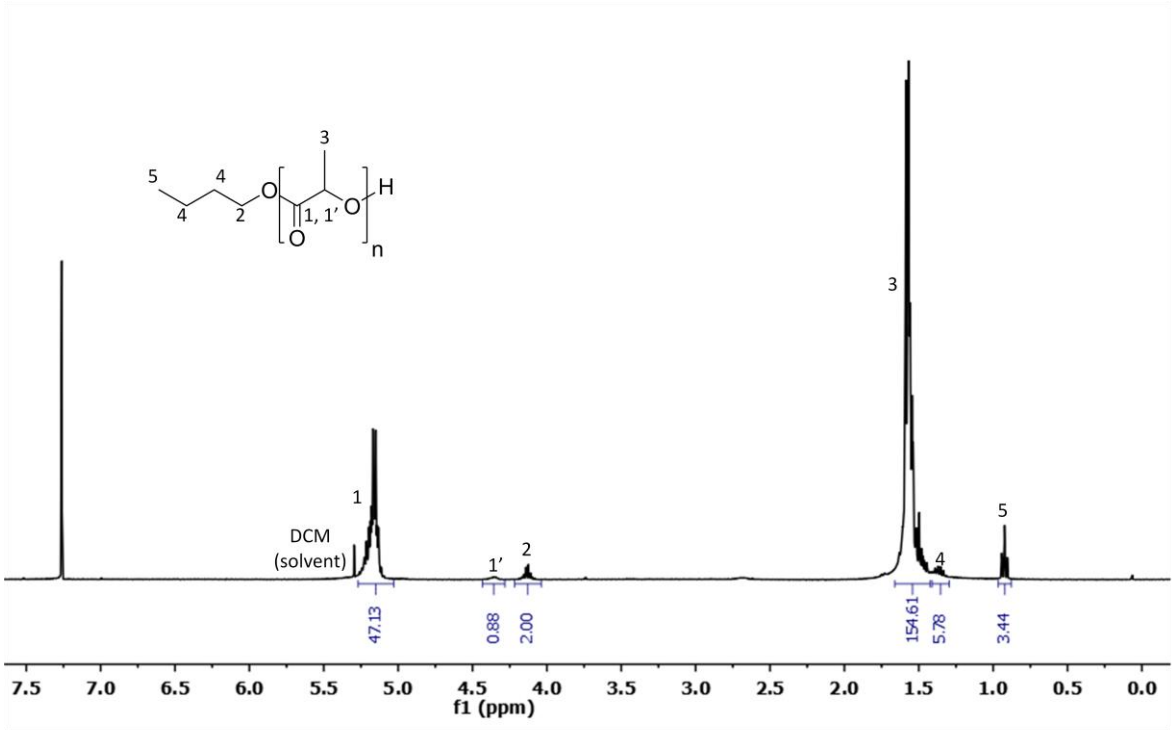

Figure 2-10. ^{1}H NMR spectrum (400 MHz, $CDCl_3$) of PLA_{50}-OH.

2.4.1.2 Post Polymerization Functionalization of PLA-OH

The derivatisation of the PLA hydroxyl end groups by simple coupling chemistry enables the synthesis of macroRAFT agents. Barz *et al.*[127] reported the coupling of PLA with CPADB RAFT agent via an activated ester and Hillmyer *et al.*[179] similarly reacted PLA with a trithiocarbonate RAFT agent via an acyl chloride intermediate. The RAFT agent CPADB has been demonstrated to control the polymerization of methacrylates including MPC, giving polymers of PDI less than 1.1.[13, 180]

The PLA macroRAFT agents with a DP of 50 and 200 were synthesized in 72 % and 92 % yield via a Steglich esterification; activating the carboxyl moiety of CPADB utilising dicyclohexylcarbodiimide to form the *o*-acylisourea intermediate which reacts with dimethylaminopyridine forming an active intermediate.[181] The formation of this active intermediate suppresses intramolecular side reactions and is highly electrophilic and prone to attack by PLA hydroxyl end groups.

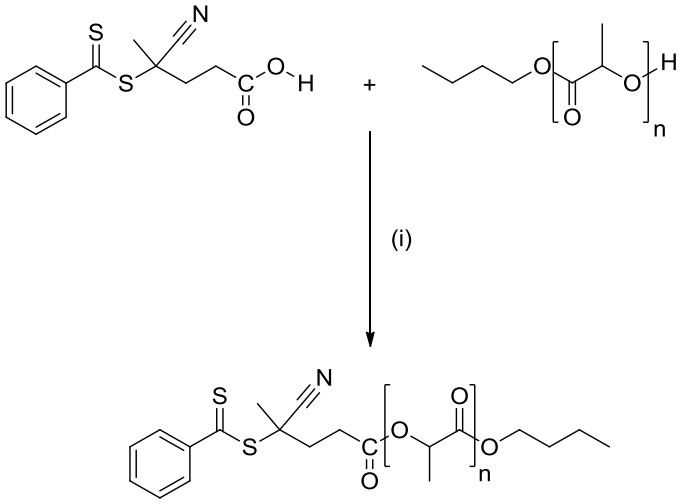

Figure 2-11. Synthesis of PLA_{50}-R. (i) DCC (1.2 eq.), DMAP (0.1 eq.), CPADB(1.5 eq.), DCM, RT, 16 h.

The initial method for coupling CPADB to PLA is described in **Figure 2-11**. A ratio of 1.5:1 mols of CPADB to hydroxyl end groups was used, however, this proved unsuccessful resulting in only 38 % functionalization of PLA chains. This method was optimised by employing a larger excess of CPADB to hydroxyl end groups (4.5:1), which resulted in the complete conversion of PLA hydroxyl end groups. The integral ratio of the methylene end group signal at 4.10 ppm to the aromatic signals of the RAFT end group was given as $i_{1\text{-}3}$:i_5 =5:2 which is in agreement with the target ratio. The ^{1}H NMR spectrum (**Figure 2-12**) of the macroRAFT agent showed the disappearance of the PLA methine end group signal at 4.32 ppm (**Figure 2-10**, peak 1') as a result of the formation of a carboxylate linkage. The high excess of CPADB is critical to gain high functionalization, Barz *et al.* showed that 69 % conversion was achieved with a 3 times molar excess.[127] The large excess of RAFT agent was removed by precipitating twice into methanol, a good solvent for CPADB. The shortcoming of the DCC/DMAP coupling method is the use of a large excess of RAFT agent which could potentially be recovered using column chromatography. The method described by Hillmyer only uses a twofold excess of the RAFT agent obtaining the polymer at 93 % yield with 100 % functionalisation.[179] The coupling reaction via an acid chloride is therefore more efficient. The degree of functionalization of PLA_{200}-OH was determined by ^{1}H NMR spectroscopy to be 99 %. The GPC trace for PLA_{200}-R showed a small shoulder corresponding to a higher molecular weight oligomer which was not observed in the trace of the unfunctionalised chain **Figure 2-13**, which suggests the occurrence of side reactions during the coupling reaction.

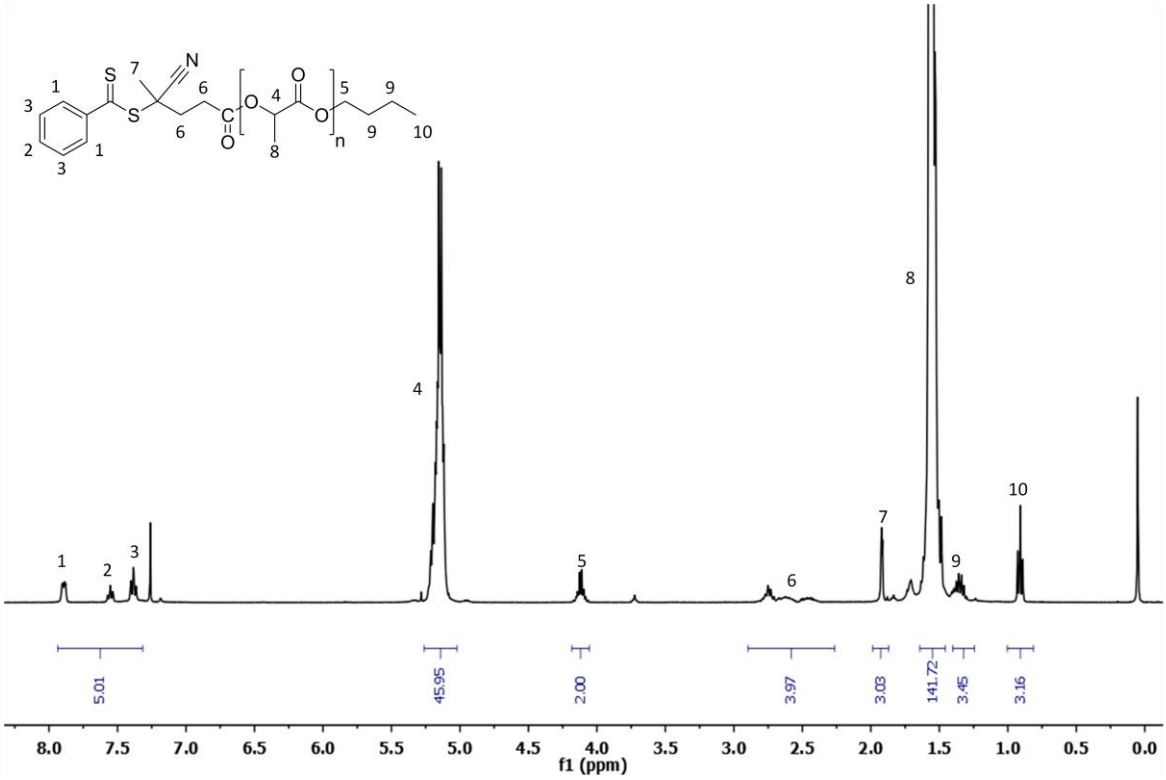

Figure 2-12. ^{1}H NMR spectrum (400 MHz, $CDCl_3$) of PLA_{50}-R.

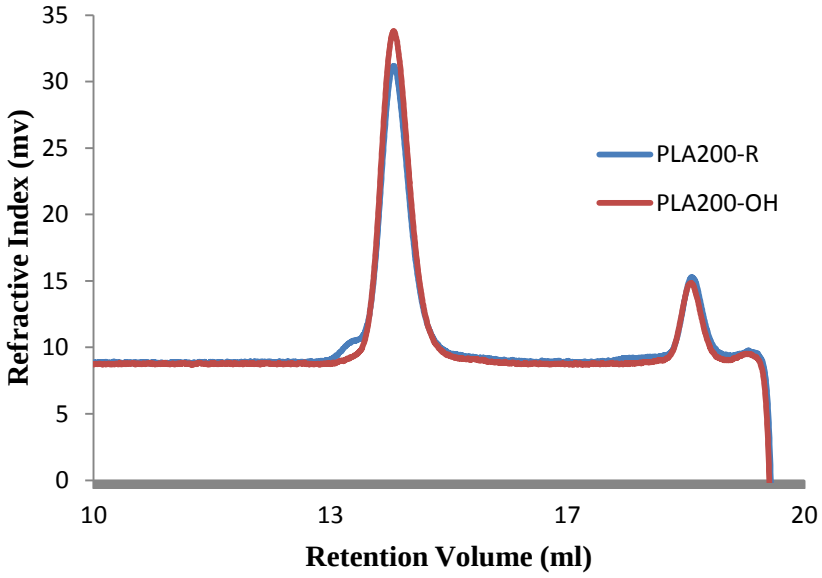

Figure 2-13. GPC traces for PLA_{200}-OH and PLA_{200}-R.

2.4.2 Synthesis of Bifunctionalized MacroRAFT agent

2.4.2.1 ROP of Lactide Initiated by Butanediol.

Recently the synthesis of an ABA-type triblock copolymer has been reported in which a di-hydroxy polycaprolactone was functionalised with cyanopentanoic acid

dithionaphthalenoate to form a bifunctional macroRAFT agent which was chain extended at both ends with 2-(*N*, *N*-dimethylaminoethyl)methacrylate.[147] There are reports of the ROP of lactide initiated by polyethylene glycol to generate triblock copolymers PLA-PEG-PLA which have two terminal hydroxyl end groups, but to our knowledge there are no prior reports of the post polymerization modification to generate PLA-based bifunctional macroRAFT agents. [182, 183]

Dihydroxyl-polylactide was synthesized following the conditions described in **Figure 2-14**; using butanediol to initiate polymerization. The monomer:initiator ratio was varied to target PLA of DP 50, 200 and 400. The DP was determined by the integral ratio of the initiator methylene signal at 4.13 ppm to the PLA methine signal at 5.15 ppm from the ^{1}H NMR spectrum (**Figure 2-15**). Polymerizations reached high conversions (72-83%) and generated polymers with narrow molecular weight distributions (1.07-1.16, **Table 2-1**).

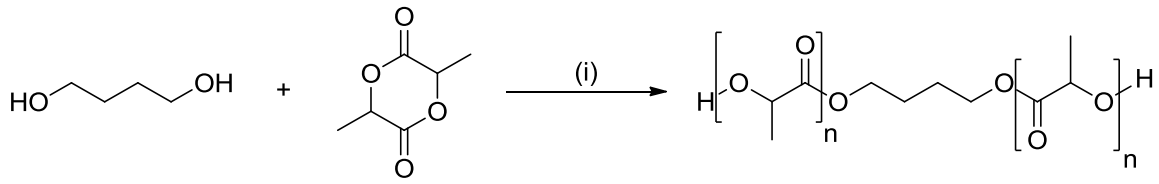

Figure 2-14. DBU catalyzed ROP of lactide. (i) DBU (0.9 eq.), THF, RT, 55 min.

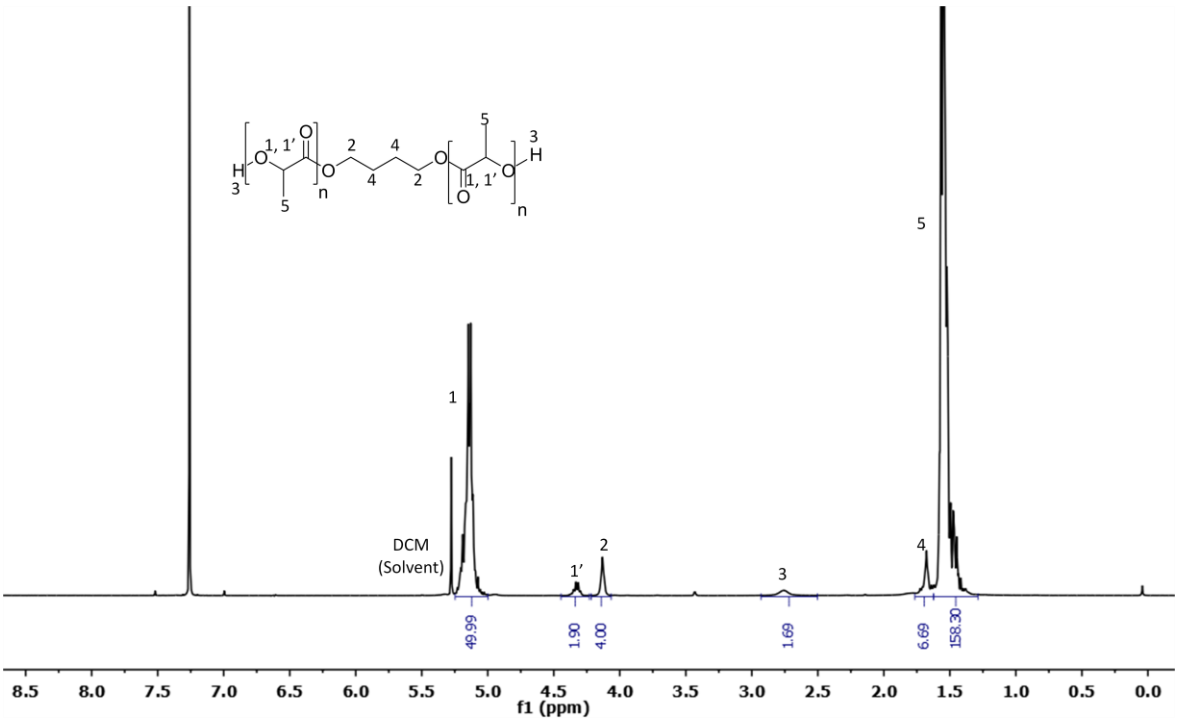

Figure 2-15. ^{1}H NMR spectrum (400 MHz, $CDCl_3$) of HO-PLA_{50}-OH

2.4.2.2 Post Polymerization Functionalization of HO-PLA-OH

An analogous method to that used in the synthesis of the mono functional PLA-macroRAFT agent was utilised to synthesize bifunctional PLA-macroRAFT agents (**Figure 2-16**). The hydroxyl end groups were successfully derivatized to obtain a bifunctional PLA-macroRAFT agent; this was confirmed by the ^{1}H NMR spectrum (**Figure 2-17**) with the complete loss of the methine end group signal at 4.33 ppm due to the formation of an ester bond. The RAFT aromatic signals integrated against the methylene butanediol initiator signal (4.14 ppm) corresponds to the expected ratio of 10:4. Similarly to the purification of R-PLA-OH, the polymer was precipitated twice into methanol to ensure complete removal of excess of the RAFT agent. The sensitivity of ^{1}H NMR spectroscopy towards quantifying the degree of functionalization diminishes with increasing molecular weight of the polymer (M_n>2500 $gmol^{-1}$) due to the low concentration of end groups. The end group signals (**Figure 2-17**, peaks 1-3 and 5) were discrete and better resolution of these signals was achieved with the use of a higher field NMR (500 MHz). The end groups signals for R-PLA_{50}-R (Mn = 4300 $gmol^{-1}$) as shown in **Figure 2-17** are strong and highly resolved facilitating the determination of the level of RAFT functionalization.

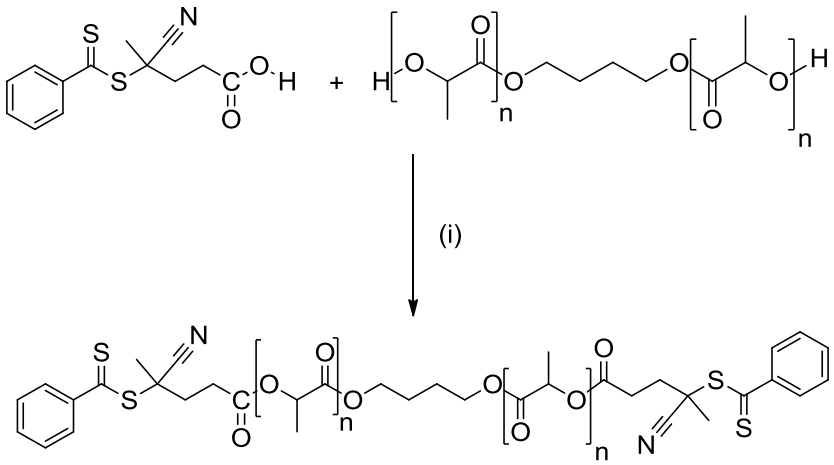

Figure 2-16. Synthesis of R-PLA_{50}-R. (i) DCC (1.2 eq.), DMAP (0.1 eq.), DCM, RT, 16 h.

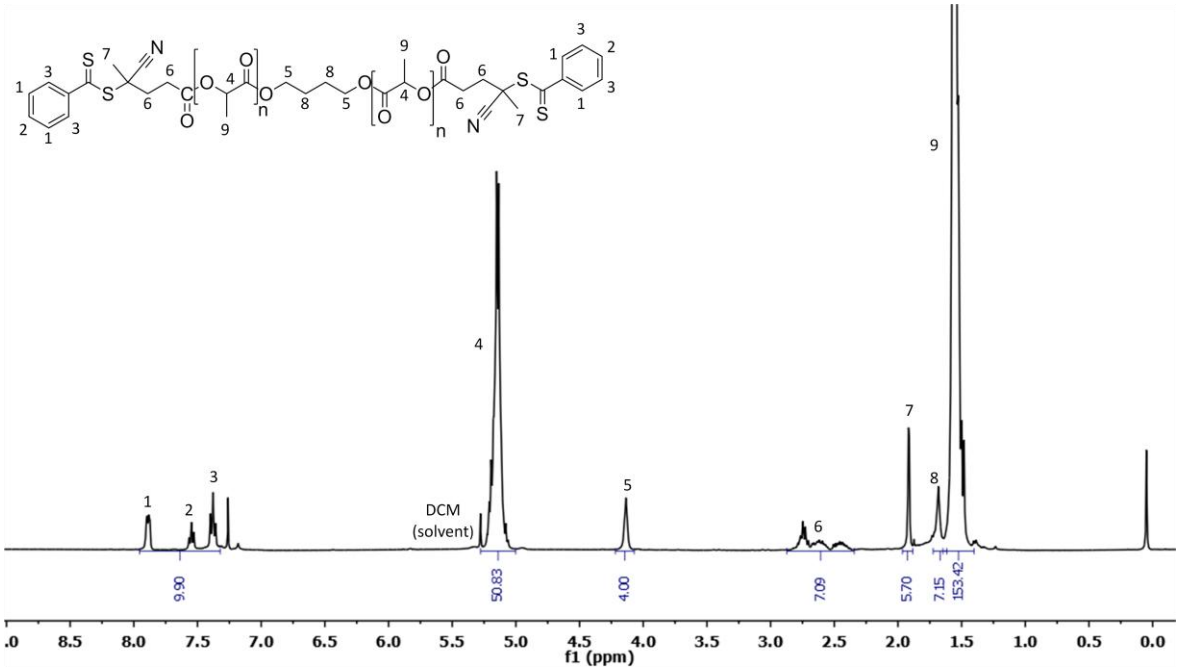

Figure 2-17. ^{1}H NMR spectrum (400 MHz, $CDCl_3$) of R-PLA_{50}-R.

2.5 Conclusion

PLA macroRAFT agents were synthesized via two strategies; RAFT agent initiated ROP and derivatization of the preformed PLA hydroxyl end group by esterification. The first route is preferred, the RAFT agent is generated using a high yielding facile synthetic method which effectively initiates ROP of lactide, however, the efficacy of this RAFT agent for the polymerization of MPC is unknown. The alternative utilises CPADB which is an expensive starting material utilised in excess to functionalize the PLA homopolymer but is widely used for the effective polymerization of MPC. An analogous method can generate bifunctionalized macroRAFT agents which can be used to form triblock copolymers. Bifunctionalized PLA-macroRAFT agents were synthesized by ROP initiated by a diol followed by the functionalization of both hydroxyl end groups with a dithiobenzoate RAFT agent. Polymers were obtained with a narrow PDI range of 1.02-1.17 with near 100 % RAFT functionalization of PLA chains achieved.

3. Synthesis of PLA-PMPC Block Copolymers

3.1 Introduction

Amphiphilic block copolymers are of great interest for biomedical applications e.g. drug delivery. PMPC is used as the hydrophilic block as a means of increasing the biocompatibility of the block copolymers.[184-186] A range of block copolymers composed of PMPC have been synthesized using ATRP and more recently RAFT polymerization.[13, 22, 28, 31] Our target copolymer PLA-PMPC has been previously synthesized by combining ROP with ATRP but not with RAFT to the best of our knowledge. Furthermore PMPC-PLA-PMPC triblocks have not been reported up to now. The initial strategy to prepare PLA-PMPC block copolymers used macroRAFT agents synthesized as described in **Chapter 2** which would be chain extended with MPC. However, before embarking on this work it was decided to investigate the ability of BSTSE (as a model RAFT agent) to control the polymerization of methacrylates

3.2 Model RAFT Polymerizations using BSTSE

3.2.1 RAFT Polymerization of *n*-Butyl Methacrylate

A model system was chosen which could be readily analysed to enable the comparison of RAFT agents for the polymerization of methacrylates. Poly(*n*-butyl methacrylate) is soluble in THF and therefore the M_n and PDI of the polymer could be determined easily. *n*-Butyl methacrylate (BMA) was polymerized using the conditions specified in **Figure 3-1** with a target DP of 50. The polymerization was quenched after 14 h reaching 97 % conversion of the monomer. The aromatic signals of the RAFT end group at 7.25-7.4 ppm were not observed in the ^{1}H NMR spectrum of the purified polymer. Molecular weight data (**Table 3-1**) showed that the RAFT agent lacked control over the polymerization of BMA generating polymers with a broad PDI and molecular weight comparable with that obtained by free radical polymerization. It was concluded that BSTSE would be ineffective for the RAFT polymerization of MPC.

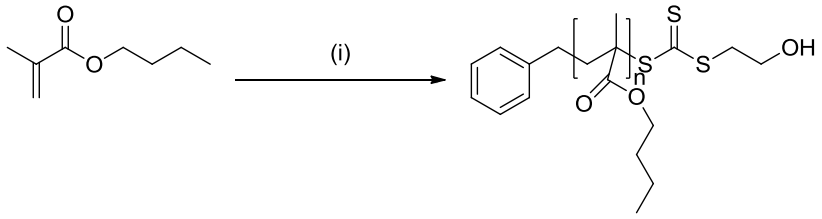

Figure 3-1. RAFT polymerization of BMA (i) BSTSE 0.02 eq., AIBN $5.0x10^{-3}$ eq, MeOH, 75 ^{o}C, 14 h.

Table 3-1. Molecular weight data for PBMA homopolymer.

PBMA	$M_{n, thr.}$ [a]	M_n [b]	PDI [b]
Free Radical Polymerization	-	30000	3.01
RAFT Polymerization	7000	40000	1.57

[a] M_n value for 100 % conversion of monomer

[b] data obtained by THF GPC using triple detection. Calibrated with a single narrow molecular weight distribution PS standard. Sample concentration used was ~ 5mg/ml.

3.2.2 Choice of RAFT Agents

The efficiency of RAFT is dependent on the choice of monomer, the properties of the leaving radical group R and the Z group which acts to activate or deactivate the thiocarbonyl double bond. In the pre-equilibrium step of the RAFT mechanism (**Figure 3-2**) the RAFT agent (**2**) and polymeric RAFT agent (**4**) should possess a reactive thiocarbonyl bond resulting in high k_{add}, R (**5**) must be a good leaving group to allow rapid fragmentation of radical intermediate (**3**) i.e. high k_{β} and must be able to reinitiate polymerization efficiently. The radical intermediate (**3**) should also partition in favour of the polymeric RAFT agent (**4**) i.e. $k_{\beta 2} > k_{\beta 1}$ in order to keep the concentration of P_n (**1**) low at all times.[119] The benzyl R group of BSTSE is regarded as a poor leaving group with respect to the propagating radical of the methacrylate monomer resulting in the radical intermediate partitioning in favour of reactants (**1** and **2**).[123] R groups of RAFT agents utilised for the polymerization of methacrylates generally possess an electron-withdrawing group and are more sterically hindered in order to increase the rate of fragmentation of the S-R bond.

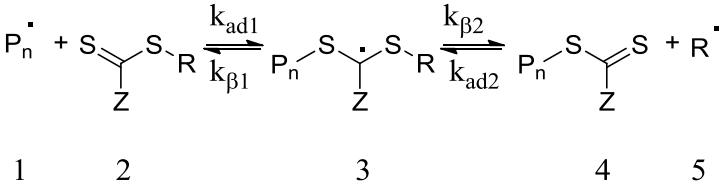

Figure 3-2. RAFT - Pre-equilibrium mechanism.

3.3 Alternative RAFT agents

Ishihara *et al.* showed that RAFT agents 4-cyano-4-[(dodecylsulfanylthiocarbonyl)sulfanyl]pentanoic acid (CPAD) and CPADB are effective RAFT agents for the polymerization of MPC providing good control over methacrylate polymerization.[11-13] A model polymerization was thus carried out to confirm the efficacy of the RAFT agent CPADB for the polymerization of methacrylates.

BMA was polymerized with a target DP of 50, using the conditions described in **Figure 3-3** analogous to the BSTSE RAFT polymerization. The polymerization was quenched after 8 h at which point 90 % conversion of the monomer had been reached. GPC analysis of the purified homopolymer gave M_n = 6400 $gmol^{-1}$ (theoretical M_n = 8800 $gmol^{-1}$) and a narrow molecular weight distribution of 1.11 which is typical of a controlled polymerization in comparison to the broad PDI observed for the BSTSE RAFT polymerization of BMA. Therefore CPADB appeared to be more suitable for the polymerization of BMA than BSTSE.

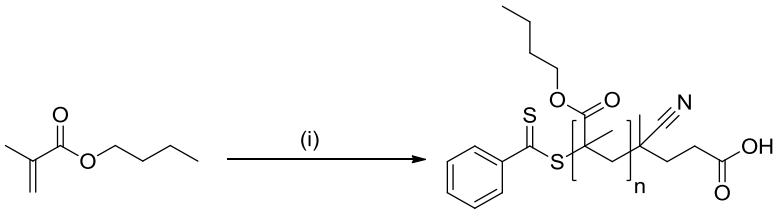

Figure 3-3. RAFT polymerization of BMA. (i) CPADB 0.02 eq., ACVA $5.0x10^{-3}$ eq., BMA 50.0 eq., THF , 75 ^{o}C, 8 h.

3.4 RAFT Polymerization of APC

Stenzel *et al.* reported the synthesis of amphiphilic block copolymer poly(butyl acrylate)-poly(acryloyloxyethyl phosphorylcholine) (APC) with the RAFT agent 2-

benzylsulfanylthiocarbonylsulfanyl propionic acid, an analogue of BSTSE.[187] However, due to the difficulty in analysing these block copolymers a model experiment was designed in which APC was replaced by the structurally similar 2-hydroxyethyl acrylate (HEA). GPC results showed the formation of HEA block copolymers with narrow weight distributions ranging from 1.15-1.27.[187] Therefore in this work BSTSE was used for the RAFT polymerization of APC as a possible route to synthesize PLA-PAPC block copolymers using PLA-macroRAFT agent with a BSTSE end group.

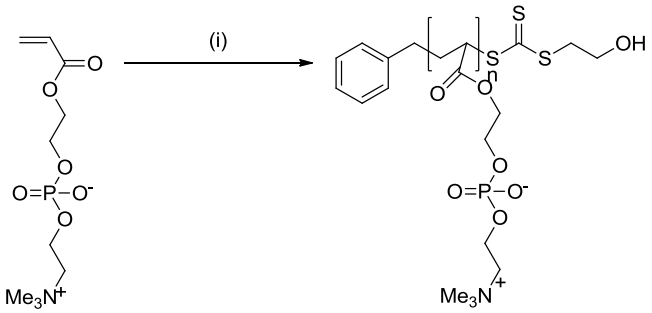

Figure 3-4. RAFT polymerization of APC. (i) BSTSE 0.04 eq., ACVA 0.01 eq., MeOH , 75 ^{o}C, 17 h.

APC was polymerized following the conditions shown in **Figure 3-4** with a target DP of 25. The polymerization was quenched after 17 h and the ^{1}H NMR spectrum of the crude mixture showed that 94 % conversion was achieved. The polymer was purified by dialysis against water to remove unreacted monomer and RAFT agent. The DP of the homopolymer was determined as 34 from the ^{1}H NMR spectrum (**Figure 3-5**) by end group analysis comparing the integral ratio of the aromatic signal 7.41-7.05 ppm (**Figure 3-5**, peak 1), to the methylene signal of PAPC at 3.70 ppm (**Figure 3-5**, peak 5). Molecular weight data obtained by aqueous GPC with RI detection gave M_n = 3500 gmol^{-1} (theoretical M_n = 7700 gmol^{-1}) and PDI of 1.34. BSTSE has demonstrated control over the polymerization of APC and there is scope to achieve narrower molecular weight distributions by quenching the polymerization at lower conversions. From the literature it is known that bimodal molecular weight distributions are often observed for the RAFT polymerization of acrylates and become more pronounced for higher molecular weights and at higher monomer conversions.[119] In the case of the RAFT polymerization of poly(butyl acrylate) using a trithiocarbonate the source of the high molecular weight shoulder had been determined by end group analysis.[188] The data supports the hypothesis that the high molecular weight polymer arises from the copolymerization of a polyacrylate macroRAFT agent formed during polymerization by a backbiting β-scission mechanism.[188] The PLA-macroRAFT agent could therefore be extended by APC, however, thus far

CPADB is the RAFT agent which has demonstrated the greatest control over the polymerization of methacrylates and in the literature Bhuchar *et al.* reported the synthesis of MPC homopolymer by RAFT polymerization with a PDI of 1.08 with CPADB.[13] From this point forward our focus will be on the use of PLA macroRAFT agents possessing the CPADB end group.

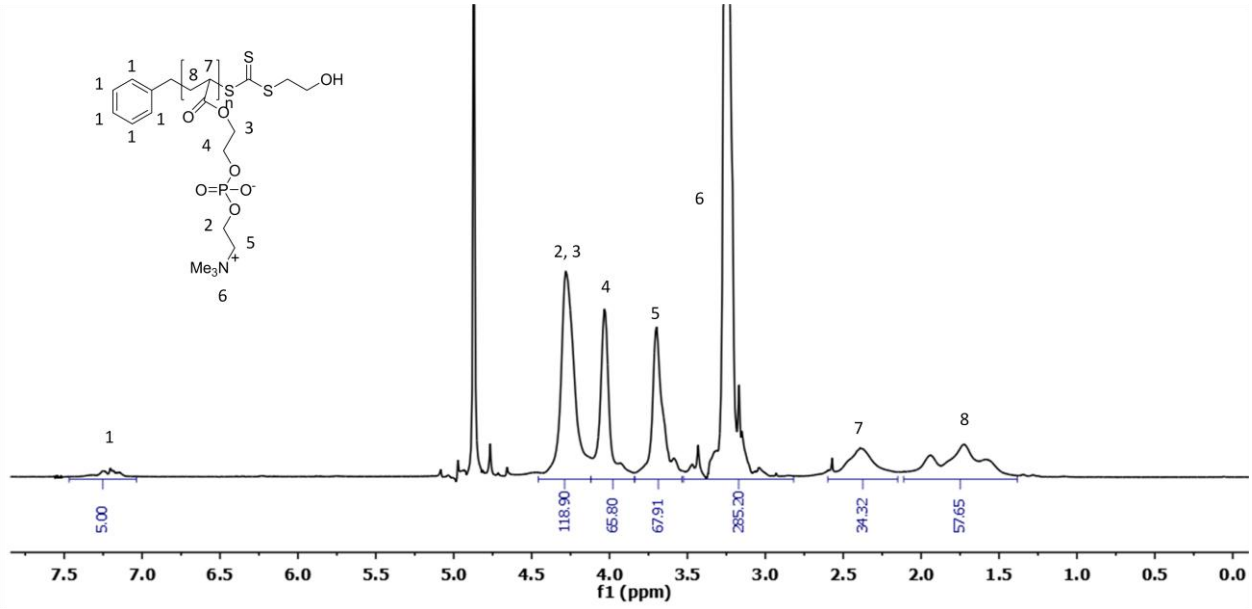

Figure 3-5. ^{1}H NMR spectrum (400 MHz, MeOD-d4) of PAPC with BSTSE end group.

3.5 Synthesis of PLA-PMPC

A range of PLA_{46}-$PMPC_x$ polymers were synthesized varying the MPC block length where x=50, 75 and 100. The polymerization of MPC was carried out under the conditions described in **Figure 3-6.** The polymerizations were quenched after 12 h at which high conversions were obtained, these polymers were subsequently purified by first precipitating into methanol to remove unreacted PLA-macroRAFT agent followed by dialysis to remove DMSO and residual monomer. Triblock copolymer $PMPC_{100}$-PLA_{51}-$PMPC_{100}$ was synthesized using a bifunctionalised macroinitiator under similar conditions utilised for the synthesis of the diblock copolymer except the ratio of PLA-macroRAFT agent to initiator used was 2:1. The DP of the MPC block was determined from the ^{1}H NMR spectrum (**Figure 3-7**) using the ratio of the methine signal of PLA at 5.27 ppm (**Figure 3-7**, peak 1) to the methylene signal of PMPC at 3.81 ppm (**Figure 3-7**, peak 5) as DP 43. The M_n value of the block copolymer was obtained by combining the M_n of the PMPC and the macroRAFT agent determined previously by ^{1}H NMR spectroscopy (**Table 3-2**).

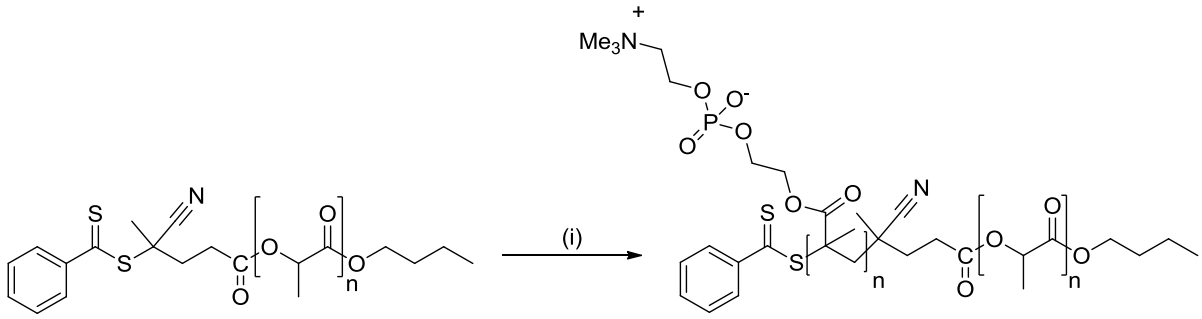

Figure 3-6. Synthesis of PLA_{46}-$PMPC_{50}$. (i) ACVA 0.25 eq., MPC 50.0 eq., DMSO/MeOH (3:7), 75 ^{o}C, 12 h.

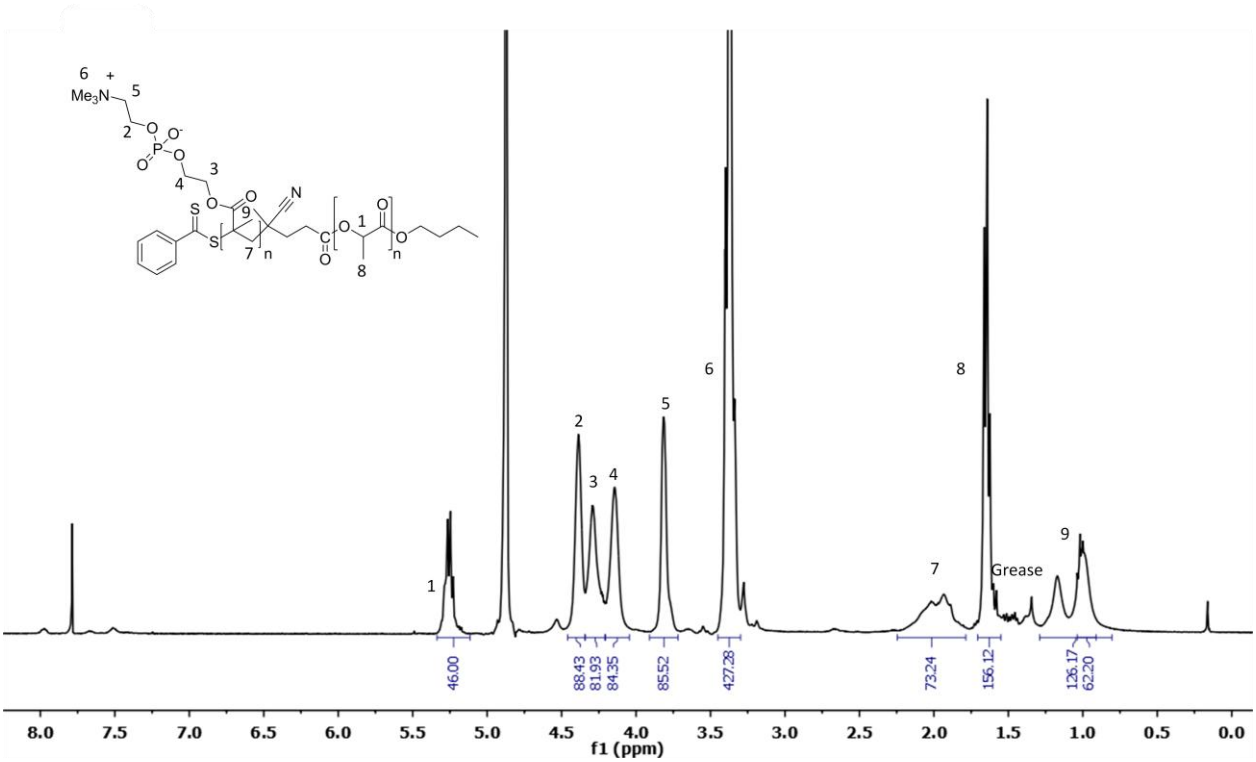

Figure 3-7. ^{1}H NMR spectrum (400 MHz, MeOD-d4/$CDCl_3$ (2:1)) of PLA_{46}-$PMPC_{50}$.

The molecular weight data for the PLA-PMPC block copolymers are given in **Table 3-2**. The M_n values of the block copolymers determined by ^{1}H NMR spectroscopy were in agreement with the target M_n however there is in most cases a large discrepancy between the M_n determined by ^{1}H NMR spectroscopy and by GPC. Block copolymers were analysed using GPC with a conventional calibration using a series of near monodisperse polymethyl methacrylate standards. The M_n determined by ^{1}H NMR spectroscopy has approximately a 10% error but it is absolute. The GPC separates polymers by hydrodynamic volume using polymethyl methacrylate calibrants and can lead to an inaccurate M_n which can explain the differences with the values obtained by ^{1}H NMR

spectroscopy. However GPC traces in **Figure 3-8** show multimodal distributions; the traces for the diblock copolymers are similar displaying two lower molecular weight shoulders whereas the triblock copolymer gives a bimodal distribution. The presence of a multimodal distribution means the M_n determined by ^{1}H NMR spectroscopy results is therefore unreliable. It was not possible to determine the peak due to unreacted PLA-macroRAFT agent as a GPC trace of the macroRAFT agent had not been obtained using a methanol/chloroform system.

Table 3-2. Molecular data for PLA-PMPC block Copolymers prepared by RAFT polymerization.

Block Copolymer	Conv. (%)	$M_{n,\ Thr.}$ [a]	M_n [b] (^{1}H NMR)	M_n [c] (GPC)	PDI[c]	Yield (%)
PLA_{46}-$PMPC_{50}$	75	18400	16300	16000	1.30	60
PLA_{46}-$PMPC_{75}$	83	25800	21700	12300	1.38	73
PLA_{46}-$PMPC_{100}$	70	33200	24900	15600	1.40	65
$PMPC_{100}$-PLA_{51}-$PMPC_{100}$	91	63300	52700	9000	1.28	90

[a] M_n value for 100 % conversion of monomer

[b] Molecular weight determined by ^{1}H NMR in MeOD-d4/$CDCl_3$(2:1)

[c] Molecular weight data obtained by methanol/chloroform (1:3) GPC with RI detector. Calibrated with a series of near-monodisperse polymethylmethacrylate standards. Sample concentration used was ~1mg/ml.

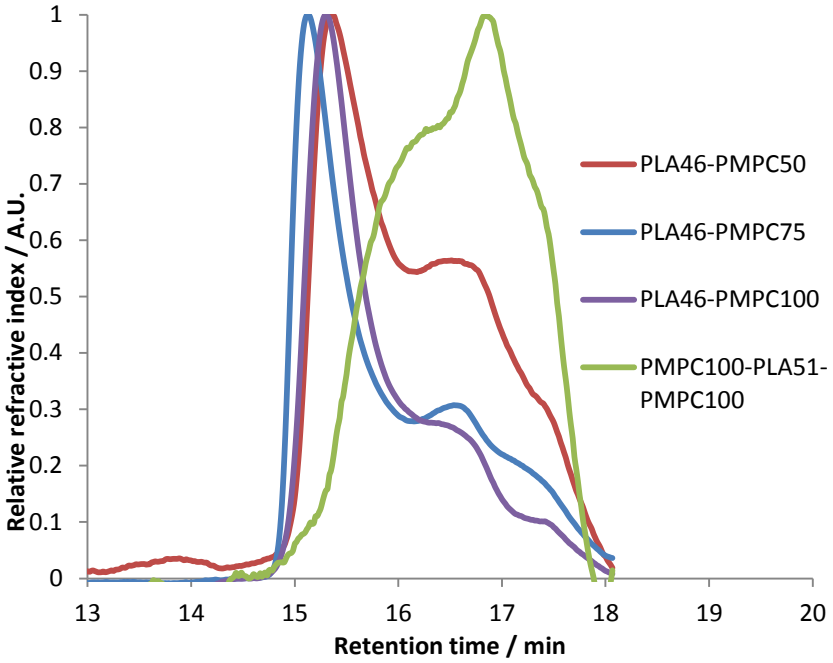

Figure 3-8. GPC traces of PLA_{46}-$PMPC_x$ block copolymers obtained by methanol/chloroform (1:3) GPC.

The additional peaks observed in the GPC traces do not represent unreacted macroRAFT agent as PLA was removed by precipitating into methanol. To account for the multimodal distributions the stability of the PLA-macroRAFT agent was investigated in the polymerization solvent mixture. A sample of the macroRAFT agent was heated at 70 ^{o}C for 5h and subsequently analysed by ^{1}H NMR spectroscopy. As evidenced by the ^{1}H NMR spectrum (**Figure 3-9A**), the PLA-macroRAFT agent had degraded under polymerization conditions which explains the GPC results (**Figure 3-8**). Further stability experiments were carried out in DMSO and THF/ethanol (1:1) mixture and in both systems PLA retained its structural integrity as shown by the ^{1}H NMR spectra (**Figure 3-9B, 3-9C)**). Methanol/DMSO proved an effective solvent mixture for the polymerization of MPC by ATRP at room temperature, but PLA is not stable in the presence of methanol at high temperatures due to the nucleophilicity of methanol. THF/ethanol has proved to be a potential alternative solvent mixture for the synthesis of PLA-PMPC block copolymers.

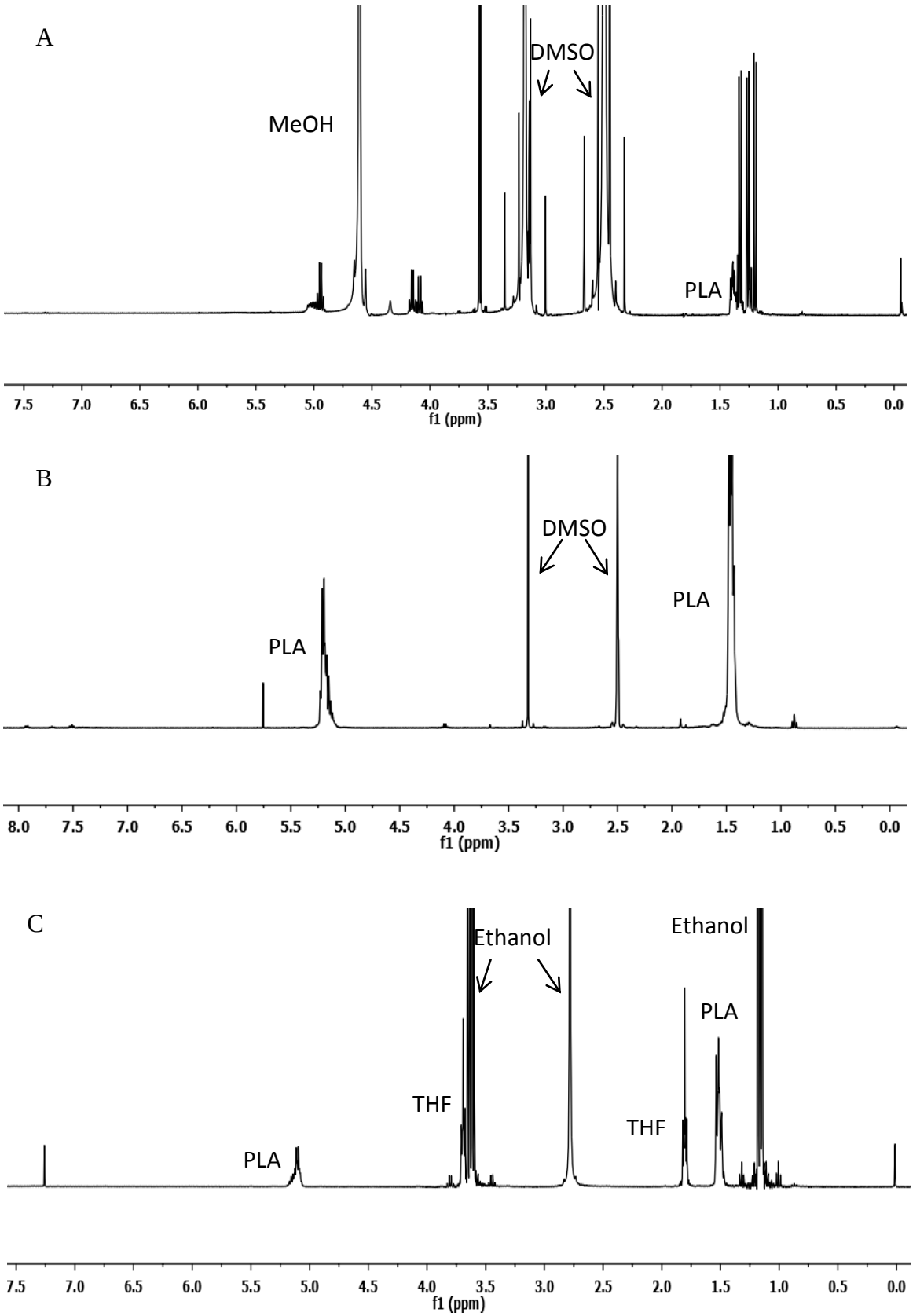

Figure 3-9. PLA-macroRAFT stability test; A)^{1}H NMR spectrum of PLA-R heated in MeOH-d4/DMSO-d6 (7:3), B) ^{1}H NMR spectrum of PLA-R heated in DMSO-d6, C) ^{1}H NMR spectrum of PLA-R heated in THF/ethanol (1:1).

3.6 Model System: PLA-P(HEMA)

2-Hydroxyethyl methacrylate (HEMA) is a hydrophilic methacrylate like MPC but soluble in a wider range of solvents and therefore its polymer can be more readily analysed. Additionally, PLA-PHEMA block copolymers have not to our knowledge been synthesized by combining ROP and RAFT polymerization and PLA-PHEMA triblock copolymers have yet to be reported. The knowledge gleaned from these polymerization experiments will be applied to the synthesis of PLA-PMPC block copolymers in which both blocks are not soluble in a common solvent.

3.6.1 Synthesis of PLA-PHEMA Diblock Copolymer

HEMA was polymerized using PLA_x-R where x= 46 and 219 under conditions described in **Figure 3-10**. The target DP of PHEMA was chosen to obtain block copolymers with a hydrophilic weight fraction (*f,* **Equation 1**) of 0.35±0.1 which was proposed by Discher and Eisenberg to give vesicle morphology upon self-assembly.[189] PLA_{46}-$PHEMA_{100}$ was synthesized to examine the morphological effects of increasing the hydrophilic block length. The ratio of macroRAFT agent to initiator used for the synthesis of diblocks was maintained at 4:1. The initiator chosen was 4,4'-azobis(4-cyanopentanoic acid (ACVA) based on the work by Liu *et al.* who showed that better control over the polymerization of 2-(dimethylamino)ethyl methacrylate was achieved when the CPADB was combined with ACVA and not AIBN.[180]

$$f = M_n \text{ of PHEMA block} / M_n \text{ of PLA-PHEMA di/triblock copolymers} \quad (\mathbf{1})$$

The ^{1}H NMR spectrum of the purified PLA_{46}-$PHEMA_{100}$ polymer is shown in **Figure 3-11** in a solvent mixture of $CDCl_3$/MeOD-d4 to ensure the solubilisation of both blocks. The M_n of the PHEMA block was determined by comparing the integral ratio of the PLA methine signal at 4.93ppm (**Figure 3-11**, peak 1) to the PHEMA methylene adjacent to the carboxylate moiety signal at 3.55 ppm (**Figure 3-11**, peak 3). The molecular weight data for PLA-PHEMA diblock copolymers is provided in **Table 3-3** and GPC traces are given in **Figure 3-12**. The M_n obtained by GPC is in agreement with that determined by ^{1}H NMR spectroscopy for PLA_{46}-$PMPC_x$ copolymers albeit higher in the case of PLA_{219}-$PHEMA_{67}$. The GPC trace of PLA_{219}-$PHEMA_{67}$ (**Figure 3-12**) shows a high molecular weight shoulder which suggests that the shoulder observed in the GPC trace of the macroRAFT agent possessed a RAFT functionality. The conditions utilised for the

synthesis of PLA-PHEMA generated mono-modal polymers with narrow molecular weight distribution (PDI = 1.1-1.2). PLA-PHEMA block copolymers generated by the ROP-ATRP method gave PDIs ranging from 1.18-1.32.[171]

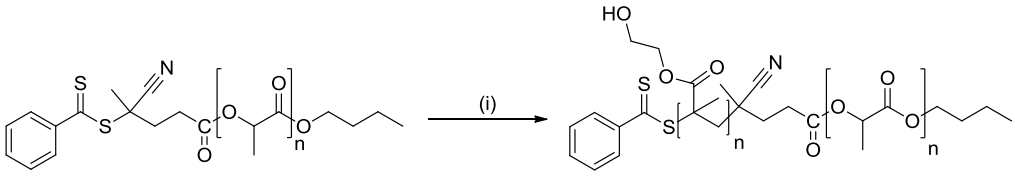

Figure 3-10. Synthesis of PLA_{46}-$PHEMA_{100}$. (i) ACVA 0.25 eq., HEMA 50.0 eq., THF, 70 ^{o}C, 12 h.

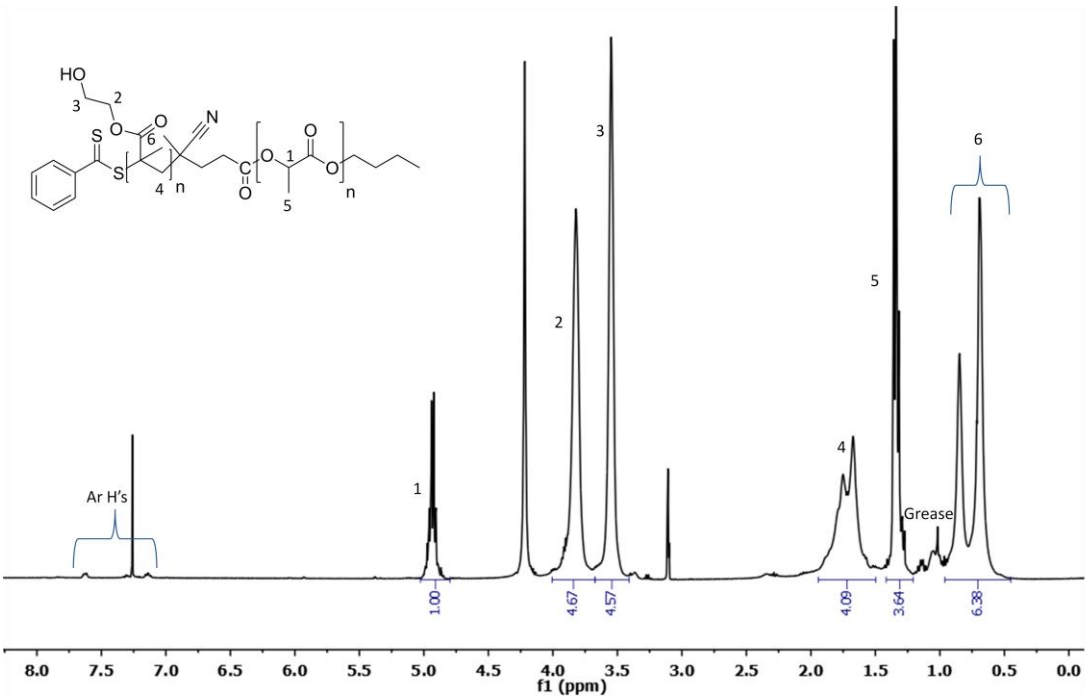

Figure 3-11. ^{1}H NMR spectrum (400 MHz, MeOD-d4/$CDCl_3$ (1:2)) of PLA_{46}-$PHEMA_{100}$.

Table 3-3. Molecular weight data for PLA-PHEMA/PHEMA-PLA-PHEMA block copolymers.

PLA Polymer[a]	Conv. (%)	f_{HEMA}	$M_{n,\ Thr.}$[b]	M_n[c] (^{1}H NMR)	M_n[d] (GPC)	PDI[d]	M_n[e] (GPC)	PDI[e]	Yield (%)
PLA_{46}-$PHEMA_{15}$	94	0.35	5600	6100	10000	1.15	14700	1.82	89
PLA_{46}-$PHEMA_{100}$	89	0.78	16700	16300	18300	1.09	25200	1.46	97
PLA_{219}-$PHEMA_{67}$	70	0.35	24800	23300	38400	1.20	36100	1.76	96
$PHEMA_{62}$-PLA_{390}-$PHEMA_{62}$	67	0.36	45000	42500	36700	1.24	39900	1.41	60
$PHEMA_{62}$-PLA_{390}-$PHEMA_{62}$	85	0.36	45000	44500	50700	1.29	-	-	76
$PHEMA_{20}$-PLA_{390}-$PHEMA_{20}$	63	0.15	33900	32900	34500	1.41	33700	1.96	74
$PHEMA_{53}$-PLA_{51}-$PHEMA_{53}$	84	0.76	18100	17000	53100	1.14	27600	2.25	91

[a]RAFT polymerization performed at 70 ^oC in THF

[b]M_n value for 100 % conversion of monomer

[c]Molecular weight determined by ^{1}H NMR in MeOD-d4/$CDCl_3$(1:2)

[d]Molecular weight data obtained by THF GPC using triple detection. Calibrated with a single narrow molecular weight distribution PS standard. Sample concentration used was ~1mg/ml.

[e]Molecular weight data obtained by DMF GPC using RI detector. Calibrated with a series of narrow polydispersity PS standards. Sample concentration used was ~1mg/ml.

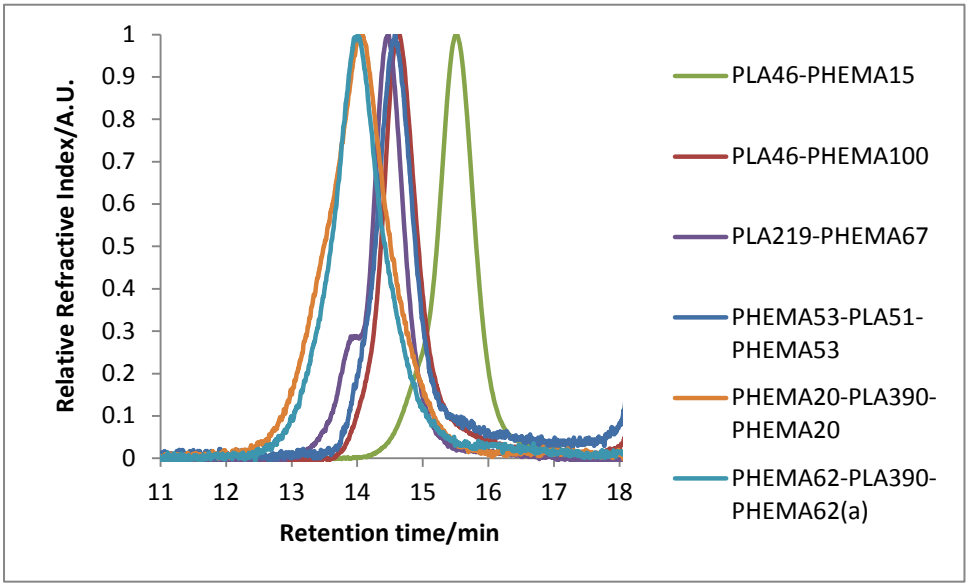

Figure 3-12. GPC traces of PLA_{46}-$PMPC_x$ and $PMPC_x$-PLA_y-$PMPC_x$ block obtained by THF GPC.

3.6.2 Synthesis of PHEMA-PLA-PHEMA

PHEMA-PLA-PHEMA triblock copolymers were synthesized utilising R-PLA_x-R where x=51 and 390. The compositions of the two $PHEMA_y$-PLA_x-$PHEMA_y$ triblock copolymers were chosen to target a f_{HEMA} of 0.36 and 0.15. As mentioned in section **3.6.1** amphiphilic block copolymers with f=0.35±0.1 form vesicles, it was also proposed that when f<0.25 inverted microstructures will be generated upon self-assembly.[189] $PHEMA_{53}$-PLA_{51}-$PHEMA_{53}$ with a composition ratio of 1:1:1 was synthesized to compare the self-assembly behaviour with the diblock copolymer PLA_{46}-$PHEMA_{100}$ of the same f_{HEMA} and M_n.

The effects of the macroRAFT agent to initiator ratio and time on the PDI of $PHEMA_{53}$-PLA_{51}-$PHEMA_{53}$ were investigated. The triblock copolymers were synthesized as described in **Figure 3-13**, under these conditions a narrow PDI of 1.13 was obtained. Lowering the MRA:initiator ratio to 2:1 resulted in a slight increase in PDI to 1.17. Additionally an increase in polymerization time from 12 h to 24 h saw little change in the PDI obtained. The polymerization conditions for the triblock copolymers chosen were analogous to those utilised for the diblock synthesis; MRA:initiator ratio 4:1 and 12 h polymerization time. Under these conditions high degrees of conversion and narrowly dispersed polymers were obtained. However, the degree of conversion was lower when chain extending PLA with a DP of 390 due to the higher viscosity. Increased viscosity leads to reduced initiator efficiency which results in a lower concentration of radicals.[190] An ^{1}H NMR spectrum of the purified triblock copolymer is shown in **Figure 3-14**. The

DP of PHEMA block was determined by the integral ratio of the PLA methine signal at 4.88 ppm (**Figure 3-14**, peak 1) to the methylene signal at 3.77 ppm (**Figure 3-14**, peak 2**)** as DP 112. The DP is usually determined using signal 3 however the solvent THF was often difficult to remove and the THF signals overlap with peaks 3 and 4 (**Figure 3-14**).

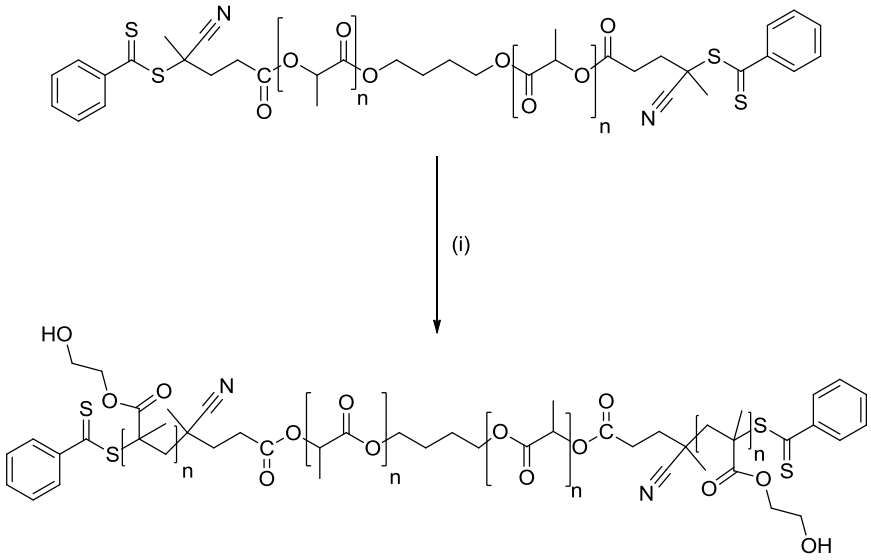

Figure 3-13. Synthesis of $PHEMA_{53}$-PLA_{51}-$PHEMA_{53}$. (i) ACVA 0.25 eq., HEMA 106.0 eq., THF, 70 ^{o}C, 12 h.

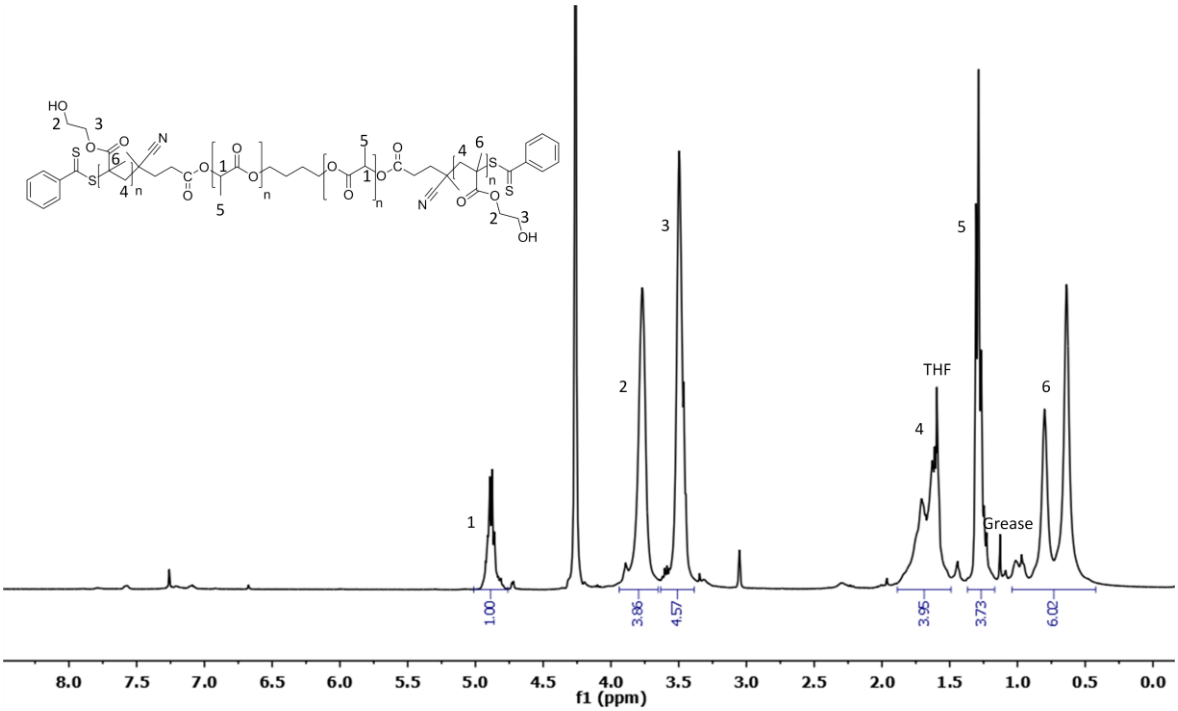

Figure 3-14. ^{1}H NMR spectrum (400 MHz, MeOD-d4/$CDCl_3$ (1:2)) of $PHEMA_{53}$-PLA_{51}-$PHEMA_{53}$.

The M_n of $PHEMA_y$-PLA_{400}-$PHEMA_y$ was also determined by GPC using THF as the solvent and this data (**Table 3-3**) was comparable with M_n determined by ^1H NMR spectroscopy when the DP of PHEMA is small. However, there are larger deviations as the length of the PHEMA blocks increase. Interestingly, for the monomodal trace of $PHEMA_{53}$-PLA_{51}-$PHEMA_{53}$ the M_n obtained by GPC was 53,100 $gmol^{-1}$ which is over double that determined by ^1H NMR spectroscopy. The GPC M_n and dn/dc should be similar to that of the diblock copolymer PLA_{46}-$PHEMA_{100}$. The refractive index (RI) and light scattering (LS) signal are both dependent on the refractive index increment (dn/dc) of the polymer in THF. The dn/dc is the change of the solution refractive index with solute concentration. The dn/dc of the diblock copolymer was 0.093 mg/g which was three times that of the triblock copolymer which was given as 0.027 mg/g. The dn/dc is determined by the length of both the hydrophilic and hydrophobic block length thus the two values would be approximately the same since both the di- and triblock copolymer are composed of similar PLA and PHEMA block lengths; the dn/dc values must be incorrect. The use of an inaccurate concentration or an issue with solubility would lead to differences between dn/dc values.

It has been reported that PHEMA has limited solubility in THF and often the hydroxyl moieties of HEMA/PHEMA are protected by esterification.[191] However, PHEMA-P(MPS)-PHEMA was both synthesized and analyzed using THF without the use of protecting groups.[192] To identify whether THF was affecting the characterization, each block copolymer was reanalyzed utilising GPC in which the solvent used was DMF (**Figure 3-15**). The GPC traces obtained by DMF GPC (**Figure 3-15**) are multimodal and broader in comparison to the GPC curves observed by THF GPC (**Figure 3-14**). The drifting of the baseline observed for the PLA_{46}-$PHEMA_{15}$ GPC trace (**Figure 3-15**) is due to the use of a low concentrated sample. The block copolymers have a broad molecular weight distribution between 1.4-2.25 (**Table 3-3**); based on these results either the synthesis of the PLA-PHEMA block copolymers was not as controlled as the initial GPC traces portrayed or DMF is not an appropriate solvent for analysis of these block copolymers. The polymerization solvent was to be changed to include a more polar component such as ethanol which is known to solubilise the PHEMA homopolymer.

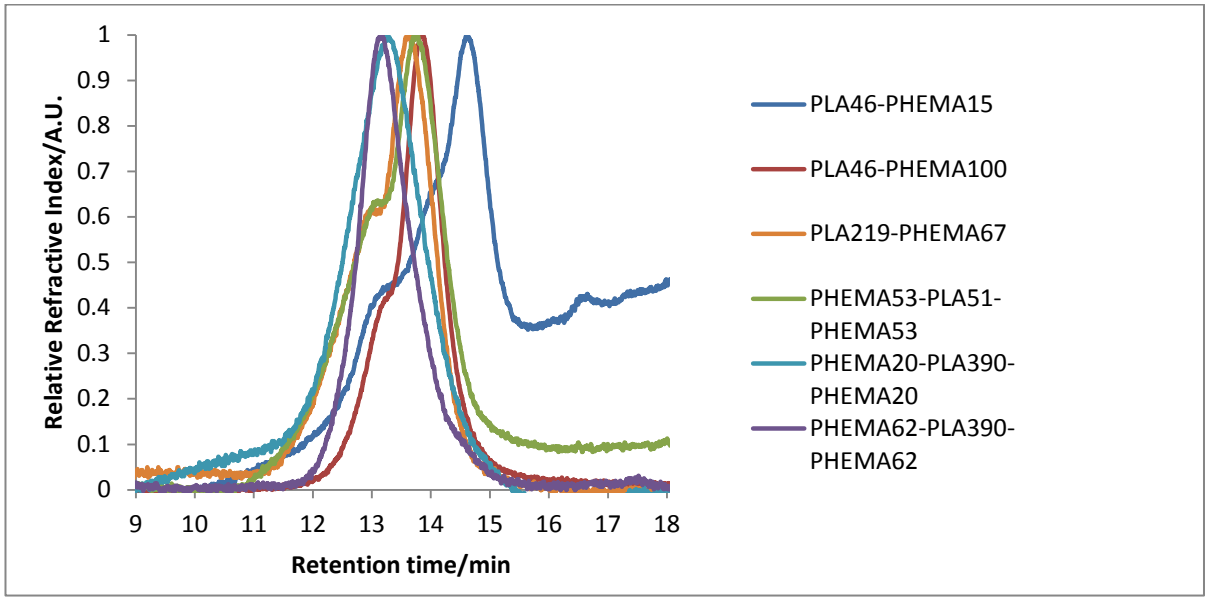

Figure 3-15. GPC traces of PLA_{46}-$PMPC_x$ and $PMPC_x$-PLA_y-$PMPC_x$ block obtained by DMF GPC.

3.6.3 Synthesis of PLA-PHEMA- alternative method

The synthesis of diblock and triblock copolymers was repeated in a mixture of ethanol and THF to investigate whether THF was affecting the polymerization of HEMA in addition to the characterization. The macroRAFT agent was shown in **Figure 3-9** to be stable in this solvent mixture at 70 ^{o}C and these conditions would be a more representative of model system for the synthesis of PLA-PMPC diblock and triblock copolymer.

HEMA was polymerized using PLA_x-R where x= 46 and 197 and R-PLA_y-R where y=181 and 390 under the same conditions described in **Figure 3-10**. Polymerizations were carried out in a 1:1 mixture of THF/ethanol except for when R-PLA_{390}-R was used, a mixture of 6:4 THF:ethanol was required to solubilise the PLA-macroRAFT agent. Block copolymers were analysed using GPC with a conventional calibration using narrow molecular weight distribution polystyrene standard and a dn/dc value of 0.165. The M_n obtained from GPC is comparable with M_n determined by ^{1}H NMR spectroscopy (**Table 3-4**). There still remains a discrepancy between the GPC M_n and ^{1}H NMR M_n of $PHEMA_{50}$-PLA_{51}-$PHEMA_{50}$, however, GPC separates polymer chains based on hydrodynamic volume which in this case is estimated using polystyrene calibrants and can lead to inaccurate M_n. The polymers synthesized give narrower molecular distributions ranging from 1.16 to 1.28 (**Table 3-4**) in comparison to the previous method (PDI = 1.4-2.25). The GPC traces (**Figure 3-16)** are narrow monomodal peaks and in the case of $PHEMA_{50}$-PLA_{51}-$PHEMA_{50}$ a high molecular weight shoulder was observed.

PLA-PHEMA di- and triblocks have been successfully synthesized by the chain extension of the PLA-macroRAFT agents with HEMA. The polymerizations were shown to be controlled generating block copolymers with a low polydispersity range. In the mixed solvent system of THF and ethanol, the PLA-macroRAFT is shown to be stable under RAFT conditions and both components of the block copolymer are solubilised which are important factors for the synthesis of the target PLA-PMPC block copolymers. Therefore the methodology established for the PLA-PHEMA system should overcome the problems experienced with the initial synthetic method for PLA-PMPC block copolymers.

Table 3-4. Molecular weight data for PLA-PHEMA/PHEMA-PLA-PHEMA block copolymers prepared by alternative method.

PLA Polymer	Conv. (%)	f_{HEMA}	$M_{n,\ Thr.}$[d]	M_n[e] (^{1}H NMR)	M_n[f] (GPC)	PDI[e]	Yield (%)
PLA_{46}-$PHEMA_{100}$[a]	77	0.78	16700	13900	18000	1.17	81
PLA_{197}-$PHEMA_{60}$[b]	85	0.35	22300	21200	21500	1.16	71
$PHEMA_{50}$-PLA_{51}-$PHEMA_{50}$[a]	73	0.75	17300	14200	23800	1.28	70
$PHEMA_{25}$-PLA_{181}-$PHEMA_{25}$[a]	60	0.32	20200	17300	23300	1.21	73
$PHEMA_{25}$-PLA_{181}-$PHEMA_{25}$[b]	58	0.32	20200	17800	21300	1.22	78
$PHEMA_{40}$-PLA_{390}-$PHEMA_{40}$[c]	37	0.27	39100	31600	29200	1.27	79

[a]RAFT polymerization performed in THF/ethanol (1:1) at 70 ^oC for 12 h.

[b] RAFT polymerization performed in THF/ethanol (1:1) at 70 ^oC for 24 h.

[c]RAFT polymerization performed in THF/ethanol (6:4) at 70 ^oC for 24 h.

[d]M_n value for 100 % conversion of monomer

[e]Molecular weight determined by ^{1}H NMR in MeOD-d4/$CDCl_3$(1:2)

[f]Molecular weight data obtained by DMF GPC using RI detector. Calibrated with a series of narrow polydispersity PS standards. Sample concentration used was ~1mg/ml.

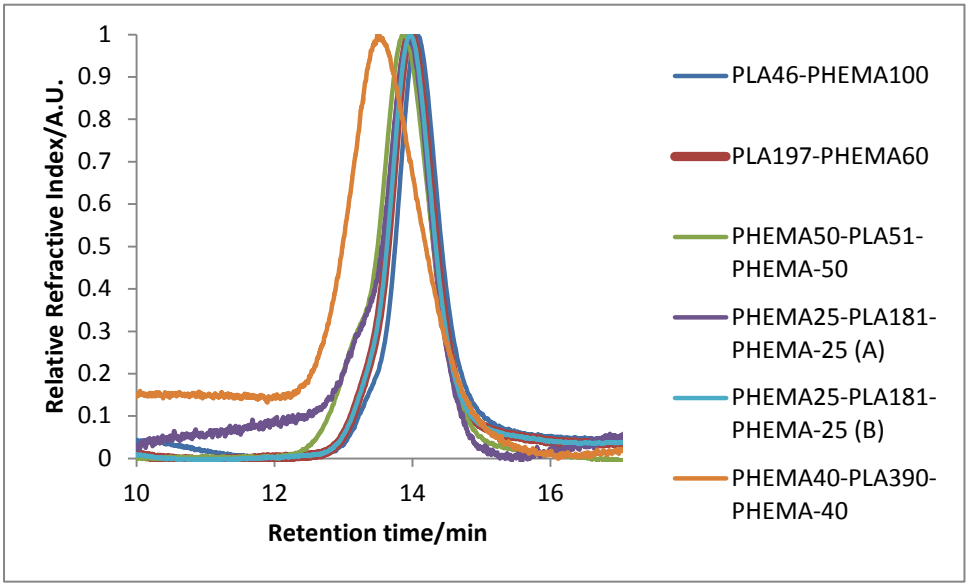

Figure 3-16. GPC traces of PLA_x-$PMPC_y$ and $PMPC_y$-PLA_x-$PMPC_y$ block copolymers prepared by alternative method.

3.7 Synthesis of PLA-PMPC block Copolymers

The PLA-PHEMA model system aided the derivation of a synthetic methodology for the synthesis of PLA-PMPC block copolymers. PLA_{46}-$PMPC_x$ was synthesized following conditions described in **Figure 3-17** varying the targeted MPC block length; x=25 and 100. Generally the polymerization was quenched at 12 h after reaching high levels of conversion. The polymer was purified by precipitation into THF to remove unreacted PLA macroRAFT agent, the precipitate was dissolved in methanol and dialysed to remove residual monomer. The ^{1}H NMR spectrum of the purified polymer is given in **Figure 3-18**, the M_n of the block copolymer was determined as described in section **3.5**.

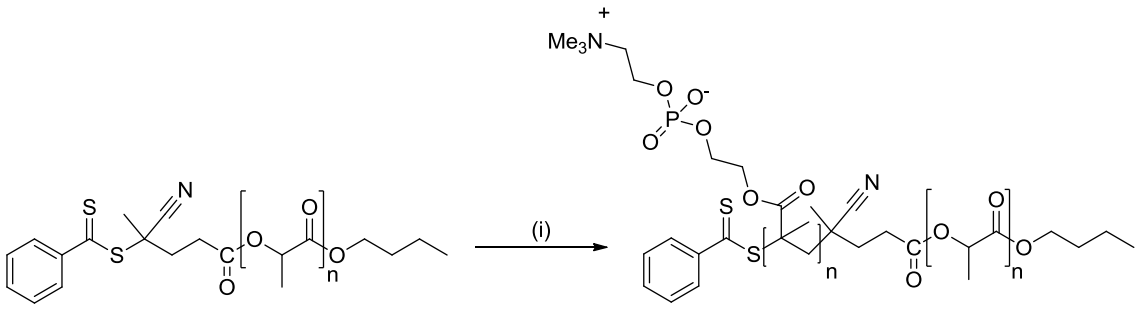

Figure 3-17. Synthesis of PLA_{46}-$PMPC_{100}$. (i) ACVA 0.25 eq., MPC 100.0 eq., ethanol/THF (1:1), 70 ^{o}C, 12 h.

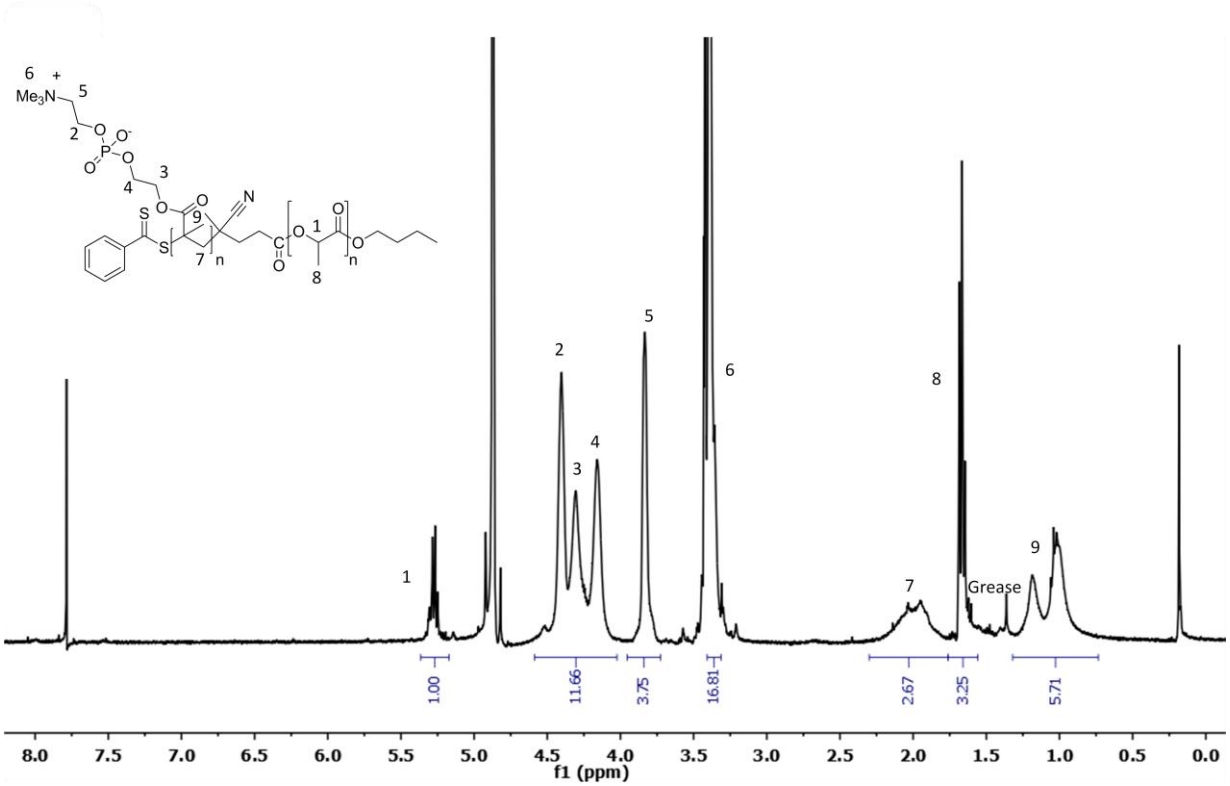

Figure 3-18. ^{1}H NMR spectrum (400 MHz, MeOD-d4/$CDCl_3$ (2:1)) of PLA_{46}-$PMPC_{100}$.

The molecular weight data for MPC based diblock copolymers (**Table 3-5)** was obtained via GPC with an RI detector using a mixture of methanol/chloroform (1:3) as the solvent. **Table 3-5** highlights the discrepancies observed between the M_n determined by ^{1}H NMR spectroscopy and GPC analysis. The M_n obtained by GPC for the diblock copolymer PLA_{46}-$PMPC_{25}$ is approximately the same as that of PLA_{46}-$PMPC_{100}$. Given the symmetric weight distribution of polymer chains (**Figure 3-24**) the M_n obtained by ^{1}H NMR spectroscopy can be taken as a more reliable value. The GPC M_n is determined by the hydrodynamic volume of the polymer chain which is itself partly determined by the conformation of the polymer. Conventional calibration requires that the hydrodynamic volume of the polymer sample and standard are comparable, if they are not this results in an inaccurate M_n. However, the GPC can still provide a measure of the polydispersity of the sample as the PDI is a ratio of M_w to M_n. The diblock copolymers synthesized possess narrow molecular weight distributions ranging from 1.16-1.21, these polymers prepared previously by a combination of ROP and ATRP have been reported with PDIs ranging from 1.18-1.52.[42, 44]

Table 3-5. Molecular weight data for PLA-PMPC/PMPC-PLA-PMPC block copolymers.

Block Copolymer	Conv. (%)	f_{MPC}	$M_{n, Thr.}$[d]	M_n[e] (^{1}H NMR)	M_n[f](GPC)	PDI[f]
PLA_{46}-$PMPC_{25}$[a]	93	0.67	11000	13400	18000	1.16
PLA_{46}-$PMPC_{25}$[b]	92	0.67	11000	12800	18400	1.15
PLA_{46}-$PMPC_{100}$[a]	91	0.89	33200	33500	19300	1.21
PLA_{46}-$PMPC_{100}$[b]	83	0.89	33200	29500	19400	1.24
$PMPC_{53}$-PLA_{51}-$PMPC_{53}$[a]	85	0.88	35600	33800	24600	1.24
$PMPC_{55}$-PLA_{390}-$PMPC_{55}$[c]	72	0.53	61200	52900	44800	1.36

[a] RAFT polymerization performed in THF/ethanol (1:1)

[b] RAFT polymerization performed in DMSO/IPA (3:7)

[c] RAFT polymerization performed in THF/ethanol (6:4)

[d] Mn value for 100 % conversion of monomer

[e] Molecular weight determined by ^{1}H NMR in MeOD-d4/$CDCl_3$(2:1)

[f] Molecular weight data obtained by methanol/chloroform (1:3) GPC using RI detector. Calibrated with a series of narrow polydispersity polymethylmethacrylate standards. Sample concentration used was ~1mg/ml.

It was shown in section 3.5 that the PLA-macroRAFT agent was stable in DMSO at high temperatures. The polarity of DMSO is significantly higher than THF, and would be more effective at solubilising the PMPC block, thus another solvent mixture was utilised to potentially increase control over the polymerization of MPC. A mixture of DMSO/isopropanol (3:7) was also utilised for the synthesis of PLA_{46}-$PMPC_x$ diblock copolymers. The polymers obtained in DMSO/IPA possessed a narrow molecular weight distribution with a PDI range of 1.15-1.24. **Table 3-5** shows little difference between the PDI of polymers synthesized in a DMSO/IPA and THF/ethanol mixture and thus MPC based triblock copolymers would be synthesized using a THF/ethanol mixture which can be more easily removed during purification of the polymer than DMSO.

Triblock copolymers $PMPC_{53}$-PLA_{51}-$PMPC_{53}$ and $PMPC_{55}$-PLA_{390}-$PMPC_{55}$ were synthesized as described in **Figure 3-20** utilizing bifunctionalized PLA-macroRAFT agents with a DP of 51 and 390. The polymerization method is analogous to that utilised

for the synthesis of PLA-PMPC diblock copolymer, however, a solvent mixture of THF/ethanol (6:4) was utilised for the chain extension of R-PLA_{390}-R. The ratio of the first triblock copolymer was chosen for comparing the self-assembly behaviour with the diblock copolymer PLA_{46}-$PMPC_{100}$ with the same f_{MPC} target. The composition of the latter was chosen to compare the self-assembly of triblock copolymers with varying PLA block lengths. The ^{1}H NMR spectrum of the purified polymer $PMPC_{53}$-PLA_{51}-$PMPC_{53}$ is given in **Figure 3-21**, the M_n of the block copolymer was determined as described in section **3.5**. The molecular weight data is given in **Table 3-5**, the polymerizations were shown to be controlled with PDI's of 1.24 and 1.36. The higher PDI of 1.36 is likely due to the increased PLA block length of the macroRAFT agent.

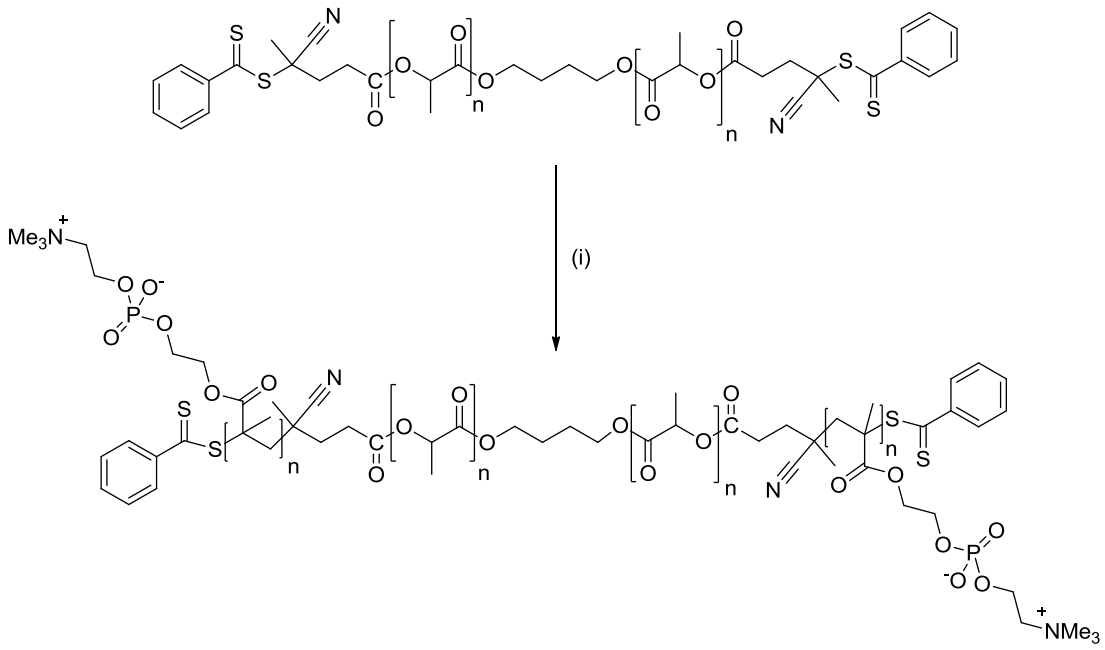

Figure 3-19. Synthesis of $PMPC_{100}$-PLA_{51}-$PMPC_{100}$. (i) ACVA 0.25 eq., MPC 106.0 eq., ethanol/THF (1:1), 70 ^{o}C, 24 h.

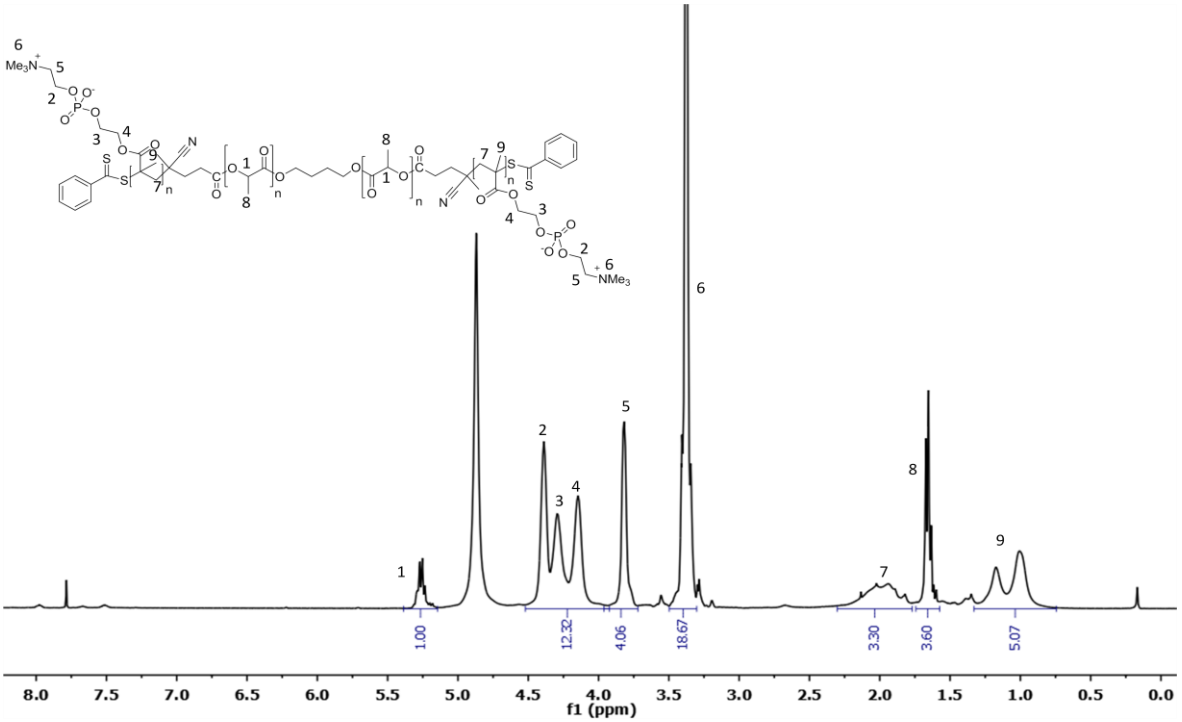

Figure 3-20. ^{1}H NMR spectrum (400 MHz, MeOD-d4/$CDCl_3$ (2:1)) of $PMPC_{53}$-PLA_{51}-$PMPC_{53}$.

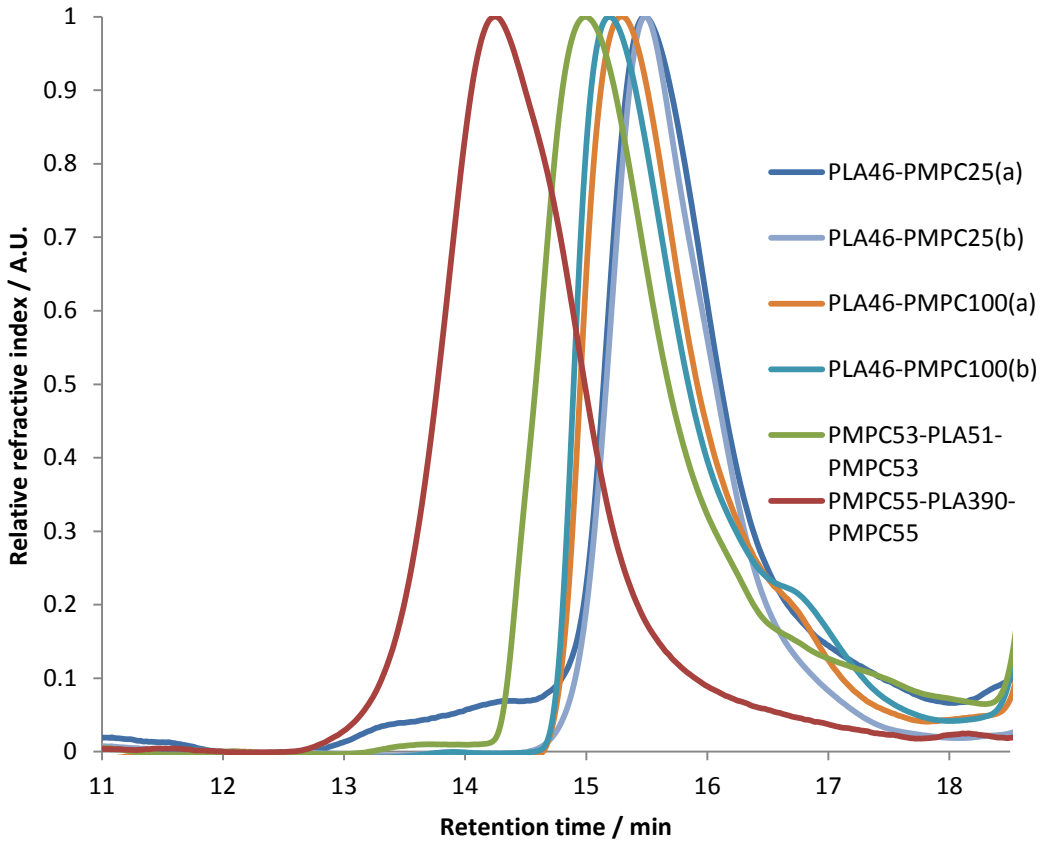

Figure 3-21. GPC traces of PLA_{46}-$PMPC_x$ and $PMPC_x$-PLA_y-$PMPC_x$ block copolymers prepared by alternative method.

3.8 Conclusions

The RAFT agent BSTSE was shown not to effectively control the polymerization of methacrylates and therefore PLA-PMPC cannot be synthesized using the BSTSE end capped PLA macroRAFT agent. PLA-macroRAFT agents with CPADB end groups were chain extended with MPC in a solvent mixture of methanol and DMSO at elevated temperatures, however, the PLA macroRAFT agent was subject to hydrolysis which was evidenced by ^{1}H NMR spectroscopy. The synthesis of PLA-PHEMA block copolymers was used as a model polymerization to determine the conditions required for the synthesis of the target polymer, PLA-PMPC. Chain extension of both PLA macroRAFT agents PLA-R and R-PLA-R with MPC was successful in a mixture of THF and ethanol dependent on the DP of the PLA macroRAFT agent. A range of diblock and triblock copolymers of PLA-PMPC with varied compositions were synthesized with narrow molecular weight distributions ranging from 1.15-1.36.

4. Self-Assembly of PLA block Copolymers

4.1 Self-Assembly of Block Copolymers

The morphology of self-assembled structures is predominantly determined by the critical packing parameter p=v/al, where v is the hydrophobic volume, a is the maximum area of the hydrophilic chain and l is the length of the hydrophobic block.[156, 168] The critical packing parameter has proved effective at predicting various morphologies: when p is less than ⅓, micelles are obtained, when p falls between ½ and ⅓, cylindrical micelles are formed; and vesicles were observed when p is approximately 1 (**Figure 4-1**).[156, 193] Inverted structures are formed when p is greater than 1.[156] The morphologies of aggregates in solution are influenced by several factors including the stretching ability of the core block, the repulsive interactions between the corona forming block and the interfacial tension between the micelle core and the solvent outside the core.[153, 155, 156] These factors can be controlled by varying several parameters; temperature, additives, preparation method of aggregates, block length and concentration. [153, 156]

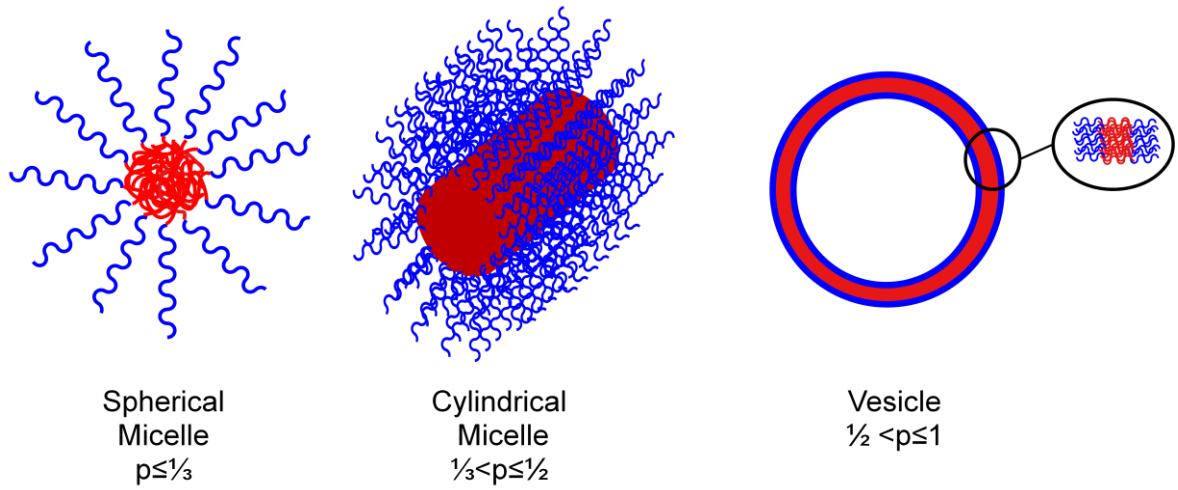

Figure 4-1. Self-assembly of block copolymers, defined by the packing parameter, into spherical micelles, cylindrical micelles and vesicles.[168, 193]

4.2 Self-Assembly of PLA-PHEMA Block Copolymers

4.2.1 Copolymer Composition

PLA-PHEMA block copolymers possess similar properties to the target system of PLA-PMPC being both partially biodegradable and demonstrating excellent blood compatibility such properties are of interest for biomedical applications e.g. drug delivery. The self-assembly of PLA-PHEMA has not to our knowledge been investigated. The morphogenic effects of copolymer composition, the preparation method and temperature on PLA-

PHEMA aggregates were examined. The effects of copolymer composition were investigated using a range of diblock and triblock copolymers. The aggregates were prepared by the solvent swap method (i.e. the addition of water to the polymer solution or *vice versa*) which will now be referred to as nanoprecipitation. The block copolymer was dissolved in a solvent mixture of THF/methanol (1:1) ensuring both blocks were solubilised before water was slowly added inducing self-assembly to give a final concentration of 1 mg/ml. THF and methanol were removed gradually by evaporation. The morphology and size of the aggregates formed were analysed by transmission electron microscopy (TEM) using 1 %(w/v) aqueous uranyl acetate and dynamic light scattering (DLS) (**Table 4-1**). The morphologies observed for the self-assembly of diblock copolymers have generally been shown to follow the trends proposed by Discher and Eisenberg in which amphiphilic molecules which possess a hydrophilic weight fraction (*f*) = 35±10% are expected to form vesicles, *f*>45% self-assemble into micelle structures and *f*<25% results in inverted microstructures.[189]

PLA-PHEMA diblock copolymers of varied composition were prepared to target different morphologies. Vesicles enable the delivery of both hydrophilic and hydrophobic compounds e.g. dyes and drugs, whereas the core of micelles can encapsulate hydrophobic drugs for the delivery.[194, 195] Block copolymers with a hydrophilic weight fraction (*f*) of 0.75 and 0.32 were studied and shown to self-assemble in water to form spherical aggregates. PLA_{46}-$PHEMA_{79}$ yielded aggregates with a broad diameter range of 127-242 nm determined by TEM (**Figure 4-2A**). An enlarged image (**Figure 4-2B**) illustrates that the larger aggregates are composed of smaller micelles with a diameter range of 13-19 nm. Micelles were expected based on the higher $f_{HEMA.}$ DLS revealed a dual distribution; the diameter range of the predominant particle size 244-275 nm, the individual micelles were not detected by DLS (**Figure 4-4**) which suggests aggregation is extensive through the solution. The diameter determined by TEM is often smaller than that obtained by DLS due to dehydration caused by solvent evaporation, which could explain the discrepancy between the particle size determined by TEM (127-242 nm) of that by DLS (244-275 nm).

Lowering f_{HEMA} resulted in the formation of associating aggregates similar to that observed for PLA_{46}-$PHEMA_{79}$ (**Figure 4-2C**). The smaller aggregates were identified as micelles by TEM, which possessed a narrow diameter range 24-32 nm. The individual micelles were not detected by DLS. DLS studies did, however, detect two size distributions corresponding to micellar aggregates; the predominant particle size was 121-145 nm with a narrow size distribution (**Figure 4-4**). 'Higher order' morphologies were targeted by

increasing the hydrophobic block length, however, aggregation of micelles were formed exclusively. Longer block copolymers with a higher PLA content are known to precipitate faster upon the addition of water leading to the formation of smaller aggregates.[196] Similar TEM images were observed for aggregates of ethylene cellulose-graft-PHEMA and amphiphilic chitosan based block copolymers which were explained by strong interactions between hydroxyl groups.[197, 198] Additionally Holder *et al.* obtained aggregating micelle clusters for the self assembly of PHEMA-PMPS-PHEMA triblock copolymer.[192]

ABA block copolymers based on PEG-PLA-PEG have demonstrated great promise as drug delivery vehicles due to their increased stealthiness i.e. inability to be detected by the immune system and higher PEG density due to their U-shaped conformation.[199, 200] PEG-PLA-PEG has also been shown to generate smaller particles than their BAB counterparts with similar LA/EG ratio; the average diameter for ABA type polymer (109±4.6 nm) was approximately twice that of the BAB type polymer (215±12.2 nm).[199, 200] With respect to vesicle formation ABA block copolymer can adopt two possible conformations; I-shape in which the hydrophilic segments are at opposite sides of the membrane and U-shape in which a curved loop forms; the hydrophilic segments are pointed towards the outside of the membrane.[169] Additionally PLA-PEG ABA polymers have been shown to have higher entrapment efficiencies and can repel protein adsorption more effectively than AB or BAB block copolymers.[200] For these reasons several triblock copolymer were synthesized. ABA block copolymers are expected to self-assemble to form micelles but by changing the block copolymer composition we aim to observe higher order morphologies.[192, 201]

The self-assembly of triblock copolymers PHEMA-PLA-PHEMA with f_{HEMA} = 0.09, 0.24 and 0.72 prepared by nanoprecipitation was thus studied. $PHEMA_{11}$-PLA_{390}-$PHEMA_{11}$ which possesses the longest PLA block length yielded vesicles as evidenced by the TEM (**Figure 4-2D**) characterised by the darker outer ring which represents the bilayer. Vesicles were formed with a broad diameter range of 39-173 nm which is comparable with that measured by DLS, in which a dual distribution was observed; size distributions with a diameter range of 59-69 nm and 136-166 nm (**Figure 4-5**). Vesicle formation was not expected, however, a reduced hydrophilic block length can lead to an increase in aggregation number resulting in an increase in core size and stretching of the PLA chains resulting in larger aggregates. The self-assembly of $PHEMA_{16}$-PLA_{181}-$PHEMA_{16}$ with a similar f_{HEMA} to the diblock copolymer PLA_{197}-$PHEMA_{51}$ resulted in the formation of associating micelles as expected (**Figure 4-3C**) with a diameter range of 58-118 nm determined by TEM which is similar to that obtained by DLS (**Figure 4-5**). The broad size

distribution between 350-450 nm demonstrates the occurrence of aggregation in solution (**Figure 4-5**). The range of f_{HEMA} selected saw the formation of both micelles commonly associated with ABA systems and also achieved higher order structures. No trends were observed based on the f_{HEMA}; further analysis of the self-assembly of triblock copolymers is required investigating differences between triblocks with a constant hydrophobic block length. Holder *et al*. showed that larger aggregates formed when the hydrophilic block length was increased for POEGMA-PMPS triblock copolymers.[192] The f_{HEMA} was increased to 0.72 for $PHEMA_{38}$-PLA_{51}-$PHEMA_{38}$. TEM analysis showed the formation of a mixture of vesicles and aggregating micelles (**Figure 4-3A**). The vesicles were small with a diameter range of 40-96 nm. Aggregating micelles (**Figure 4-3B**) were observed which were also formed by the diblock copolymer with a similar f_{HEMA} value. The diameter range determined by TEM for the individual micelles was 42-102 nm which was in agreement with that determined by DLS (**Figure 4-5**). The coexistence of different morphologies can arise due to the broad polydispersity of the block copolymer or can be a thermodynamic phenomenon whereby the free energy difference between different morphologies is small.[159] The PDI of this triblock copolymer was broader than the other block copolymers synthesized, with a PDI of 1.28 giving rise to the mixture of aggregates observed. The morphologies for both di-and triblock copolymers shown by TEM are 'real', these structures were observed extensively across the carbon grids and the diameters measured were generally in agreement with those obtained by DLS.

Table 4-1. Nanoprecipitation of PLA-PHEMA block Copolymers-Aggregate Morphologies and Particle Size from TEM

Block Copolymer[a]	f_{HEMA}	**Diameter Range**[b] **(nm)**	**Morphology**[c]	**Soln Appearance**[d]
PLA_{46}—$PHEMA_{79}$	0.75	13-19, 190-354	Micellar Aggregates	Opaque
PLA_{197}-$PHEMA_{51}$	0.32	24-32, 213-224	Micellar Aggregates	Translucent Blue
$PHEMA_{11}$-PLA_{390}-$PHEMA_{11}$	0.09	39-173	Vesicles	Translucent Blue
$PHEMA_{16}$-PLA_{181}-$PHEMA_{16}$	0.24	58-118	Spherical	Translucent Blue
$PHEMA_{38}$-PLA_{51}-$PHEMA_{38}$	0.72	42-102, 40-96	Micelle/ Vesicle	Translucent Blue

[a]Self-assembled structures prepared by the slow addition of water to a solution of polymer in THF/methanol (1:1). The polymer concentration of each solution was 1 mg/ml.

[b]Diameter range determined by TEM

[c] Morphology observed by TEM

[d] The appearance of the solution indicates particle size. An opaque solution is a result of increased scattering from larger size aggregates

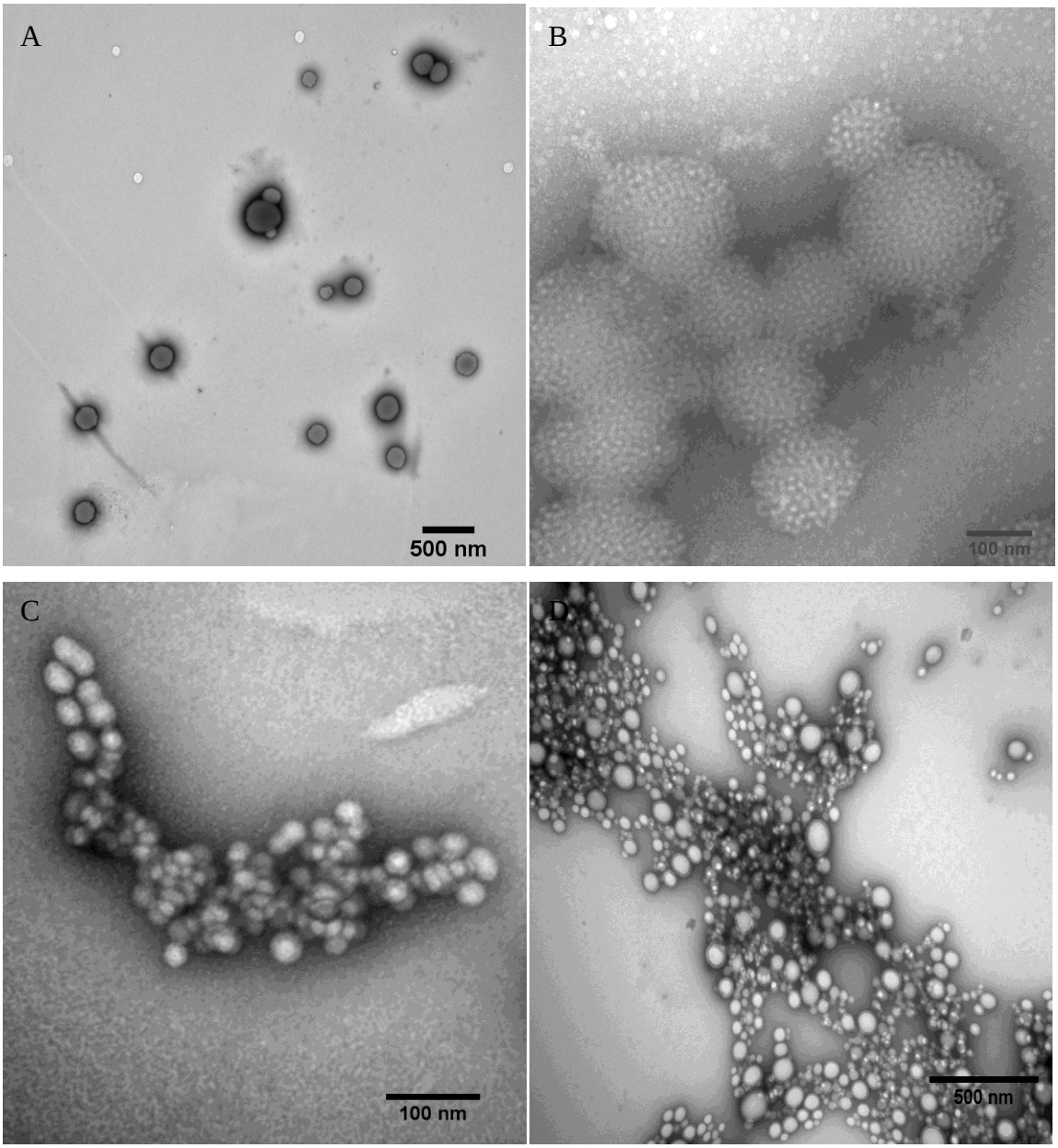

Figure 4-2. TEM images obtained for negatively stained spherical aggregates prepared by nanoprecipitation of (A) PLA_{46}-$PHEMA_{79}$ and (B) an enlarged TEM image of the spherical aggregates in (A), (C) PLA_{197}-$PHEMA_{51}$ (D) vesicles formed from $PHEMA_{11}$-PLA_{390}-$PHEMA_{11,}$

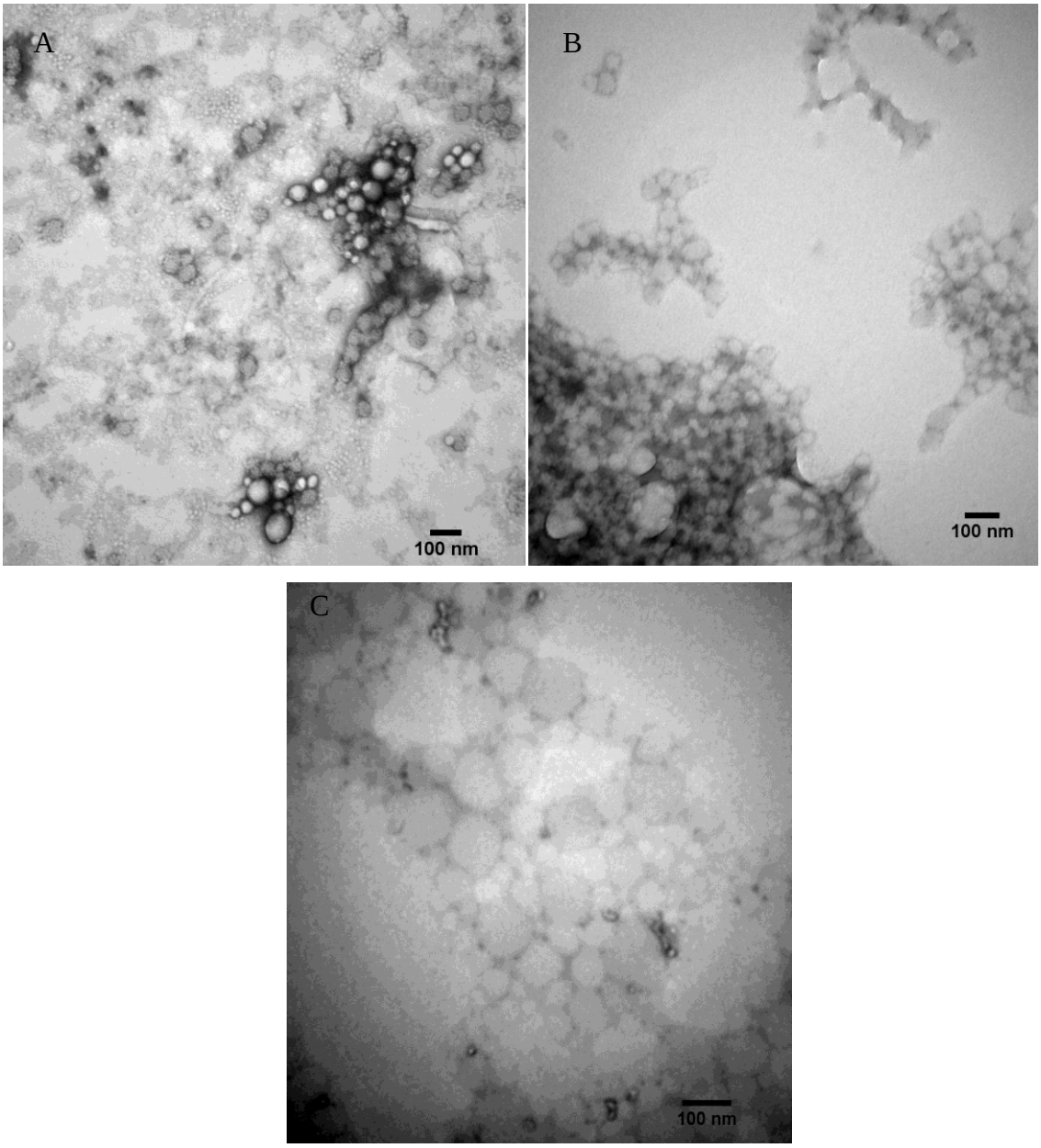

Figure 4-3. TEM images for negatively stained spherical aggregates prepared by nanoprecipitation (A) spherical aggregates formed from $PHEMA_{38}$-PLA_{51}-$PHEMA_{38}$ (B) Micelle clusters formed from $PHEMA_{38}$-PLA_{51}-$PHEMA_{38}$, (C) $PHEMA_{16}$-PLA_{181}-$PHEMA_{16}$.

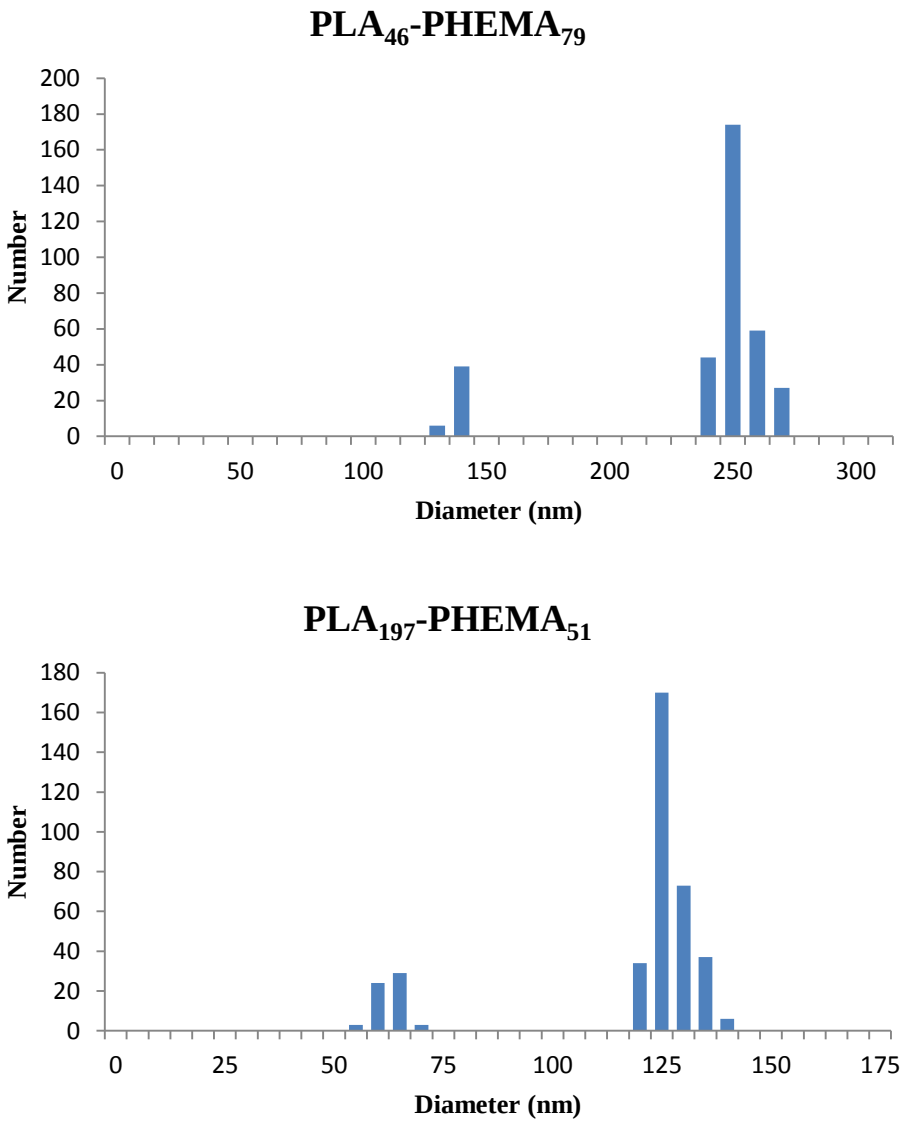

Figure 4-4. DLS results for PLA-PHEMA diblock copolymers (1 mg/ml) prepared by nanoprecipitation.

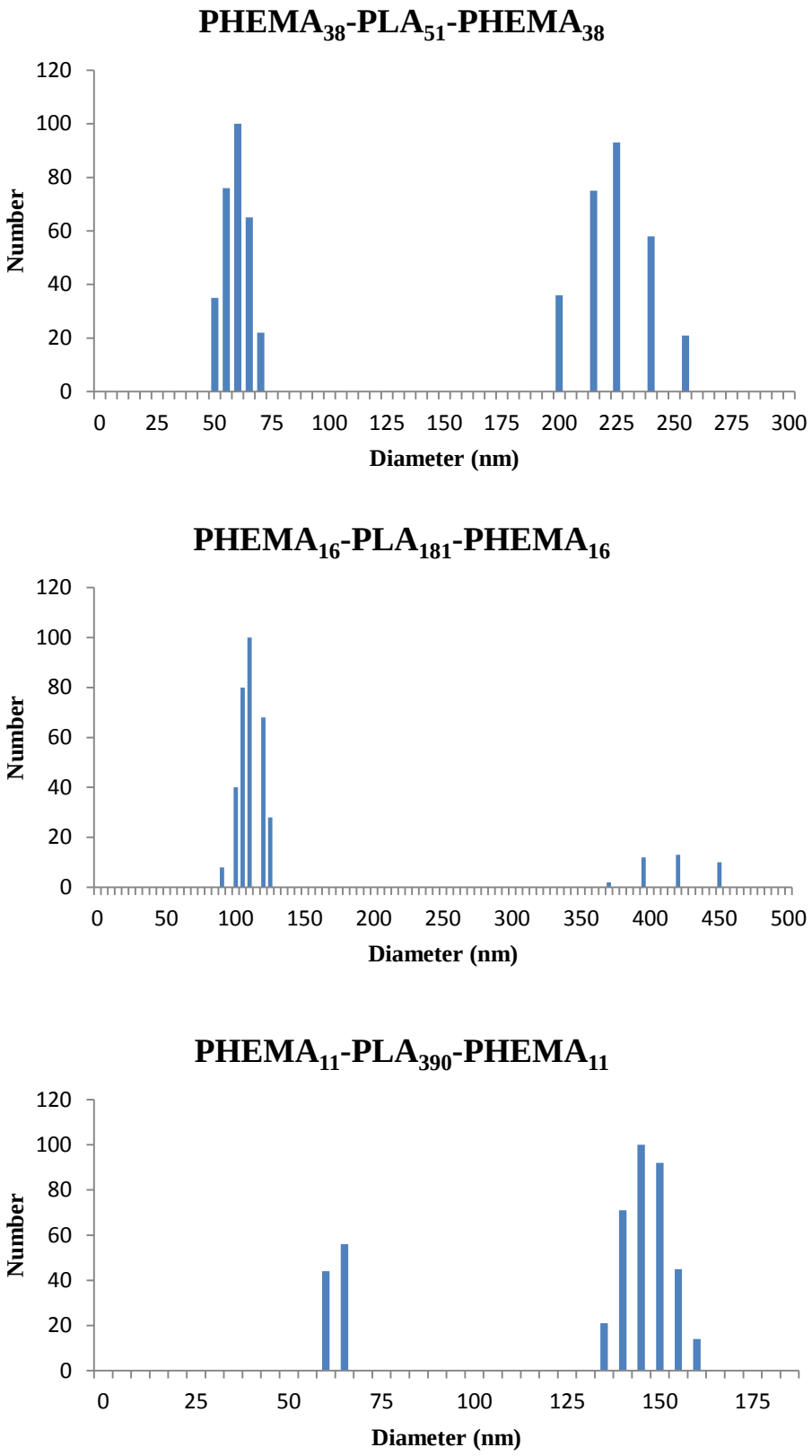

Figure 4-5. DLS results for PLA-PHEMA triblock copolymers (1 mg/ml) prepared by nanoprecipitation.

4.2.2 Alternative Methods of Self-Assembly

The initial self-assembly study showed that the two diblock copolymers PLA_{46}-$PHEMA_{79}$ and PLA_{197}-$PHEMA_{51}$ and a triblock copolymer $PHEMA_{16}$-PLA_{181}-$PHEMA_{16}$ were all shown to form micellar structures. These three block copolymers were selected to investigate the morphogenic effects of alternative methods for aggregate preparation in order to observe different morphologies. Aggregates were prepared via three methods: nanoprecipitation; the addition of water to the polymer dissolved in acetone, a common solvent for both blocks; and the reverse addition approach. The order of addition with respect to nanoprecipitation is important, the addition of the polymer in a water miscible solvent to a large volume of water results in an increased rate of precipitation in comparison to the reverse addition leading to the formation of smaller particles.[196] Aggregates were also prepared by dissolving the polymer in an alternative common solvent, DMSO which is favourable for both segments. The solvent was removed by exchange with water via dialysis over a 24 h period. The particle size data obtained by DLS and TEM for the self-assembled structures are summarized in **Table 4-3**.

The common solvent determines the nature of the polymer solvent interaction which influences the coil dimensions and as a result the degree of core stretching.[202] The polymer solvent interaction is dependent on both the solubility parameter of the polymer and solvent in addition to the dielectric constant of the solvent (**Table 4-2)**.[202] From **Table 4-2** it can be concluded that the interaction between PLA and the solvent is stronger in acetone than in DMSO, the closer the solubility parameter of the polymer and solvent the greater the dissolution of the polymer. Due to the polarity of PHEMA, the polymer solvent interaction is dependent on the dielectric constant therefore the strength of the PHEMA-solvent interaction is greater in DMSO than in acetone.[196] At the beginning of self-assembly the core during the water addition becomes more swollen when the solvent favours the core forming block.[202] As the core becomes more swollen the degree of core chain stretching increases which is entropically unfavourable and the penalty for high stretching leads to changes in morphology in order to reduce the free energy of micellization.[153] The degree of core chain stretching decreases in order of spherical to cylindrical to vesicle morphologies.[202]

Table 4-2. Solvent and Polymer Physical Properties[203, 204]

Solvent/Polymer	Solubility Parameter$(J/cm^3)^{1/2}$	Dielectric Constant
Acetone	20.1	20.7
DMSO	29.7	46.7
Water	47.9	80.1
PLA	19.2-21.0	
PHEMA	27.5	

Table 4-3. Alternative Methods for the Self-Assembly of PLA-PHEMA Block copolymers-Aggregate Morphologies and Particle Size from TEM

Block Copolymer	Method[a]	f_{HEMA}	Diameter Range (nm) [b]	Morphology[c]	Soln Appearance
PLA_{46}-$PHEMA_{79}$	1	0.75	12-18	Micelles	Translucent Blue
	2		10-14, 39-125	Micelles, Vesicles	Opaque
	3		15-23	Micelles	Translucent Blue
PLA_{197}-$PHEMA_{51}$	1	0.32	90-126 (Cluster)	Micelles, aggregating clusters	Translucent Blue
	2		34-48	Micelles, aggregating clusters	Translucent Blue
	3		___	___	Translucent Blue
	4		41-55	Micelles, aggregating clusters	Translucent Blue
$PHEMA_{16}$-PLA_{181}-$PHEMA_{16}$	1	0.24	___	___	Translucent Blue
	2		31-43	Micelles, aggregating clusters	Translucent Blue
	3		27-45	Micelles, aggregating clusters	Translucent Blue
	4		63-139	Micelles, Vesicles	Translucent Blue

[a]Aggregates of PLA-PHEMA block copolymers were prepared via several methods; (1) dialysing the block copolymer in DMSO against water, (2) the slow addition of water to the polymer dissolved in acetone, (3) the

slow addition of the polymer in acetone to water, (4) heating aggregates prepared by method (2) at 80°C for 2h before cooling rapidly. The polymer concentration of each solution was 1 mg/ml.

[b]Diameter range determined by TEM

[c]Morphology observed by TEM

The self-assembly of PLA-PHEMA via nanoprecipitation is evidenced by ^{1}H NMR spectroscopy, **Figure 4-6** shows the ^{1}H spectrum of the block copolymer in $CDCl_3$/MeOD and in D_2O demonstrating the loss of PLA signals. The self-assembly of PLA_{46}-$PHEMA_{79}$ by nanoprecipitation (addition of water to polymer solution) yielded vesicles the target morphology and structures similar to that observed in **Figure 4-2B**; large aggregates (**Figure 4-7B**) composed of micelles which is more apparent in the enlarged TEM image (**Figure 4-7C**). The aggregates identified by TEM were larger than previously measured with a diameter range of 300-900 nm. Vesicles (**Figure 4-7A**) were observed with a broad diameter range of 39-125 nm. DLS measured a narrowly disperse population ranging between 350-404 nm (**Figure 4-9A**). By reversing the addition i.e. addition of polymer solution to water, micelles were formed exclusively with a diameter range of 15-23 nm measured by TEM (**Figure 4-7D**) which was expected under kinetic control. The TEM images shown in **Figure 4-7** show a layering which is a drying effect of the dye on the grid. DLS detected larger aggregates with a diameter range of 151-171 nm (**Figure 4-9B**). Dialysis-induced self-assembly of PLA_{46}-$PHEMA_{79}$ was shown to have little effect on the morphology of the self-assembled structures. Similarly to those observed previously the micelles appear to be interacting, forming larger aggregates (**Figure 4-8**), which are detected by DLS with a particle size range of 208-275 nm (**Figure 4-9C**). Larger aggregates were expected due to the slower mixing rates of DMSO with water, however, the result is in keeping with the dependence on the compatibility between blocks and the solvents calculated by Hildebrand solubility parameters. The self-assembly study has demonstrated the morphogenic effect of solvent; utilising a solvent which interacts strongly with the hydrophobic block had resulted in the formation of vesicles in contrast to DMSO which yielded micelles which is attributed to the greater mobility of PLA chains and swelling of the core of the micelle in acetone.

The self-assembly of PLA_{197}-$PHEMA_{51}$ via the addition of water to the polymer solution yielded clustered micelles (**Figure 4-10A**) which are more visible in the enlarged TEM image (**Figure 4-10B**). The clusters are detected by DLS but not the individual micelles (**Figure 4-11A**). The diameter range of the micelle clusters formed was determined by TEM as 90-126 nm which is comparable with that determined by DLS (**Figure 4-11A**). With the polymer possessing a longer hydrophobic block and using acetone as the common

solvent; vesicles were the targeted morphology however micelles formed exclusively. The overriding factor in determining the morphology of the diblock copolymers must be the length of the hydrophobic block; longer PLA chains are prone to faster precipitation leading to smaller aggregates.[196] Reverse addition was analyzed by DLS alone, two particle distributions were observed with a diameter range of 105-127 nm and 224-261 nm (**Figure 4-11B**). The morphology observed does not differ from the previous method based on DLS results although in this case micelle structures were expected due to rapid precipitation. The self-assembly of the block copolymer by dialysis resulted in the same morphology; aggregation of micelle clusters, with a diameter range of 87-91 nm (**Figure 4-10C, 4-10D**) which was comparable with that determined by DLS (**Figure 4-11C**). The frequency of micelle clusters is lower than that observed by nanoprecipitation due to the change of concentration upon dialysis. DMSO was utilised to obtain larger aggregates, however, similarly to PLA_{46}-$PHEMA_{79}$ micelle structures were formed. The aggregates formed from PLA_{197}-$PHEMA_{51}$ were reproducible by each method.

The triblock copolymer $PHEMA_{16}$-PLA_{181}-$PHEMA_{16}$ self-assembled via the addition of the. aqueous phase to the polymer solution, to form micelle clusters (**Figure 4-12A, 4-12B**) similar to that of the diblock copolymer PLA_{197}-$PHEMA_{51}$. The diameter range was determined by TEM for the individual micelles as 31-43 nm and the micelle clusters as 104-138nm which was detected by DLS (**Figure 4-13A**). The self-assembly of $PHEMA_{16}$-PLA_{181}-$PHEMA_{16}$ via nanoprecipitation is further demonstrated by ^{1}H NMR spectroscopy; **Figure 4-14** shows a ^{1}H NMR spectrum of the block copolymer in D_2O showing the absence of PLA signals. Reversing the addition for nanoprecipitation resulted in the aggregation of micelles (**Figure 4-12C, 4-12D**) producing a different aggregate structure from the previous self-assembled structures observed for $PHEMA_{16}$-PLA_{181}-$PHEMA_{16}$. The predominant size distribution measured by DLS was 127-221 nm (**Figure 4-13B**), and the width of these structure as measured by TEM as 27-45 nm. The larger particle sizes (> 400 nm) observed were a result of aggregation (**Figure 4-13B**). The self-assembly of the triblock by dialysis was unsuccessful as mass precipitation occurred which was not observed during the self-assembly of the diblock copolymers. As stated in section **4.2.1** ABA block copolymers tend to form micelles via a U-shape structure and the self assembly of the triblock with f_{HEMA} of 0.24 has been shown to be reproducible for each method used for aggregate preparation. The self-assembly of the triblock copolymer has a greater dependency on the block copolymer composition than the methods used for the preparation of aggregates. The structures of di-and triblock copolymers observed by TEM were present across the grid and the inability for the individual micelles to be detected by DLS

shows that these micellar aggregates exist and are present extensively through the solution. The CMC's of the PLA-PHEMA di- and triblock copolymers have yet to be determined however based on the ability to form self-assembled structures at 1 mg/ml for analysis it can be concluded that the CMC's of these materials must be smaller than 1 mg/ml.

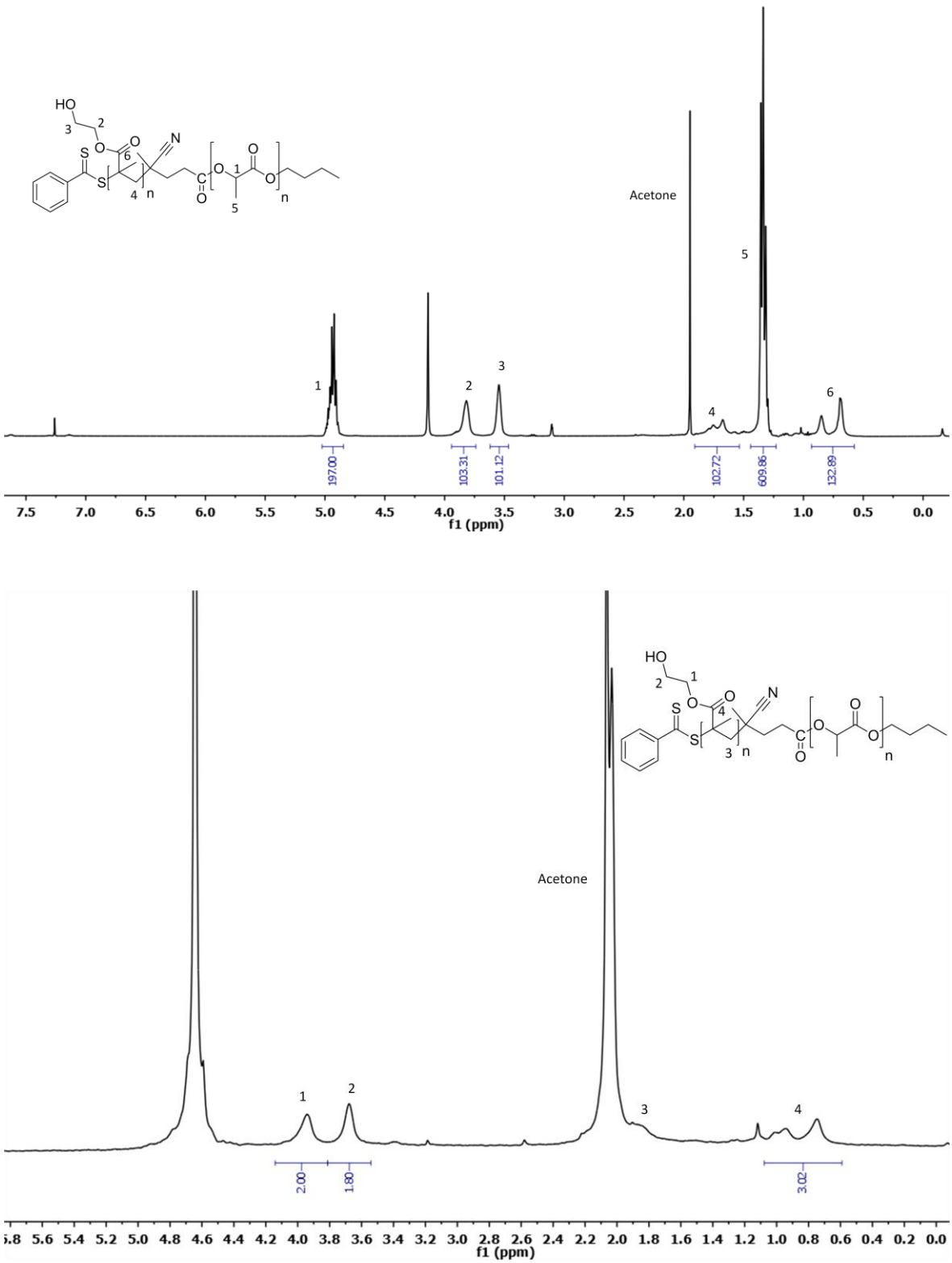

Figure 4-6. ^{1}H NMR spectra of PLA_{197}-$PHEMA_{51}$ in $CDCl_3$/MeOD-d4 (top) and in D_2O (bottom).

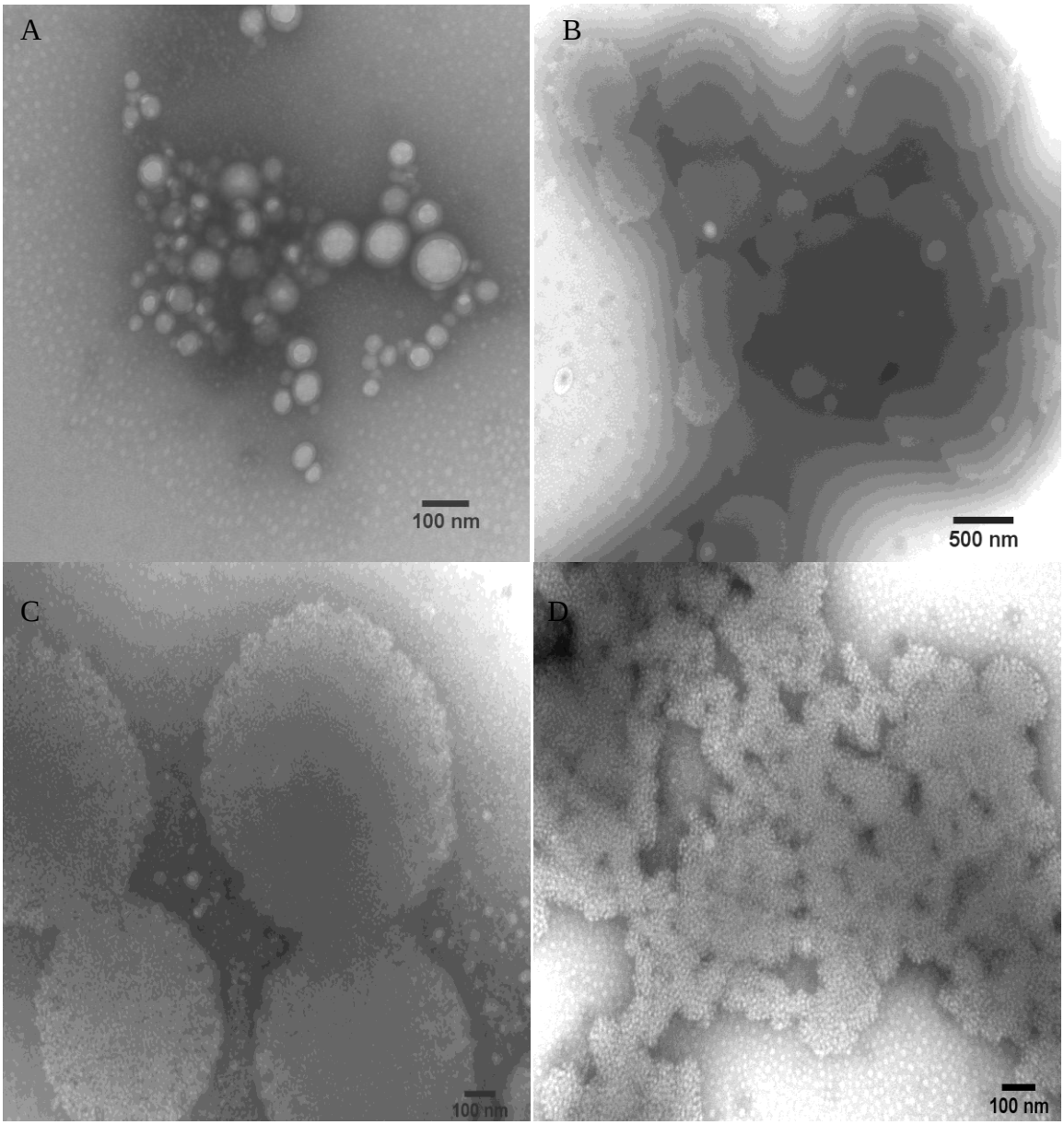

Figure 4-7. TEM images obtained for negatively stained spherical aggregates formed from PLA_{46}-$PHEMA_{79}$ by various preparation methods; (A) nanoprecipitation (water added to polymer solution), (B) nanoprecipitation (water added to polymer soln), (C) an enlarged image of (B), (D) nanoprecipitation (polymer solution added to water).

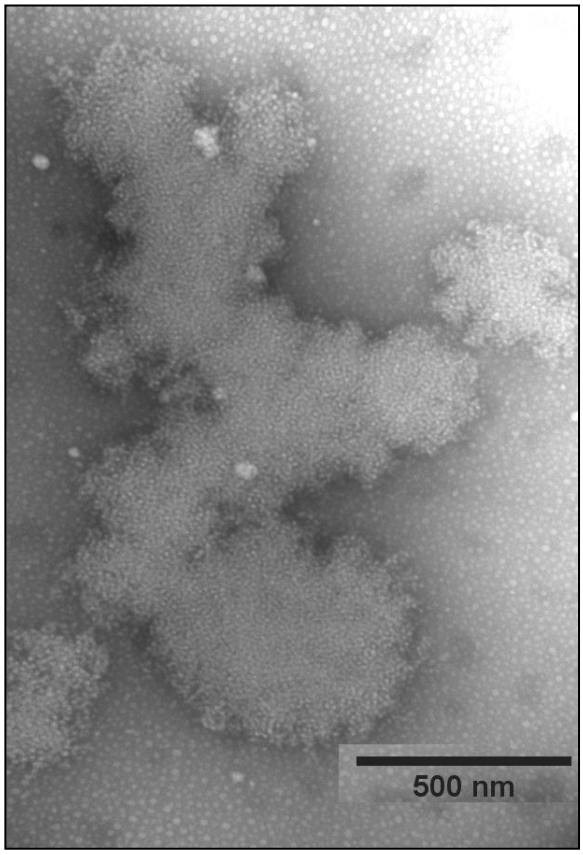

Figure 4-8. TEM images for negatively stained spherical aggregates prepared by dialysis of PLA_{46}-$PHEMA_{79}$.

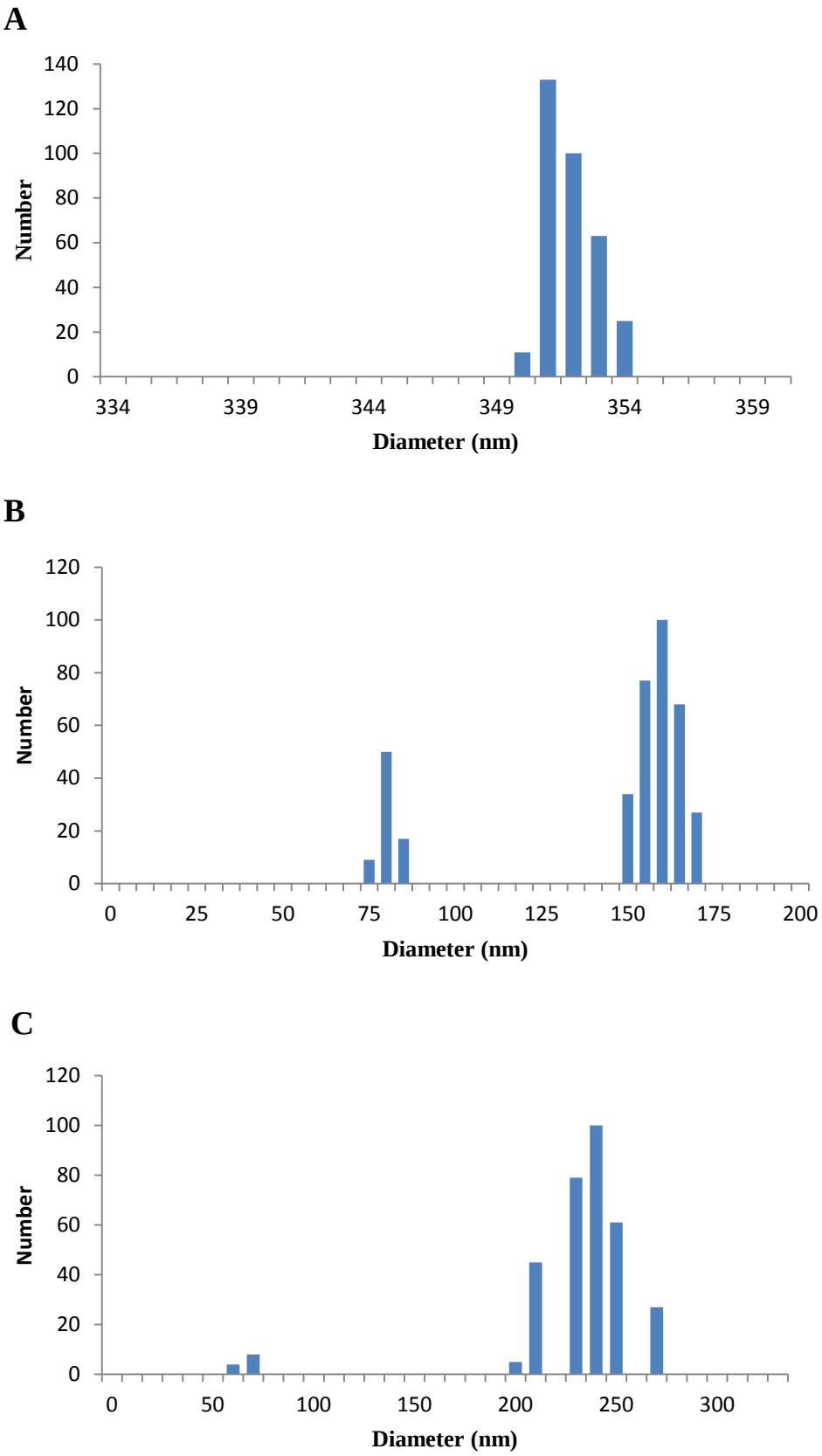

Figure 4-9 DLS results for PLA_{46}—$PHEMA_{79}$ (1 mg/ml) prepared by A) nanoprecipitation, B) reverse nanoprecipitation, C) dialysis.

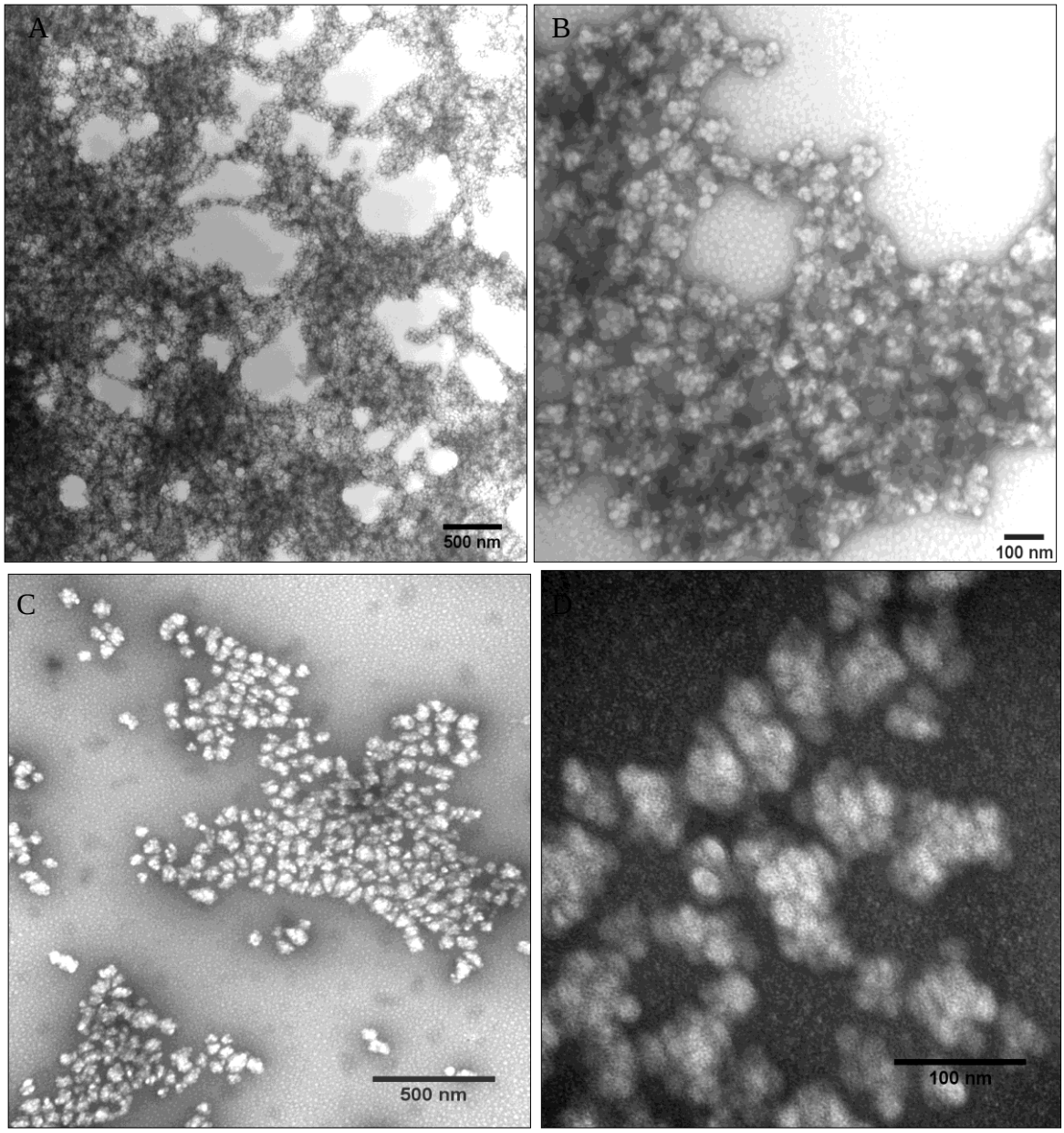

Figure 4-10. TEM images obtained for negatively stained aggregates formed from PLA_{197}-$PHEMA_{51}$ by various preparation methods; (A) nanoprecipitation (water added to polymer solution), (B) an enlarged image of (A), (C) dialysis (DMSO against water), (D) an enlarged image of (C).

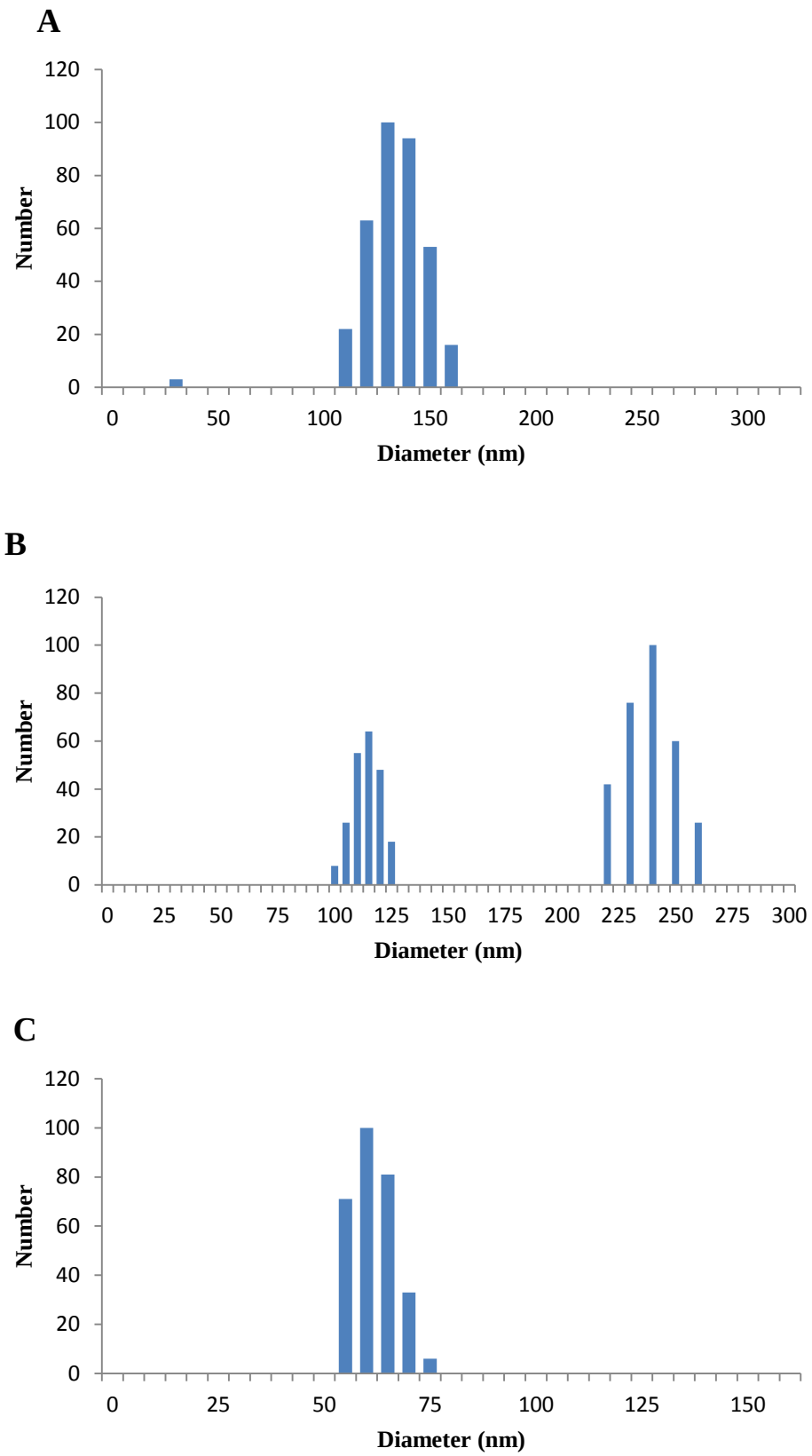

Figure 4-11. DLS results for PLA_{197}-$PHEMA_{51}$ (1 mg/ml) prepared by A) nanoprecipitation, B) reverse nanoprecipitation, C) dialysis.

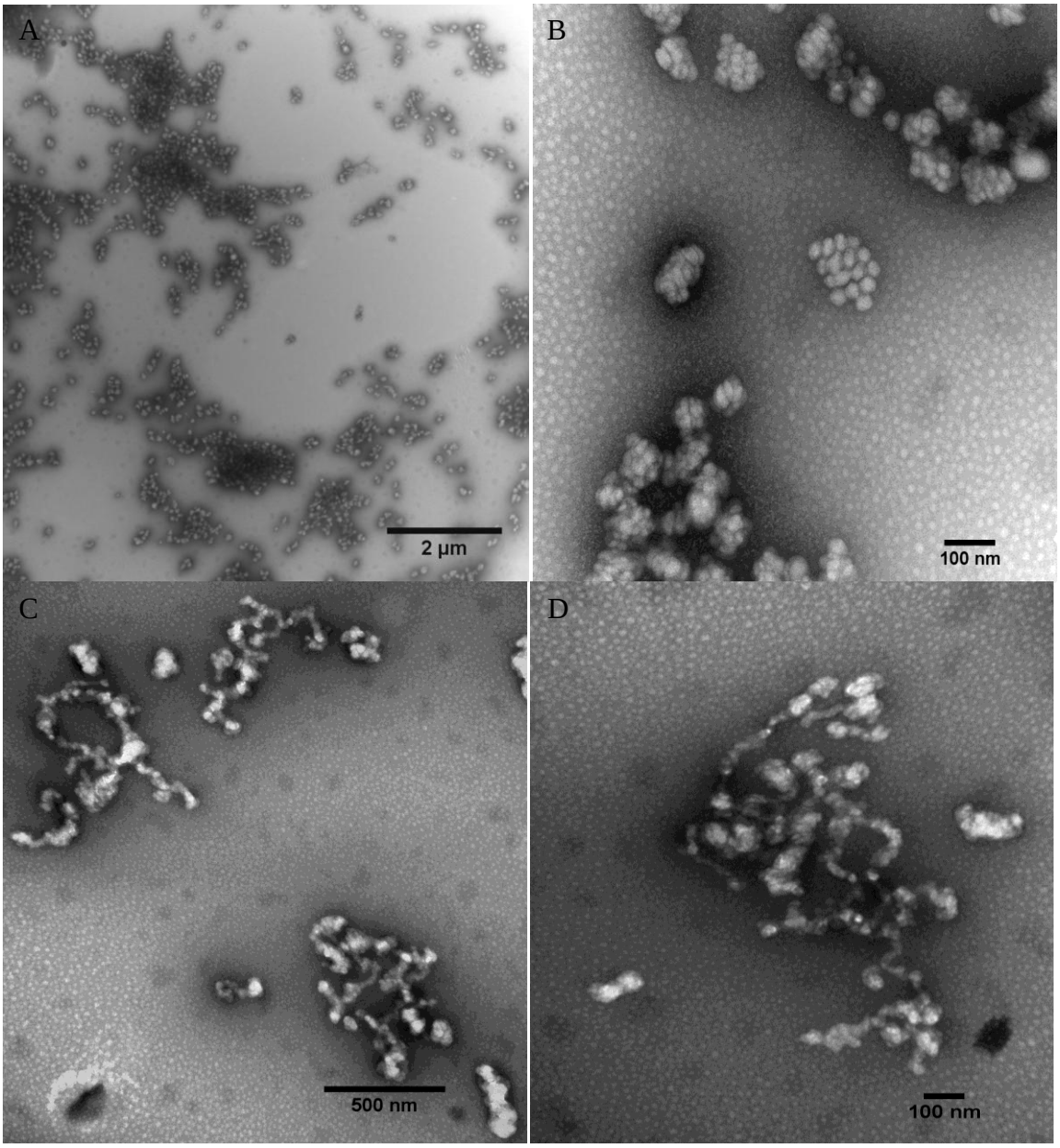

Figure 4-12. TEM images obtained for negatively stained spherical aggregates formed from $PHEMA_{16}$-PLA_{181}-$PHEMA_{16}$ by various preparation methods; (A) nanoprecipitation (water added to polymer solution), (B) an enlarged image of (A), (C) nanoprecipitation (polymer solution added to water), (D) an enlarged image of (C).

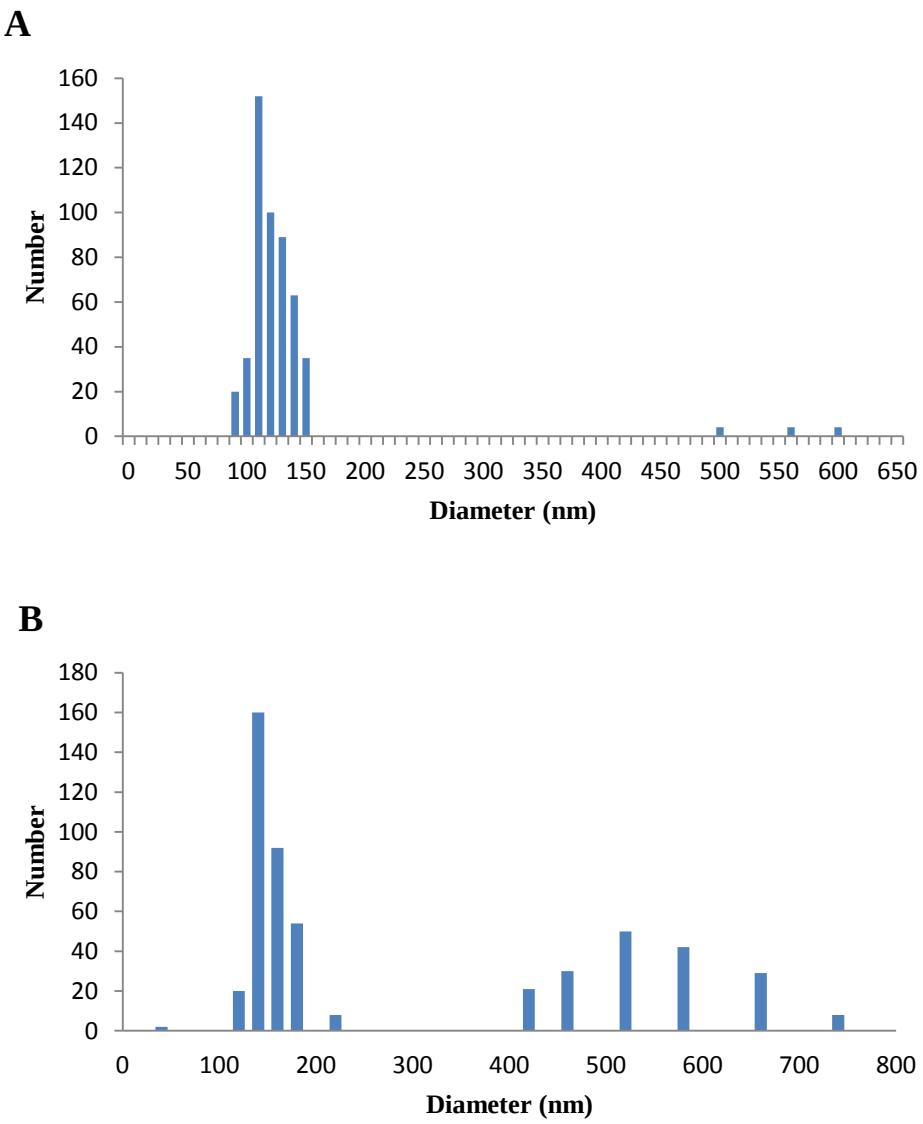

Figure 4-13. DLS results for $PHEMA_{16}$-PLA_{181}-$PHEMA_{16}$ (1 mg/ml) prepared by A) nanoprecipitation, B) reverse nanoprecipitation.

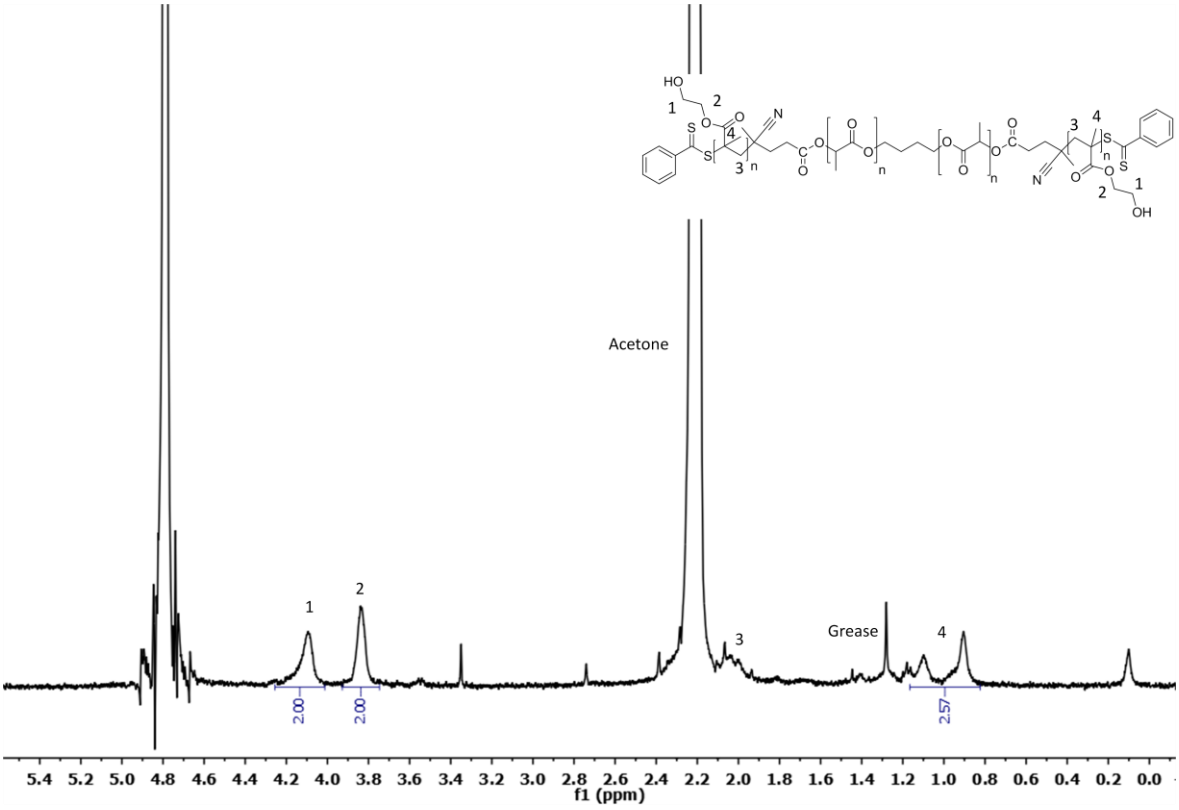

Figure 4-14. ^{1}H NMR spectrum (400 MHz, D_2O) of $PHEMA_{16}$-PLA_{181}-$PHEMA_{16}$.

4.2.3 Effects of Temperature on Self Assembly

Block copolymers which possess glass transition temperatures (T_g) above ambient temperature have been shown to form spherical and cylindrical micelles which possess "glassy" cores and vesicles with glassy wall interiors.[201] These aggregates are considered more stable in water; due to the reduced molecular motion of the hydrophobic block, these chains are kinetically frozen therefore preventing interaggregate migration of block copolymer chains.[201] The T_g of polylactide is 60 ^{o}C, therefore aggregates formed upon self-assembly at room temperature are potentially more stable than aggregates which are composed of a core with a T_g less than ambient temperature. Solutions of a diblock and triblock copolymer of PLA-PHEMA self-assembled by nanoprecipitation were each heated to 75 ^{o}C for 2 h before rapidly cooling in ice to examine the effects of temperature on self-assembled structures. The nanoparticles were prepared at elevated temperatures to increase mobility of PLA chains at a water content whereby the aggregates are effectively frozen encouraging morphological transitions. The effects of temperature upon the aggregates formed are given in **Table 4-3**.

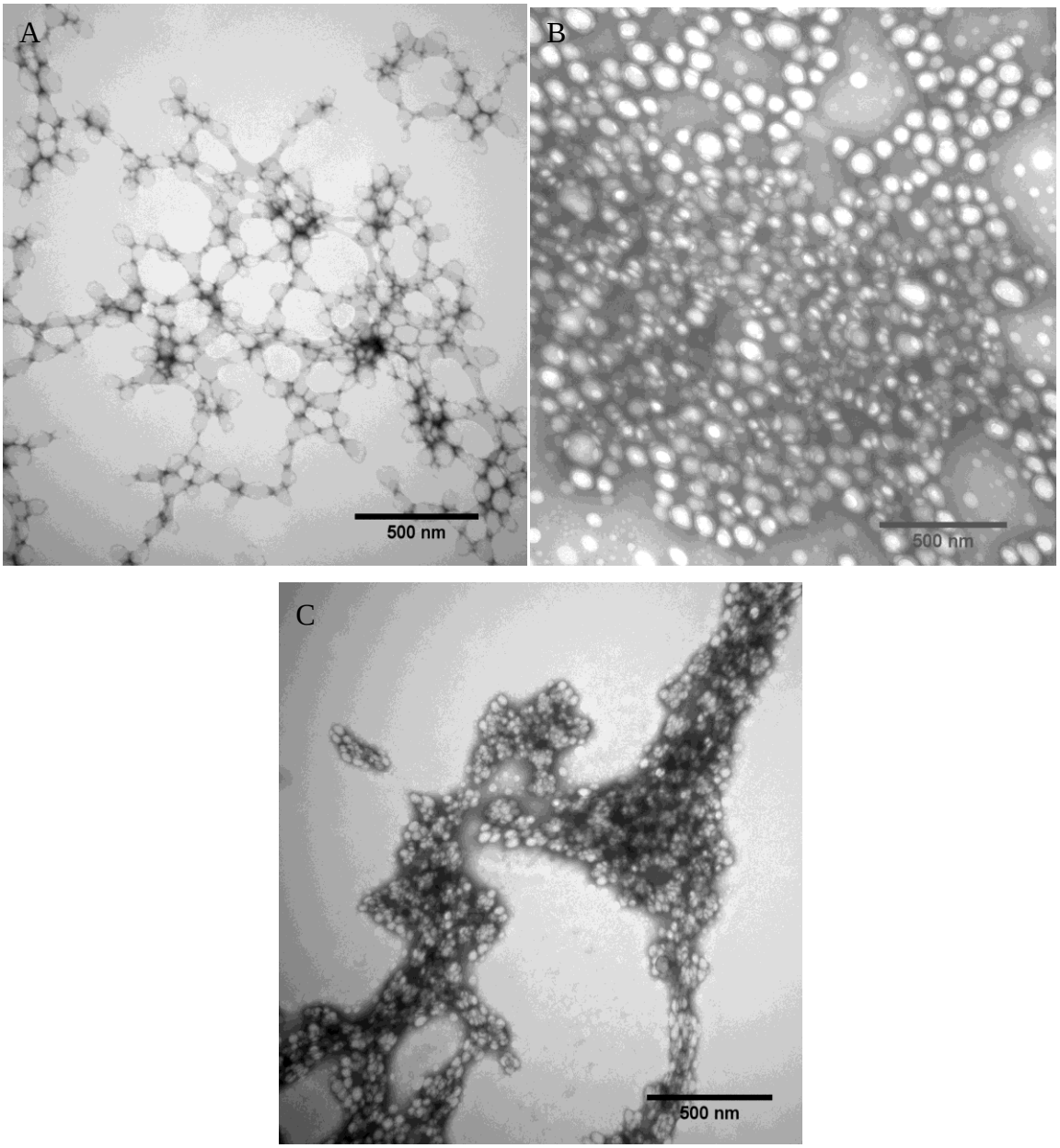

Figure 4-15. TEM images obtained for negatively stained aggregates formed by heating block copolymers prepared by nanoprecipitation (addition of water to acetone); (A) $PHEMA_{16}$-PLA_{181}-$PHEMA_{16}$; (B) $PHEMA_{16}$-PLA_{181}-$PHEMA_{16}$, (C) PLA_{197}-$PHEMA_{51}$.

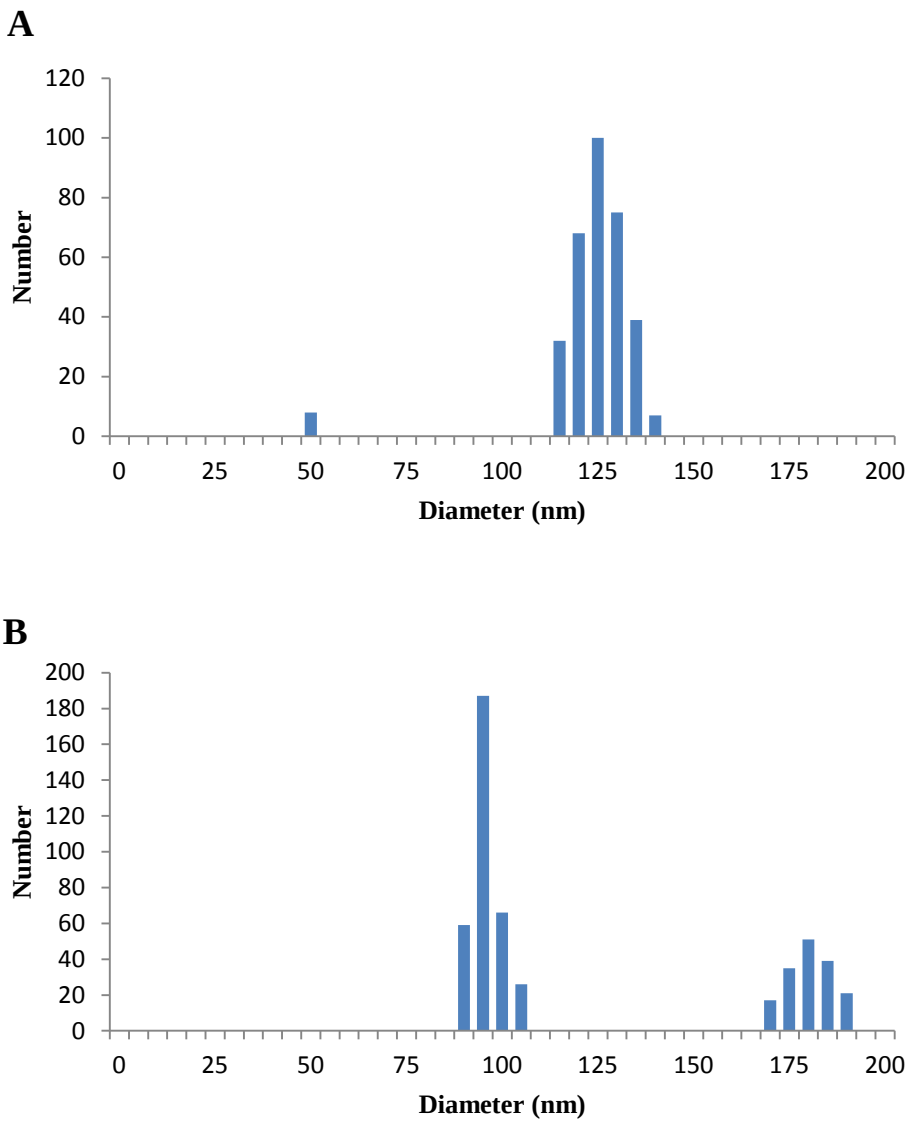

Figure 4-16. DLS results for A) PLA_{197}-$PHEMA_{51}$ (1 mg/ml) and B) $PHEMA_{16}$-PLA_{181}-$PHEMA_{16}$ (1 mg/ml) after heating at 80°C.

The self-assembly of the triblock copolymer $PHEMA_{16}$-PLA_{181}-$PHEMA_{16}$ has consistently reproduced micelle structures. Upon heating the solution above the T_g associating micelles (**Figure 4-15A**) with a broad diameter range of 63-127 nm and vesicles characterized by the darker outer ring (**Figure 4-15B**) with a diameter range of 61-139 nm were formed. The particle size measured by TEM was comparable with that determined by DLS (**Figure 4-16**). ABA block copolymers are known to form micelles, however, increasing the mobility of the PLA chains led to the formation of vesicles. The morphology of diblock copolymer PLA_{197}-$PHEMA_{51}$ was unaffected by the rise in temperature as demonstrated in **Figure 4-10C and Figure 4-11C** forming micelle clusters indicating a solid core. The morphological transition observed may be attributed to the

configuration of triblock copolymer chains present in micelles which differs to that of the diblock copolymer.

4.3 Self-Assembly of PLA-PMPC Block Copolymers

4.3.1 Copolymer Composition

Nanoparticles of PLA-PMPC are of great interest as potential drug delivery devices due to its biodegradability and biocompatibility. The self-assembly of PLA-PMPC diblock copolymers has been previously studied, Hsiue *et al.* reported the effects of cosolvents on morphology obtaining spherical structures with diameters ranging between 249-432 nm.[42] PLA-PMPC block copolymers which possessed a f_{MPC} = 0.23 have been shown to self-assemble to form large compound micelles.[43] Giant vesicles have also been reported for PLA-PMPC block copolymers with a f_{MPC} =0.48-0.53.[44] Several triblock copolymers were prepared in addition to diblock copolymers because of the increased stealthiness of ABA copolymers based on PLA-PEG over AB and BAB type copolymers due to the increased PEG density which arises from the adopted U-shaped structure.[199, 200] In this work the f_{MPC} of the diblock and triblock was varied to target different morphologies. The aggregates were prepared by nanoprecipitation utilising an analogous method to that described in section **4.2.1**. No one solvent can solubilise both the PLA and PMPC block therefore a mixture of THF/methanol (1:1) was used to dissolve block copolymers.

Spherical morphologies were observed when PLA_{46}-$PMPC_x$ diblock copolymers with varied MPC block lengths were self-assembled via nanoprecipitation. PLA_{46}-$PMPC_{101}$ formed predominantly vesicles (**Figure 4-17A**) with a wide size distribution of 86-200 nm which was in agreement with results obtained by DLS (**Figure 4-18**) thus particles with sizes greater than 350 nm observed by DLS were due to aggregation.. Micelles were also identified by TEM (**Figure 4-17B**), with a diameter range of 31-43 nm. Upon decreasing the MPC hydrophilic block length larger vesicles were formed with a diameter range of 226-412 nm (**Figure 4-17C**). Additionally, smaller aggregates were observed by TEM with a diameter range of 65-167 nm. The particle size measured by TEM (**Table 4-4**) was comparable with that determined by DLS (**Figure 4-18)**. The morphology was reproducible upon reducing the MPC block length of the diblock copolymer with a larger particle size which is attributed to reduced repulsion between corona chains resulting in an increase in aggregation number.

Based on the reports of Disher *et al*. the relationship between *f* and morphology, micelles should have formed from the self-assembly for both diblock copolymers however the dominant morphology were vesicles.[189] Block copolymers composed of a small PLA segment are known to precipitate slowly which would lead to the formation of larger aggregates. Additionally Liu *et al*. showed that morphologies observed for PLA-PMPC block copolymers were not in agreement with those predicted obtaining vesicles for f_{MPC} > 0.45 and observing micelles with f_{MPC} above 0.6 which was ascribed to the zwitterionic side chain of MPC.[44]

ABA block copolymers generally form micelles, however, polymersomes were targeted by varying the hydrophobic block length. $PMPC_{50}$-PLA_{51}-$PMPC_{50}$ was self-assembled by nanoprecipitation yielding large spherical aggregates with a broad diameter range of 160-406 nm and 48-106 nm (**Figure 4-19A**) which corresponds to the data obtained by DLS (**Figure 4-20**). Micelles were observed from the self-assembly of the triblock copolymer $PMPC_{41}$-PLA_{390}-$PMPC_{41}$ in which the f_{MPC} is significantly less, **Figure 4-19B,** shows a high concentration of particles with a diameter range of 33-59 nm. The predominant particle size determined by DLS was 264-412 nm, this is most likely due to the aggregation of micelles. There are a few larger non spherical particles observed (**Figure 4-19B**) with a diameter range of 298-394 nm which are suspected artefacts of the grid as these were not observed across the grid. Similarly to the diblock copolymer, triblock copolymers with a smaller PLA block resulted in larger aggregates suggesting that the length of hydrophobic block determines the morphology. Further analysis of the self-assembly of triblock copolymers is required to examine the morphological effects of altering the f_{MPC} of the PMPC-PLA_{51}-PMPC triblock copolymer; varying the hydrophilic block length.

Table 4-4. Nanoprecipitation of PLA-PMPC Block copolymers-Aggregate Morphologies and Particle Size from TEM.

Block Copolymer[a]	f_{MPC}	**Diameter Range (nm)** [b]	**Morphology**[c]	**Soln Appearance**
PLA_{46}-$PMPC_{33}$	0.74	65-167, 226-412	Vesicles	Transparent
PLA_{46}-$PMPC_{101}$	0.90	31-43, 86-200	Micelles, Vesicles	Transparent
$PMPC_{50}$-PLA_{51}-$PMPC_{50}$	0.89	48-106, 160-406	Micelles, Vesicles	Transparent
$PMPC_{41}$-PLA_{390}-$PMPC_{41}$	0.46	33-59	Micelles	Transparent

[a]Self-assembled structures prepared by the slow addition of water to the polymer dissolved in a solvent mixture of THF/methanol (1:1). The polymer concentration of each solution was 1 mg/ml.

[b]Diameter range determined by TEM

[c]Morphology observed by TEM

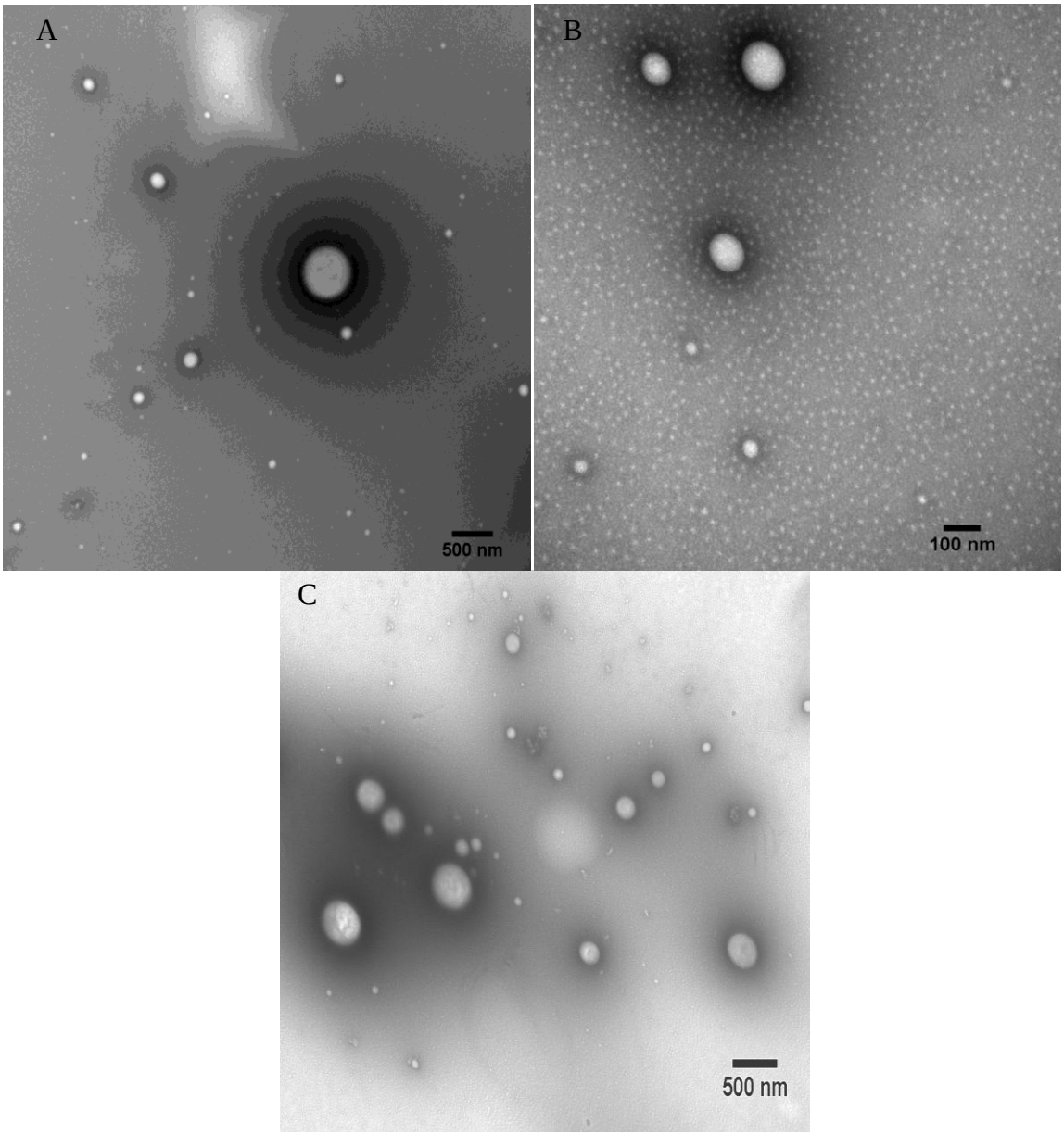

Figure 4-17. TEM images for negatively stained spherical aggregates prepared by nanoprecipitation (A) PLA_{46}-$PMPC_{101}$ (B) an enlarged image of (B), (C) PLA_{46}-$PMPC_{33}$.

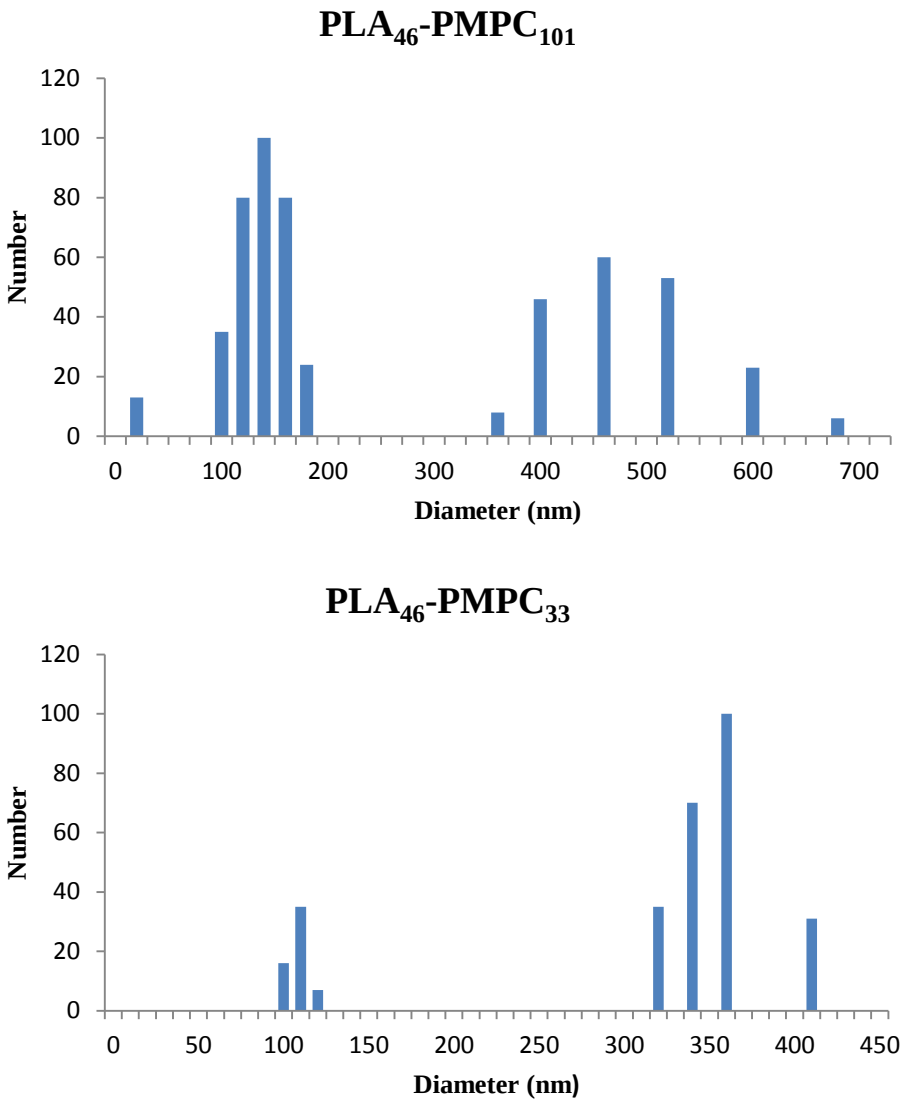

Figure 4-18. DLS results for PLA-PMPC diblock copolymers (1 mg/ml) prepared by nanoprecipitation.

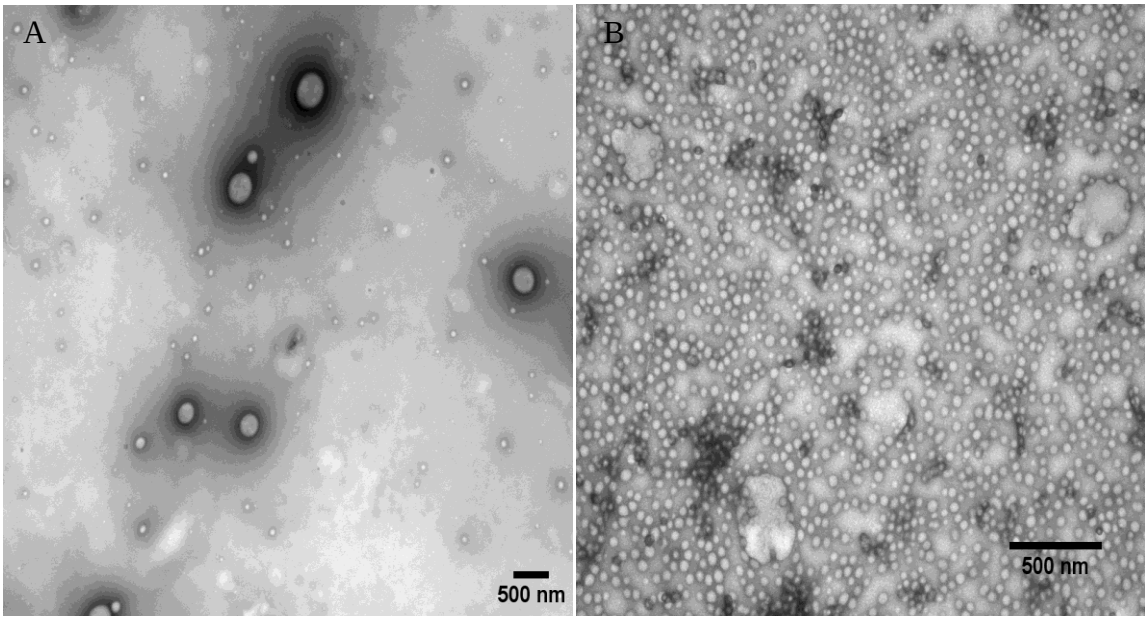

Figure 4-19. TEM images obtained for negatively stained spherical aggregates prepared by nanoprecipitation of (A) $PMPC_{50}$-PLA_{51}-$PMPC_{50}$ and (B) $PMPC_{41}$-PLA_{390}-$PMPC_{41}$.

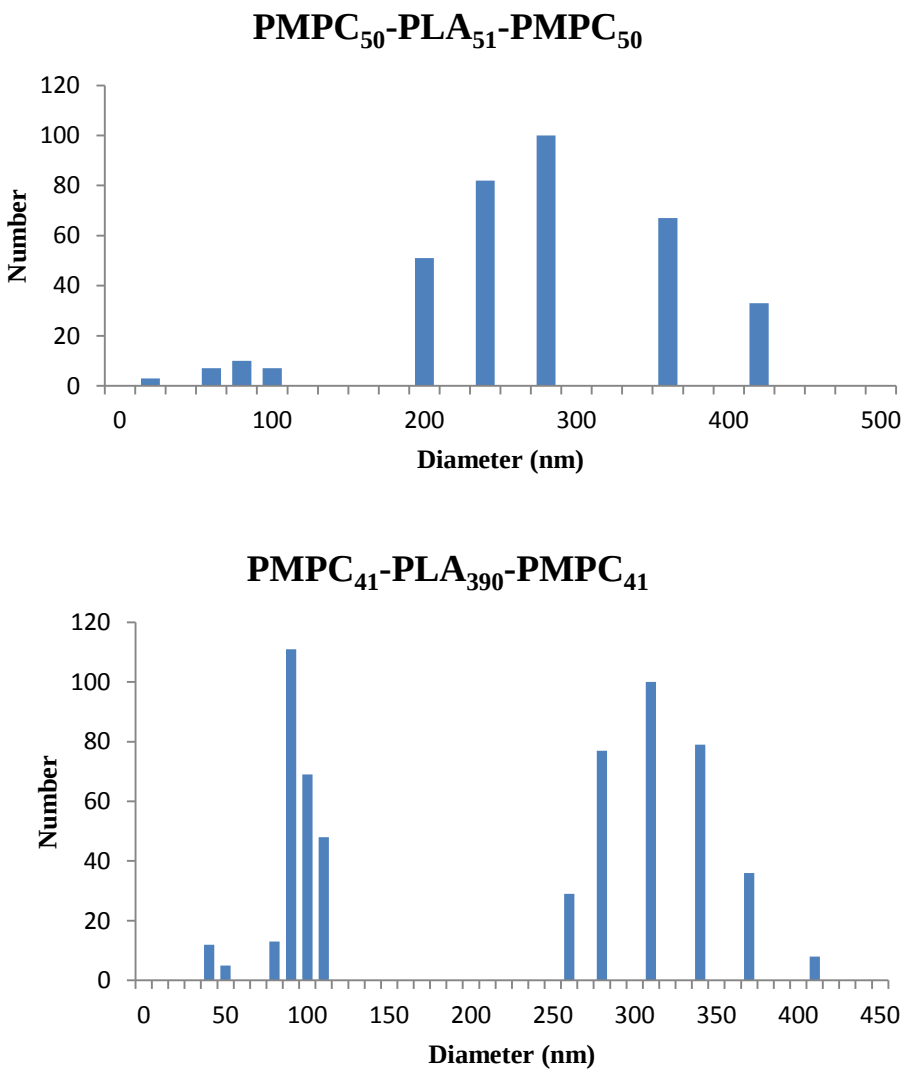

Figure 4-20. DLS results for PLA-PMPC triblock copolymers (1 mg/ml) prepared by nanoprecipitation.

4.3.2 Alternative Methods for the Preparation of Self-Assembled Structures

The self-assembly of PLA-PMPC triblock copolymers has not to our knowledge been investigated. The effects of the self-assembly method on the morphology of the two triblock copolymers (**Table 4-5**) was therefore investigated. Aggregates were prepared by direct dissolution and by dialysis; triblock copolymers were initially dissolved in the solvent mixture of THF/methanol (1:1) used for nanoprecipitation and dialysed against water.

Significantly larger vesicles with a diameter of 710-1250 nm (**Figure 4-21A**) were observed when the self-assembly of $PMPC_{53}$-PLA_{51}-$PMPC_{53}$ was induced by dialysis in addition to a small population of aggregates with a diameter of 210-406 nm (**Figure 4-21A**). Particle size data obtained by TEM was in close agreement with that determined by DLS (**Figure 4-22A)**. The morphology was reproducible by dialysis which was expected, however, the size of aggregates is larger than that obtained by nanoprecipitation as evidenced by TEM and DLS (**Figure 4-21A, 4-22A**). Due to the hydrophilicity of the MPC block, direct dissolution can be utilised for the preparation of self-assembled structures. **Figure 4-23** demonstrates the self assembly of $PMPC_{53}$-PLA_{51}-$PMPC_{53}$ by direct dissolution showing the disappearance of PLA signals from the ^{1}H NMR spectrum of the block copolymer in deuterium oxide. $PMPC_{53}$-PLA_{51}-$PMPC_{53}$ yields small micelles with a narrow diameter range of 29-46 nm (**Figure 4-21B**) which is comparable with the DLS results (**Figure 4-22B)**, showing that in this case the morphology of the aggregates is influenced by the method of preparation.

The morphology of aggregates of $PMPC_{55}$-PLA_{390}-$PMPC_{55}$ has been shown to be consistent despite changing the method by which aggregates were prepared (**Figure 4-24A, 4-24B**). It was thought that removal of the polymer solvent mixture would be slower by dialysis thus increasing the mobility of the chains which would lead to the formation of larger aggregates. However, the size of the micelles formed by dialysis was comparable with that of aggregates obtained by the nanoprecipitation method with a diameter range of 46-72 nm. Micelles formed by direct dissolution were smaller under kinetic control with a diameter range of 24-48 nm. The size of the aggregates measured by TEM is comparable with DLS studies (**Figure 4-25A, 4-25B)**. In direct dissolution the block copolymers are solubilised in a solvent which favours the hydrophilic block, thermodynamic equilibrium may not occur between unimers and aggregates which results in the formation of micelles as demonstrated by the self-assembly of both triblock copolymers. The micelle

morphology shown by TEM was observed across the grid for both triblock copolymers which was supported by DLS these structures must therefore exist.

Table 4-5. Alternative Methods for the Self-Assembly of PLA-PMPC Block copolymers-Aggregate Morphologies and Particle Size from TEM and DLS Measurements.

	Method[a]	f_{MPC}	Diameter Range (nm)[b]	Morphology[c]	Soln Appearance
$PMPC_{53}$-PLA_{51}-$PMPC_{53}$	1	0.89	29-46	Micelles	Transparent
	2	0.89	210-406, 710-1250	Vesicles	Translucent white
$PMPC_{55}$-PLA_{390}-$PMPC_{55}$	1	0.46	24-48	Micelles	Transparent
	2	0.46	46-72	Micelles	Translucent White

[a]Aggregates of PMPC-PLA-PMPC block copolymers were prepared by two methods; (1) direct dissolution of the triblock copolymer in water, (2) dialysing the polymer in a solvent mixture of THF/methanol (1:1) against water. The polymer concentration of each solution was 1 mg/ml.

[b]Diameter range determined by TEM

[c]Morphology observed by TEM

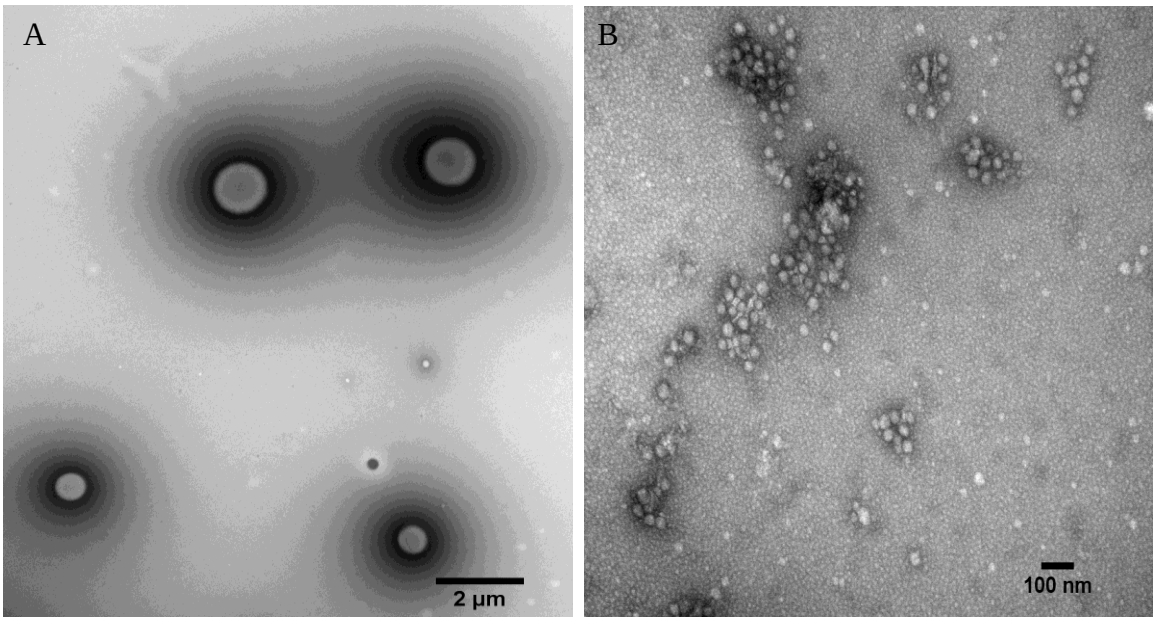

Figure 4-21. TEM images obtained for negatively stained spherical aggregates formed from $PMPC_{50}$-PLA_{51}-$PMPC_{50}$ by various preparation methods; (A) dialysis (THF/methanol (1:1) against water), (B) direct dissolution.

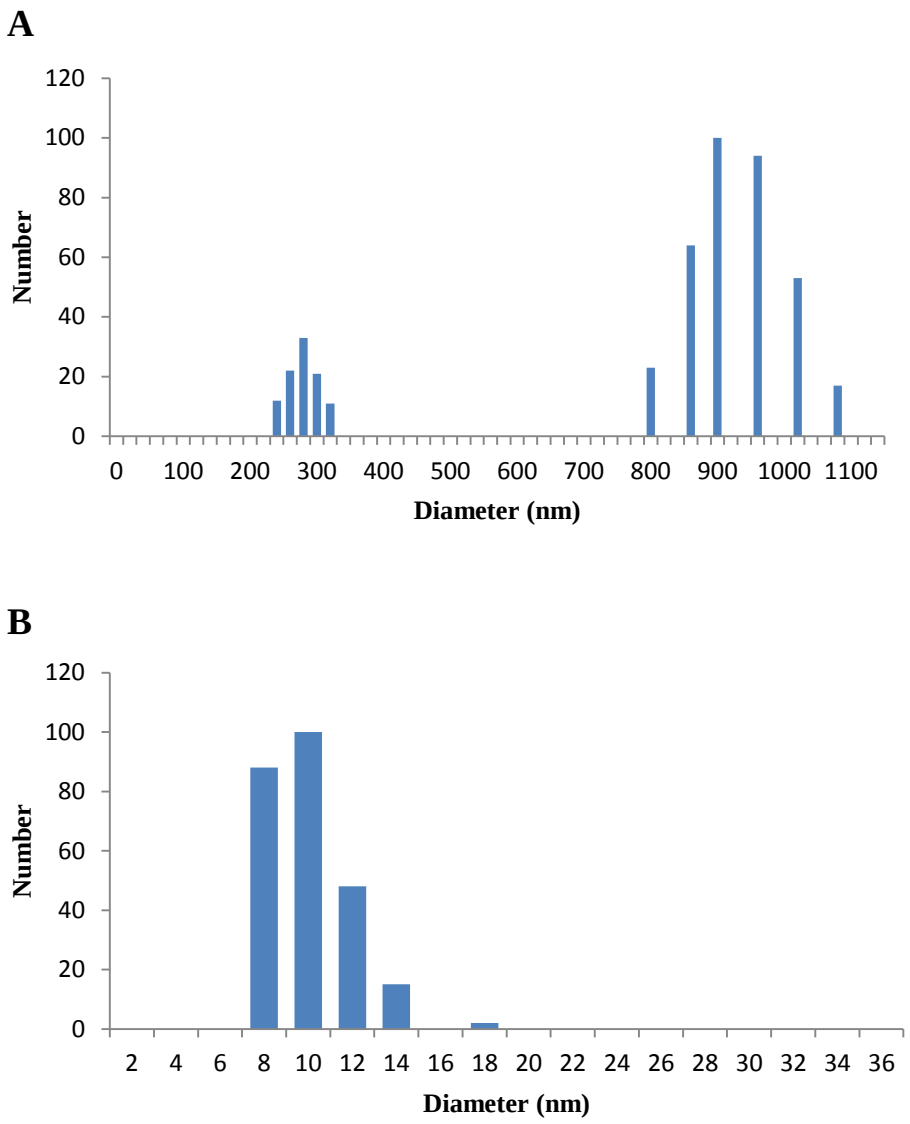

Figure 4-22. DLS results for $PMPC_{50}$-PLA_{51}-$PMPC_{50}$ (1 mg/ml) prepared by A) dialysis, B) direct dissolution.

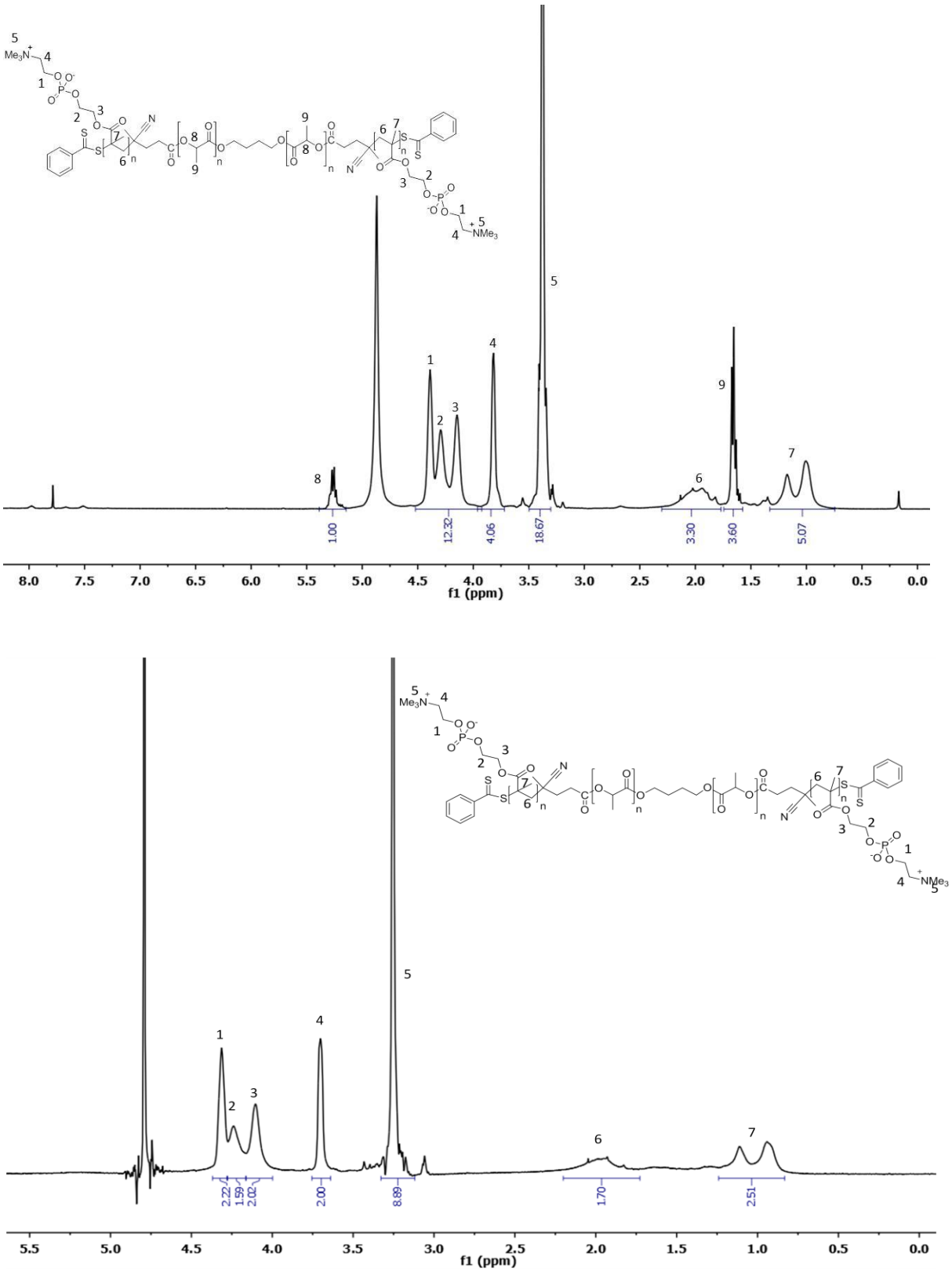

Figure 4-23. ^{1}H NMR spectrum (400 MHz) of $PMPC_{53}$-PLA_{51}-$PMPC_{53}$ in $CDCl_3$/MeOD-d4 (top) and in D_2O (bottom).

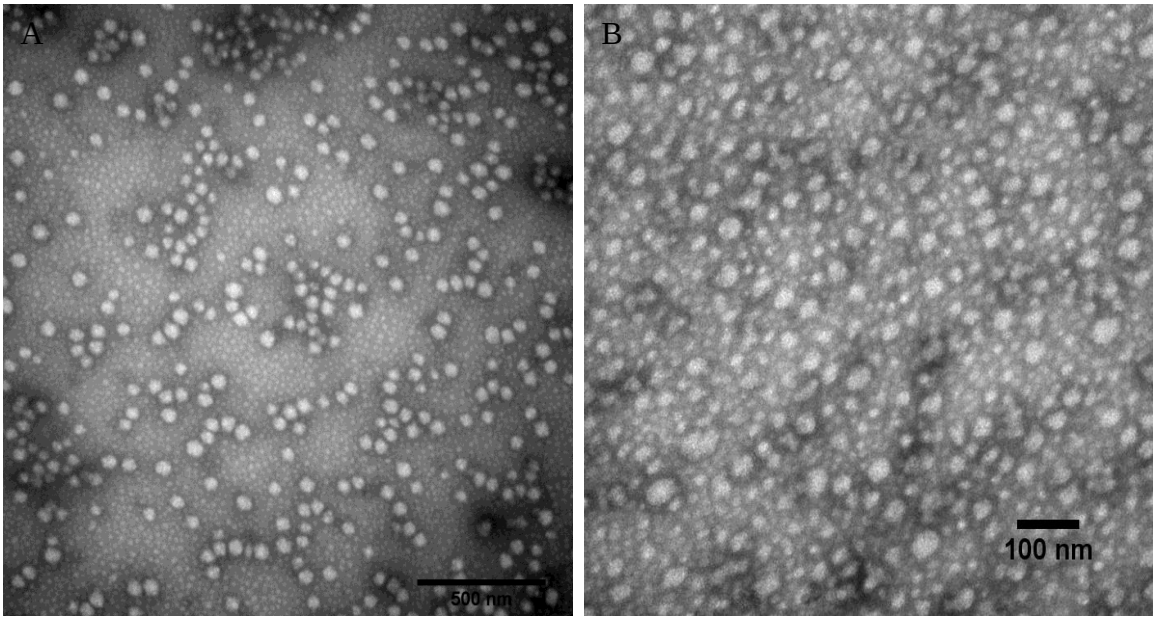

Figure 4-24. TEM images obtained for negatively stained spherical aggregates formed from $PMPC_{41}$-PLA_{390}-$PMPC_{41}$ by various preparation methods; (A) dialysis (THF/methanol (1:1) against water), (B) direct dissolution.

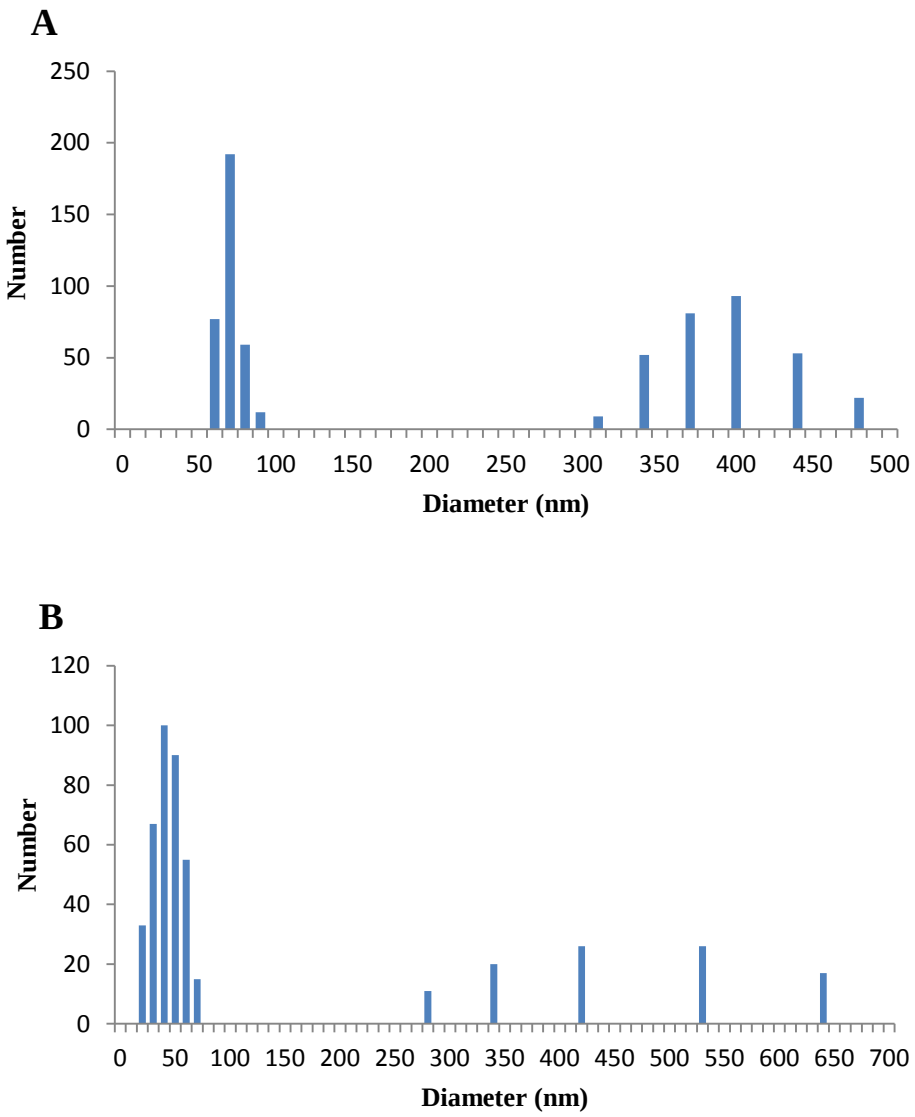

Figure 4-25. DLS results for $PMPC_{41}$-PLA_{390}-$PMPC_{41}$ (1 mg/ml) prepared by A) dialysis, B) direct dissolution.

4.4 Encapsulation of a Dye

To demonstrate the ability of PLA-PMPC block copolymers as potential drug carriers a qualitatitve test was carried out using the fluorescent hydrophobic dye nile red. The block copolymer PLA_{46}-$PMPC_{101}$ was self-assembled by nanoprecipitation with THF/methanol at a concentration of 3mg/ml in the presence of nile red. The hydrophobic dye is insoluble in aqueous solution but can be solubilised in the hydrophobic core or membrane of the nanoparticle. The successful encapsulation of the dye by PLA-PMPC diblock copolymer in aqueous media is shown by the presence of a light pink colour (**Figure 4-26B**) and under UV light the dye is shown to fluorescence (**Figure 4-26C**). Several drops of sodium hydroxide (1M) was subsequently added to the dye loaded nanoparticles to demonstrate the

pH responsive release of the dye as PLA degrades (**Figure 26D**). The qualitative tests show that there is scope for these amphiphilic block copolymers in biomedical applications.

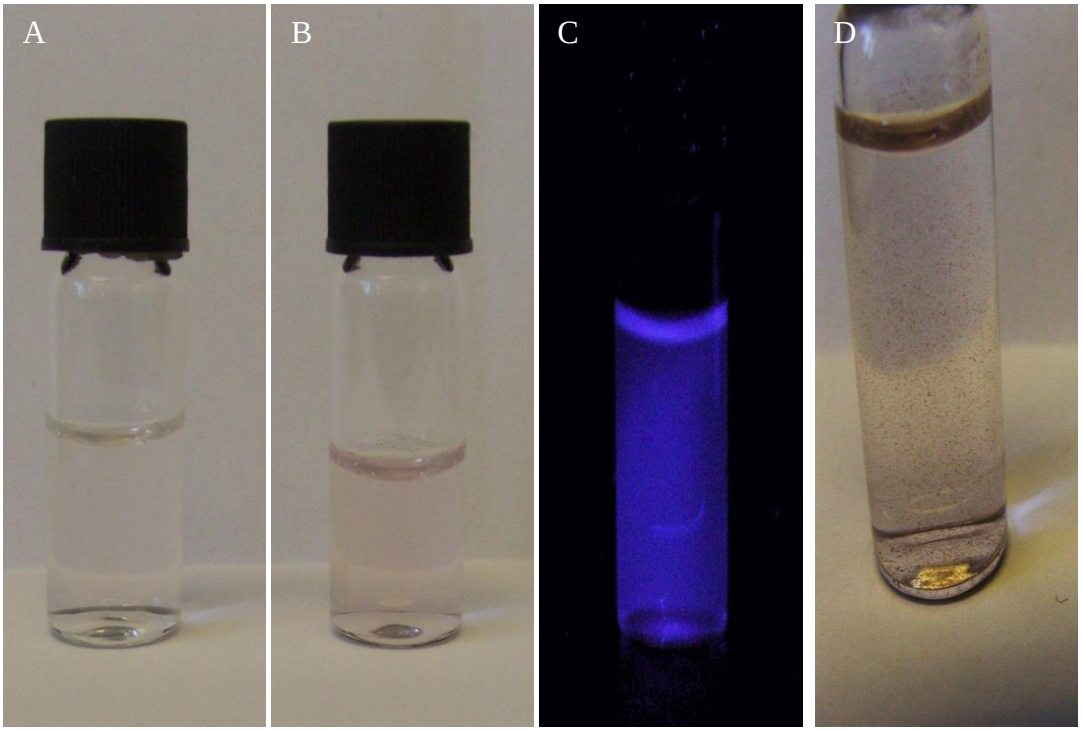

Figure 4-26. Encapsulation of Nile red (A) self-assembled PLA-PMPC block copolymer, (B) Nile red encapsulated by PLA-PMPC, (C) (B) under UV light, (D) (B) in the presence of base.

4.5 Conclusion

The self-assembly of a range of PLA-PHEMA and PLA-PMPC block copolymers was studied investigating the morphological effects of temperature, the common solvent, copolymer composition and preparation methods. Generally the diblock copolymers of PLA-PHEMA which possessed a longer PLA segment self-assembled to form micelles due to the increased rate of precipitation. Vesicles were only observed when the common solvent favoured the hydrophobic block of PLA_{46}-$PHEMA_{79}$. ABA triblock copolymers were shown to self-assemble to yield micelles over a range of copolymer compositions and via various preparation methods as expected. Vesicles were achieved for triblock copolymers with significantly low f_{HEMA} and when temperatures were raised above the T_g to increase the fluidity of the core.

A range of PLA-PMPC block copolymers with varied compositions were self-assembled using several techniques to target different morphologies. Similarly to the self-assembly of

PLA-PHEMA systems diblock and triblock copolymers with larger PLA block length were shown to yield smaller aggregates. The morphologies observed for the various block copolymers were consistent amongst different preparative techniques. Vesicle structures were reproducible by the self-assembly of $PMPC_{50}$-PLA_{51}-$PMPC_{50}$, however, by preparing nanoparticles by direct dissolution the system was no longer in thermodynamic equilibrium thus resulting in micelle formation.

Based on the self-assembly study of both block copolymer systems the PLA block length appears to be the major factor affecting the morphology. Usually block copolymers consisting of a larger hydrophobic block generate larger aggregates however, with PLA block copolymers smaller aggregates are formed. Further analysis of these systems is required to investigate the morphological effects of higher $f_{HEMA/MPC}$ values.

5. Conclusions and Future Work

In summary of the two initial strategies investigated for the synthesis of PLA-PMPC block copolymers, it was shown that the macroRAFT agent prepared by the covalent attachment of a RAFT agent to a pre-formed polylactide polymer via the R group was more effective for the chain extension of MPC. Mono and di-functionalised PLA macroRAFT agents were successfully synthesized with a narrow PDI range of 1.02-1.17 with close to 100% RAFT functionalization of PLA chains obtained.

The main issue with the RAFT polymerization of MPC was the selection of a solvent which could solubilise both MPC and PLA and the resultant block copolymer. It was confirmed by ^{1}H NMR spectroscopy that the PLA-macroRAFT agent was subject to hydrolysis when heated in the solvent mixture of DMSO/methanol used for the ATRP synthesis of these block copolymers which explained the multi-modal molecular weight distributions observed for the PLA-PMPC block copolymers. The PLA-macroRAFT agent was subject to stability tests to confirm the integrity of the polymeric structure in several solvents and solvent mixtures by ^{1}H NMR spectroscopy. The RAFT polymerization of MPC in a mixture of ethanol and THF proved to be effective, generating diblock and triblock copolymers with a narrow PDI. A PDI range of 1.15-1.24 was observed for diblock copolymer and 1.24-1.36 for the novel triblock copolymers. The discrepancy between the M_n determined by ^{1}H NMR spectroscopic and GPC analyses demonstrates the difference in the hydrodynamic volume of the polymer standard and sample. By preparing these block copolymers by RAFT polymerization polymers with narrower molecular weight distribution were obtained in comparison to the studies of Hsiue *et al*. and the use of metallic catalyst impurities was avoided.[42]

PLA-PMPC block copolymers with a larger PLA block length generally self-assembled to form smaller aggregates showing the morphogenic effect of the polymer composition. The morphologies observed for the triblock copolymers were consistent for different preparative techniques i.e. solvent switch and direct dissolution. $PMPC_{50}$-PLA_{51}-$PMPC_{50}$ was shown to self-assemble to form vesicles however by preparing nanoparticles by direct dissolution micelles formed showing that the system was no longer in thermodynamic equilibrium. Amphiphilic block copolymers are targeted for their potential as drug carriers, the ability of PLA-PMPC block copolymers to act as possible vehicles was demonstrated by the encapsulation of a hydrophobic fluorescent dye and shown to release the dye upon an increase in pH.

PLA-PHEMA provided an effective model for the target system which could be readily analyzed by GPC. A range of diblock and triblock copolymers were synthesized with varied f_{HEMA} compositions. Polymers were shown to be prepared with controlled molecular weight and narrow molecular weight distributions with a PDI range of 1.16-1.28. PLA-PHEMA block copolymers have not been synthesized previously by RAFT and ROP techniques and their self-assembly has not been studied to a great extent. The self-assembly study showed that the majority of block copolymers formed micellar aggregates by nanoprecipitation except when f_{HEMA} was significantly low resulting in the formation of vesicles. Micellar aggregates are believed to form due to the lower solubility of HEMA in water. Aggregates were also prepared using different methods which in certain cases had a morphological effect. Further characterization of PLA-PHEMA di- and triblock copolymer is required in order to determine the cmc's for the aggregates.

Both PLA-PHEMA and PLA-PMPC block copolymers should be evaluated as potential as drug carriers investigating drug loading and release, cytotoxicity and degradation. The PLA-PMPC diblock copolymers have previously been investigated for the delivery of cancer drugs thus any future work should focus on the PLA-PMPC triblock copolymer. Properties such as cmc's will need to be determined by fluorescent spectroscopy to evaluate the stability of the aggregates.

A methodology has been determined for the synthesis of PLA ABA based triblock copolymers which has not been previously reported. A range of PLA based triblock copolymers could be synthesized with advantageous properties for biomedical applications. Polymer drug carriers have also been widely studied for gene delivery as non-viral vectors.[205] Non-viral vectors have been researched due the immunogenic shortcomings of viral vectors.[206] Polymeric vectors are usually composed of a cationic segment to form a polyplex with the negatively charged phosphate ions of DNA. Triblock vectors such as PDMAEMA-PCL-PDMAEMA and pentablock vectors PDEAEM-PEO-PPO-PEO-PDEAEM have been previously investigated showing effective transfection efficiency.[147, 207] Incorporation of a hydrophobic segment has been shown to improve transfection.[208] PLA-PMPC di- and triblock copolymers could be chain-extended by cationic monomers e.g. DMAEMA, and evaluated for gene delivery investigating DNA complexation, cellular uptake and gene expression.

6. General Experimental

6.1 Materials

All chemicals were purchased from Sigma Aldrich unless otherwise specified. 3, 6-Dimethyl-1, 4-dioxane-2, 5-dione (>96 %), potassium phosphate tribasic (>98 %), carbon disulfide (99.9 %), sodium bicarbonate (>99.5 %), *N*,*N*-dicyclohexylcarbodiimide (99 %), 4-dimethylaminopyridine (99 %), 2-propanol (anhydrous) (99.5 %), ethanol (anhydrous) (≥99.5 %), DMSO (anhydrous) (≥99.9 %), 4-cyano-4-(phenylcarbothioylthio)pentanoic acid (>97 %) were used without further purification. *n*-Butyl acrylate (>99 %), *n*-butyl methacrylate (99 %) and 2-hydroxyethyl methacrylate (HEMA) (97 %) were passed though a basic alumina column prior to use. 1-Butanol (99.9 %) and 1, 4-butanediol (99 %) were dried by distillation and stored over 4 Å molecular sieves under nitrogen. DBU (9 8%) was stirred over calcium hydride (90-95 %), vacuum distilled and stored over 4 Å molecular sieves under nitrogen. DMSO-d6 (>99.8 %D), chloroform-d (99.8 %D) and methanol-d4 (>99.8 %) were purchased from Apollo Scientific. Chloroform (>99 %), ethyl acetate (99.97 %), dichloromethane (99.99 %), methanol (99.99 %), acetone (99.99 %), THF (>99.5 %), diethyl ether (>99 %) and hexane (95 %) were purchased from Fisher Scientific. AIBN (98 %) was purchased from Acros and 4, 4'-azobis(4-cyano-pentanoic acid) (>98 %) was purchased from Fluka. Mercaptoethanol (99 %) and benzyl bromide (99 %) were purchased from Alfa Aesar and HEMA-PC (>98 %) and HEA-PC(98 %) was supplied by Vertellus. Dry solvents; DCM, chloroform, THF and methanol (>99.5 %) were purchased from Fisher Scientific and purified using an Innovative Technology Inc. solvent purification system which involves the passage of solvent though two alumina columns and, in the case of THF, two copper catalyst columns and storage under nitrogen.

6.2 Analysis

NMR spectra were recorded using a Varian Inova 500 spectrometer at 499.87 MHz (^{1}H), a Varian VNMRS-700 spectrometer at 699.73 MHz (^{1}H) and a Bruker Avance 400 spectrometer at 400.13 MHz (^{1}H) or 100.26 MHz (^{13}C). NMR spectra were analysed using MestRE Nova 6.2 software.

TEM was performed on a Hitachi H-7600 operating at 100 kV. One drop (10 µl) of prepared aggregate solution (1 mg/ml) was applied onto a glow discharged, carbon coated, 400 mesh copper grid for 30 seconds, blotted with filter paper and negatively stained with 1 w/v% aqueous uranyl acetate for 30 seconds. The grids were glow discharged for 20 seconds to increase the hydrophilicity which assists sample spreading.

All IR spectra were collected on a Nexus Nicolet FT-IR spectrometer by creating a film on NaCl plates from acetone or methanol and analyzed using omnic E.S.P. 5.1 software. Elemental analysis was carried out on an Exeter analytical E-440 elemental analyser for C, H and N content and Dionex DX 120 Ion chromatograph to determine S content. Dynamic light scattering was conducted on Brookhaven ZetaPlus Zeta potential analyser, particle size of the prepared aggregate solution (1 mg/ml) was determined using BIC Particle sizing software.

THF GPC was conducted on a Viscotek TDA 302 with 2 x 300 ml PLgel 5 μm mixed C columns, having refractive index, viscosity and light scattering detectors. THF was used as the eluent at a flow rate of 1.0 ml/min and at constant temperature of 35 ^{o}C. Molecular weights were obtained using triple detection; the detectors were calibrated with a single narrow molecular weight distribution polystyrene standard using a value of dn/dc of 0.185. Data analysis was carried out using Omnisec 4.0 software. THF (conventional calibration), samples were analysed using a conventional calibration generated with a series of narrow polydispersity polystyrene standards (192-1,111,200 gmol^{-1}) obtained from Polymer Laboratories. The polymer concentration of each solution analyzed was approximately 1 mg/ml.

Chloroform/methanol GPC was carried out using a Hewlett Packard HP1090Liquid Chromatograph and two Polymer Laboratories PL Gel 5 μm Mixed-C (7.5 x 300 mm) columns in series with a guard column at 40 °C connected to a Gilson Model 131 refractive index detector. The eluent was a 3:1 v/v % chloroform/methanol mixture containing 2 mM LiBr at a flow rate of 1.0 ml min^{-1}. A series of near-monodisperse polymethylmethacrylate standards were used as calibration standards. Data analysis was carried out using Cirrus GPC software supplied by Polymer Laboratories (UK). The polymer concentration of each solution analyzed was approximately 1 mg/ml.

DMF GPC was performed on Viscotek 301 with refractive index, viscosity and light scattering detectors and 2 x 300 mm PLgel 5μm mixed C columns, DMF containing 0.1 % by mass of LiBr was used as the eluent with a flow rate of 1.0 ml/min and at a constant temperature of 70 ^{o}C. Molecular weights were obtained using triple detection; the detectors were calibrated with a single narrow molecular weight distribution polystyrene standard using a value of dn/dc of 0.165. The polymer concentration of each solution analyzed was approximately 1 mg/ml.

6.3 Methods

6.3.1 Synthesis of RAFT Agent BSTSE[172]

Mercaptoethanol (1.05 ml, 14.98 mol., 1.0 eq.) was added to a fine suspension of potassium phosphate tribasic (3.18 g, 14.98 mol., 1.0 eq.) in acetone (36 ml) and stirred for 10 min. Carbon disulfide (2.7 ml, 44.94 mol., 3.0 eq.) was subsequently added and after stirring for 10 min. benzyl bromide (1.76 ml, 14.98 mol., 1.0 eq.) was added. The solution was then stirred a further 15 mins before filtering the suspension, the cake was washed with acetone (3x15 ml). Acetone was then removed *in vacuo* to yield a viscous orange oil. Yield 3.28 g (90 %).

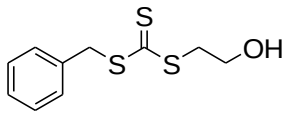

Figure 6-1. Chemical structure of RAFT agent BSTSE.

^{1}H NMR (700 MHz, $CDCl_3$): δ 7.40-7.25 (5H, m, Ar H's), 4.62 (2H, s, $ArCH_2$), 3.88 (2H, t, *J*=6.0Hz, CH_2OH), 3.61 (2H, t, *J*=6.0Hz, SCH_2), 2.37 (1H, br S, OH).
^{13}C NMR (126 MHz, $CDCl_3$): δ 223.51 (CS_3), 134.85 (Ar), 129.30 (Ar), 128.77 (Ar), 127.87 (Ar), 60.54 (CH_2OH), 41.76 ($PhCH_2S$), 39.22 (SCH_2).
Elemental (found %): C, 49.29; H, 4.96; S, 39.36; $C_{10}H_{12}OS_3$ (expected %) C, 49.14; H, 4.95; S, 39.16.
MS (ES+): m/z 91 $PhCH_2^+$, m/z 199.9 $PhCH_2CS_2^+$, m/z 45 $^+(CH_2)_2OH$.

6.3.2 Synthesis of PLA-MacroRAFT agent

6.3.2.1 Tin Catalyzed ROP of Lactide

To tin octanoate (0.06 g, 0.07 mmol., 0.5 eq.) and BSTSE (0.07 g, 0.28 mmol., 1.0 eq.) under nitrogen, D, L-lactide (1.0 g, 6.9 mmol., 25 eq.) in dry toluene (60 ml) was added. The reaction was heated at reflux (110 ^oC) for 24 h. The polymer was precipitated from toluene into methanol and dried *in vacuo*. Yield 0.65 g (61 %).

^{1}H NMR (400 MHz, $CDCl_3$): δ 7.36 – 7.26 (4H, m, Ar H's), 5.27 – 5.06 (74H, m, CH), 4.60 (2 H, s, $PhCH_2$, end group), 4.44 – 4.28 (4H, m, SCH_2 + CH, end group), 3.65(2 H, t, *J* = 6.3 Hz, SCH_2CH_2O, end group), 1.71 – 1.36 (273H, m, CH_3).

6.3.2.2 DBU Catalyzed ROP of Lactide

DBU (0.18 ml, 1.2 mmol., 0.9 eq.) was added to a solution of D, L-lactide (5.09 g, 35 mmol., 25.0 eq.), RAFT agent (0.34 g, 1.4 mmol., 1.0 eq.) in chloroform (120 ml) under nitrogen, the solution was stirred for 50 min. before being quenched with benzoic acid (0.2 g, 1.6 mmol., 1.17 eq.) in chloroform. The reaction mixture underwent an aqueous wash followed by a sodium hydrogen carbonate wash. The polymer was subsequently precipitated from chloroform into hexane and dried *in vacuo* to yield a yellow crystalline solid. Yield 5.21 g (96 %).

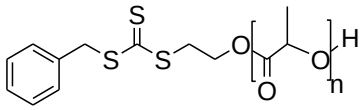

Figure 6-2. Chemical structure of PLA macroRAFT agent with BSTSE end group.

^{1}H NMR (400 MHz, $CDCl_3$): δ 7.36-7.27 (5 H, m, Ar H's), 4.67 – 4.55 (49H, m, CH), 4.62 (2H, s, $PhCH_2$, end group), 4.44 – 4.29 (3H, m, SCH_2 + CH, end group), 3.66 (2H, t, *J* = 6.3 Hz, SCH_2CH_2O, end group), 1.67 – 1.49 (153H, m, CH_3).

^{13}C NMR (101 MHz, $CDCl_3$): δ 169.77-169.19 (CO), 134.77 (Ar), 129.30 (Ar), 128.80 (Ar), 127.94 (Ar), 69.47-69.05 (CH), 66.72-66.67 (CHOH, end group), 62.66 (CH_2O, end group), 41.72 ($PhCH_2$, end group), 34.68 (SCH_2, end group), 20.56 (CH_3, end group), 16.79-16.67 (CH_3).

GPC (THF): M_n=3,900 gmol^{-1}, M_w=4,100 gmol^{-1}, PDI=1.03.

IR (cm^{-1}): 1755 (C=O).

6.3.3 Synthesis of PLA-PMPC

6.3.3.1 PLA_{50}-$PMPC_{100}$

MPC (0.8 g, 2.7 mmol., 100.0 eq.), ACVA (1.9x10^{-3} g, 6.8x10^{-3} mmol., 0.25 eq.) and macroRAFT agent (0.12 g, 0.03 mmol., 1.0 eq.) in a solvent mixture of methanol/DMSO (7:3) (3.68 g) was degassed by purging with nitrogen for 30min. The mixture was heated at 75 ^{o}C and stirred for 12 h. The polymer was precipitated from methanol/DMSO into methanol. The precipitant was filtered then concentrated under reduced pressure and subsequently dialyzed against water over 24 h. and lyophilised. Yield 0.6 g (65 %).

^{1}H NMR (400 MHz, MeOD:$CDCl_3$ (2:1)): δ 5.36 – 5.16 (50H, m, CH, PLA), 4.39 (165H, br s, $CH_2CH_2NMe_3$, PMPC), 4.30 (143H, br s, $CO_2CH_2CH_2$, PMPC), 4.15 (147H, br s, CO_2CH_2, PMPC), 3.82 (156H, br s, CH_2NMe_3, PMPC), 3.38 (762H, s, NMe_3, PMPC),

2.18-1.68 (125H, br s, CH_2, PMPC, backbone), 1.71 – 1.58 (185H, m, CH_3, PLA), 1.17, 1.01(220H, br s, CH_3, PMPC, backbone).

GPC (MeOH/$CHCl_3$(1:3)): M_n=15,600 $gmol^{-1}$, M_w=21,800 $gmol^{-1}$, PDI = 1.40.

6.3.3.2 PLA_{50}-$PMPC_{50}$

PLA_{50}-$PMPC_{50}$ was synthesized using an analogous method to 6.3.3.1 adding to a Schlenk tube: PLA-macroRAFT agent (0.18 g, 0.04 mmol., 1.0 eq.), MPC (0.6 g, 2.0 mmol., 50.0 eq.) and ACVA ($2.8x10^{-3}$ g, $1.0x10^{-2}$ mmol., 0.25 eq.) in DMSO/MeOH (3:7) (3.11 g). Yield 0.47 g (60 %).

^{1}H NMR (400 MHz, MeOD:$CDCl_3$ (2:1)): δ 5.35 – 5.15 (50H, m, CH, PLA), 4.39 (96H, br s, C*H*$_2$$CH_2NMe_3$, PMPC), 4.29 (89H, br s, CO_2CH_2C*H*$_2$, PMPC), 4.15 (92H, br s, CO_2CH_2, PMPC), 3.81 (93H, br s, C*H*$_2$$NMe_3$, PMPC), 3.37 (464H, s, NMe_3, PMPC), 2.18 – 1.82 (80H, m, CH_2, PMPC, backbone), 1.72 – 1.55 (170H, m, CH_3, PLA), 1.17, 1.00(137H, br s, CH_3, PMPC, backbone).

GPC (MeOH/$CHCl_3$(1:3)): M_n=16,000 $gmol^{-1}$, M_w =20,800 $gmol^{-1}$, PDI = 1.30.

6.3.3.3 PLA_{50}-$PMPC_{75}$

PLA_{50}-$PMPC_{75}$ was synthesized using an analogous method to 6.3.3.1 adding to a Schlenk tube: PLA-macroRAFT agent (0.16 g, 0.04 mmol., 1.0 eq.), MPC (0.8 g, 2.7 mmol., 75.0eq.) and ACVA ($2.5x10^{-3}$ g, $9.0x10^{-3}$ mmol., 0.25 eq.) in DMSO/MeOH (3:7) (3.84 g). Yield 0.68 g (73 %).

^{1}H NMR (400 MHz, MeOD:$CDCl_3$ (2:1)): δ 5.33 – 5.19 (50H, m, CH, PLA), 4.39 (135H, br s, C*H*$_2$$CH_2NMe_3$, PMPC), 4.29 (121H, br s, CO_2CH_2C*H*$_2$, PMPC), 4.15 (134H, br s, CO_2CH_2, PMPC), 3.82 (132H, br s, C*H*$_2$$NMe_3$, PMPC), 3.38 (533H, br s, NMe_3, PMPC), 2.18 – 1.83 (110H, m, CH_2, PMPC, backbone), 1.74 – 1.53 (165H, m, CH_3, PLA), 1.18, 1.01(174H, br s, CH_3, PMPC, backbone).

GPC (MeOH/$CHCl_3$(1:3)): M_n=12,300 $gmol^{-1}$, M_w=17,000 $gmol^{-1}$, PDI = 1.38.

6.3.4 Synthesis of Triblock Copolymer PMPC-PLA-PMPC

MPC (0.8 g, 2.7 mmol., 200.0 eq.), ACVA ($1.9x10^{-3}$ g, $6.8x10^{-3}$ mmol., 0.5 eq.) and macroRAFT agent (0.07 g, 0.01 mmol., 1.0 eq.) in a solvent mixture of methanol/DMSO (7:3) (3.49 g) was degassed by purging with nitrogen for 30 min. The mixture was heated at 70 ^oC and stirred for 12 h. The polymer was precipitated from methanol/DMSO into

methanol. The precipitant was filtered then concentrated under reduced pressure and subsequently dialyzed against water over 24 h. and lyophilised. Yield 0.78 g (90 %).

^{1}H NMR (400 MHz, MeOD:$CDCl_3$ (2:1)): δ 5.33 – 5.15 (50H, m, CH, PLA), 4.37 (340H, br s, C*H*$_2$$CH_2NMe_3$, PMPC), 4.28 (289H, br s, CO_2CH_2C*H*$_2$, PMPC), 4.13 (315H, br s, CO_2CH_2, PMPC), 3.80 (322H, br s, C*H*$_2$$NMe_3$, PMPC), 3.36 (1477H, s, NMe_3, PMPC), 2.20-1.78 (269H, m, CH_2, PMPC, backbone), 1.74 – 1.51 (179H, m, CH_3, PLA), 1.16, 1.0 (410H, br s, CH_3, PMPC, backbone).
GPC (MeOH/$CHCl_3$(1:3)): M_n=9,000 gmol^{-1}, M_w=11,500 gmol^{-1}, PDI = 1.28.

6.3.5 APC

6.3.5.1 Free Radical Polymerization

APC (0.51 g, 1.8 mmol., 100.0 eq.) and ACVA (5x10^{-3} g, 1.8x10^{-2} mmol., 1.0 eq.) in methanol (2.5 ml) was degassed by several freeze pump thaw cycles before stirring at 75 ^oC for 17 h. The polymer in methanol was dialysed against water for 24 h. and lyophilized. Yield 0.31 g (61 %).

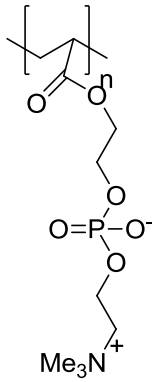

Figure 6-3. Chemical structure of PAPC.

^{1}H NMR (400 MHz, MeOD): δ 4.34 (4H, br s, C*H*$_2$$CH_2NMe_3$ + CO_2CH_2C*H*$_2$), 4.09 (2H, br s, CO_2CH_2), 3.76 (2H, br s, C*H*$_2$$NMe_3$), 3.31 (9H, s, NMe_3), 2.43 (1H, br s, CH, backbone), 1.98, 1.78, 1.62 (2H, br s, CH_2, backbone).
GPC (Aqueous): M_n=5,800 gmol^{-1}, M_w=12,300 gmol^{-1}, PDI=2.12.

6.3.5.2 RAFT Polymerization

APC (1.00 g, 3.6 mmol., 23.0 eq.), BSTSE RAFT agent (3.8x10^{-2} g, 0.16 mmol., 1.0 eq.) and ACVA (1.1x10^{-2} g, 0.04 mmol., 0.25 eq.) in methanol (5 ml) was degassed by several

freeze pump thaw cycles before stirring at 75 °C for 17 h. The polymer was precipitated into diethyl ether then redissolved in methanol and dialysed against water for 24 h. and lyophilized. Yield 0.65 g (65 %).

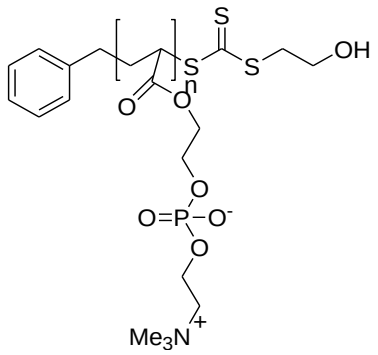

Figure 6-4. Chemical structure of PAPC with BSTSE end group.

^{1}H NMR (400 MHz, MeOD): δ 7.41 – 7.05 (5H, m, Ar), 4.27 (120H, br s, C*H*$_2$CH$_2$NMe$_3$ + CO$_2$CH$_2$C*H*$_2$), 4.03 (66H, br s, CO$_2$CH$_2$), 3.70 (68H, s, C*H*$_2$NMe$_3$), 3.25 (288H, s, NMe$_3$), 2.39 (35H, br s, CH, backbone), 1.94, 1.73, 1.58 (58H, br s, CH$_2$, backbone).
^{13}C NMR (101 MHz, MeOD) δ 176.09(CO), 129.64 (Ar, end group), 67.41 (*C*H$_2$NMe$_3$), 65.71 (*C*H$_2$CH$_2$NMe$_3$), 64.64 (CO$_2$CH$_2$), 60.66 (CO$_2$CH$_2$*C*H$_2$), 54.80 (NMe$_3$), 42.80 (CHCO$_2$, backbone), 36.33 (CH$_2$, backbone).
GPC (Aqueous): M_n=3,500 gmol^{-1}, M_w=4,700 gmol^{-1}, PDI=1.34.
IR (cm^{-1}): 1720 (C=O PMPC), 1232 (P-O), 968 (N-Me).

6.3.6 Model System – *n*-Butyl Methacrylate

6.3.6.1 RAFT Polymerization of n-Butyl Methacrylate

6.3.6.1.1 BSTSE

n-Butyl Methacrylate (1.1 ml, 7.0 mmol., 45.0 eq.), BSTSE agent (0.038 g, 0.16 mmol., 1.0 eq.) and AIBN (0.0064 g, 0.04 mmol., 0.25 eq.) in THF (4.5 ml) was degassed by purging with nitrogen for 30 min. before stirring at 75 °C for 14 h. The polymer was precipitated from THF into cold methanol. The polymer was dried *in vacuo*. Yield 0.47 g (48 %).

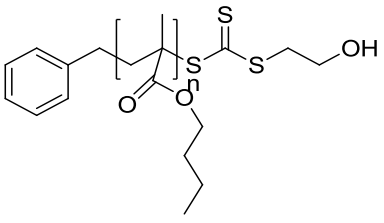

Figure 6-5. Chemical structure of poly(*n*-butyl methacrylate) with BSTSE end group.

^{1}H NMR (400 MHz, $CDCl_3$): δ 3.94 (2H, s, CO_2CH_2), 2.09 – 1.74 (2 H, m, CH_2, backbone), 1.60 (2 H, s, OCH_2CH_2), 1.38 (2 H, s, CH_2CH_3), 0.94 (6H, t, *J* = 31.9 Hz, CH_2CH_3 + CH_3, backbone).

GPC (THF): M_n=39,800gmol^{-1}, M_w=62,500 gmol^{-1}, PDI = 1.57.

6.3.6.1.2 4-Cyano-4-phenylcarbonothio) pentanoic acid

n-Butyl Methacrylate (1.12 ml, 7.0 mmol., 50.0 eq.), RAFT agent (0.0393 g, 0.14 mmol., 1.0 eq.) and ACVA (0.01 g, 0.04 mmol., 0.25 eq.) in THF (4.5 ml) was degassed by purging with nitrogen for 30 min. before stirring in an oil bath set at 75 ^oC for 8 h. The polymer was precipitated from THF into cold methanol. The polymer was dried *in vacuo.* Yield 0.89 g (89 %).

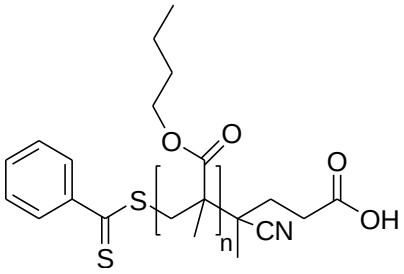

Figure 6-6. Chemical structure of poly(*n*-butyl methacrylate) with CPADB end group.

^{1}H NMR (400 MHz, $CDCl_3$): δ 7.84 (2H, d, *J*=7.3 Hz, Ar), 7.50 (1H, t, *J*=7.4 Hz, Ar), 7.34 (2H, t, *J*=7.5 Hz, Ar), 3.92 (122H, s, CO_2CH_2), 2.06-1.69 (115H, m, CH_2, backbone), 1.60 (128H, s, OCH_2CH_2), 1.39 (139H, s, CH_2CH_3), 0.93 (360H, t, *J*=33.0 Hz, CH_2CH_3 + CH_3, backbone).

GPC (THF): M_n=6,200 gmol^{-1}, M_w=6, 900 gmol^{-1}, PDI = 1.11.

6.3.6.2 Free Radical Polymerization

n-Butyl Methacrylate (1.12 ml, 7.0 mmol., 200.0 eq.) and ACVA (0.01 g, 0.04 mmol., 1.0 eq.) in THF (4.5 ml) was degassed by purging with nitrogen for 30 min. before stirring at 75 ^oC for 8 h. The polymer was precipitated from THF into cold methanol. The polymer was dried *in vacuo*. Yield 0.76 g (76 %).

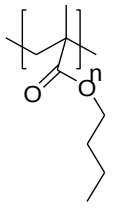

Figure 6-7. Structure of poly(*n*-butyl methacrylate).

^{1}H NMR (400 MHz, $CDCl_3$): δ 3.93 (2H, s, CO_2CH_2), 2.08-1.73 (2 H, m, CH_2, backbone), 1.60 (2 H, s, OCH_2CH_2), 1.40 (2H, s, CH_2CH_3), 1.07-0.75 (6H, t, J=31.9 Hz CH_2CH_3 + CH_3, backbone).

GPC (THF): M_n=29,600 gmol^{-1}, M_w=60,300 gmol^{-1}, PDI = 2.03.

6.3.7 Ring Opening Polymerization of Lactide with Butanediol Initiator

6.3.7.1 General Procedure

To a round bottomed flask containing D, L-lactide, dry THF was added via a cannula. Under nitrogen, butanediol followed by DBU were added via a syringe to the lactide solution. After stirring for one hour the reaction mixture was quenched by the addition of benzoic acid in dry THF (10 ml). The reaction mixture was concentrated under reduced pressure and precipitated twice into methanol. The resulting white polymer was dried over anhydrous magnesium sulfate and *in vacuo* to yield a white solid.

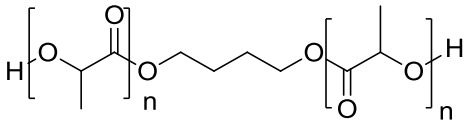

Figure 6-8. Chemical structure of HO-PLA-OH.

Table 6-1. ROP of lactide initiated by butanediol – quantities of each chemical and solvent utilised.

Poly(lactide)	**Lactide**			**Butanediol**			**DBU**			**Benzoic Acid**			**Dry THF**
	Mass (g)	Mols.	Eq.	Vol. (ml)	mmols.	Eq.	Vol. (ml)	mmols.	Eq.	Mass(g)	mmols.	Eq.	Vol. (ml)
HO-PLA$_{50}$-OH	4	0.028	25.0	0.98	1.1	1.0	0.16	1.1	1.0	0.16	1.3	1.2	80
HO-PLA$_{200}$-OH	16.27	0.11	100.0	0.1	1.1	1.0	0.68	4.5	4.1	0.71	5.8	5.2	150
HO-PLA$_{400}$-OH	22.06	0.15	200.0	0.06	0.77	1.0	0.22	1.5	2.0	0.25	2.0	2.7	200

6.3.7.1.1 HO-PLA$_{50}$-OH

HO-PLA$_{50}$-OHwas synthesized following the general procedure 6.3.7.1 and the masses of starting materials given in Table 6-1. Yield 2.90 g (72.5 %).

^{1}H NMR (400 MHz, $CDCl_3$): δ 5.27 – 5.06 (50H, m, CH), 4.42 – 4.25 (2H, m, CH, end group), 4.13 (4H, s, OC*H*$_2$CH$_2$CH$_2$C*H*$_2$O), 2.76 (2H, brs, OH), 1.68 (4H, dt, *J*=5.2, 2.6 Hz, CH$_2$C*H*$_2$C*H*$_2$CH$_2$), 1.60 – 1.40 (158H, m,CH_3).

^{13}C NMR(101 MHz, $CDCl_3$): δ 170.11-169.20 (CO), 69.33-69.09 (CH), 66.78 (CHOH, end group), 64.85 (O*C*H$_2$CH$_2$CH$_2$*C*H$_2$O), 25.10 (CH$_2$*C*H$_2$*C*H$_2$CH$_2$), 20.58 (CH_3, end group), 16.87-16.72 (CH_3).

GPC (THF): M_n=4,400 gmol^{-1}, M_w=4,700 gmol^{-1}, PDI=1.07.

IR (cm^{-1}): 1755 (C=O).

6.3.7.1.2 HO-PLA$_{200}$-OH

HO-PLA$_{200}$-OH was synthesized following the general procedure 6.3.7.1 and the masses of starting materials given in Table 6-1. Yield 12.06 g (74 %).

^{1}H NMR (400 MHz, $CDCl_3$): δ 5.25 – 5.03 (187H, m, CH), 4.39 – 4.26 (2H, m, CH, end group), 4.13 (4H, s, C*H*$_2$CH$_2$CH$_2$C*H*$_2$), 1.62 – 1.42 (572H, m, CH_3).

^{13}C NMR (101 MHz, $CDCl_3$): δ 169.63-169.37 (CO), 69.06 (CH), 66.72 (CHOH, end group), 64.82 (O*C*H$_2$CH$_2$CH$_2$*C*H$_2$O), 25.07 (CH$_2$*C*H$_2$*C*H$_2$CH$_2$), 16.69 (CH_3).

GPC (THF): M_n=11,100 gmol^{-1}, M_w=12,000 gmol^{-1}, PDI=1.09.

IR (cm^{-1}): 1756 (C=O).

6.3.7.1.3 HO-PLA$_{400}$-OH

HO-PLA$_{400}$-OH was synthesized following the general procedure 6.3.7.1 and the masses of starting materials given in Table 6-1. Yield 18.34 g (83 %).

^{1}H NMR (400 MHz, $CDCl_3$): δ 5.27 – 5.04 (400H, m, CH), 4.34 (1H, q, *J* = 7.1 Hz, CH, end group), 4.14 (4H, s, OC*H*$_2$ CH$_2$ CH$_2$C*H*$_2$O), 1.66 – 1.42 (1252H, m, CH_3).

^{13}C NMR (101 MHz, $CDCl_3$): δ 169.72- 169.22 (CO), 69.53- 69.10 (CH), 16.85- 16.73 (CH_3).

GPC (THF): M_n=17,600 gmol^{-1}, M_w=20,500 gmol^{-1}, PDI=1.16.

IR (cm^{-1}): 1753 (C=O).

6.3.8 Ring Opening Polymerization of Lactide with Butanol Initiator

6.3.8.1 General Procedure

To a round bottomed flask containing lactide dry chloroform was added via a cannula. Under nitrogen, butanol followed by DBU, were added via a syringe to the lactide solution. After stirring for one hour the reaction mixture was quenched by the addition of benzoic acid in dry chloroform (10 ml). The reaction mixture was concentrated under reduced pressure and precipitated twice into methanol. The resulting white polymer was dried over anhydrous magnesium sulfate and *in vacuo*.

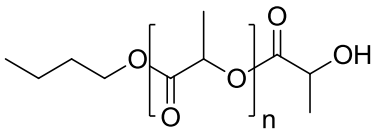

Figure 6-9. Chemical structure of PLA-OH.

Table 6-2. ROP of lactide initiated by butanol – quantities of each chemical and solvent utilised.

Poly(lactide)	**Lactide**			**Butanol**			**DBU**			**Benzoic Acid**			**Dry Chloroform**
	Mass (g)	Mols.	Eq.	Vol. (ml)	mmols.	Eq.	Vol. (ml)	mmols.	Eq.	Mass(g)	mmols.	Eq.	Vol. (ml)
PLA_{50}-OH	15.0	0.1	25.0	0.38	4.2	1.0	0.62	4.2	1.0	0.6	4.9	1.2	150
PLA_{200}-OH	16.72	0.12	100.0	0.11	1.2	1.0	0.69	4.6	4.0	0.73	5.8	5.2	170
PLA_{200}-OH-Alternative method	17.08	0.12	100.0	0.11	1.2	1.0	0.35	2.3	2.0	0.38	3.1	3.2	170

6.3.8.1.1 PLA_{50}-OH

PLA_{50}-OH was synthesized following the general procedure 6.3.8.1 and the masses of starting materials given in Table 6-2. Yield: 12.0 g (80 %).

^{1}H NMR (400 MHz, $CDCl_3$): δ 5.25 – 5.07 (47H, m, CH), 4.40 – 4.27 (1H, m, CH, end group), 4.17 – 4.05 (2H, m, CH_2O, end group), 1.60 – 1.40 (155H, m, CH_3), 1.39 – 1.28 (4H, m, C*H*$_2$$CH_3$, end group), 0.90 (3H, t, *J* = 7.4 Hz, CH_3, alkyl end group).
^{13}C NMR (101 MHz, $CDCl_3$): δ 169.74-169.20 (CO), 69.50- 69.07 (CH), 66.74 (CHOH, end group), 65.45 (CH_2O, end group), 30.53 (*C*H_2CH_2O, group), 20.58 (CH_3, PLA end group), 19.04 (*C*H_2CH_3, end group), 16.81-16.69 (CH_3), 13.70 (CH_3, alkyl end group).
GPC (THF): M_n=3,600 gmol^{-1}, M_w=4,100 gmol^{-1}, PDI=1.14.
IR (cm^{-1}): 1755 (C=O PLA).

6.3.8.1.2 PLA_{200}-OH

PLA_{200}-OH was synthesized following the general procedure 6.3.8.1 and the masses of starting materials given in Table 6-2. Yield 14.67 g (87 %).

^{1}H NMR (400 MHz, $CDCl_3$): δ 5.23 – 4.96 (230H, m, CH), 4.41 – 4.20 (1H, m, C*H*OH, end group), 4.18 – 3.98 (2H, m, CH_2O, end group), 1.67 – 1.26 (713H, m, CH_3), 0.94 – 0.83 (3H, t, *J*=7.4 Hz, CH_3, alkyl end group).
^{13}C NMR (101 MHz, $CDCl_3$): δ 169.60-169.12 (CO), 69.45-69.04 (CH), 66.70 (CHOH, end group), 65.38 (CH_2, end group), 30.51 (*C*H_2CH_2O, end group), 20.51 (CH_3, PLA end group), 18.99 (*C*H_2CH_3, end group), 16.77-16.65 (CH_3), 13.64 (CH_3, alkyl end group).
GPC (THF): M_n=12,000 gmol^{-1}, M_w=13,100 gmol^{-1}, PDI=1.08.
IR (cm^{-1}): 1751 (C=O).

6.3.8.1.3 PLA_{200}-OH - Alternative Method

PLA_{200}-OH was synthesized following the general procedure 6.3.8.1 and the masses of starting materials given in Table 6-2. Yield 16.82 g (98 %).

^{1}H NMR (400 MHz, $CDCl_3$): δ 5.27 – 5.07 (224H, m, CH), 4.41 – 4.31 (1H, m, C*H*OH, end group), 4.18 – 4.09 (2H, m, CH_2O, end group), 1.69 – 1.43 (715H, m, CH_3), 0.92 (3H, t, *J* = 7.4 Hz, CH_3, alkyl end group).

^{13}C NMR (101 MHz, $CDCl_3$): δ 169.70-169.21 (CO), 69.51-69.08 (CH), 65.47 (CH_2, end group), 30.55 (CH_2CH_2O, end group), 20.60 (CH_3, PLA end group), 19.05 (CH_2CH_3, end group), 16.83-16.70 (CH_3), 13.71 (CH_3, alkyl end group).

GPC (THF): M_n=12,300 gmol^{-1}, M_w=12,600 gmol^{-1}, PDI=1.02.

IR (cm^{-1}): 1754 (C=O).

6.3.9 Functionalization of PLA_x-OH and HO- PLA_x-OH

6.3.9.1 General Procedure

DCC and DMAP in dry DCM was added dropwise to a solution of CPADB and polylactide in DCM at 0 ^oC under nitrogen. Following the addition of the reactants, the reaction mixture was stirred for a further 10 min. at 0 ^oC before allowing the mixture to warm to room temperature then stirring overnight. The reaction mixture was subsequently cooled and filtered; the filtrate was concentrated under reduced pressure and precipitated twice into methanol. The resulting pink polymer was dried over anhydrous magnesium sulfate and *in vacuo*.

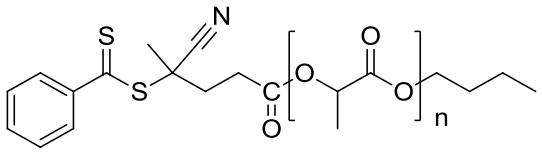

Figure 6-10. Chemical structure of PLA-macroRAFT agent; CPADB endcapped PLA (PLA-R).

Table 6-3. Functionalization of PLA-OH/HO-PLA-OH- quantities of chemicals and solvents utilised.

Functionalized PLA	**PLA-OH/HO-PLA-OH**			**CPADB**			**DCC**			**DMAP**			**Dry DCM**
	Mass (g)	mmols.	Eq.	Mass (g)	mmols.	Eq.	Mass (g)	mmols.	Eq.	Mass(g)	mmols.	Eq.	Vol. (ml)
PLA_{50}-R	1.8	0.48	0.2	0.65	2.34	1.0	0.58	2.8	1.2	0.029	0.23	0.1	55
PLA_{200}-R	3.07	0.19	0.22	0.24	0.85	1.0	0.21	1.0	1.2	0.01	$8.5x10^{-5}$	0.1	70
PLA_{200}-R[a]	2.5	0.15	0.22	0.19	0.67	1.0	0.19	0.67	1.2	0.008	$6.7x10^{-5}$	0.1	60
R-PLA_{50}-R	1.08	0.29	0.11	0.72	2.6	1.0	0.6	2.9	1.1	0.029	0.24	0.09	55
R-PLA_{200}-R	2.5	0.18	0.11	0.46	1.6	1.0	0.41	2.0	1.2	0.02	0.16	0.1	55
R-PLA_{400}-R	4.05	0.14	0.11	0.35	1.3	1.0	0.31	1.5	1.2	0.015	0.13	0.1	80

[a]PLA_{200}-OH utilised was prepared by alternative method

6.3.9.1.1 PLA_{50}-OH

PLA_{50}-R was synthesized following general procedure 6.3.9.1 and the masses of starting materials given in Table 6-3. Yield: 1.3 g (67 %). Degree of functionalization : 100 % (^{1}H NMR).

^{1}H NMR (400 MHz, $CDCl_3$): δ 7.89 (2H, dd, *J* = 8.0, 3.1 Hz, Ar), 7.55 (1H, t, *J* = 7.4 Hz, Ar), 7.38 (2H, t, *J* = 7.7 Hz, Ar), 5.24 – 5.07 (46H, m, PLA), 4.18 – 4.06 (2H, m, OCH_2, end group), 2.84 – 2.36 (4H, m, CH_2CH_2, RAFT end group), 1.92 (3H, S, CH_3, RAFT end group), 1.64 – 1.46 (142H, m, CH_3), 1.42-1.29 (4H, m, CH_2CH_2, end group), 0.91 (3H, t, *J* = 7.4 Hz, CH_3 ,end group).

^{13}C NMR (101 MHz, $CDCl_3$): δ 169.68-169.22 (CO), 144.60 (Ar), 133.12 (Ar), 128.67 (Ar), 126.78 (Ar), 118.50 (CN), 69.52- 68.93 (CH), 65.48 (CH_2O, end group), 45.82-45.75 (CSR_2CN, end group), 33.32-33.22 (CH_2CH_2, RAFT end group), 30.56 (OCH_2CH_2, end group), 29.60 (CH_2CH_2, RAFT end group), 24.28-24.13 (CH_3, RAFT end group), 19.06 (CH_2CH_3, end group), 16.92- 16.74 (CH_3), 13.73 (CH_2CH_3, end group).

GPC (THF): M_n=3,700 gmol^{-1}, M_w=3,800 gmol^{-1}, PDI=1.02.

IR (cm^{-1}): 1756 (C=O).

6.3.9.1.2 PLA_{200}-OH[a]

PLA_{200}-R was synthesized following general procedure 6.3.9.1 and the masses of starting materials given in Table 6-3. Yield: 2.82 g (90 %). Degree of functionalization: 99 % (^{1}H NMR).

^{1}H NMR (400 MHz, $CDCl_3$) δ 7.89 (2H, dd, *J* = 7.7, 2.7 Hz, Ar), 7.55 (1H, t, *J* = 7.3 Hz, Ar), 7.38 (2H, t, *J* = 7.8 Hz, Ar), 5.24 – 5.06 (219H, m, CH), 4.18 – 4.04 (2H, m, OCH_2, end group), 2.84 – 2.35 (4H, m, CH_2CH_2, RAFT end group), 1.91 (3H, s, CH_3, RAFT end group), 1.60 – 1.47 (669H, m, CH_3), 0.90 (3H, t, *J* = 7.4 Hz, CH_3, end group).

^{13}C NMR (101 MHz, $CDCl_3$): δ 169.69-169.20 (CO), 133.11 (Ar), 128.65 (Ar), 126.76 (Ar), 69.50-69.07 (CH), 65.46 (OCH_2, end group), 30.54 (OCH_2CH_2, end group), 19.04 (CH_2CH_3, end group), 16.82-16.70 (CH_3), 13.71 (CH_2CH_3, end group).

GPC (THF): M_n=13,600 gmol^{-1}, M_w=14,100 gmol^{-1}, PDI=1.03.

IR (cm^{-1}): 1756(C=O).

6.3.9.1.3 PLA_{200}-OH[b]

PLA_{200}-R was synthesized using general procedure 6.3.9.1. with PLA_{200}-OH prepared by method 6.3.9.1 and the masses of starting materials given in Table 6-3. Yield: 2.37 g (93 %). Degree of functionalization: 99 % (^{1}H NMR).

^{1}H NMR (400 MHz, $CDCl_3$): δ 7.91(2H, dd, *J* = 7.8, 2.7 Hz, Ar), 7.57 (1H, t, *J* = 7.7 Hz, Ar), 7.40 (2H, t, *J* = 7.7 Hz, Ar), 5.25 – 5.09 (197, m, CH), 4.18 – 4.06 (2H, m, OCH_2, end group), 2.88 – 2.36 (4H, m, CH_2CH_2, RAFT end group), 1.97 – 1.88 (3H, s, CH_3, RAFT end group), 1.68 – 1.44 (692H, m, CH_3), 0.96 – 0.82 (3H,t, *J* = 7.4 Hz, CH_3, end group).
^{13}C NMR (101 MHz, $CDCl_3$): δ 169.64-169.17 (CO), 128.64 (Ar), 126.75 (Ar), 69.48-69.07 (CH), 30.54 (OCH_2CH_2, end group), 19.03 (CH_2CH_3, end group), 16.80-16.68 (CH_3), 13.67 (CH_2CH_3, end group).
GPC (THF): M_n=10,300 gmol^{-1}, M_w=11,000 gmol^{-1}, PDI=1.07.
IR (cm^{-1}): 1754 (C=O).

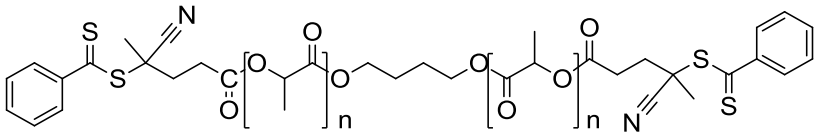

Figure 6-11. Chemical structure of difunctionalised PLA-macroRAFT agent, R-PLA-R.

6.3.9.1.4 HO-PLA_{50}-OH

R-PLA_{50}-R was synthesized following general procedure 6.3.9.1 and the masses of starting materials given in Table 6-3. Yield: 0.98 g (79 %). Degree of functionalization: 99 % (^{1}H NMR).

^{1}H NMR (400 MHz, $CDCl_3$): δ 7.89 (4H, dd, *J* = 7.6, 2.7 Hz, Ar), 7.55 (2H, t, *J* = 7.3 Hz, Ar), 7.38 (4H,t, *J* = 7.6 Hz, Ar), 5.25 – 5.05 (51H, m, CH), 4.14 (4H, s, $OCH_2CH_2CH_2CH_2O$), 2.85 – 2.35 (8H, m, CH_2CH_2, RAFT end group), 1.91 (6H, s, CH_3, end group), 1.68 (4H, s, $CH_2CH_2CH_2CH_2$), 1.64 – 1.42 (153H, m, CH_3).
^{13}C NMR (101 MHz, $CDCl_3$): δ 171.08-169.21 (CO), 144.59 (Ar), 133.11 (Ar), 128.65 (Ar), 126.76 (Ar), 118.53-118.48 (CN, end group), 69.31-68.91 (CH), 64.84 ($OCH_2CH_2CH_2CH_2O$), 45.81-45.73 (CSR_2CN, end group), 33.29-33.19 (CH_2CH_2, RAFT end group), 29.58 (CH_2CH_2, RAFT end group), 25.07 ($CH_2CH_2CH_2CH_2$), 24.25-24.10 (CH_3, RAFT end group), 16.86-16.71 (CH_3).
GPC (THF): M_n=4,400 gmol^{-1}, M_w=4,500 gmol^{-1}, PDI=1.02.

IR (cm^{-1}): 1755 (C=O PLA).

6.3.9.1.5 HO-PLA_{200}-OH

R-PLA_{200}-R was synthesized following general procedure 6.3.9.1 and the masses of starting materials given in Table 6-3. Yield 2.3 g (88 %). Degree of functionalization: 100 % (^{1}H NMR).

^{1}H NMR (400 MHz, $CDCl_3$): δ 7.91 (4H, dd, *J* = 7.2, 3.2 Hz, Ar), 7.57 (2H, t, *J* = 7.4 Hz, Ar), 7.40 (4H, t, *J* = 7.7 Hz, Ar), 5.28 – 5.03 (181H, m, CH), 4.15 (4H, s, C*H*$_2$$CH_2CH_2$C*H*$_2$), 2.87 – 2.32 (8H, m, CH_2CH_2, raft end group), 1.93 (6H, s, CH_3, end group), 1.66 – 1.44 (608H, m, CH_3).

^{13}C NMR (101 MHz, $CDCl_3$): δ 169.70-169.23 (CO), 133.13 (Ar), 128.68 (Ar), 126.79 (Ar), 69.10 (CH), 16.74 (CH_3).

GPC (THF): M_n=12,400 $gmol^{-1}$, M_w=13,100 $gmol^{-1}$, PDI=1.06.

IR (cm^{-1}): 1753 (C=O).

6.3.9.1.6 HO-PLA_{400}-OH

R-PLA_{400}-R was synthesized following general procedure 6.3.9.1 and the masses of starting materials given in Table 6-3. Yield: 3.7 g (90 %). Degree of functionalization: 96 % (^{1}H NMR).

^{1}H NMR (400 MHz, $CDCl_3$): δ 7.89 (4H, dd, *J* = 7.8, 2.5 Hz, Ar), 7.55 (2H, t, *J* = 7.4 Hz, Ar), 7.38 (4H, t, *J* = 7.7 Hz, Ar), 5.26 – 5.05 (390H, m, CH), 4.13 (4H, s, OC*H*$_2$ CH_2CH_2C*H*$_2$O), 2.85 – 2.35 (8H, m, CH_2CH_2, RAFT end group), 1.91 (6H, s, CH_3, end group), 1.75 – 1.34 (1227H, m, CH_3).

^{13}C NMR (101 MHz, $CDCl_3$): δ 169.67-169.20 (CO), 128.66 (Ar), 126.78 (Ar), 69.51-69.09 (CH), 16.83- 16.73 (CH_3).

GPC (THF): M_n=18,500 $gmol^{-1}$, M_w=21,600 $gmol^{-1}$, PDI=1.17.

IR (cm^{-1}): 1750 (C=O).

6.3.10 Synthesis of PLA -PHEMA Diblock Copolymer

6.3.10.1 PLA_{46}-$PHEMA_{15}$

PLA-macroRAFT agent (0.46 g, 0.12 mmol., 1.0 eq.), HEMA (0.22 ml, 1.8 mmol., 15.0 eq.) and ACVA ($8.6x10^{-3}$ g, 0.03 mol., 0.25 eq.) in THF (3.14 ml) was degassed by purging with nitrogen for 25 min. and heated at 70 ^oC for 12 h. The solution was cooled before

diluting with THF and precipitated twice into diethyl ether. The polymer obtained was dried under reduced pressure. Yield 0.62 g (89 %).

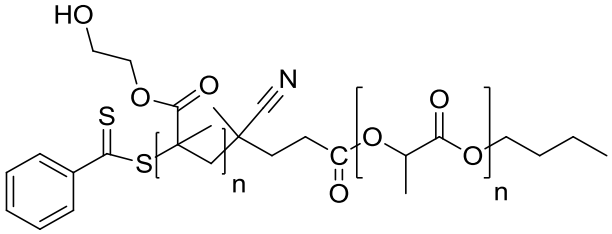

Figure 6-12. Chemical structure of PLA -PHEMA diblock copolymer.

^{1}H NMR (400 MHz, $CDCl_3$:MeOD (2:1)): δ) δ 5.06 – 4.81 (47H, m, CH, PLA),, 3.84 (42H, br s, CO_2CH_2, PHEMA), 3.57 (38H, br s, C*H*$_2$OH, PHEMA), 1.92-1.57(42H, m, CH_2, PHEMA backbone), 1.47 – 1.27 (148H, m, CH_3, PLA), 0.87, 0.71 (53H, br s, CH_3, PHEMA backbone).

^{13}C NMR (101 MHz, $CDCl_3$:MeOD (2:1)): δ 178.11-177.10 (CO, PHEMA), 169.41-169.25 (CO, PLA), 69.22-68.84 (CH, PLA), 66.28 (CO_2CH_2, PHEMA), 59.24 (CH_2OH, PHEMA), 53.98-51.65 (CH_2, PHEMA backbone), 44.86-44.52 (CCH_3CO_2, PHEMA backbone), 18.42 (CH_3, PHEMA backbone), 16.45-16.10 (CH_3, PLA).

GPC (THF): M_n=10,000 gmol^{-1}, M_w=11,400 gmol^{-1}, PDI=1.15.

GPC (DMF): M_n=14,700 gmol^{-1}, M_w=26,700 gmol^{-1}, PDI=1.82.

IR (cm^{-1}): 1758 (C=O PLA), 1722 (C=O PHEMA).

6.3.10.2 PLA_{47}-$PHEMA_{100}$

PLA_{47}-$PHEMA_{100}$ was synthesized using an analogous method to 6.3.10.1 adding to a Schlenk tube: PLA-macroRAFT agent (0.14 g, 0.04 mmol., 1.0 eq.), HEMA (0.47 ml, 3.8 mmol., 100.0 eq.) and ACVA ($2.7x10^{-3}$ g, $9.6x10^{-3}$ mmol., 0.25 eq.) in THF (2.89 ml). Yield 0.62 g (97 %).

^{1}H NMR (400 MHz, $CDCl_3$:MeOD (2:1)): δ 5.00 – 4.86 (47H, m, CH, PLA), 3.82 (204H, br s, CO_2CH_2, PHEMA), 3.55 (198H, br s, CH_2OH, PHEMA), 1.98-1.54 (187H, m, CH_2, PHEMA backbone), 1.43 – 1.19 (162H, m, CH_3, PLA), 0.85, 0.69 (283H, br s, CH_3, PHEMA backbone).

^{13}C NMR (101 MHz, $CDCl_3$:MeOD (2:1)): δ 178.16-177.18 (CO, PHEMA), 169.48-169.31 (CO, PLA), 69.03-68.87 (CH, PLA), 66.32 (CO_2CH_2, PHEMA), 59.43-59.28 (CH_2OH, PHEMA), 54.02-51.62 (CH_2, PHEMA backbone), 44.87-44.54 (CCH_3CO_2), 18.47 (CH_3, PHEMA backbone), 16.52- 16.16 (CH_3, PLA).

GPC (THF): M_n=18,300 gmol^{-1}, M_w=19,800 gmol^{-1} PDI=1.09.

GPC (DMF): M_n=25,200 gmol^{-1}, M_w=36,800 gmol^{-1} PDI=1.46.
IR (cm^{-1}): 1758 (C=O PLA), 1722 (C=O PHEMA).

6.3.10.3 PLA_{219}-$PHEMA_{67}$

PLA_{219}-$PHEMA_{67}$ was synthesized using an analogous method to 6.3.10.1 adding to a Schlenk tube: PLA-macroRAFT agent (0.46 g, 0.03 mmol., 1.0 eq.), HEMA (0.23 ml, 1.9 mmol., 67.0 eq.) and ACVA (2.0x10^{-3} g, 7.2x10^{-3} mmol., 0.25 eq.) in THF (3.21 ml). Yield 0.68 g (96 %).

^{1}H NMR (400 MHz, $CDCl_3$:MeOD (2:1)): δ 5.04 – 4.84 (219H, m, CH, PLA), 3.82 (114H, br s, CO_2CH_2, PHEMA), 3.55 (110H, br s, CH_2OH, PHEMA), 1.88 – 1.57 (115H, m CH_2, PHEMA backbone), 1.40 – 1.24 (672H, m, CH_3, PLA), 0.85, 0.69 (165H, br s, CH_3, PHEMA backbone).
^{13}C NMR (101 MHz, $CDCl_3$:MeOD (2:1)) δ 178.17-177.19 (CO, PHEMA), 169.47-169.29 (CO, PLA), 68.86 (CH, PLA), 66.32 (CO_2CH_2, PHEMA), 59.41-59.26 (CH_2OH, PHEMA), 54.00-51.71 (CH_2, PHEMA, backbone), 44.85-44.52 (*C*CH_3CO_2, PHEMA), 18.43 (CH_3, PHEMA, backbone), 16.17(CH_3, PLA).
GPC (THF): M_n=38,400 gmol^{-1}, M_w=46,100 gmol^{-1}, PDI=1.20.
GPC (DMF): M_n=36,100 gmol^{-1}, M_w=63,600 gmol^{-1}, PDI=1.76.

6.3.10.4 PLA_{46}-$PHEMA_{100}$

PLA_{46}-$PHEMA_{100}$ was synthesized using an analogous method to 6.3.10.1 adding to a Schlenk tube: PLA-macroRAFT agent (0.13 g, 0.03 mmol., 1.0 eq.), HEMA (0.41 ml, 3.4 mmol., 100.0 eq.) and ACVA (2.4x10^{-3} g, 8.5x10^{-3} mmol., 0.25 eq.) in ethanol/THF (1:1) (2.28 g). Yield 0.46 g (81 %).

^{1}H NMR (400 MHz, $CDCl_3$:MeOD (2:1)): δ 4.98 – 4.77 (47H, m CH, PLA), 3.78 (162H, br s, CO_2CH_2, PHEMA), 3.50 (163H, br s, CH_2OH, PHEMA), 1.88 – 1.48 (136H, m, CH_2, PHEMA backbone), 1.39 – 1.18 (140H, m, CH_3, PLA), 0.81, 0.64 (226H, br s, CH_3, PHEMA backbone).
^{13}C NMR (101 MHz, $CDCl_3$:MeOD (2:1)): δ 178.10-177.10 (CO, PHEMA), 169.40-169.19 (CO, PLA), 68.95-68.79 (CH, PLA), 66.22 (CO_2CH_2, PHEMA), 59.30-59.16 (CH_2OH, PHEMA), 53.93-51.59 (CH_2, PHEMA, backbone), 44.78-44.45 (*C*CH_3CO_2, PHEMA), 18.35 (CH_3, PHEMA, backbone), 16.36-16.03 (CH_3, PLA).
GPC (DMF): M_n=18,800 gmol^{-1}, M_w=22,100 gmol^{-1}, PDI=1.17.

IR (cm^{-1}): 1759 (C=O PLA), 1722 (C=O PHEMA).

6.3.10.5 PLA_{197}-$PHEMA_{60}$

PLA_{197}-$PHEMA_{60}$ was synthesized using an analogous method to 6.3.10.1 adding to a Schlenk tube: PLA-macroRAFT agent (0.34 g, 0.02 mmol., 1.0 eq.), HEMA (0.17 ml, 1.4 mmol., 60.0 eq.) and ACVA ($1.6x10^{-3}$ g, $5.8.x10^{-3}$ mmol., 0.25 eq.) in ethanol/THF (1:1) (2.08 g) and heated for 24 h. Yield 0.37 g (71 %).

^{1}H NMR (400 MHz, $CDCl_3$:MeOD (2:1)): δ 5.02 – 4.81 (197H, m, CH, PLA), 3.82 (103H, br s, CO_2CH_2, PHEMA), 3.55 (101H, br s, CH_2OH, PHEMA), 1.87 – 1.55 (103H, m, CH_2, PHEMA backbone), 1.45 – 1.25 (610H, m, CH_3, PLA), 0.85, 0.69 (133H, br s, CH_3, PHEMA backbone).
^{13}C NMR (101 MHz, $CDCl_3$:MeOD (2:1)): δ 178.15-177.16 (CO, PHEMA), 169.46-169.20 (CO, PLA), 69.24-68.84 (CH, PLA), 66.31 (CO_2CH_2, PHEMA), 59.39-59.24 (CH_2OH, PHEMA), 53.99-51.62 (CH_2, PHEMA, backbone), 44.84-44.51 (CCH_3CO_2, PHEMA), 18.42 (CH_3, PHEMA, backbone), 16.22-16.11 (CH_3, PLA).
GPC (DMF): M_n=21,500 $gmol^{-1}$, M_w=24,900 $gmol^{-1}$, PDI=1.16.
IR (cm^{-1}): 1756 (C=O PLA), 1726 (C=O PHEMA).

6.3.11 Synthesis of PHEMA-PLA-PHEMA Triblock Copolymer

6.3.11.1 $PHEMA_{62}$-PLA_{390}-$PHEMA_{62}$

PLA-macroRAFT agent (0.53 g, 0.02 mol., 1.0 eq.), HEMA (0.28 ml, 2.3 mol., 125.0 eq.) and ACVA ($1.3x10^{-3}$ g, $4.6x10^{-3}$ mmol., 0.25 eq.) in THF (3.73 ml) was degassed by purging with nitrogen for 25 min. and heated at 70 ^oC for 12 h. The solution was cooled before diluting with THF and precipitated twice into diethyl ether. The polymer obtained was dried under reduced pressure. Yield 0.5 g (60 %).

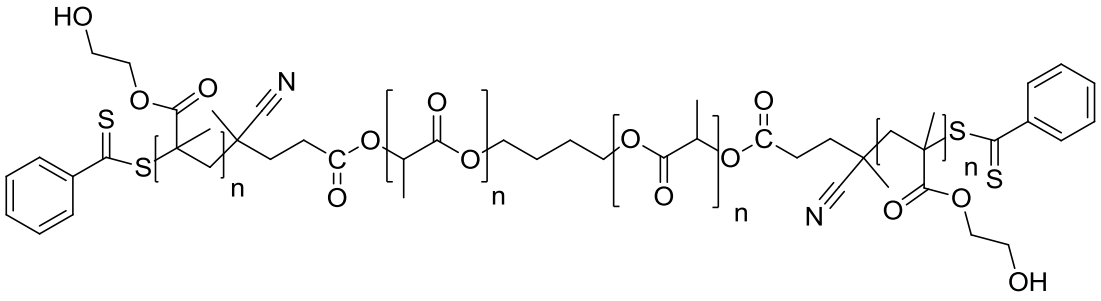

Figure 6-13. Chemical structure of PHEMA-PLA-PHEMA triblock copolymer.

^{1}H NMR (400 MHz, $CDCl_3$:MeOD (2:1)): δ 5.02 – 4.87 (390H, m CH PLA), 3.82 (217H, br s, CO_2CH_2, PHEMA), 3.55 (258H, br s, C*H*$_2$OH, PHEMA), 1.94-1.55 (248H, br s, CH_2, PHEMA backbone), 1.40 – 1.27 (1217H, m, CH_3, PLA), 0.85, 0.69 (300H, br s, CH_3, PHEMA backbone).

^{13}C NMR (101 MHz, $CDCl_3$:MeOD (2:1)): δ 178.09-177.10 (CO, PHEMA), 169.39-169.17 (CO, PLA), 68.95-68.79 (CH, PLA), 66.22 (CO_2CH_2, PHEMA), 59.15 (CH_2OH, PHEMA), 53.89-52.92 (CH_2, PHEMA backbone), 44.79-44.45 (*C*CH_3CO_2, PHEMA backbone), 18.33 (CH_3, PHEMA backbone), 16.06 (CH_3, PLA).

GPC (THF): M_n=36,700 gmol^{-1}, M_w=45,300 gmol^{-1}, PDI=1.24.

GPC (DMF): M_n=39,900 gmol^{-1}, M_w=56,100 gmol^{-1}, PDI=1.41.

IR (cm^{-1}): 1757 (C=O PLA), 1720 (C=O HEMA).

6.3.11.2 $PHEMA_{62}$-PLA_{390}-$PHEMA_{62}$

$PHEMA_{62}$-PLA_{390}-$PHEMA_{62}$ was synthesized using an analogous method to 6.3.11.1 adding to a Schlenk tube an additional 0.5 eq of initiator and repeating the polymerization for a further 12 h.

^{1}H NMR (400 MHz $CDCl_3$:MeOD (2:1)): δ 5.09-4.70 (390H, m, CH, PLA), 3.79 (239H, br s, O_2CH_2, PHEMA), 3.52 (237H, br s, C*H*$_2$OH, PHEMA), 1.85-1.51 (240H, m, CH_2, PHEMA backbone), 1.44-1.13 (1227H, m, CH_3, PLA), 0.82, 0.66 (287H, br s, CH_3, PHEMA backbone).

^{13}C NMR (101 MHz, $CDCl_3$:MeOD (2:1)): δ 178.12-177.11 (CO, PHEMA), 169.41-169.20 (CO, PLA), 68.80 (CH, PLA), 66.24 (CO_2CH_2, PHEMA), 59.17 (CH_2OH, PHEMA), 54.59-51.72 (CH_2, PHEMA backbone), 44.79-44.44 (*C*CH_3CO_2, PHEMA backbone), 18.35 (CH_3, PHEMA backbone), 16.09(CH_3, PLA).

GPC (THF): M_n=50,700 gmol^{-1}, M_w=65,200 gmol^{-1}, PDI=1.29.

6.3.11.3 $PHEMA_{20}$-PLA_{390}-$PHEMA_{20}$

$PHEMA_{20}$-PLA_{390}-$PHEMA_{20}$ was synthesized using an analogous method to 6.3.11.1 adding to a Schlenk tube: PLA-macroRAFT agent (0.61 g, 0.02 mmol., 1.0 eq.), HEMA (0.1 ml, 8.5 mmol., 40.0 eq.) and ACVA ($3.0x10^{-3}$ g, $1.0x10^{-2}$ mmol., 0.5 eq.) in THF (4.0 ml). The polymerization mixture was charged with an additional 0.5 eq. of initiator and heated for a further 12 h. Yield 0.53 g (74 %).

^{1}H NMR (400 MHz $CDCl_3$:MeOD (2:1)): δ 5.02 – 4.89 (390H, m, CH, PLA), 3.82 (63H, br s, CO_2CH_2, PHEMA), 3.54 (109H, br s, C*H*$_2$OH, PHEMA), 1.90-1.56 (113H, m, CH_2,

PHEMA backbone), 1.46 – 1.22 (1187H, m, CH_3, PLA), 0.86, 0.69 (89H, br s, CH_3, PHEMA backbone).

^{13}C NMR(101 MHz, $CDCl_3$:MeOD (2:1)): δ 178.15-176.71 (CO, PHEMA), 169.41-169.23 (CO, PLA), 68.83 (CH, PLA), 66.24 (CO_2CH_2, PHEMA), 59.23 (CH_2OH, PHEMA), 54.01- 53.42 (CH_2, PHEMA backbone), 44.85-44.51 (CCH_3CO_2, PHEMA backbone), 18.45 (CH_3, PHEMA backbone), 16.10 (CH_3, PLA).

GPC (THF): M_n=34,500 gmol^{-1}, M_w=48,600 gmol^{-1}, PDI=1.41.

GPC (DMF): M_n=33,700 gmol^{-1}, M_w=65,900 gmol^{-1}, PDI=1.96.

6.3.11.4 $PHEMA_{53}$-PLA_{51}-$PHEMA_{53}$

$PHEMA_{53}$-PLA_{51}-$PHEMA_{53}$ was synthesized using an analogous method to 6.3.11.1 adding to a Schlenk tube: PLA-macroRAFT agent (0.16 g, 0.04 mmol., 1.0 eq.), HEMA (0.47 ml, 3.8 mmol., 106.0 eq.) and ACVA ($2.5x10^{-3}$ g, $9.1x10^{-3}$ mmol., 0.25 eq.) in THF (2.98 ml). Yield 0.6 g (91 %).

^{1}H NMR (400 MHz, $CDCl_3$:MeOD (2:1)): δ 4.95-4.77 (51H, m, CH, PLA), 3.77 (196H, br s, CO_2CH_2, PHEMA), 3.50 (224H, br s, C*H_2*OH, PHEMA), 1.87-1.68 (203H, m, CH_2, PHEMA backbone), 1.35 – 1.18 (190H, m, CH_3, PLA), 0.80, 0.64 (281H, br s, CH_3, PHEMA backbone).

^{13}C NMR (101 MHz, $CDCl_3$:MeOD (2:1)): δ 178.11-177.10 (CO, PHEMA), 169.99-169.18 (CO, PLA), 68.95-68.79 (CH, PLA), 66.22 (CO_2CH_2, *P*HEMA), 59.30- 59.15 (CH_2OH, PHEMA), 53.88-51.58 (CH_2, PHEMA backbone), 44.79-44.45 (CCH_3CO_2, PHEMA backbone), 18.34 (CH_3, PHEMA backbone), 16.38-16.03 (CH_3, PLA).

GPC (THF): M_n=53,100 gmol^{-1}, M_w=60,700 gmol^{-1} PDI=1.14.

GPC (DMF): M_n=27,600 gmol^{-1}, M_w=61,900 gmol^{-1}, PDI=2.25.

6.3.11.5 $PHEMA_{40}$-PLA_{390}—$PHEMA_{40}$

$PHEMA_{40}$-PLA_{390}-$PHEMA_{40}$ was synthesized using an analogous method to 6.3.11.1 adding to a Schlenk tube: PLA-macroRAFT agent (0.31 g, 0.01 mmol., 1.0 eq.), HEMA (0.11 ml, 0.87 mmol., 80.0 eq.) and ACVA ($8.0x10^{-4}$ g, $2.7x10^{-3}$ mmol., 0.25 eq.) in ethanol/THF (4:6) (1.71 g) and heated for 24 h. Yield 0.34 g (79 %).

^{1}H NMR (400 MHz, $CDCl_3$:MeOD (2:1)): δ 5.01 – 4.80 (390H, m, CH, PLA), 3.79 (53H, br s, CO_2CH_2, PHEMA), 3.52 (47H, br s, C*H_2*OH, PHEMA), 1.73 – 1.63 (43H, m, CH_2,

PHEMA backbone), 1.39 – 1.19 (1189H, m, CH_3, PLA), 0.83, 0.66 (61H, br s, CH_3, PHEMA backbone).

^{13}C NMR (101 MHz, $CDCl_3$:MeOD (2:1)): δ 177.87-176.46 (CO, PHEMA), 169.42-169.28 (CO, PLA), 68.81 (CH, PLA), 66.26 (CO_2CH_2, PHEMA), 59.18 (CH_2OH, PHEMA), 54.26-52.51 (CH_2, PHEMA backbone), 44.82-44.45 (CCH_3CO_2, PHEMA backbone), 18.36 (CH_3, PHEMA backbone), 16.08(CH_3, PLA).

GPC (DMF): M_n=29,200 gmol^{-1}, M_w=37,100 gmol^{-1}, PDI=1.27.

IR (cm^{-1}): 1757 (C=O PLA), 1714 (C=O PHEMA).

6.3.11.6 $PHEMA_{25}$-PLA_{181}—$PHEMA_{25}$

$PHEMA_{25}$-PLA_{181}-$PHEMA_{25}$ was synthesized using an analogous method to 6.3.11.1 adding to a Schlenk tube: PLA-macroRAFT agent (0.41 g, 0.03 mmol., 1.0 eq.), HEMA (0.20 ml, 1.7 mmol., 50.0 eq.) and ACVA ($2.3x10^{-3}$ g, $8.4x10^{-3}$ mmol., 0.25 eq.) in ethanol/THF (1:1) (2.49 g). Yield 0.45 g (73 %).

^{1}H NMR (400 MHz, $CDCl_3$:MeOD (2:1)): δ 5.01 – 4.79 (181H, CH, PLA), 3.79 (63H, br s, CO_2CH_2, PHEMA), 3.51 (58H, br s, CH_2OH, PHEMA), 1.79 – 1.56 (44H, m, CH_2, PHEMA backbone), 1.41 – 1.17 (558H, m, CH_3, PLA), 0.82, 0.65 (81H, br s, CH_3, PHEMA backbone).

^{13}C NMR (101 MHz, $CDCl_3$:MeOD (2:1)): δ 178.10-176.10 (CO, PHEMA), 169.38-169.16 (CO, PLA), 68.97-68.82 (CH, PLA), 66.25 (CO_2CH_2, PHEMA), 59.20 (CH_2OH, PHEMA), 53.78-51.62 (CCH_3CO_2, PHEMA backbone), 44.84-44.50 (CCH_3CO_2, PHEMA backbone), 18.40 (CH_3, PHEMA backbone), 16.10 (CH_3, PLA).

GPC (DMF): M_n=23,300 gmol^{-1}, M_w=28,200 gmol^{-1}, PDI=1.21.

IR (cm^{-1}): 1756 (C=O PLA)

6.3.11.7 $PHEMA_{25}$-PLA_{181}-$PHEMA_{25}$

$PHEMA_{25}$-PLA_{181}-$PHEMA_{25}$ was synthesized using an analogous method to 6.3.11.1 adding to a Schlenk tube: PLA-macroRAFT agent (0.33 g, 0.03 mmol., 1.0 eq.), HEMA (0.16 ml, 1.4 mmol., 50.0 eq.) and ACVA ($1.9x10^{-3}$ g, $6.7x10^{-3}$ mmol., 0.25 eq.) in ethanol/THF (1:1) (2.03 g) and heated for 24 h. Yield 0.4 g (78 %).

^{1}H NMR (400 MHz, $CDCl_3$): δ 5.05 – 4.89 (181H, m, CH, PLA), 3.85 (68H, br s, CO_2CH_2, PHEMA), 3.58 (65H, br s, CH_2OH, PHEMA), 1.91-1.64 (54H, m, CH_2,

PHEMA backbone), 1.43 – 1.28 (564H, m, CH_3, PLA), 0.88, 0.72 (93H, br s, CH_3, PHEMA backbone).

^{13}C NMR (101 MHz, $CDCl_3$:MeOD (2:1)): δ 178.18-176.86 (CO, PHEMA), 169.48-169.21 (CO, PLA), 69.02-68.87 (CH, PLA), 66.33 (CO_2CH_2, PHEMA), 59.40-59.26 (CH_2OH, PHEMA), 54.04-52.00 (*C*CH_3CO_2, PHEMA backbone), 44.86-44.52 (*C*CH_3CO_2, PHEMA backbone), 18.44 (CH_3, PHEMA backbone), 16.23-16.18 (CH_3, PLA).

GPC (DMF): M_n=21,300 gmol^{-1}, M_w=25,900 gmol^{-1}, PDI=1.22.

IR (cm^{-1}): 1757(C=O PLA)

6.3.11.8 $PHEMA_{50}$-PLA_{51}—$PHEMA_{50}$

$PHEMA_{50}$-PLA_{51}-$PHEMA_{50}$ was synthesized using an analogous method to 6.3.11. adding to a Schlenk tube: PLA-macroRAFT agent (0.15 g, 0.03 mmol., 1.0 eq.), HEMA (0.42 ml, 3.4 mmol., 100.0 eq.) and ACVA (2.4x10^{-3} g, 8.6x10^{-3} mmol., 0.25 eq.) in ethanol/THF (1:1) (2.40 g). Yield 0.42 g (70 %).

^{1}H NMR (400 MHz, $CDCl_3$:MeOD (2:1)): δ 5.06 – 4.84 (51H, m, CH, PLA), 3.85 (153H, br s, CO_2CH_2, PHEMA), 3.58 (152H, br s, C*H*$_2$OH, PHEMA), 1.98-1.60 (137H, m, CH_2, PHEMA backbone), 1.48– 1.26 (169H, m, CH_3, PLA), 0.88, 0.72 (218H, br s, CH_3, PHEMA backbone).

^{13}C NMR (101 MHz, $CDCl_3$:MeOD (2:1)): δ 178.16- 177.18 (CO, PHEMA), 169.48-169.26 (CO, PLA), 69.17-68.86 (CH, PLA), 66.32 (CO_2CH_2, *P*HEMA), 59.42-59.28 (CH_2OH, PHEMA), 53.99-51.72 (*C*CH_3CO_2, PHEMA backbone), 44.86-44.53 (*C*CH_3CO_2, PHEMA backbone), 18.46 (CH_3, PHEMA backbone), 16.23-16.15 (CH_3, PLA).

GPC (DMF): M_n=23,800 gmol^{-1}, M_w=30, 500 gmol^{-1}, PDI=1.28.

IR (cm^{-1}): 1756 (C=O PLA), 1726 (C=O PHEMA).

6.3.12 Synthesis of PLA-PMPC Diblock Copolymer

6.3.12.1 PLA_{46}-$PMPC_{100}$ Diblock Copolymer

PLA-macroRAFT agent (0.08 g, 0.02 mmol., 1.0 eq.), MPC (0.6 g, 2.02 mmol., 100.0 eq.) and ACVA (1.4x10^{-3} g, 5.1x10^{-3} mmol., 0.25 eq.) and DMSO/IPA (3:7) (2.71 g) was degassed by purging with nitrogen for 25min. and heated at 70 ^{o}C for 12 h. The solution was cooled before diluting with methanol and precipitated into THF. The resulting solid was dissolved in methanol and dialyzed against water over 24 h. and lyophilised. Yield 0.5 g (74 %).

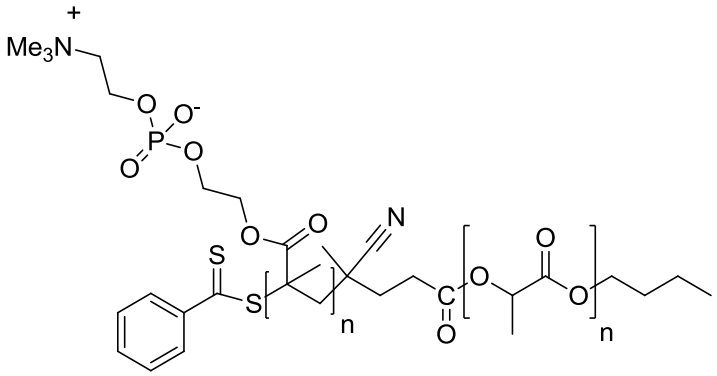

Figure 6-14. Chemical structure of PLA-PMPC Diblock Copolymer.

^{1}H NMR (400 MHz, MeOD/$CDCl_3$ (2:1)): δ 5.3 – 5.16 (46H, m, CH, PLA), 4.40 (188H, br s, C*H*$_2$$CH_2NMe_3$, PMPC), 4.30 (167H, br s, CO_2CH_2C*H*$_2$, PMPC), 4.16 (169H, br s, CO_2C*H*$_2$), 3.83 (175H, br s, C*H*$_2$$NMe_3$), 3.39 (776H, s, 6H, NMe_3), 2.27-1.76 (125H, br S, CH_2 MPC backbone), 1.71 – 1.58 (148H, m, CH_3 PLA backbone), 1.18, 1.01 (257H, br s, CH_3 MPC backbone).

^{13}C NMR (101 MHz, MeOD/$CDCl_3$ (2:1)): δ 178.79-177.66 (CO MPC), 170.52 (CO PLA), 69.99(CH PLA), 67.01 (CO_2C*H*$_2$), 65.76 (*CH*$_2$$PO_4$), 63.82 ($PO_4$$CH_2$), 60.17 (C*H*$_2$$NMe_3$), 54.61 ($NMe_3$), 46.01-45.68 (*C*$CH_3COO_2$), 19.58 ($CH_3$ MPC), 17.83-17.01 (CH_3 PLA).

GPC (methanol/chloroform(1:3)): M_n=19,400 $gmol^{-1}$, M_w=24,000 $gmol^{-1}$, PDI=1.24.

IR (cm^{-1}): 1756 (C=O PLA), 1720 (C=O PMPC), 1232 (P-O), 968 (N-Me).

6.3.12.2 PLA_{50}-$PMPC_{100}$ Diblock Copolymer

The synthesis of the block copolymer was repeated in ethanol/THF(1:1). Yield 0.47 g (69 %).

^{1}H NMR (400 MHz, MeOD/$CDCl_3$ (2:1)): δ 5.34 – 5.17 (46H, m, CH, PLA), 4.39 (221H, br s, C*H*$_2$$CH_2NMe_3$, PMPC), 4.29 (188H, br s, CO_2CH_2C*H*$_2$, PMPC), 4.14 (200H, br s, CO_2C*H*$_2$, PMPC), 3.82 (203H, s, C*H*$_2$$NMe_3$, PMPC), 3.38 (869H, s, NMe_3, PMPC), 2.26 – 1.77 (153H, m, CH_2, PMPC backbone), 1.71 – 1.55 (152H, m, CH_3, PLA), 1.17, 1.01 (275H, br s, CH_3, PMPC backbone).

GPC (methanol/chloroform(1:3)): M_n=19,300 $gmol^{-1}$, M_w=23,300 $gmol^{-1}$, PDI=1.21.

IR (cm^{-1}): 1756 (C=O PLA), 1723 (C=O PMPC), 1241 (P-O), 967 (N-Me).

6.3.12.3 PLA_{46}-$PMPC_{25}$ Diblock Copolymer

PLA_{46}-$PMPC_{25}$ was synthesized using an analogous method to 6.3.12.1 adding to a Schlenk tube: PLA-macroRAFT agent (0.24 g, 0.06 mmol., 1.0 eq.), MPC (0.45 g, 1.5 mmol., 25.0 eq.) and ACVA ($4.3x10^{-3}$ g, $1.5x10^{-2}$ mmol., 0.25 eq.) in THF:ethanol (1:1) (2.75 g). Yield 0.39 g (57 %).

^{1}H NMR (400 MHz, MeOD/$CDCl_3$ (2:1)): δ 5.35-5.17 (46H, m, CH, PLA), 4.42 (70H, br s, C*H*$_2$$CH_2NMe_3$, PMPC), 4.31 (67H, br s, CO_2CH_2C*H*$_2$, PMPC), 4.17 (70H, br s, CO_2C*H*$_2$, PMPC), 3.83 (65H, br s, C*H*$_2$$NMe_3$, PMPC), 3.39 (291H, s, NMe_3, PMPC), 2.27 – 1.80 (58H, m, CH_2, PMPC, backbone), 1.73 – 1.55 (144H, m, CH_3, PLA), 1.19, 1.02 (94H, br s, CH_3, PMPC, backbone).

^{13}C NMR (101 MHz, MeOD/$CDCl_3$ (2:1)): δ 178.85-177.71 (CO, PMPC), 170.55-170.39 (CO, PLA), 70.17-70.00 (CH, PLA), 66.97 (*C*H_2NMe_3, PMPC), 65.73 (*C*$H_2CH_2NMe_3$, PMPC), 63.92 (CO_2CH_2, PMPC), 60.23 (CO_2CH_2*C*H_2, PMPC), 54.58 (NMe_3, PMPC), 45.94, 45.61 (*C*CH_3CO_2, PMPC, backbone), 19.47 (CH_3, PMPC, backbone), 17.58-17.00 (CH_3, PLA).

GPC (methanol/chloroform(1:3)): M_n=18,000 $gmol^{-1}$, M_w=20,900 $gmol^{-1}$, PDI=1.16.

IR (cm^{-1}): 1757 (C=O PLA), 1723 (C=O PMPC), 1240 (P-O), 968 (N-Me).

6.3.12.4 PLA_{46}-$PMPC_{25}$ Diblock Copolymer

The synthesis of the block copolymer was repeated in DMSO/IPA (3:7) (2.75 g). Yield 0.5 g (72 %).

^{1}H NMR (400 MHz, MeOD/$CDCl_3$ (2:1)): δ 5.35 – 5.17 (46H, m, CH, PLA), 4.42 (65H, br s, C*H*$_2$$CH_2NMe_3$, PMPC), 4.31 (64H, br s, CO_2CH_2C*H*$_2$, PMPC), 4.18 (64H, br s, CO_2C*H*$_2$, PMPC), 3.83 (61H, br s, C*H*$_2$$NMe_3$, PMPC), 3.39 (287H, s, NMe_3, PMPC), 2.26 – 1.80 (49H, m, CH_2, PMPC, backbone), 2.05-1.78(143H, m, CH_3 PLA backbone), 1.18, 1.02 (90H, br s, CH_3, PMPC, backbone).

GPC (methanol/chloroform (1:3)): M_n=18,400 $gmol^{-1}$, M_w=21,200 $gmol^{-1}$, PDI=1.15.

IR (cm^{-1}): 1756 (C=O PLA), 1723 (C=O PMPC), 1241 (P-O), 967 (N-Me).

6.3.13 Synthesis of PMPC-PLA-PMPC Triblock Copolymer

6.3.13.1 $PMPC_{55}$-PLA_{390}-$PMPC_{55}$

PLA-macroRAFT agent (0.29 g, 0.01 mmol., 1.0 eq.), MPC (0.33 g, 1.11 mmol., 110.0 eq.) and ACVA ($1.4x10^{-3}$ g, $5.1x10^{-3}$ mmol., 0.5 eq.) and THF:ethanol (6:4) (2.74 g) was degassed by purging with nitrogen for 25 min. and heated at 70 ^{o}C for 12 h. The solution was cooled before diluting with methanol and precipitated into THF. The resulting solid was dissolved in methanol and dialyzed against water over 24 h and lyophilised. Yield 0.55 g, (89 %).

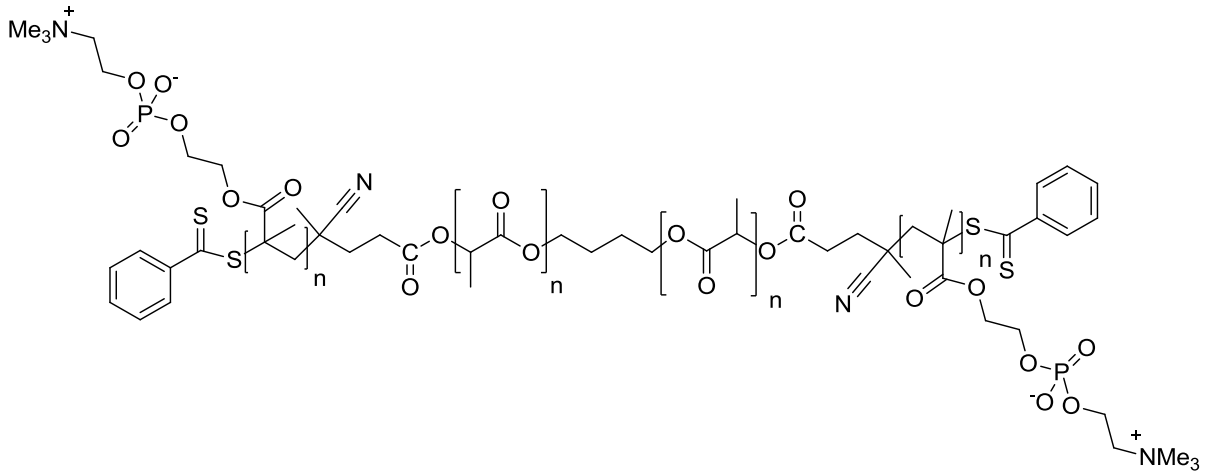

Figure 6-15. Chemical structure of PMPC-PLA-PMPC triblock copolymer.

^{1}H NMR (400 MHz, MeOD:$CDCl_3$(2:1)): δ 5.34-5.16 (390H, m, CH, PLA), 4.39 (178H, br s, C*H*$_2$$CH_2NMe_3$, PMPC), 4.29 (146H, br s, CO_2CH_2C*H*$_2$, PMPC), 4.14 (159H, br s, CO_2C*H*$_2$, PMPC), 3.81 (126H, br s, C*H*$_2$$NMe_3$, PMPC), 3.37 (769H, s,$NMe_3$, PMPC), 2.23-1.83 (113H, m, CH_2, PMPC, backbone), 1.73-1.53 (1167H, m, CH_3, PLA), 1.17, 1.01 (240H, br s, CH_3, PMPC, backbone).

^{13}C NMR (101 MHz, MeOD:$CDCl_3$(2:1)): δ 178.88-177.71 (CO, PMPC), 170.57 (CO, PLA), 70.01 (CH, PLA), 66.99 (*C*H_2NMe_3, PMPC), 65.82 (*C*$H_2CH_2NMe_3$, PMPC), 63.87 (CO_2CH_2, PMPC), 60.20 (CO_2CH_2*C*H_2, PMPC), 54.58 (NMe_3, PMPC), 46.02-45.67 (*C*CH_3CO_2, PMPC, backbone), 19.58 (CH_3, PMPC, backbone), 17.07 (CH_3, PLA).

GPC (methanol/chloroform(1:3)): M_n=44,800 gmol^{-1}, M_w=60,900 gmol^{-1}, PDI=1.36.

IR (cm^{-1}): 1756 (C=O PLA), 1723 (C=O PMPC), 1218 (P-O), 969 (N-Me).

6.3.13.2 $PMPC_{53}$-PLA_{51}-$PMPC_{53}$ Triblock Copolymer

PLA_{53}-$PMPC_{51}$-$PLA_{53}$was synthesized using an analogous method to 6.3.13.1 adding to a Schlenk tube: PLA-macroRAFT agent (0.089 g, 0.02 mmol., 1.0 eq.), MPC (0.63 g, 2.1 mmol., 106.0 eq.) and ACVA ($1.4x10^{-3}$ g, $5.0x10^{-3}$ mmol, 0.25 eq.) in THF:ethanol (1:1) (2.88 g) and heated for 24 h. Yield 0.48 g (67 %).

^{1}H NMR (400 MHz, MeOD $CDCl_3$ (2:1)): δ 5.34 – 5.15 (51H, m, CH, PLA), 4.39 (215H, br s, C*H*$_2$$CH_2NMe_3$, PMPC), 4.29 (187H, br s, CO_2CH_2C*H*$_2$, PMPC), 4.15 (206H, br s, CO_2C*H*$_2$, PMPC), 3.82 (201H,br s, C*H*$_2$$NMe_3$, PMPC), 3.38 (908H, s, NMe_3, PMPC), 2.18-1.80 (174H, m, CH_2, PMPC, backbone), 1.71 – 1.57 (186H, m, CH_3, PLA), 1.17, 1.01(266H, br s, CH_3, PMPC, backbone).

^{13}C NMR (101 MHz, MeOD:$CDCl_3$(2:1)): δ 178.81-177.66 (CO, PMPC), 171.17-170.43 (CO, PLA), 70.35-69.96 (CH, PLA), 66.94 (*C*H_2NMe_3, PMPC), 65.74 (*C*$H_2CH_2NMe_3$, PMPC), 63.79 (CO_2CH_2, PMPC), 60.13 (CO_2CH_2*C*H_2, PMPC), 54.56 (NMe_3, PMPC), 45.94-45.61 (*C*CH_3CO_2, PMPC, backbone), 19.47 (CH_3, PMPC, backbone), 17.70-17.01 (CH_3, PLA)

GPC (methanol/chloroform(1:3)): M_n=24,600 $gmol^{-1}$, M_w=30,600 $gmol^{-1}$, PDI=1.24.

IR (cm^{-1}): 1758 (C=O PLA), 1722 (C=O PMPC), 1236 (P-O), 966 (N-Me).

Bibliography

1. R. F. A. Zwaal, P. Comfurius and L. L. M. Vandeenen, *Nature*, 1977, **268**, 358-360.
2. H. Chen, L. Yuan, W. Song, Z. K. Wu and D. Li, *Prog. Polym. Sci.*, 2008, **33**, 1059-1087.
3. S. Clarke, M. C. Davies, C. J. Roberts, S. J. B. Tendler, P. M. Williams, V. O'Byrne, A. L. Lewis and J. Russell, *Langmuir*, 2000, **16**, 5116-5122.
4. J. A. Hayward and D. Chapman, *Biomaterials*, 1984, **5**, 135-142.
5. D. S. Johnston, S. Sanghera, M. Pons and D. Chapman, *Biochim. Biophys. Acta*, 1980, **602**, 57-69.
6. Y. Kadoma, N. Nakabayashi, E. Masuhara and J. Yamauchi, *Kobunshi Ronbunshu*, 1978, **35**, 423-427.
7. E. J. Lobb, I. Ma, N. C. Billingham, S. P. Armes and A. L. Lewis, *J. Am. Chem. Soc.*, 2001, **123**, 7913-7914.
8. I. Y. Ma, E. J. Lobb, N. C. Billingham, S. P. Armes, A. L. Lewis, A. W. Lloyd and J. Salvage, *Macromolecules*, 2002, **35**, 9306-9314.
9. D. M. Haddleton, S. G. Jackson and S. A. F. Bon, *J. Am. Chem. Soc.*, 2000, **122**, 1542-1543.
10. S. Faucher, P. Okrutny and S. P. Zhu, *Macromolecules*, 2006, **39**, 3-5.
11. S. I. Yusa, K. Fukuda, T. Yamamoto, K. Ishihara and Y. Morishima, *Biomacromolecules*, 2005, **6**, 663-670.
12. B. Yu, A. B. Lowe and K. Ishihara, *Biomacromolecules*, 2009, **10**, 950-958.
13. N. Bhuchar, Z. Deng, K. Ishihara and R. Narain, *Polym. Chem.*, 2011, **2**, 632-639.
14. A. L. Lewis, *Colloids Surf., B*, 2000, **18**, 261-275.
15. K. Ishihara, H. Oshida, Y. Endo, T. Ueda, A. Watanabe and N. Nakabayashi, *J. Biomed. Mater. Res.*, 1992, **26**, 1543-1552.
16. K. Ishihara, H. Oshida, Y. Endo, A. Watanabe, T. Ueda and N. Nakabayashi, *J. Biomed. Mater. Res.*, 1993, **27**, 1309-1314.
17. E. J. O. B. Campbell, Vincent; Stratford, Peter W.; Quirk, Ian; Vick, Terrence A.; Wiles, Martin C.; Yianni, Yiannakis P., *ASAIO J.*, 1994, **40**, M853-M857.
18. K. Ishihara and Y. Iwasaki, *J. Biomater. Appl.*, 1998, **13**, 111-127.
19. E. Dickinson, *Colloids Surf., B*, 1999, **15**, 161-176.

20. J. M. Anderson, A. Rodriguez and D. T. Chang, *Semin. Immunol.*, 2008, **20**, 86-100.
21. S. I. Jeon, J. H. Lee, J. D. Andrade and P. G. Degennes, *J. Colloid Interf. Sci.*, 1991, **142**, 149-158.
22. H. Y. Chu, N. Liu, X. Wang, Z. Jiao and Z. M. Chen, *Int. J. Pharm.*, 2009, **371**, 190-196.
23. J. P. Salvage, S. F. Rose, G. J. Phillips, G. W. Hanlon, A. W. Lloyd, I. Y. Ma, S. P. Armes, N. C. Billingham and A. L. Lewis, *J. Control. Release*, 2005, **104**, 259-270.
24. J. Z. Du, Y. P. Tang, A. L. Lewis and S. P. Armes, *J. Am. Chem. Soc.*, 2005, **127**, 17982-17983.
25. C. Giacomelli, L. Le Men, R. Borsali, J. Lai-Kee-Him, A. Brisson, S. P. Armes and A. L. Lewis, *Biomacromolecules*, 2006, **7**, 817-828.
26. H. Lomas, I. Canton, S. MacNeil, J. Du, S. P. Armes, A. J. Ryan, A. L. Lewis and G. Battaglia, *Adv. Mater.*, 2007, **19**, 4238-4243.
27. H. Lomas, J. Du, I. Canton, J. Madsen, N. Warren, S. P. Armes, A. L. Lewis and G. Battaglia, *Macromol. Biosci.*, 2010, **10**, 513-530.
28. S. Sugihara, A. Blanazs, S. P. Armes, A. J. Ryan and A. L. Lewis, *J. Am. Chem. Soc.*, 2011, **133**, 15707-15713.
29. J. J. Yuan, S. P. Armes, Y. Takabayashi, K. Prassides, C. A. P. Leite, F. Galembeck and A. L. Lewis, *Langmuir*, 2006, **22**, 10989-10993.
30. J.-J. Yuan, A. Schmid, S. P. Armes and A. L. Lewis, *Langmuir*, 2006, **22**, 11022-11027.
31. J. Z. Du and S. P. Armes, *Langmuir*, 2009, **25**, 9564-9570.
32. Y. H. Ma, Y. Q. Tang, N. C. Billingham, S. P. Armes and A. L. Lewis, *Biomacromolecules*, 2003, **4**, 864-868.
33. C. M. Li, Y. Q. Tang, S. P. Armes, C. J. Morris, S. F. Rose, A. W. Lloyd and A. L. Lewis, *Biomacromolecules*, 2005, **6**, 994-999.
34. C. M. Li, N. J. Buurma, I. Haq, C. Turner, S. P. Armes, V. Castelletto, I. W. Hamley and A. L. Lewis, *Langmuir*, 2005, **21**, 11026-11033.
35. C. M. Z. Cristiano, V. Soldi, C. Li, S. P. Armes, C. Rochas, I. Pignot-Paintrand and R. Borsali, *Macromol. Chem. Phys.*, 2009, **210**, 1726-1733.
36. C. M. Li, J. Madsen, S. P. Armes and A. L. Lewis, *Angew. Chem. Int. Edit.*, 2006, **45**, 3510-3513.
37. N. V. Tsarevsky and K. Matyjaszewski, *Macromolecules*, 2002, **35**, 9009-9014.

38. J. Madsen, S. P. Armes, K. Bertal, H. Lomas, S. MacNeil and A. L. Lewis, *Biomacromolecules*, 2008, **9**, 2265-2275.
39. X. Fan, L. Lin and P. B. Messersmith, *Biomacromolecules*, 2006, **7**, 2443-2448.
40. Y. Iwasaki, M. Takamiya, R. Iwata, S.-i. Yusa and K. Akiyoshi, *Colloids Surf. B.*, 2007, **57**, 226-236.
41. J.-H. Seo, R. Matsuno, M. Takai and K. Ishihara, *Biomaterials*, 2009, **30**, 5330-5340.
42. G. H. Hsiue, C. L. Lo, C. H. Cheng, C. P. Lin, C. K. Huang and H. H. Chen, *J. Polym. Sci., Part A: Polym. Chem.*, 2007, **45**, 688-698.
43. G. Liu, X. Hu, C. Chen, Q. Jin and J. Ji, *Polym. Int.*, 2011, **60**, 578-583.
44. G. Liu, X. Hu, C. Chen and J. Ji, *J. Appl. Polym. Sci.*, 2010, **118**, 3197-3202.
45. G.-Y. Liu, P. Lv, C.-J. Chen, X.-F. Hu and J. Ji, *Macromol. Chem. Phys.*, 2011, **212**, 643-651.
46. X. Zhang, J. Lu, Y. Huang, W. Zhao, Y. Chen, J. Li, X. Gao, R. Venkataramanan, M. Sun, D. B. Stolz, L. Zhang and S. Li, *Bioconjugate Chem.*, 2013, **24**, 464-472.
47. G. Y. Liu, L. P. Lv, C. J. Chen, X. S. Liu, X. F. Hu and J. Ji, *Soft Matter*, 2011, **7**, 6629-6636.
48. O. Coulembier, P. Degee, J. L. Hedrick and P. Dubois, *Prog. Polym. Sci.*, 2006, **31**, 723-747.
49. L. S. Nair and C. T. Laurencin, *Prog. Polym. Sci.*, 2007, **32**, 762-798.
50. C. Chu, in *The Biomedical Engineering Handbook,* CRC Press, Boca Ranton, Editon edn., 2000.
51. A. Gopferich, *Biomaterials*, 1996, **17**, 103-114.
52. J. Tamada and R. Langer, *J. Biomater. Sci., Polym. Ed.*, 1992, **3**, 315-353.
53. C. K. Williams, *Chem. Soc. Rev.*, 2007, **36**, 1573-1580.
54. K. M. Stridisberg, M. Ryner and A.-C. Albertsson, in *Degradable Aliphatic Polyesters*, Springer, Berlin, Editon edn., 2002, pp. 41-66.
55. C. Jerome and P. Lecomte, *Adv. Drug Deliv. Rev.*, 2008, **60**, 1056-1076.
56. S. Kobayashi, H. Uyama and S. Kimura, *Chem. Rev.*, 2001, **101**, 3793-3818.
57. G. Odian, *Principles of Polymerization*, Wiley, New Jersey, 2004.
58. A. Duda, in *Renewable Resources: Biopolyesters and Biocatalysis*, Oxford University Press, Washington DC, Editon edn., 2000, vol. 764, pp. 160-199.
59. K. N. Houk, A. Jabbari, H. K. Hall and C. Aleman, *J. Org. Chem.*, 2008, **73**, 2674-2678.

60. C. Aleman, O. Betran, J. Casanovas, K. N. Houk and H. K. Hall, *J. Org. Chem.*, 2009, **74**, 6237-6244.
61. P. Dubois, N. Ropson, R. Jerome and P. Teyssie, *Macromolecules*, 1996, **29**, 1965-1975.
62. H. R. Kricheldorf, M. Berl and N. Scharnagl, *Macromolecules*, 1988, **21**, 286-293.
63. A. Amgoune, C. M. Thomas and J. F. Carpentier, *Pure Appl. Chem.*, 2007, **79**, 2013-2030.
64. I. Barakat, P. Dubois, R. Jerome and P. Teyssie, *Macromolecules*, 1991, **24**, 6542-6545.
65. A. C. Albertsson and I. K. Varma, *Biomacromolecules*, 2003, **4**, 1466-1486.
66. A. C. Albertsson and I. K. Varma, in *Degradable Aliphatic Polymers*, Springer, Berlin, Editon edn., 2001, vol. 157, pp. 1-40.
67. B. Gupta, N. Revagade and J. Hilborn, *Prog. Polym. Sci.*, 2007, **32**, 455-482.
68. J. C. Middleton and A. J. Tipton, *Biomaterials*, 2000, **21**, 2335-2346.
69. P. B. Maurus and C. C. Kaeding, *Oper. Techn. Sport Med.*, 2004, **12**, 158-160.
70. J. A. Cooper, H. H. Lu, F. K. Ko, J. W. Freeman and C. T. Laurencin, *Biomaterials*, 2005, **26**, 1523-1532.
71. H. H. Lu, J. A. Cooper, S. Manuel, J. W. Freeman, M. A. Attawia, F. K. Ko and C. T. Laurencin, *Biomaterials*, 2005, **26**, 4805-4816.
72. J. Tiainen, M. Veiranto, E. Suokas, P. Tormala, T. Waris, M. Ninkovic and N. Ashammakhi, *J. Craniofac. Surg.*, 2002, **13**, 427-433.
73. C. G. Pitt, M. M. Gratzl, G. L. Kimmel, J. Surles and A. Schindler, *Biomaterials*, 1981, **2**, 215-220.
74. M. Rutkowska, A. Dereszewska, M. Jastrzebska and H. Janik, *Macromol. Symp.*, 1998, **130**, 199-204.
75. L. S. Nair and C. T. Laurencin, *Adv. Biochem. Eng. Biot.*, 2006, **102**, 47-90.
76. S. P. Lyu, J. Schley, B. Loy, D. Lind, C. Hobot, R. Sparer and D. Untereker, *Biomacromolecules*, 2007, **8**, 2301-2310.
77. S. M. Li and S. McCarthy, *Biomaterials*, 1999, **20**, 35-44.
78. H. Antheunis, J. C. van der Meer, M. de Geus, W. Kingma and C. E. Koning, *Macromolecules*, 2009, **42**, 2462-2471.
79. C. G. Pitt, F. I. Chasalow, Y. M. Hibionada, D. M. Klimas and A. Schindler, *J. Appl. Polym. Sci.*, 1981, **26**, 3779-3787.
80. L. T. Fan and S. K. Singh, *Controlled Release - A Qualitative Treatment.*, Berlin: Springer-Verlag, 1989.

81. K. Park, W. S. W. Shalaby and H. Park, *Biodegradable Hydrogels for Drug Delivery*, Techromic Publ., Lancaster, 1993.
82. T. St. Pierre and E. Chiellini, *J. Bioact. Compat Pol.*, 1986, **1**, 467 - 497.
83. K. W. Leong, B. C. Brott and R. Langer, *J. Biomed. Mater. Res.*, 1985, **19**, 941-955.
84. E. Ron, T. Turek, E. Mathiowitz, M. Chasin, M. Hageman and R. Langer, *Proc. Natl. Acad. Sci. U. S. A.*, 1993, **90**, 4176-4180.
85. M. Hakkarainen, A. C. Albertsson and S. Karlsson, *Polym. Degrad. Stab.*, 1996, **52**, 283-291.
86. C. C. Chu, *Ann. Surg.*, 1982, **195**, 55-59.
87. M. Vert, S. Li and H. Garreau, *J. Control. Release*, 1991, **16**, 15-26.
88. E. Lavik and R. Langer, *Appl. Microbiol. Biotechnol.*, 2004, **65**, 1-8.
89. R. Langer, *Acc. Chem. Res.*, 2000, **33**, 94-101.
90. E. S. Place, J. H. George, C. K. Williams and M. M. Stevens, *Chem. Soc. Rev.*, 2009, **38**, 1139-1151.
91. R. Langer and J. P. Vacanti, *Science*, 1993, **260**, 920-926.
92. Y. Ikada, in *Polymer Based Systems on Tissue Engineering, Replacement and Regeneration*, Springer, Dordrecht, Editon edn., 2002, vol. 86, pp. 357-370.
93. B. L. Seal, T. C. Otero and A. Panitch, *Mat. Sci. Eng. R.*, 2001, **34**, 147-230.
94. C. M. Agrawal and R. B. Ray, *J. Biomed. Mater. Res.*, 2001, **55**, 141-150.
95. S. C. Baker, G. Rohman, J. Southgate and N. R. Cameron, *Biomaterials*, 2009, **30**, 1321-1328.
96. A. P. Pego, B. Siebum, M. J. A. Van Luyn, X. Van Seijen, A. A. Poot, D. W. Grijpma and J. Feijen, *Tissue Eng.*, 2003, **9**, 981-994.
97. A. P. Pego, M. J. A. Van Luyn, L. A. Brouwer, P. B. van Wachem, A. A. Poot, D. W. Grijpma and J. Feijen, *J. Biomed. Mater. Res., Part A*, 2003, **67A**, 1044-1054.
98. M. Martina and D. W. Hutmacher, *Polym. Int.*, 2007, **56**, 145-157.
99. M. Heyde, K. A. Partridge, S. M. Howdle, R. O. C. Oreffo, M. C. Garnett and K. M. Shakesheff, *Biotechnol. Bioeng.*, 2007, **98**, 679-693.
100. I. C. Bonzani, R. Adhikari, S. Houshyar, R. Mayadunne, P. Gunatillake and M. M. Stevens, *Biomaterials*, 2007, **28**, 423-433.
101. R. Verdejo, G. Jell, L. Safinia, A. Bismarck, M. M. Stevens and M. S. P. Shaffer, *J. Biomed. Mater. Res.*, 2009, **88A**, 65-73.
102. C. Gualandi, L. J. White, L. Chen, R. A. Gross, K. M. Shakesheff, S. M. Howdle and M. Scandola, *Acta Biomater.*, 2010, **6**, 130-136.

103. E. S. Place, R. Nair, H. N. Chia, G. Szulgit, E.-h. Lim and M. M. Stevens, *Adv. Healthcare Mater.*, 2012, **1**, 480-484.
104. C. Gentilini, Y. Dong, J. R. May, S. Goldoni, D. E. Clarke, B.-H. Lee, E. T. Pashuck and M. M. Stevens, *Adv. Healthcare Mater.*, 2012, **1**, 308-315.
105. A. C. Albertsson and U. Edlund, in *Degradable Aliphatic Polymers*, Springer, Berlin, Editon edn., 2002, pp. 67-112.
106. S. Ghosh, *J. Chem. Res-S.*, 2004, 241-246.
107. R. Yoshida, K. Sakai, T. Okano and Y. Sakurai, *Polym. J.*, 1991, **23**, 1111-1121.
108. C. M. Agrawal, in *Polymer Based Systems on Tissue Engineering, Replacement and Regeneration*, Springer, Dordrecht, Editon edn., 2002, vol. 86, pp. 25-36.
109. B. Meier, in *The New York Times*, The New York Times Company, New York, Editon edn., 2013.
110. C. M. Agrawal and K. A. Athanasiou, *J. Biomed. Mater. Res.*, 1997, **38**, 105-114.
111. K. A. Athanasiou, G. G. Niederauer and C. M. Agrawal, *Biomaterials*, 1996, **17**, 93-102.
112. D. H. R. Barton and S. W. McCombie, *J. Chem. Soc., Perkin Trans. 1*, 1975, 1574-1585.
113. G. F. Meijs, E. Rizzardo and S. H. Thang, *Macromolecules*, 1988, **21**, 3122-3124.
114. G. F. Meijs, E. Rizzardo and S. H. Thang, *Polym. Bull.*, 1990, **24**, 501-505.
115. G. F. Meijs, E. Rizzardo, T. P. T. Le and Y. C. Chen, *Macromol. Chem. Phys.*, 1992, **193**, 369-378.
116. J. Krstina, C. L. Moad, G. Moad, E. Rizzardo and C. T. Berge, *Macromol. Symp.*, 1996, **111**, 13-23.
117. J. Krstina, G. Moad, E. Rizzardo, C. L. Winzor, C. T. Berge and M. Fryd, *Macromolecules*, 1995, **28**, 5381-5385.
118. J. Chiefari, Y. K. Chong, F. Ercole, J. Krstina, J. Jeffery, T. P. T. Le, R. T. A. Mayadunne, G. F. Meijs, C. L. Moad, G. Moad, E. Rizzardo and S. H. Thang, *Macromolecules*, 1998, **31**, 5559-5562.
119. *Handbook of RAFT Polymerization*, Wiley-VCH, Weinheim, 2008.
120. G. Moad, E. Rizzardo and S. H. Thang, *Aust. J. Chem.*, 2005, **58**, 379-410.
121. G. Moad, E. Rizzardo and S. H. Thang, *Aust. J. Chem.*, 2012, **65**, 985-1076.
122. C. Boyer, V. Bulmus, T. P. Davis, V. Ladmiral, J. Liu and S. Perrier, *Chem. Rev.*, 2009, **109**, 5402-5436.
123. Y. K. Chong, J. Krstina, T. P. T. Le, G. Moad, A. Postma, E. Rizzardo and S. H. Thang, *Macromolecules*, 2003, **36**, 2256-2272.

124. M. Benaglia, E. Rizzardo, A. Alberti and M. Guerra, *Macromolecules*, 2005, **38**, 3129-3140.
125. D. Pissuwan, C. Boyer, K. Gunasekaran, T. P. Davis and V. Bulmus, *Biomacromolecules*, 2010, **11**, 412-420.
126. A. Gregory and M. H. Stenzel, *Prog. Polym. Sci.*, 2012, **37**, 38-105.
127. M. Barz, F. K. Wolf, F. Canal, K. Koynov, M. J. Vicent, H. Frey and R. Zentel, *Macromol. Rapid Commun.*, 2010, **31**, 1492-1500.
128. M. Seo, M. A. Amendt and M. A. Hillmyer, *Macromolecules*, 2011, **44**, 9310-9318.
129. G. J. Liu, S. B. Ma, S. K. Li, R. Cheng, F. H. Meng, H. Y. Liu and Z. Y. Zhong, *Biomaterials*, 2010, **31**, 7575-7585.
130. J. Rieger, C. Grazon, B. Charleux, D. Alaimo and C. Jerome, *J. Polym. Sci., Part A: Polym. Chem.*, 2009, **47**, 2373-2390.
131. X. Xu, C. Liu and J. Huang, *J. Appl. Polym. Sci.*, 2008, **108**, 2180-2188.
132. T. Boursier, I. Chaduc, J. Rieger, F. D'Agosto, M. Lansalot and B. Charleux, *Polym. Chem.*, 2011, **2**, 355-362.
133. X. W. Xu, J. D. Flores and C. L. McCormick, *Macromolecules*, 2011, **44**, 1327-1334.
134. A. K. Mishra, V. K. Patel, N. K. Vishwakarma, C. S. Biswas, M. Raula, A. Misra, T. K. Mandal and B. Ray, *Macromolecules*, 2011, **44**, 2465-2473.
135. K. P. Chen, N. Grant, L. Y. Liang, H. F. Zhang and B. Tan, *Macromolecules*, 2010, **43**, 9355-9364.
136. C. E. Lipscomb and M. K. Mahanthappa, *Macromolecules*, 2011, **44**, 4401-4409.
137. C. D. Petruczok, R. F. Barlow and D. A. Shipp, *J. Polym. Sci., Part A: Polym. Chem.*, 2008, **46**, 7200-7206.
138. M. Hales, C. Barner-Kowollik, T. P. Davis and M. H. Stenzel, *Langmuir*, 2004, **20**, 10809-10817.
139. A. O. Saeed, S. Dey, S. M. Howdle, K. J. Thurecht and C. Alexander, *J. Mater. Chem.*, 2009, **19**, 4529-4535.
140. S. R. S. Ting, A. M. Gregory and M. H. Stenzel, *Biomacromolecules*, 2009, **10**, 342-352.
141. C. Schmid, J. Falkenhagen and C. Barner-Kowollik, *J. Polym. Sci., Part A: Polym. Chem.*, 2011, **49**, 1-10.

142. C. Lefay, D. Gle, M. Rollet, J. Mazzolini, D. Bertin, S. Viel, C. Schmid, C. Boisson, F. D'Agosto, D. Gigmes and C. Barner-Kowollik, *J. Polym. Sci., Part A: Polym. Chem.*, 2011, **49**, 803-813.
143. T. Gruendling, M. Dietrich and C. Barner-Kowollik, *Aust. J. Chem.*, 2009, **62**, 806-812.
144. J. Akimoto, M. Nakayama, K. Sakai and T. Okano, *J. Polym. Sci., Part A: Polym. Chem.*, 2008, **46**, 7127-7137.
145. S. Sinnwell, A. J. Inglis, T. P. Davis, M. H. Stenzel and C. Barner-Kowollik, *Chem. Commun.*, 2008, 2052-2054.
146. K. J. Thurecht, A. M. Gregory, S. Villarroya, J. X. Zhou, A. Heise and S. M. Howdle, *Chem. Commun.*, 2006, 4383-4385.
147. C. H. Zhu, S. Jung, S. B. Luo, F. H. Meng, X. L. Zhu, T. G. Park and Z. Y. Zhong, *Biomaterials*, 2010, **31**, 2408-2416.
148. M. Achilleos, T. M. Legge, S. Perrier and C. S. Patrickios, *J. Polym. Sci., Part A: Polym. Chem.*, 2008, **46**, 7556-7565.
149. R. Karunakaran and J. P. Kennedy, *J. Polym. Sci., Part A: Polym. Chem.*, 2008, **46**, 4254-4257.
150. Q. Zheng and S. Zheng, *J. Polym. Sci., Part A: Polym. Chem.*, 2012, **50**, 1717-1727.
151. Y. Y. Tong, Y. Q. Dong, F. S. Du and Z. C. Li, *J. Polym. Sci., Part A: Polym. Chem.*, 2009, **47**, 1901-1910.
152. C. Chang, H. Wei, C. Y. Quan, Y. Y. Li, J. Liu, Z. C. Wang, S. X. Cheng, X. Z. Zhang and R. X. Zhuo, *J. Polym. Sci., Part A: Polym. Chem.*, 2008, **46**, 3048-3057.
153. N. S. Cameron, M. K. Corbierre and A. Eisenberg, *Can. J. Chem.*, 1999, **77**, 1311-1326.
154. W.-D. He, X.-L. Sun, W.-M. Wan and C.-Y. Pan, *Macromolecules*, 2011, **44**.
155. L. F. Zhang and A. Eisenberg, *Polym. Adv. Technol.*, 1998, **9**, 677-699.
156. P. L. Soo and A. Eisenberg, *J. Polym. Sci., Part B: Polym. Phys.*, 2004, **42**, 923-938.
157. G. Riess, *Prog. Polym. Sci.*, 2003, **28**, 1107-1170.
158. N. Rodriguez, F. Pincet and S. Cribier, *Colloids Surf., B*, 2005, **42**, 125-130
159. Y. Mai and A. Eisenberg, *Chem. Soc. Rev.*, 2012, **41**, 5969-5985.
160. A. J. Parnell, N. Tzokova, P. D. Topham, D. J. Adams, S. Adams, C. M. Fernyhough, A. J. Ryan and R. A. L. Jones, *Faraday Discuss.*, 2009, **143**, 29-46.
161. F. M. Menger and M. I. Angelova, *Acc. Chem. Res.*, 1998, **31**, 789-797

162. M. I. Angelova and D. S. Dimitrov, *Faraday Discuss.*, 1986, **81**, 303-311.
163. L. Theogarajan, S. Desai, M. Baldo and C. Scholz, *Polym. Int.*, 2008, **57**, 660-667.
164. H. C. Shum, J.-W. Kim and D. A. Weitz, *J. Am. Chem. Soc.*, 2008, **130**, 9543–9549.
165. K. Letchford and H. Burt, *Eur. J. Pharm. Biopharm.*, 2007, **65**, 259-269.
166. S. Ezrahi, E. Tuval and A. Aserin, *Adv. Colloid Interface Sci.*, 2006, **128**, 77-102.
167. S. Ikeda and Y. Maruyama, *J. Colloid Interface Sci.*, 1994, **166**, 1-5.
168. M. Antonietti and S. Forster, *Adv. Mater.*, 2003, **15**, 1323-1333.
169. J. S. Lee and J. Feijen, *J. Control. Release*, 2012, **161**, 473-483.
170. T. Azzam and A. Eisenberg, *Angew. Chem., Int. Ed.*, 2006, **45**, 7443-7447.
171. F. F. Wolf, N. Friedemann and H. Frey, *Macromolecules*, 2009, **42**, 5622-5628.
172. J. Skey and R. K. O'Reilly, *Chem. Commun.*, 2008, 4183-4185.
173. D. Garlotta, *J. Polym. Environ.*, 2001, **9**, 63-84.
174. M. K. Kiesewetter, E. J. Shin, J. L. Hedrick and R. M. Waymouth, *Macromolecules*, 2010, **43**, 2093-2107.
175. A. Stjerndahl, A. Finne-Wistrand, A. C. Albertsson, C. M. Backesjo and U. Lindgren, *J. Biomed. Mater. Res.*, 2008, **87A**, 1086-1091.
176. B. G. G. Lohmeijer, R. C. Pratt, F. Leibfarth, J. W. Logan, D. A. Long, A. P. Dove, F. Nederberg, J. Choi, C. Wade, R. M. Waymouth and J. L. Hedrick, *Macromolecules*, 2006, **39**, 8574-8583.
177. L. Mespouille, F. Nederberg, J. L. Hedrick and P. Dubois, *Macromolecules*, 2009, **42**, 6319-6321.
178. D. J. Coady, K. Fukushima, H. W. Horn, J. E. Rice and J. L. Hedrick, *Chem. Commun.*, 2011, **47**, 3105-3107.
179. J. Rzayev and M. A. Hillmyer, *J. Am. Chem. Soc.*, 2005, **127**, 13373-13379.
180. L. Liu, C. L. Wu, J. C. Zhang, M. M. Zhang, Y. W. Liu, X. J. Wang and G. Q. Fu, *J. Polym. Sci., Part A: Polym. Chem.*, 2008, **46**, 3294-3305.
181. B. Neises and W. Steglich, *Angew. Chem., Int. Ed. Engl.*, 1978, **17**, 522-524.
182. Y. Q. Wan, W. N. Chen, J. Yang, J. Z. Bei and S. G. Wang, *Biomaterials*, 2003, **24**, 2195-2203.
183. W. N. Chen, W. J. Luo, S. G. Wang and J. Z. Bei, *Polym. Adv. Technol.*, 2003, **14**, 245-253.
184. X. B. Zhao, Z. Q. Zhang, F. Pan, Y. H. Ma, M. P. Armes, A. L. Lewis and J. R. Lu, *Langmuir*, 2005, **21**, 9597-9603.

185. J. Madsen, S. P. Armes, K. Bertal, S. MacNeil and A. L. Lewis, *Biomacromolecules*, 2009, **10**, 1875-1887.
186. X. B. Zhao, F. Pan, Z. Q. Zhang, C. Grant, Y. H. Ma, S. P. Armes, Y. Q. Tang, A. L. Lewis, T. Waigh and J. R. Lu, *Biomacromolecules*, 2007, **8**, 3493-3502.
187. M. H. Stenzel, C. Barner-Kowollik, T. P. Davis and H. M. Dalton, *Macromol. Biosci.*, 2004, **4**, 445-453.
188. A. Postma, T. P. Davis, G. Li, G. Moad and M. S. O'Shea, *Macromolecules*, 2006, **39**, 5307-5318.
189. D. E. Discher and A. Eisenberg, *Science*, 2002, **297**, 967-973.
190. K. H. Wong, T. P. Davis, C. Bamer-Kowollik and M. H. Stenzel, *Polymer*, 2007, **48**, 4950-4965.
191. M. F. Zhang, T. Breiner, H. Mori and A. H. E. Muller, *Polymer*, 2003, **44**, 1449-1458.
192. S. J. Holder, N. A. A. Rossi, C. T. Yeoh, G. G. Durand, M. J. Boerakker and N. Sommerdijk, *J. Mater. Chem.*, 2003, **13**, 2771-2778.
193. S. J. Holder and N. A. J. M. Sommerdijk, *Polym. Chem.*, 2011, **2**, 1018-1028.
194. D. E. Discher and F. Ahmed, *Annu. Rev. Biomed. Eng.*, 2006, **8**, 323-341.
195. F. Ahmed, R. I. Pakunlu, A. Brannan, F. Bates, T. Minko and D. E. Discher, *J. Control. Release*, 2006, **116**, 150-158.
196. P. Vangeyte, S. Gautier and R. Jerome, *Colloids Surf., A*, 2004, **242**, 203-211.
197. X. Qu, V. V. Khutoryanskiy, A. Stewart, S. Rahman, B. Papahadjopoulos-Sternberg, C. Dufes, D. McCarthy, C. G. Wilson, R. Lyons, K. C. Carter, A. Schatzlein and I. F. Uchegbu, *Biomacromolecules*, 2006, **7**, 3452-3459.
198. H. L. Kang, W. Y. Liu, R. G. Liu and Y. Huang, *Macromol. Chem. Phys.*, 2008, **209**, 424-430.
199. X. Shan, C. Liu, Y. Yuan, F. Xu, X. Tao, Y. Sheng and H. Zhou, *Colloids Surf., B*, 2009, **72**, 303-311.
200. A. K. Jain, A. K. Goyal, P. N. Gupta, K. Khatri, N. Mishra, A. Mehta, S. Mangal and S. P. Vyas, *J. Control. Release*, 2009, **136**, 161-169.
201. S. J. Holder, G. G. Durand, C.-T. Yeoh, E. Illi, N. J. Hardy and T. H. Richardson, *J. Polym. Sci., Part A: Polym. Chem.*, 2008, **46**, 7739-7756.
202. Y. S. Yu, L. F. Zhang and A. Eisenberg, *Macromolecules*, 1998, **31**, 1144-1154.
203. A. Y. Kwok, G. G. Qiao and D. H. Solomon, *Polymer*, 2004, **45**, 4017-4027.
204. J. Brandrup, Immergut, E.H, *In Polymer Handbook*, 3rd edn., Wiley-Interscience, New York, 1989.

205. F. J. Xu and W. T. Yang, *Prog. Polym. Sci.*, 2011, **36**, 9742-9746.
206. A. R. Thierry, Y. Lunardiiskandar, J. L. Bryant, P. Rabinovich, R. C. Gallo and L. C. Mahan, *Proc. Natl. Acad. Sci. U. S. A.*, 1995, **92**, 9742-9746.
207. A. Agarwal, R. Unfer and S. K. Mallapragada, *J. Control. Release*, 2005, **103**, 245-258.
208. M. Kurisawa, M. Yokoyama and T. Okano, *J. Control. Release*, 2000, **68**, 1-8.